PB-223 626

DESIGN AND CONTROL OF INCINERATORS

VOLUME I

MASSACHUSETTS INSTITUTE OF TECHNOLOGY

PREPARED FOR
ENVIRONMENTAL PROTECTION AGENCY
PUBLIC HEALTH SERVICE

SEPTEMBER 1973

DISTRIBUTED BY:
NTIS
National Technical Information Service
U. S. DEPARTMENT OF COMMERCE

BIBLIOGRAPHIC DATA SHEET

1. Report No. EPA-670/2-73-089A

2.

PB 223 626

4. Title and Subtitle

DESIGN AND CONTROL OF INCINERATORS
VOLUME I

5. Report Date 1973-issuing date

6.

7. Author(s) A. F. Sarofim, G. C. Williams, J. B. Howard, and J. E. L. Rogers

8. Performing Organization Rept. No.

9. Performing Organization Name and Address

Fuels Research Laboratory
Chemical Engineering Department
Massachusetts Institute of Technology
Cambridge, Massachusetts

10. Project/Task/Work Unit No.

11. Contract/~~Grant No.~~ EC-00330-03

12. Sponsoring Organization Name and Address

U.S. Environmental Protection Agency
National Environmental Research Center
Office of Research & Development
Cincinnati, Ohio 45268

13. Type of Report & Period Covered Final

14.

15. Supplementary Notes

The report describes that

16. Abstracts

A versatile batch incinerator was designed and built in order to determine the effect of operational variables on the ignition and burning rates in a fuel bed under conditions similar to those encountered in municipal incinerators. Detailed concentration and temperature profiles within and above the fuel bed were obtained for different distributions of overfire and underfire air rates. These results were used to evaluate both the rate controlling processes and control strategies. It was concluded that for the synthetic refuse beds studied, internal diffusion within the burning elements was limiting and that drying, pyrolysis, and gasification were contemporaneous through most of the runs giving rise to burning rates and overfire gas compositions that were constant over most of a run. From the oxygen concentrations in the bed, it is concluded that low underfire air rates are desirable early and late in a burn, and that for a fully ignited bed the maximum air rate is determined more by consideration of ash carryover and channelling than by the bed's ability to consume the oxygen. The fraction of the heat released above the bed, which determines the overfire air requirements, is governed by the energy requirements of the bed, and decreases with bed moisture and with heat loss from the bed. Towards the end of a burn, the carbon dioxide concentration above the bed falls off dramatically and provides a parameter that could possibly be used for control purposed.

17. Key Words and Document Analysis. 17a. Descriptors

Waste disposal, Wastes, Refuse disposal, Tests, *Incinerators, *Ignition, *Burning rate, Concentration (composition), Temperature, Control, Diffusion, Drying, Pyrolysis, Gasification, Oxygen, Gases, Heat, Moisture, Carbon dioxide, *Fuels

Reproduced by
NATIONAL TECHNICAL
INFORMATION SERVICE
US Department of Commerce
Springfield, VA. 22151

17b. Identifiers/Open-Ended Terms

Solid waste disposal, *Operational variables, *Fuel bed, Air rates, Rate controlling, Synthetic refuse, *Batch incinerator

17c. COSATI Field/Group 13-B

18. Availability Statement

Release to public

19. Security Class (This Report) UNCLASSIFIED

20. Security Class (This Page UNCLASSIFIED

21. No. of Pages ~~300~~ 299

22. Price

EPA-670/2-73-089A
September 1973

DESIGN AND CONTROL OF INCINERATORS

VOLUME I

By

A. F. Sarofim, G. C. Williams,
J. B. Howard, and J. E. L. Rogers
Fuels Research Laboratory
Chemical Engineering Department
Massachusetts Institute of Technology
Cambridge, Massachusetts

Grant No. EC-00330-03
Program Element No. 1D2063

Project Officer

Donald Oberacker
Solid Waste Research Laboratory
National Environmental Research Center
Cincinnati, Ohio 45268

Prepared for
OFFICE OF RESEARCH AND DEVELOPMENT
U.S. ENVIRONMENTAL PROTECTION AGENCY
WASHINGTON, D.C. 20460

REVIEW NOTICE

The Solid Waste Research Laboratory of the National Environmental Research Center - Cincinnati, U.S. Environmental Protection Agency, has reviewed this report and approved its publication. Approval does not signify that the contents necessarily reflect the views and policies of this laboratory or of the U.S. Environmental Protection Agency, nor does mention of trade names or commercial products constitute endorsement or recommendation for use.

The text of this report is reproduced by the National Environmental Research Center - Cincinnati in the form received from the Grantee; new preliminary pages have been supplied.

FOREWORD

Man and his environment must be protected from the adverse effects of pesticides, radiation, noise and other forms of pollution, and the unwise management of solid waste. Efforts to protect the environment require a focus that recognizes the interplay between the components of our physical environment--air, water, and land. The National Environmental Research Centers provide this multidisciplinary focus through programs engaged in

- studies on the effects of environmental contaminants on man and the biosphere, and
- a search for ways to prevent contamination and to recycle valuable resources.

In an attempt to solve the problems involved in solid waste disposal, this study investigated a batch incinerator that was designed and built to determine the effect of operational variables on the ignition and burning rates in a fuel bed. The test conditions were similar to those encountered in municipal incinerators.

A. W. Breidenbach, Ph.D.
Director
National Environmental
Research Center, Cincinnati

ABSTRACT

A versatile batch incinerator was designed and built in order to determine the effect of operational variables on the ignition and burning rates in a fuel bed under conditions similar to those encountered in municipal incinerators. Detailed concentration and temperature profiles within and above the fuel bed were obtained for different distributions of over- and underfire air rates. These results were used to evaluate both the rate controlling processes and control strategies. It was concluded that for the synthetic refuse beds studied, internal diffusion within the burning elements was limiting and that drying, pyrolysis, and gasification were contemporaneous through most of the runs giving rise to burning rates and overfire gas compositions that were constant over most of a run. From the oxygen concentrations in the bed it is concluded that low underfire air rates are desirable early and late in a burn, and that for a fully ignited bed the maximum air rate is determined more by consideration of ash carryover and channelling than by the bed's ability to consume the oxygen. The fraction of the heat released above the bed, which determines the overfire air requirements, is governed by the energy requirements of the bed, and decreases with bed moisture and with heat loss from the bed. Towards the end of a burn, the carbon dioxide concentration above the bed falls off dramatically and provides a parameter that could possibly be used for control purposes.

TABLE OF CONTENTS

Page

ABSTRACT i

TABLE OF CONTENTS ii

LIST OF FIGURES . . . . iii-viii

LIST OF TABLES . . . . ix-x

CONCLUSIONS xi

RECOMMENDATIONS xi

INTRODUCTION 1

SURVEY OF EXPERIMENTAL AND THEORETICAL TREATMENT OF FUEL BED COMBUSTION 21

PROCESSES OCCURRING WITHIN A FUEL BED 130

EXPERIMENTAL EQUIPMENT AND PROCEDURE 152

RESULTS AND DISCUSSION 184

ACKNOWLEDGMENTS 262

REFERENCES 263

NOMENCLATURE 278

APPENDIX A 1

APPENDIX B 16

APPENDIX C 21

APPENDIX D 45

APPENDIX E 64

APPENDIX F 84

APPENDIX G 92

APPENDIX H 112

LIST OF FIGURES

Figure Page

1 Different Modes of Operating a Fuel Bed 16

2 Common Incinerator Types 19

3 Deissler-Eian Correlation for the Thermal Conductivity of Packed Beds 29

4 Schematic of Apparatus Used by Kreisinger et al.. 41

5 Equipment Used by Kolodtsev 42

6 Gas Compositions and Temperature Profiles in an Overfeed Fuel Bed 43

7 Overall Reaction Rate Coefficient for the Combustion of a Pure Carbon Particle 45

8 Schematic of Nicholls' Apparatus for Underfeed Burning Tests 47

9 Underfeed Burning, High Temperature Coke: rate of ignition and rate of burning with rate of primary air and size of coke as variables 49

10 Rate of Ignition of Different Fuels, 1 - 1 1/2 in. size, 80°F air temperature 52

11 Temperature below Ignition Plane for Different Fuels 53

12 Gas Compositions and Temperature Profile within an Underfeed Bed 55

13 Underfeed Burning, Action through Fuel Bed Expressed as Weight of Fuel Products Carried per Pound of Dry Air Supplied, 3/4 - 1 in. Illinois Coal. 57

14 Volatile Matter and Ash Content of Fuel Bed Layers at Different Air Flow Rates 58

15 Representation of Mayers' Simplified Fuel Bed . . 62

16 Gas Analysis in a Fuel Bed 66

17 Temperature in Underfeed Fuel Bed 67

18 Mayers' Correlation of $\mu l/\dot{G}$ as a Function of the Underfire Air Flow Rate 70

Preceding page blank

LIST OF FIGURES
(Continued)

Figure Page

19 Comparison of Mass Transfer Correlation and Data of Kreisinger, Ovitz and Augustine for Oxygen Consumption in Fuel Beds 71

20 Mayers' Theoretical Relationship between Combustion and Ignition Rates and Air Flow Rates . . . 74

21 Theoretical Gas Composition Profiles Calculated Using the Three-Zone Theory of M. W. Thring . . . 78

22 Comparison between Theoretical and Experimental Relative Carbon Saturation Factors for Air-Coal Beds 79

23 CO_2 Reduction Rates in a Bed of 1 - 1 1/2 in. Coke Particles with Various Preheat Temperatures. 81

24 Gas Composition and Temperature in a Fuel Bed . . 83

25 Gas Composition within a Fuel Bed, Calculated by Silver. 87

26 Apparatus Used by the U.S. Bureau of Mines for Studying Combustion Characteristics of Refuse . . 91

27 Bed Thermocouple History, Incineration of Synthetic Feed with 50% Moisture 92

28 Travel of Evaporation and Burning Fronts and Total Weight Loss as Functions of Test Time in a Typical Bed of Synthetic Refuse Having a Moisture Content of 50% and a Bed Depth of 18 in. 93

29 Schematic of Test Incinerator Used by Essenhigh et al. 96

30 Comparison of Predicted and Experimental Profiles through the Solid Bed (normalized axes) . . 102

31 Sketch of Dimensionless Heat Generation and Heat Loss Curves 115

32 Variation of Gas Composition, Temperature and Reaction Rate in the Vicinity of Ignition Front . 119

33 Comparison of Vortmeyer's Ignition Theory with Experimental Data of P. Nicholls 123

LIST OF FIGURES

(Continued)

Figure		Page
34	Comparison of Ignition Theories with Experimental Data of P. Nicholls	127
35	Surface Temperature and Depth of Penetration of the Vaporization Plane in a Semi-Infinite Slab for Convective Heating of Surface by Gas at T_∞. .	133
36	Surface Temperature and Depth of Penetration of the Vaporization Plane in a Semi-Infinite Slab for Constant Heat Flux Condition	134
37	Drying Times for Spherical Particles of Different Moisture Content	138
38	Simplified Schematic of Processes Occurring in the Fuel Bed on a Traveling Grate	142
39	Equilibrium Constant of Common Fuel Bed Reactions	146
40	Equilibrium Gas Compositions at Various Assumed Fuel Bed Temperatures	149
41	Variation of Burning Rates with Temperature for Different Fuels	150
42	Diagrammatic Representation of Direction of Ignition Wave Propagation Relative to the Direction of Grate Travel and Underfire Air Flow . . .	155
43	Sketch of Experimental Incinerator	158
44	Experimental Incinerator, Gas Analysis Train and Peripheral Equipment	159
45	Interior of Fuel Bed Section with Thermocouple Probes Installed	160
46	Schematic of Overfire and Underfire Air Supply. .	164
47	Gas Sampling and Analysis Train	169
48	(a) Stack Gas Moisture Content Measurement; (b) Details of Sampling Probe	170
49	Instrument to Data Acquisition Connections . . .	173
50	Fuel Bed Temperatures (Run 10).	193

LIST OF FIGURES

(Continued)

Figure Page

51 Fuel Bed Temperature Profiles at Different Times throughout Run. Data from Run 18 197

52 Fuel Bed Temperatures (Run 5) 199

53 Fuel Bed Temperatures (Run 7) 200

54 Fuel Bed Temperatures (Run 9) 201

55 Fuel Bed Temperatures Below the Ignition Front for Different Fuel Types and Underfire Air Rates. 207

56 Ignition Wave Propagation (Run 10). 210

57 Ignition Wave Propagation (Runs 17 and 18). . . . 211

58 Burning Rates (Run 10). 214

59 Burning Rates (Run 17). 215

60 Burning Rates (Run 18). 216

61 Ignition and Burning Rates as a Function of Underfire Air Rate 218

62 Estimation of Fuel Bed Thickness and Accumulated Inert Layer (Run 17). 225

63 Estimation of Fuel Bed Thickness and Accumulated Inert Layer (Run 18). 226

64 Burning and Ignition Rates (Run 17) 228

65 Burning and Ignition Rates (Run 18) 229

66 Accumulated Carbon, Hydrogen and Oxygen Weight Loss of Fuel (Run 17) 234

67 Accumulated Carbon, Hydrogen and Oxygen Weight Loss of Fuel (Run 18) 235

68 Hydrogen/Oxygen and Carbon/Hydrogen Ratio of Fuel Burnt as a Function of Fraction of Combustible Consumed (Runs 17 and 18). 236

69 Gas Compositions from Fuel Bed Probe 1 (Run 17) . 238

70 Gas Compositions from Fuel Bed Probe 2 (Run 17) . 239

LIST OF FIGURES

(Continued)

Figure Page

71 Gas Compositions from Fuel Bed Probe 1 (Run 18) . 240

72 Gas Compositions from Fuel Bed Probe 2 (Run 18) . 241

73 Gas Compositions as a Function of Distance Above Ignition Front (Run 17) 242

74 Gas Compositions as a Function of Distance Above Ignition Front (Run 18) 243

75 Gas Compositions as a Function of Distance Above Ignition Front (Run 18) 244

76 Oxygen Concentration as a Function of Distance Below Ignition Front 246

77 Stack Gas Compositions (Run 17) 251

78 Stack Gas Compositions (Run 18) 252

List of Figures for Appendices

A.1 Cross Section and Plan of Fuel Bed Section . . . 2

A.2 (a) Schematic of Locating Probe; (b) Support Plate for Fuel Bed Section 5

A.3 Bearing Housing and Movable Base for Fuel Bed Section 7

A.4 Cross Section and Plan of Overfire Section . . . 9

A.5 Thermocouple and Gas Burner Locations in the Overfire Section 11

A.6 Sliding Refractory Shield 13

B.1 Estimate of Accumulative Heat Loss Through Fuel Bed Walls 19

C.1 Load Cell Circuit Diagram 21

C.2 Distribution of Forces in Weighing System 25

C.3 Schematic of Apparatus for Load Cell Calibration 27

D.1 Schematic of Orifice Plate Installation 45

F.1 Schematic of Incinerator Showing Material Inputs and Outputs 84

LIST OF FIGURES
(Continued)

Figure / Page

H.1 Fuel Bed Temperatures (Run 17). 144

H.2 Fuel Bed Temperature (Run 17) 145

H.3 Fuel Bed Heat Loss Probe Temperatures (Run 17). . 146

H.4 Overfire Refractory Temperatures (Run 17) 147

H.5 Overfire Shell, Inlet Air and Refractory Shield Temperatures (Run 17). 148

H.6 Fuel Bed Weight Loss (Run 17) 149

LIST OF TABLES

Table Page

1 Parameters of Design for Refuse Incinerators. . . 5

2 Air Requirements of Complete Combustion for Different Fuels on a Dry Basis. 6

3 Classification of Refuse Components 10

4 Composition and Ultimate Analysis of Refuse . . . 11

5 Analysis of a Composite Municipal Refuse 12

6 Projected Average Generated Refuse Composition, Heating Value and Quantity, 1970-2000 15

7 Comparison of Predicted and Experimental Values of Maximum Bed Temperatures and Combustion Zone Depth 101

8 Common Fuel Bed Reactions and Their Heats of Reaction 145

9 Relative Rates of Common Fuel Bed Reactions . . . 147

10 Synthetic Fuel Composition and Analysis 185

11 Summary of Experimental Conditions 186

12 Maximum Temperature Observed at Ignition Front with Varying Underfire Air Rates and Fuel Compositions 205

13 Material Balance Calculations (Run 17). 231

14 Material Balance Calculations (Run 18). 232

15 Check on Water Gas Shift Equilibrium within Fuel Bed (Run 17) 249

16 Check on Water Gas Shift Equilibrium within Fuel Bed (Run 18) 250

List of Tables for Appendices

C.I Specifications for BLH Precision C3P1 Load Cell . 24

C.II Load Cell Test 1: Diaphragm Disconnected; Weights Added. (a) Least squares fit to data; (b) Comparison of calculated and actual weights using least squares calibration curve; (c) Comparison of calculated and actual weights using calibration curve from load cell test alone . . . 30-32

LIST OF TABLES

(Continued)

Table Page

C.III Load Cell Test 2: Diaphragm Disconnected; Weights Subtracted. (a) Least squares fit to data; (b) Comparison of calculated and actual weights using least squares calibration curve; (c) Comparison of calculated and actual weights using calibration curve from load cell test alone. 33-38

C.IV Load Cell Test 3: Diaphragm Connected; Weights Subtracted. (a) Least squares fit to data; (b) Comparison of calculated and actual weights using least squares calibration curve; (c) Comparison of calculated and actual weights using calibration curve from load cell test alone. . . 39-44

D.I Factors for Orifice Plate Calculations 50

D.II Calculation of Flow Rates through Orifice Plate as a Function of Orifice Pressure Drop and Air Temperature and Static Upstream Pressure ($\beta = 0.4129$). 52

D.III Calculation of Flow Rates through Orifice Plate as a Function of Orifice Pressure Drop and Air Temperature and Static Upstream Pressure ($\beta = 0.6347$) 56

D.IV Compressibility Correction Factor (γ) for Orifice Plates 62

E.I Instrument Connections 67

H.I Instrument to Data Acquisition System Connections for Run 17 113

H.II Output Voltages for Run 17 115

H.III Listing of Temperatures, Gas Compositions and Fuel Bed Weight Loss for Run 17 118

CONCLUSIONS AND RECOMMENDATIONS

The major effort expended under the grant was in developing a versatile test incinerator. The conclusions enumerated below were derived from the preliminary twenty runs made on synthetic refuse mixtures. The conclusions are being tested and added to using shredded refuse in a follow-on grant. The study demonstrated that the major features of refuse burning on a travelling grate can be simulated in a batch incinerator in which time in a run corresponds to transit time of an element of refuse in the prototype. The extensive instrumentation available in the batch incinerator permit measurements to be made which would be extremely costly or impossible to duplicate in the field.

(a) The burning of refuse is not ignition limited over the air flow rates of interest. Burning rate increases with increasing air rate being limited only by the tendency to excessive channelling at high air flow-rates. When channelling occurred the fuel bed could be considered to be burning in two parallel modes, with the core behaving as a gasifier and the edges as a by-pass for underfire air.

(b) The major combustible gases emerging from the top of the fuel bed are carbon monoxide and hydrogen although significant amounts of methane are evolved within the bed near the ignition front. The gases evolved are relatively easy to burn and complete combustion was achieved above the bed in all cases by using overfire air jets with high momentum. The results suggest that the volume of the combustion chambers of incinerators may be reduced considerably if good overfire mixing is provided.

(c) The gases evolved by the bed satisfied the water-gas shift equilibrium. This permits the development of simple models for the burning rate.

(d) For refuse, the burning rate increases with factors that increase the CO/CO_2 ratio and H_2/H_2O ratios. Both ratios are increased by decreasing moisture content of the refuse and decreasing heat losses from the bed.

(e) Drying, pyrolysis, gasification and burnout reactions occurred contemporaneously within the bed. With the exception of very short periods at the beginning and end of a run the ratio of H_2O/CO_2 in the combustion products remained constant.

(f) During the initial and final periods oxygen from the underfire air broken through the bed indicating that the oxygen consumption was limited by the mass transfer rate to the burning bed. Underfire air rates should therefore be kept low at the ignition and discharge ends of a grate and should be raised as high as practicable once full ignition is achieved.

(g) The carbon dioxide concentration above the bed drops sharply as complete burn-out is approached. This observation might provide a means of monitoring bed burn-out.

(h) Material balances using stack gas composition provide good measures of burning rate and are a better indicator of short-range transients than the load-cell used to weigh the bed in the present system.

INTRODUCTION

Definition of the Solid Waste Problem and the Role of Incineration

The Nature of the Solid Waste Problem. Solid wastes are generated in five major areas: industrial, agricultural, commercial, household and institutional. The health and safety of the community in highly populated urban areas, where the disposal of the commercial, institutional and household waste is of major concern, have necessitated the development of municipal disposal systems. The general aversion to spending money on what is discarded as worthless and the apparent "out of sight, out of mind" philosophy of urban residents have made it evident to local governments that the first criteria for any waste disposal program would be low cost and ease of operation. Rising sanitary and environmental standards and increased public interest in the quality of the environment have added to these criteria of acceptability. Public concern over air and water pollution problems and the depletion of natural resources, among other considerations, has handed technology a serious challenge to improve the methods of solid waste disposal.

Three hundred billion pounds of solid wastes are collected by municipalities throughout the United States annually and the problem of how to dispose of them in an acceptable way has been receiving a surge of attention over the past few years. Considerable impetus and financial backing for this long-needed attack on the mounting problem of solid waste were provided by the Solid Waste Disposal Act, PL 89-272, of October 1965. Consequently, the solid waste management area has attracted the attention of a number of individuals and companies and several ways to deal with the old problem have been suggested. These have included high-temperature incineration, compaction followed by either landfill or offshore dumping, shredding followed by either burning or composting, as well as numerous ways of sorting out and classifying the reusable portions of solid wastes.

Traditionally, there have been three main methods of disposing of solid waste--open dumping, landfill and incineration, with dumping and landfill being the more widely practiced. The disposal of refuse by open dumping is an old concept. In the Middle Ages the streets of European cities were used as a dumping ground, and even in the Golden Age of ancient Greece "the narrow crooked streets of Athens were heaped with refuse" (1). The concept of modern sanitary landfill dates back to Biblical times, when wastes were disposed of by burial (2). Furnaces designed to burn refuse were not built until the end of the nineteenth century, with Nottingham, England, being credited as the birthplace of the first municipal incinerator in 1874 (3).

Of the refuse collected in the United States in 1967, 86 percent was disposed of at landfill sites, 8 percent was burned in municipal incinerators and 6 percent was disposed of in sanitary landfill operations (4). Much of the refuse disposed of in landfill sites other than by sanitary landfill is ultimately burned under poorly controlled open-burning conditions. The quantity of solid waste disposed of by each method has been traditionally determined primarily on the basis of cost. Concern, however, over the quality of the environment has generated a willingness to spend higher sums of money on solid waste disposal -- in particular on methods that involve recycling reusable portions of solid waste. Act PL 89-272 was instrumental in promoting recycling, as it specifically outlined that attention be given to the conservation of natural resources by reducing waste and unsalvageable material.

It is expected that the portion of solid waste that is recycled will increase over the next decade or so, as it becomes apparent that the "economic rents" associated with environmental decay and the depletion of natural resources are deemed to be greater than the costs of other disposal methods. Recycling of solid waste is not a new idea, but the low resale value of the salvageable items (rags, paper, glass, rubber and tin cans) made these operations economically unsuccessful except as sidelines for other methods of disposal. Conceptually, the recycling of all the reusable portions of solid waste is the most attractive method of disposal but attainment of this halcyon position will take the time required for research effort and public education and acceptance. It is unlikely that recycling will be considered competitive with conventional methods of disposal for at least a decade, and until it is practiced on a wide basis these methods will need to be used and improved to meet the challenge of legislated environmental standards. Even when recycling has become a major method of disposal, there will be significant quantities of waste that will still be unseparable, unusable, or which will require costly pretreatment for recycling, and these will have to be disposed of by the other conventional methods. For example, of three tons of refuse collected from three locations in San Francisco,only between 29.2 and 32.2 percent was recyclable (5).

Of the conventional methods presently employed, sanitary landfill has become more popular over the past years in response to public indignation over poor landfill and dumping practices which produce unsightly, odorous areas often infested with rats and vermin. The method of disposal is not without problems -- specifically, accidental explosions, pollution of well water, and the increasing cost of the earth cover required. The anaerobic decomposition of the organic portions of the waste produce, among other gases, methane, whose concentration may build up in a confined enclosure to produce an explosive mixture. Anderson and Colliman (6) report that "dangerous explosions have occurred or persons have been seriously burned as a result of accidental ignition of methane gas which had accumulated near old landfills or refuse dumps." These problems detract from the most attractive aspect of sanitary landfill, which is the eventual use of previously unusable land after it has been filled in. In many major metropolitan areas, available landfill and dumping sites are becoming scarce and this dilemma has prompted the shipping of metropolitan waste to outlying communities. This practice, in turn, has come under sharp criticism from communities that understandably resent having to act as a dumping ground for others' problems. The pressure for more landfill sites will continue to mount. Many metropolitan areas are experiencing rapid growth and the per capita daily waste in the U. S., a function of the rising standard of living, is steadily increasing. Both of these facts suggest that disposal practices requiring large land acreages and costly earth cover may become uneconomical and impractical. The only practical alternative in these areas may be incineration.

The Role of Incineration in Solid Waste Management. Incineration at present is inefficiently practiced, as indicated by Vaughan's (7) analysis of a national solid wastes survey which revealed that of the 300 incinerators in the United States, 75 percent were inadequate, as far as air pollution control and effective residue burnout were concerned. Such statistics are not surprising, since 70 to 75 percent of the incinerators in the United States were built before 1960, with some dating back as far as the 1940's. Poor incinerator operation has caused the public to regard an incinerator as a bad neighbor and, although emissions from the burning of all solid refuse contribute less than 10 percent of the 11 million tons of particulates emitted to the atmosphere annually, they are the frequent cause of local pollution complaints by citizens (8). In addition to the air pollution problem, the poor control of municipal units, which results in incomplete combustion, yields neither full volume reduction of the refuse nor an inert residue. Potentially, incineration should offer the most significant volume reduction of all solid waste disposal methods, as according to a U. S. Bureau of Mines report (9) poor incineration will reduce the volume of refuse by 75 percent, while efficient burning can reduce it by 95 percent. The residue from an incinerator eventually must be landfilled but, if it has been rendered completely inert by good incinerator operation, none of the landfill problems mentioned above should occur, and the life of present landfill sites could be dramatically extended. Ultimately incinerator residue may have a utility other than landfill, especially its ferrous content (10), but investigations into this possibility have only just started; however, problems have been encountered in the case of tin cans with the alloying of the protective metal coating with the ferrous body at the high temperatures encountered in a fuel bed.

Inefficient incinerator design and operation mitigates against incinerators being a suitable solution for the urban solid waste problem. However, good incinerator design and the development and implementation of reliable control instruments and procedures present formidable problems as the processes occurring in an incinerator are very complex, as exemplified by the varied nature of the material being burnt. It is not surprising, therefore, to find that designers have had to rely on experience and empirical relationships rather than quantitative descriptions of the chemical kinetics and heat,mass and momentum transfer processes.

Typically, designs are based on gross overall heat and material balances, rule-of-thumb guidelines on the achievable burning rates per unit area of grate surface with different refuse types, and on allowable combustion intensities in the overfire volume (Table 1). Of these three requirements the most difficult to estimate has been the achievable burning rate. The heat and mass balances are straightforward to calculate, particularly as the air requirements for most solid fuels are remarkably uniform when expressed on a basis of energy liberated (see Table 2). The achievable burning rates per unit of grate are estimated from guidelines such as those provided by Table 1 or from the rule of thumb that the heat release rate within the fuel bed should be about 300,000 Btu hr^{-1} ft^{-2} of grate area. For a typical as-fired heating value for refuse (5000 Btu lb^{-1}), the burning rate for the latter criterion would be 60 lb hr^{-1} ft^{-2} of grate area which agrees with the Incinerator Institute of America's guideline of 60-65 lb hr^{-1} ft^{-2} for a Class V incinerator and the values given in Table 1. The establishment of these guidelines has ignored the fundamental problem in many engineering operations, namely the calculation of the rate of the process, and has perhaps established a precedent of perpetuating inefficient incinerator designs.

The maximum allowable heat release rate within a fuel bed should be determined from consideration of the maximum bed temperature that would prevail and therefore must take heat losses from the bed into account; temperatures that are too high cause difficulties with clinkering and problems with grates clogged with molten glass and aluminum. There are indications that successful operation has been achieved at

TABLE 1:

Parameters of Design for Refuse Incinerators (11)

	Type of Refuse*	Grate Loadings in Lbs. of Refuse per Hour of Operation per square foot of Grate Area	Volume in Cubic Feet per Ton of Refuse per 24 Hours	
			Furnace (Primary) Chamber	Combustion (Secondary) Chamber
Range of Values	M	58 to 109	8.5 to 25.0	12.1 to 28.0
	R	50 to 72	13.4 to 14.5	26.6 to 31.8
	C	54 to 98	9.9 to 13.8	17.2 to 28.3
Average Values	M	77	12.7	18.5
	R	58	13.6	29.9
	C	77	11.5	21.3

*M - Mixed refuse made up of garbage, rubbish, and noncombustibles.
R - Refuse comprised of burnable rubbish only.
C - Refuse containing combustibles only, such as garbage and burnable rubbish.

TABLE 2:

Air Requirements of Complete Combustion For Different Fuels on a Dry Basis (12, 13)

Fuel	Atmospheric Air Required (lb./10,000 B.t.u.)	
	Range	Avg.
Anthracite:		
New Mexico	.....	7.83
Colorado	.....	7.85
Pennsylvania	7.81-7.93	6.87
SemiAnthracite	7.68-7.82	7.74
Bituminous coal:		
Low-volatile	7.62-7.76	7.69
High-volatile A	7.51-7.73	7.63
High-volatile B	7.56-7.73	7.66
High-volatile C	7.54-7.67	7.60
Subbituminous coal	7.56-7.57	7.56
Lignite:		
North Dakota	.....	7.47
Texas	.....	7.52
Coke:		
High-temperature	.....	7.96
Low-temperature	.....	7.63
Beehive	.....	8.05
By-product	.....	8.01
Gasworks coke	8.02-8.10	8.06
Petroleum coke	.....	7.73
Pitch coke	.....	8.13
Wood:		
Softwoods	7.02-7.22	7.11
Hardwoods	7.09-7.28	7.15
Bagasse	6.25-6.99	6.59
Petroleum oils:		
Gasoline (60°A.P.I.)	.....	7.46
Kerosene (45° A.P.I.)	.....	7.42
Gas oil (30°A.P.I.)	.....	7.45
Fuel oil (15°A.P.I.)	.....	7.58
Gaseous fuels:		
Natural gas	7.32-7.41	7.37
Refinery and oil gas	6.52-7.38	7.44
Blast-furnace gas	5.73-6.27	5.82
Coke-oven gas	6.66-7.02	6.80
Miscellaneous:		
Cellulose	.....	6.80
Glucose	.....	6.90
Glycol dipalmitate	.....	7.40
Methyl alcohol	.....	6.70

heat release rates up to three times the suggested maximum value of 300,000 Btu hr^{-1} ft^{-2}, hinting at the tempting prospect of reduced investment cost per ton of refuse processed.

A similar situation to that encountered when selecting grate sizes is found in the overfire region, where few design criteria are available. The only specifications given are for furnace volumes based on guidelines such as those given in Table 1, or on the rule of thumb that the volumetric heat release should be around 20,000 Btu hr^{-1} ft^{-2}, and on allowable gas velocities at different points in the incinerator. The value of the maximum combustion intensity is given without any regard for the amount of combustible that has to be burnt in the overfire region. No guidelines are given as to the desirable ratio of primary air introduced through the fuel bed to secondary air injected into the overfire region. There is general agreement in the literature (14, 15) that the overfire air must be supplied with sufficient momentum to provide adequate mixing with the combustible gases. There are, however, no reliable methods presently available for determining how this should be accomplished.

Designs based on these methods may have been satisfactory in the past, but, with the effects of the new legislation concerning acceptable levels of gaseous and particulate emissions as well as ash and residue quality beginning to be felt, increasing numbers of practitioners are becoming interested in developing more fundamental ways of designing their incinerators. For example, Hollender (16) has pointed out the need for indicators for determining the probable burning characteristics of different fuels, and the selection of the size, number and location of overfire jet systems and the ratios of primary and secondary air. In addition, the long-term trends in refuse quality as predicted by Niessen and Alsobrook (17) and Niessen and Chansky (18) have suggested that the volatile content of refuse, which is a measure of quantity of overfire air that is required to complete the combustion of the volatile products distilling from the fuel bed, will increase over the years (Table 6). The projected increase of this component in refuse is also expected to require that more significance be placed on the successful operation of the overfire air jets. This will require a more sophisticated approach to the design of these jets, along the lines taken by Niessen et al. (19).

The problems of operating an incinerator effectively are enormous when one realizes the tremendous variation in feed material that is handled from day to day. The variation in the feedstock quality of an incinerator is orders of magnitude greater than that in a pulverized coal fired utility boiler (or its chain grate stoker predecessor), yet incinerator controls are barely existent compared to the sophisticated controls of a modern utility boiler. A few of the many operating problems connected with just the fuel bed combustion are covered below.

Discussions with incinerator operators have shown the need for operational guidelines for times when the incoming refuse has a higher than normal moisture content; however, a recent paper (20) in this area could do no better than summarize the opinion of a number of operators on what operational adjustments they made when confronted with this type of situation. Very little is understood about the burning behavior of shredded refuse on a grate system; an attempt to burn shredded refuse in New York City's East Side incinerator met with complete failure when the fire was quenched (21), due primarily to the difficulty in supplying underfire air through the shredded refuse. There are no easy and quick tests to determine if complete combustion has been achieved prior to dumping the ash in the quench tank and it is not an uncommon sight to see actively burning refuse being discharged to the quench tank.

The operational problems are further heightened by the generally low level of technical training of incinerator operators compared to their counterparts in utility boilers. The rationale behind decisions to run incinerators on what appears to be a less than professional basis seems ill founded as modern incinerators are fairly capital intensive. Koenig (22) reported that the cost for a basic incinerator, without extensive pollution control and heat recovery features, is approximately $12 per ton per year capacity, although the costs vary widely. On the basis of capital costs, therefore, a basic incinerator ranks well down among the spectrum of chemical and process plants. For example, a sulfuric acid plant costs roughly $26 per ton per year capacity while a butadiene plant costs as much as $1500 per ton per year capacity. However, a modern unit with the presently required advanced pollution control equipment, waste heat recovery and aesthetic exterior would result in an appreciably higher unit investment of around $30-40 per ton per day, depending on size.

Project Objectives

The increasing investment costs for suitable incinerators, coupled with the challenges posed by more stringent pollution codes, the difficulty of finding skilled labor, and the financial pressures on municipalities, bring out the basic need to improve the designs and to develop inexpensive and reliable methods of controlling them. These improvements will only be forthcoming as a result of extensive research on a laboratory scale and careful experimentation on full-scale units.

Detailed testing in large-scale units is both difficult and costly and it is therefore desirable to perform the basic research on small-scale units which retain some of the important features of the prototype. This approach was used in the studies of solid fuel-fired stokers where the definitive experiments on the effect of fuel size and quality and underfire air rate and preheat were carried out on small-scale units by Kreisinger, Ovitz, and Augustine (23) and Nicholls (24). Studies of a similar nature on small or pilot-scale incinerators include the pioneering work at Los Angeles (25) and the studies by the U. S. Bureau of Mines (26, 27, 28), the Public Health Service (29), and Pennsylvania State University (30-47). The incinerator studies have provided some qualitative information on the physical and chemical processes occurring in refuse beds during drying, pyrolysis and combustion. Incinerator research has yet to produce an adequate quantitative description of these processes, and consequently the major thrust of this project was directed towards developing a better understanding of combustion processes in refuse beds. A prime objective was the design of a test incinerator with sufficient instrumentation to obtain the data required to unravel the processes occurring within the bed. The experimental study was limited to a synthetic refuse which could be easily characterized but which contained many of the traits of refuse.

Background Information on Incineration and Fuel Bed Processes

The Nature of Solid Waste. Table 3 gives the generally accepted breakdown of the constituents of refuse. The domestic and commercial refuse which comprises the major portion of the refuse burnt in municipal incinerators is composed primarily of paper and paper products with quantities of garbage, grass clippings, plastic, glass, metal and various other materials. A number of analyses of refuse components have been made in the past few years (17, 18, 48, 49) and although, not surprisingly, each study differs slightly in its findings. The data of Kaiser (49) provide a satisfactory basis from which to work. Table 4 presents Kaiser's data for a composite municipal refuse. The composite was selected from the proportions of the ingredients that were reported in the literature (51, 52) and obtained from private sources. The moisture content was adjusted to a total of 20 percent by the addition of water to bring the moisture content into the range experienced by incinerators.

A proximate and ultimate analysis of the composite is shown in Table 5, from which it is possible to calculate the theoretical combustion air requirements, assuming all the sulfur content of the fuel is converted to SO_2 and that none of the metal is oxidized, using the relationship:

TABLE 3:

Classification of Refuse Components (50)

Kind		Composition	Sources
Refuse	Garbage	Wastes from preparation, cooking, and serving of food; market wastes; wastes from handling, storage, and sale of produce	Households, restaurants, institutions, stores, markets
	Rubbish	Combustible: paper, cartons, boxes, barrels, wood, excelsior, tree branches, yard trimmings, wood furniture, bedding, dunnage	
		Noncombustible: metals, tin cans, metal furniture, dirt, glass, crockery, minerals	
	Ashes	Residue from fires used for cooking and heating and from on-site incineration	
	Street Refuse	Sweepings, dirt, leaves, catch basin dirt, contents of litter receptacles	Streets, sidewalks, alleys, vacant lots
	Dead Animals	Cats, dogs, horses, cows	
	Abandoned Vehicles	Unwanted cars and trucks left on public property	
	Industrial Wastes	Food processing wastes, boiler house cinders, lumber scraps, metal scraps, shavings	Factories, power plants
	Demolition Wastes	Lumber, pipes, brick, masonry, and other construction materials from razed buildings and other structures	Demolition sites to be used for new buildings, renewal projects, expressways
	Construction Wastes	Scrap lumber, pipe, other construction materials	New construction, remodeling
	Special Wastes	Hazardous solids and liquids: explosives, pathological wastes, radioactive materials	Households, hotels, hospitals, institutions, stores, industry
	Sewage Treatment Residue	Solids from coarse screening and from grit chambers; septic tank sludge	Sewage treatment plants; septic tanks

TABLE 4:

Composition and Ultimate Analysis of Refuse (49)

(Dry Basis in Percent by Weight)

Refuse Component	Per cent	Carbon	Hydrogen	Oxygen	Nitrogen	Sulfur	Ash
Corrug. paper boxes	23.38	43.73	5.70	44.93	0.09	0.21	5.34
Newspaper	9.40	49.14	6.10	41.92	0.05	0.16	1.52
Magazine paper	6.80	32.91	4.95	38.55	0.07	0.09	23.43
Brown paper	5.57	44.90	6.08	47.84	0.00	0.11	1.07
Mail	2.75	37.87	5.41	42.74	0.17	0.09	13.72
Paper food cartons	2.06	44.74	6.10	41.92	0.15	0.16	6.93
Tissue paper	1.98	-	-	-	-	-	-
Plastic coated paper	0.76	45.30	6.17	45.50	0.18	0.08	2.77
Wax cartons	0.76	59.18	9.25	30.13	0.12	0.10	1.22
Vegetable food wastes	2.29	49.06	6.62	37.55	1.68	0.20	4.89
Citrus rinds and seeds	1.53	47.96	5.68	41.67	1.11	0.12	3.46
Meat scraps, cooked	2.29	59.59	9.47	24.65	1.02	0.19	5.08
Fried fats	2.29	73.14	11.54	14.82	0.43	0.09	0.00
Wood	2.29	53.30	6.66	35.17	1.49	0.20	3.18
Ripe tree leaves	2.29	52.15	6.11	30.34	6.99	0.16	4.25
Flower garden plants	1.53	46.65	6.61	40.18	1.21	0.26	5.09
Lawn grass, green	1.53	48.18	5.96	36.43	4.46	0.42	6.55
Evergreens	1.53	48.51	6.54	40.44	1.71	0.19	2.61
Plastics	0.76	-	-	-	-	-	-
Rags	0.76	-	-	-	-	-	-
Leather goods	0.38	42.01	5.32	22.83	5.98	1.00	22.86
Rubber composition	0.38	53.22	7.09	7.76	0.50	1.34	30.09
Paints and oils	0.76	-	-	-	-	-	-
Vacuum cleaner catch	0.76	35.69	4.73	20.08	6.26	1.15	32.09
Dirt	1.53	-	-	-	-	-	-
Metals	6.85	-	-	-	-	-	-
Glass, ceramics ash	7.73	-	-	-	-	-	-
Adjusted moisture	9.05	-	-	-	-	-	-
TOTAL	100.00						

TABLE 5:

Analysis of a Composite Municipal Refuse (49)

Proximate Analysis (in percent by weight)

Moisture	20.00
Volatile matter	52.70
Fixed carbon	7.30
Ash and metal	20.00
Total	100.00

Ultimate Analysis (in percent by weight)

	Wet Basis	Dry Basis	Dry Ash and Inert Free Basis
Moisture	20.00	-	-
Carbon	29.83	37.29	49.72
Hydrogen	3.99	4.99	6.65
Oxygen	25.69	32.11	42.81
Nitrogen	0.37	0.46	0.61
Sulfur	0.12	0.15	0.20
Ash & Metal	20.00	25.00	-
Total	100.00	100.00	100.00

$$W_a = 11.5C + 34.5(H - \frac{O}{8}) + 4.32S \qquad (1)$$

where W_a is the pounds of air per pound of fuel required for complete combustion, and C, H, and O are the weight fractions of carbon, hydrogen and oxygen in the fuel respectively. For the composite, the air requirements for complete combustion are approximately 3.71 pounds of air per pound of refuse (50.5 cubic feet at 70°F and 1 atmosphere).

The higher heating value of refuse must be determined experimentally or estimated from the heating values of its individual components. For Kaiser's composite the higher heating value is 8766 Btu/lb, on a dry ash-free basis excluding the small exothermic effect of partial oxidation of the metal content. On the basis of this heating value, 7.0 pounds of theoretical air are required per 10,000 Btu's liberated during combustion, a figure which compares well with the data presented in Table 2.

Although the composition of refuse is complex and will obviously vary with the season of the year (17), locality (17, 18) and from day to day, as a rough working approximation for theoretical calculations, the combustible portion of refuse can be assumed, on a dry basis, to have the composition of cellulose ($C_6H_{10}O_5$). On a weight basis the composition of cellulose is carbon 44.4 percent, oxygen 49.4 percent, and hydrogen 6.2 percent, and requires 5.12 pounds of air for complete combustion, or 6.8 pounds per 10,000 Btu's liberated. Using the composition of cellulose as the average composition of refuse has one disadvantage in that, unlike refuse, it contains no net hydrogen. Net hydrogen is the quantity of hydrogen in the fuel that cannot be reacted to water using the oxygen content of the fuel.

Kaiser's data suggest that a suitable synthetic refuse, especially for experimental purposes, can be made out of a mixture of wood blocks, water, and inerts. An ultimate analysis of spruce, which is a typical soft wood, shows a content of 45.5 percent oxygen, 6.5 percent hydrogen, and 48.1 percent carbon. This analysis as can be seen from Table 5 is very close to the dry ash and inert free composition of Kaiser's composite refuse. The higher heating value of this wood (approximately 9300 Btu/lb) and the theoretical air requirements per 10,000 Btu's liberated (7.1 lb) are close to that of Kaiser's composite refuse.

The other problem in the simulation of refuse for experimental purposes is to select the required size of the wood blocks so that their thermal thickness is close to that of refuse and to introduce the moisture and inert content in a way similar to that experienced in practice. The inert may be conveniently introduced by adding tin cans of suitable dimensions, while the moisture content can be built up to the desired level by soaking some of the wood blocks in water for a period of a few days (moisture levels of around 60 percent can be achieved this way). The major difficulty associated with introducing the water content in this manner is that the drying behavior of the wet wood blocks may be somewhat different from that of many constituents of refuse, for example the grass, leaves and vegetable matter.

The final consideration in the characterization of solid refuse is to examine its expected trend in composition over the next decade or so. Niessen and Alsobrook (17) and Niessen and Chansky (18) have made extensive studies of the composition of refuse from various cities throughout the United States and made some projections of an average refuse composition from 1970 through 2000 which are shown in Table 6. These results do not provide for the effect of recycle on composition and as such probably only provide a good estimate of incinerator feed up to about 1980. Their projections show that moisture content is expected to decrease while volatile carbon and plastic content will increase. The decrease in moisture content coupled with the increase in plastic content will significantly raise the higher heating value of the refuse; this will adversely affect the capacity of incinerators because of the greater flue gas volume to be handled. The projected increase in the fuel volatile content is expected to require that more emphasis be placed on the successful operation of the overfire air jets. This point has been discussed in the previous section.

Types of Fuel Beds. There are relatively few different principles embodied in the numerous different ways in which solid fuel can be burnt in a fuel bed. The purpose of this section is to review the three basic types of fuel beds (fluidized bed combustion is excluded from consideration) and to indicate the principles they embody. This section will also serve to introduce a few of the common terms used in discussing fuel beds. Nicholls (24) made the first attempt to clarify the principles involved in the different types of fuel beds and this discussion is based on his paper.

The type of fuel bed is fixed by the relative direction of the flow of fuel and air. The two major modes of firing a fuel bed are termed overfeed and underfeed. A fuel bed can be considered to be operating in the overfeed mode if the fuel and combustion air flow through the bed in opposite senses. In this arrangement the combustion gases are used to preheat and ignite the virgin fuel; a possible arrangement of this is shown in Figure 1(a). The underfeed mode occurs when the fuel and combustion air flow through the bed in the same sense and, in this case, the virgin fuel is ignited only by radiation and

TABLE 6:

Projected Average Generated Refuse Composition

Heating Value and Quantity, 1970-2000 (17)

	1970	1975	1980	1990	2000
Composition					
(weight %, as discarded)					
Paper	37.4	39.2	40.1	43.4	48.0
Yard Wastes	13.9	13.3	12.9	12.3	11.9
Food Wastes	20.0	17.8	16.1	14.0	12.1
Glass	9.0	9.9	10.2	9.5	8.1
Metal	8.4	8.6	8.9	8.6	7.1
Wood	3.1	2.7	2.4	2.0	1.6
Textiles	2.2	2.3	2.3	2.7	3.1
Leather and Rubber	1.2	1.2	1.2	1.2	1.3
Plastics	1.4	2.1	3.0	3.9	4.7
Miscellaneous	3.4	3.0	2.7	2.4	2.1
(weight %, as burned)					
Moisture	25.1	23.3	22.0	20.5	19.9
Volatile Carbon	19.6	20.1	20.6	21.8	23.4
Total Ash	22.7	23.4	23.9	22.8	20.1
Ash (excluding glass and metal)	6.5	6.2	6.1	6.0	6.0

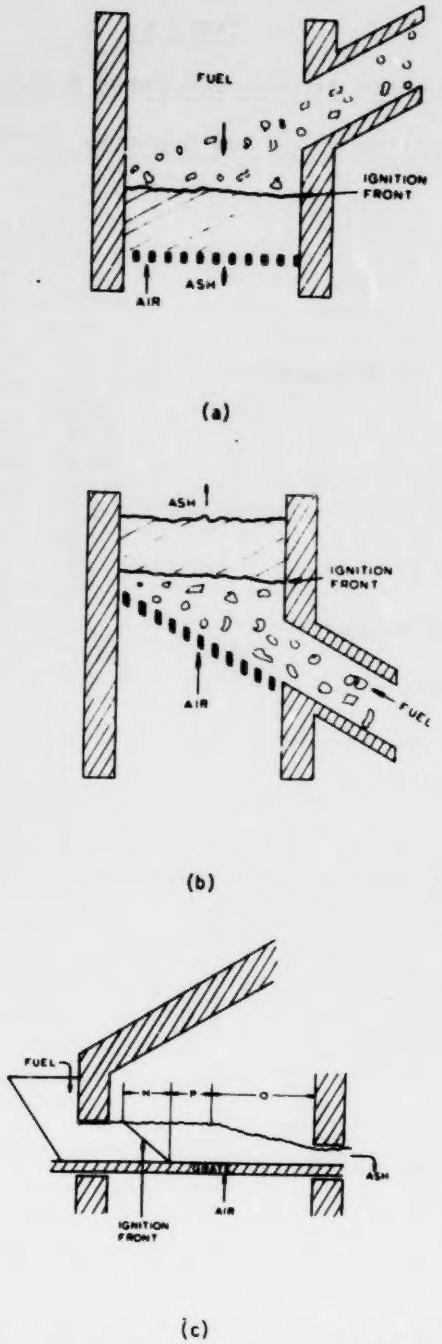
FUEL
IGNITION FRONT
AIR
ASH
(a)
ASH
IGNITION FRONT
AIR
FUEL
(b)
FUEL
H
P
O
GRATE
ASH
IGNITION FRONT
AIR
(c)

Fig. 1. Different Modes of Operating a Fuel Bed: (a) Overfeed; (b) Underfeed; (c) Traveling Grate

conduction from the combustion section located just behind the ignition plane. In this mode of combustion the underfire air (air supplied through the fuel bed and sometimes called primary air) tends to hinder ignition as it convectively cools the virgin fuel ahead of the ignition plane. Figure 1(b) shows what Nicholls (24) termed the "unrestricted-ignition underfeed principle," where the ignition rate is free to be fixed by the fuel type and size, and the underfire air rate, and degree of preheat. For this condition to exist the fuel feed rate must be equal to or greater than the ignition rate. If the fuel feed rate were lower than the ignition rate, the ignition plane would eventually reach the grate; at this point ignition would be restricted and the burning behavior of the bed would change to reflect this.

It is perhaps confusing to talk about overfeed and underfeed burning, as the major difference in the burning rate characteristics between the two types of fuel bed lies in the methods of igniting the fresh fuel. The rate of ignition can obviously provide a limiting step in the overall rate of combustion. In the overfeed bed, because the fuel is being preheated by the combustion gases, ignition does not limit the burning rate and essentially burning rates can be increased by increasing the underfire air flows up to the point where the fuel is blown out of the bed. In the underfeed bed (unrestricted ignition) the maximum rate of burning is fixed for each underfire air rate by the rate of ignition.

There are other differences in the two types of bed in addition to the burning rate characteristics. In the overfeed bed the drying and pyrolysis of the fuel take place in a region where the underfire air has little or no oxygen content and primarily consists of carbon monoxide and carbon dioxide. Under these circumstances it can be expected that fairly high quantities of pyrolysis products will be evolved from the top of the fuel bed. In the underfeed system the drying and pyrolysis of the fuel take place in a region where the underfire air is still rich in oxygen which will partially react with the pyrolysis products and any char formed; the reaction products and any remaining pyrolysis products can react with the char forming the rest of the fuel bed as they flow upward through it.

The final type of fuel bed to be discussed here is that which occurs on a traveling-grate stoker and is shown in Figure 1(c). Nicholls (24) has suggested that in this type of fuel bed length H is burning on the unrestricted ignition underfeed principle and length O on the overfeed principle since the ignition plane has reached the grate at this point and there are no further ignition constraints on burning. The burning rate in this section of the grate may well follow the type of behavior experienced in an overfeed bed, but there are obvious differences in, for example, location of pyrolysis regimes, ash build-up and volatile generation between the fuel bed shown in Figure 1(a) and the length O of Figure 1(c). Nicholls (24) also suggested that there is a length, P, located between lengths H and O, in a change-over state where the burning adjusts itself because of the cessation of ignition.

The last term which will be introduced here is "overfire air", or what is sometimes called secondary air. This is air introduced above the fuel bed in order to complete the combustion of gasification and pyrolysis products issuing from the fuel bed. These gases can be quite rich in carbon monoxide and hydrogen as well as in pyrolysis products, and adequate mixing of the overfire air with these gases at high enough temperatures is necessary to achieve complete burn-out in the residence time available in the furnace. In addition to the task of providing the air required to complete combustion, cooling air may also be brought in through the overfire air jets; this is the accepted practice in refractory lined furnaces where it is necessary to keep wall temperatures down to reasonable levels.

Description of Incinerator Types. Municipal incinerators operate on both batch and continuous bases and the average capacity of the 254 incinerators operating in the United States in 1966 was 300 tons per day (53). The larger units operate on a continuous basis and many of them are of the traveling-grate or reciprocating-grate variety. Refractory lined furnaces are the most commonly used for refuse incineration in the United States partly because of their low construction cost and the fact that licensed personnel are not required for operation, which results in a savings in labor costs. These units are limited to a maximum size of around 300 tons per day, as at this size operating and maintenance costs offset capital costs (54). Large quantities of excess air are required in these units to keep the walls from overheating; all this air must pass through the air pollution devices, which increases the cost of this equipment. A typical refractory lined incinerator is shown in Figure 2(a).

The large excess air problem can be obviated with the use of water-walled furnaces, where water-filled tubes are used to form the furnace walls. In these furnaces the excess air can be kept at the minimum required for complete combustion in the residence time available, as the extra air is not required for cooling purposes. This type of construction has been used widely in Europe, where the cost of fuel has prompted utilization of the waste heat to produce steam. Although the use of water walls reduces the cost of the pollution control equipment, the labor charges for operating these units are higher, as licensed power plant operators are needed. Problems of corrosion of the steel tubes by acid fumes and condensate and

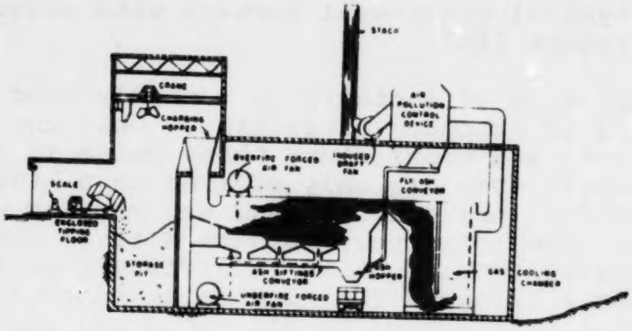
STACK
CRANE
CHARGING HOPPER
AIR POLLUTION CONTROL DEVICE
OVERFIRE FORCED AIR FAN
INDUCED DRAFT FAN
SCALE
FLY ASH CONVEYOR
ENCLOSED TIPPING FLOOR
STORAGE PIT
ASH SIFTINGS CONVEYOR
ASH HOPPER
GAS
COOLING CHAMBER
UNDERFIRE FORCED AIR FAN

TYPICAL REFRACTORY LINED INCINERATOR

(a)

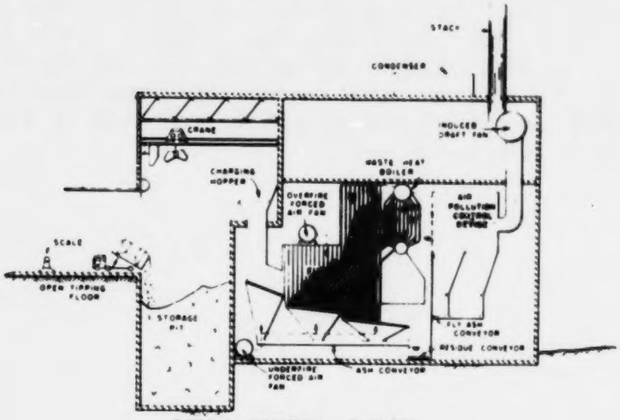
STACK
CONDENSER
CRANE
INDUCED DRAFT FAN
WASTE HEAT BOILER
CHARGING HOPPER
OVERFIRE FORCED AIR FAN
AIR POLLUTION CONTROL DEVICE
SCALE
OPEN TIPPING FLOOR
STORAGE PIT
FLY ASH CONVEYOR
RESIDUE CONVEYOR
UNDERFIRE FORCED AIR FAN
ASH CONVEYOR

TYPICAL WATERWALL FURNACE
WITH WASTE HEAT BOILER

(b)

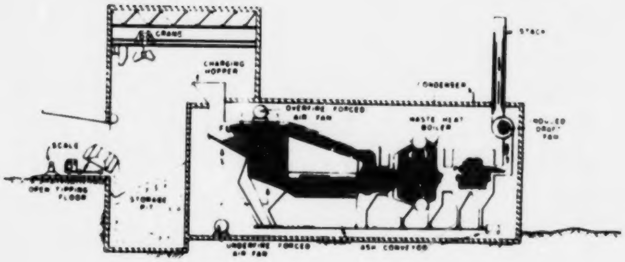
CRANE
STACK
CHARGING HOPPER
CONDENSER
OVERFIRE FORCED AIR FAN
WASTE HEAT BOILER
INDUCED DRAFT FAN
SCALE
OPEN TIPPING FLOOR
STORAGE PIT
UNDERFIRE FORCED AIR FAN
ASH CONVEYOR

TYPICAL ROTARY KILN INCINERATOR
WITH WASTE HEAT BOILER

(c)

Fig. **2.** Common Incinerator Types: (a) Typical Refractory Lined Incinerator; (b) Typical Waterwall Incinerator with Waste Heat Boiler; (c) Typical Rotary Kiln Incinerator with Waste Heat Boiler erosion by fly-ash are other factors which have to be considered. A typical water-wall furnace with waste heat boiler is shown in Figure 2(b).

The only other type of incinerator commonly used is the rotary kiln, which is of European extraction. Only one company is licensed to sell and manufacture these units in the United States; presently they are only offered in a limited size range, around 250 tons per day, and are coupled with a refractory furnace. The refractory furnace acts as the drying and initial combustion stage, while the rotary kiln is used for the final burnout stage. The slow rotary action provides bed agitation which is supposed to aid rapid and complete combustion. A typical rotary kiln is shown in Figure 2(c).

The three incinerator types discussed above are the only ones currently being used in the United States. There are a number of companies that, in the last few years, have developed their own units, the most notable of which is the high temperature incinerator (55). These and other designs are still in the development and demonstration stage and are a few years away from being in widespread use.

SURVEY OF EXPERIMENTAL AND THEORETICAL TREATMENT OF FUEL BED COMBUSTION

Outline of Material Covered

This survey will start with the development of the general equations describing the processes of heat and mass transfer within a fuel bed, along with a number of the simplifications typically used by various authors to permit these equations to be cast into tractable forms. This material will serve as a background to the discussion of a number of the theoretical treatments of fuel bed combustion that have appeared in the literature. In this section, some points will be raised on the estimation of the suitable physical properties of fuel beds necessary for use in any mathematical model. The large degree of uncertainty in the physical properties provides a rationale for the simplifications to these equations. Following this, a short survey of the more important experimental work in coal combustion will be given, which in turn will be followed by a survey of the most interesting theoretical treatments of combustion and ignition within coal beds. Both the theoretical and experimental studies on coal beds, which can be considered to be idealized refuse beds, provide some valuable insights into the behavior of fuel beds despite the fact that they lack the heterogeneity and complexity of a refuse bed.

The experimental and theoretical work on simulated refuse burning that has been reported in the literature will then be covered and the section will close with a discussion of ignition rates and combustion stability in fuel beds.

The literature in the field of coke and coal combustion, especially on the experimental side, is voluminous but somewhat dated. The survey presented here makes no pretense to be a complete literature survey and covers only the areas that the author finds pertinent. Likewise, there is a great deal published in the literature concerning experimental investigations on large-scale incinerators; no attempt is made here to cover this area, as it is not directly applicable to this work. Hence, the survey will cover only those studies that closely parallel and complement the work presented here.

To previse the reader of some of the results of this survey, there are no theories that can adequately predict the rate of ignition within a fuel bed and how it is affected by underfire air rate and fuel particle size and type. Similarly, the survey shows that there are no reliable a priori methods for calculating gas compositions and temperature profiles within fuel beds. These comments apply to the simple case of a coal bed as well as to a refuse bed.

The calculation of burning rates for deep coal beds under most conditions (except where ignition limited) can be done with reasonable accuracy since the compositions of the gases issuing from the top of the bed are not markedly altered by changes in particle size and underfire air rate and the gas compositions closely approach their equilibrium values at the prevailing bed temperature. The burning rate for these cases is thus found to vary almost linearly with the air flow rate. There are, at present, no theories that can be used to predict the burning rate of a refuse bed, given the physical and chemical characteristics of the fuel and the underfire air rate. There are therefore no methods currently available for testing the validity of the empirical guidelines discussed on pages 3 - 8. It is possible, however, to put an approximate upper bound on achievable burning rates under non ignition controlled conditions.

Mathematical Treatment of Fuel Bed Combustion

Development of General Equations. A general mathematical treatment of a fuel bed would involve material balances on the solid and gas phases for each reacting component, a continuity equation, an energy balance, and a set of appropriate boundary conditions. The solution to this set of equations would permit the prediction of temperatures, pressures, velocities, and composition changes within the bed as a function of time and position. This general problem has not yet been attempted and cannot be justified with the present state of knowledge of the physical properties of fuel beds and the various chemical processes taking place. Consequently, simplifications have to be made in order to obtain tractable models. The simplifications used in many developments are:

(i) constant total mass flow
(ii) constant fluid density; this eliminates the necessity for the continuity equation
(iii) no velocity variation in the gas flow
(iv) no pressure changes in the system; this eliminates the necessity for the momentum equation
(v) kinetic and potential energy changes are neglected
(vi) reaction is confined to the solid phase
(vii) all model parameters are considered constant

With these simplifications the general conservation equations for heat and mass are:

Gas Phase

(i) Heat Balance

$$-\nabla.(-K_g\Delta T_g + \dot{G}C_{p_g}T_g) + h_v(T_s - T_g) = \delta\rho_g C_{p_g}\frac{\partial T_g}{\partial t} \qquad (2)$$

(ii) **Mass Balance (for all j)**

$$-\nabla.(-D^E\Delta C_j + \dot{G}m_j) + \sum_{i}^{R}\nu_{ji}r_i^{eff} + \Psi_j(T_s) = \frac{\delta\partial C_j}{\partial t} \qquad (3)$$

Solid Phase

(i) **Heat Balance**

$$-\nabla.(K_s^E\Delta T_s + \dot{U}C_{p_s}T_s) - h_v(T_s - T_g) + \overset{R}{\underset{i=1}{}} r_i^{eff}\Delta H_i - \Phi(T_s)$$

$$= (1-\delta)\rho_s C_{p_s}\frac{\partial T_s}{\partial t} \qquad (4)$$

(ii) **Mass Balance**

$$-\nabla.\dot{U} + \sum_{i=1}^{R}\nu_{ji}r_i^{eff} - \sum_{i=1}^{J}\Psi_i(T_s) = (1-\delta)\frac{\partial\rho_s}{\partial t} \qquad (5)$$

The symbols used in these equations have the meaning given to them in the Nomenclature (Appendix I). An explanation of the various terms in the equations is given below.

$\nabla.(K_g\Delta T_g)$ represents the difference in heat flow into and out of a unit volume of the bed per unit time by means of conduction in the fluid phase and in the direction of maximum decreasing temperature gradient in the fluid. K_g is the effective thermal conductivity of the gas and is given by: $K_g = \delta k_g + Cp_g\rho_g E$ where k_g is the molecular conductivity and E is the turbulent eddy diffusivity, which can be estimated following Bernard and Wilhelm (56). In the similar term for the solid phase, K_s^E is the effective solid thermal conductivity, which takes into account the effect of radiation through the bed; K_s^E may be estimated by the methods outlined by Schotte (57), Yagi, Kunii and Wakao (58) and Luikov et al. (59).

$\nabla.(GC_{pg}T_g)$ is the difference in heat flow into and out of a unit volume of bed per unit time by means of mass flow through the established fluid temperature gradient. The parallel term for the solid heat balance represents a similar heat-transport mechanism due to bulk movement of the solid particles.

$h_v(T_s - T_g)$ represents the rate of heat transport per unit volume and time by convection from the solid to the gas. Values of h_v, the volumetric heat transfer coefficient, can be obtained from available correlations for heat transfer in packed beds. The extensive data in this field have been reviewed recently by Barker (60) and Handley and Heggs (61).

$\sum_{i=1}^{R} r_i^{eff} H_i$ represents the net heat liberated by the R chemical reactions of gas phase species with the solid particles; r_i^{eff} is the effective mass rate of reaction per unit volume of bed of the i^{th} reaction and ΔH_i is its heat of reaction. ΔH_i is considered positive for exothermic reactions and negative for endothermic reactions. r_i^{eff} must be calculated from consideration of the true heterogeneous chemical rate and the rate of mass transport to the solid-gas interface.

$\Phi(T_s)$ is the net heat absorbed by all the endothermic reactions occurring within the bed exclusive of the gas-solid reactions considered above. This term contains the heat effects of drying and pyrolysis of the fuel and will be a complex function of the solid temperature.

$\delta \rho_g C_{pg} \cdot \frac{\partial T_g}{\partial t}$ represents the heat absorbed in a local rise in the gas temperature weighted in proportion to the volume fraction (δ) of the bed that contains gas. The parallel term in the solid phase heat balance has equivalent significance.

$\sum_{i=1}^{R} \nu_{ji} r_i^{eff}$ is the mass rate of appearance of specie j per unit volume of the bed and per unit time through the R simultaneous gas-solid reactions taking place within the bed. The ν_{ji} are the stoichiometric coefficients of specie j in reaction i and are written positive for products and negative for reactants.

$\Psi_j(T_s)$ is the mass rate of appearance in the gas phase of specie j per unit volume of the bed and per unit time through drying and pyrolysis of the fuel and will be a complex function of the solid temperature. $\sum_{i=1}^{J} \Psi_i(T_s)$ is the loss of weight of the solid caused by the loss of all species 1 through J during the processes of drying and pyrolysis.

In form, these equations are similar to those used in studies of fixed bed reactors, but they are somewhat more complex due to the reaction behavior of the solid. The solid phase in a refuse bed undergoes drying, pyrolysis and char combustion and is continuously changing in shape and physical structure as well as chemical composition. The solution to a set of equations such as these with their appropriate boundary conditions is impossible because it is extremely difficult to adequately describe the various solid phase reactions. In addition, the various parameters of the equations (reaction rates, heat transfer coefficients, thermal conductivities, etc.) are poorly known. The following section discusses briefly how some of the more important physical properties of a fuel bed may be estimated.

Notes on the Selection of Physical Properties. Caution must be exercised in selecting appropriate values of K_s^E and h_v or h_s. The direct experimental measurement of average and local heat transfer coefficients for single particles is only practical in a bed of large spheres. Examples of methods for calculating such heat transfer coefficients are provided by the work of Furnas (62) and Gillespie, Crandell and Carberry (63). Furnas used a suction pyrometer to measure the temperature of the interstitial gas and the same pyrometer to measure the solids temperature, but without drawing any gas through it. It is likely that this technique of measuring the solids temperature did not give a true solid temperature, but rather a weighted average of the gas and solids temperatures. Gillespie et al. measured local and average heat transfer rates from an internally heated sphere (1-in.-diameter) in a bed one foot square.

The experimental difficulties associated with the direct experimental determination of local and average values of h_v have led researchers to determine overall or integral heat transfer coefficients by indirect means. In one of the more widely used techniques of this type, h_v is calculated from a suitable mathematical model of the modes of heat transfer within the packed bed and the time variation of the heating or cooling gas exit temperature obtained from unsteady-state experiments. For these experiments the mathematical model must take into account all important modes of heat transfer in the bed as well as the effects of internal resistance to heat transfer within the particles; in addition, the experimental equipment must be carefully designed to minimize end effects and radial velocity gradients. Some of the scatter observed in the various correlations of overall heat transfer coefficients may be partly due to (a) inadequate representation of the modes of heat transfer and neglect of the internal resistance to heat transfer, (b) the use of different methods and assumptions when calculating the coefficients and (c) the effect of channeling and gross variations in packing arrangements within "random" packed beds.

Under conditions in which the Biot number is large, the internal resistance to heat transfer may be accounted for by calculating an effective heat transfer coefficient (h_s^E) using the following expression developed by Bradshaw et al. (64):

$$\frac{1}{h_s^E} = \frac{1}{h_s} + \frac{D_p}{10k_s} + \frac{6K_g(1-\delta)}{D_p(G\delta\rho_g C_{p_g})^2} \tag{6}$$

where h_s is the "true" heat-transfer coefficient based on the heat-transfer area per unit volume of bed and is given, for hard spherical particles, as:

$$h_s = \frac{h_v D_p}{6(1-\delta)} \tag{7}$$

A similar expression for the effective heat-transfer coefficient was developed by Kitaev (65) from the results of a study of the heating times of thermally thick elements using the hydraulic equivalent of an analog computer. Kitaev's expression did not include the term associated with the effective gas thermal conductivity.

The data of Furnas (62) would be the best for predicting heat transfer rates within fuel beds as he worked with the widest range of materials of differing surface characteristics and with particle sizes comparable to those found in fuel beds. However, Kitaev et al. (67) have concluded from an analysis of Furnas' data that the correlation presented by him, namely

$$h_v = \frac{A w^{0.7} T^{0.3}\, 10^{1.68\delta - 3.56\delta^2}}{D_p^{0.9}} \tag{8}$$

where w = gas flow rate in standard cubic feet per hour per foot of cross-sectional area of the bed

T = average gas temperature (°F)

D_p = particle diameter (ft)

δ = voidage fraction

A = constant for each material

is in error because the internal resistance to heat transfer was not taken into account. According to Kitaev et al., the anomalous behavior noticed by Furnas in his experiments on the cooling of coke can be substantially explained by the neglect of this factor. Kitaev et al. suggest that a modified form of Furnas' equation be used, based on their recalculations of his data, using the relationship given in equation (8). The equation is:

$$h_v = \frac{0.0044\, w^{0.9} T^{0.3} M}{D_p^{0.75}} \text{ Btu hr}^{-1} \text{ ft}^{-3}\ {}^\circ\text{F}^{-1} \tag{9}$$

where M is a function of the voidage and an average value of the factor A has been used. Kitaev et al. suggest that the overall heat-transfer coefficient will be a strong function of M , but quote only one value of M ($M = 0.5$ for a voidage of 20 percent). This mitigates against the usefulness of equation (9). In addition, the dependence of h_v on the particle size and the mass flow rate of gas is different from most recent correlations (see equations (10) and (11); and the method of taking into account the temperature at which transfer takes place is only approximate. Furthermore, the rather low ratio of the diameter of the packed bed to the particle diameter, in many cases 5 to 8, probably meant that serious channeling took place near the walls, giving a high estimate of the overall heat transfer coefficient because of the greater possibility of heat loss to the containing walls. The literature (68, 69) suggests that the ratio of bed diameter to particle diameter does not affect the correlation of heat transfer at ratios greater than 18:1.

With the shortcomings indicated above, it is suggested that the standard correlations of heat transfer be used rather than the modified form of the Furnas equation. Typically, these may take the form of the empirical Chilton-Colburn j-factor correlation, a suitable form being given by Yoshida, Ramaswami and Hougen (66):

$$j_H = 0.91\ \Psi N_{Re}^{-0.51} \qquad N_{Re} < 50 \qquad (10)$$

$$j_H = 0.61\ \Psi N_{Re}^{-0.41} \qquad N_{Re} > 50 \qquad (11)$$

In these equations N_{Re} is defined as

$$N_{Re} = \frac{\dot{G}}{A_s \mu \Psi} \qquad (12)$$

where A_s is the interfacial area per unit volume of bed and Ψ is a shape factor ($\Psi = 1$ for spheres). It should be realized that estimates based on these correlations may be no better than ± 50 percent and may be worse; in addition the presence of chemical reaction within a bed may affect the heat transfer rate but in the absence of any experimental data under these conditions the standard correlations must suffice.

The effective thermal conductivity of a packed bed can be determined for stagnant conditions by using any of the methods suggested on page 23 . The method of Schotte (57) appears to fit most of the available experimental data and is relatively easy to use. However, the available data, primarily that of Yagi and Kunii (70), are only for particles up to about 11 mm diameter and bed temperatures up to 850°C. Schotte allowed for the effect of radiation with the following relationship:

$$\left[\frac{K_s^E}{k_g}\right]_{\text{stagnant}} = \left[\frac{K_s}{k_g}\right]_{DE} + \frac{h_r D_p}{k_g} + \frac{1 - \delta}{\frac{k_g}{h_r D_p} + \frac{k_g}{k_s}} \qquad (13)$$

where $(K_s/k_g)_{DE}$ is taken from the semi-empirical correlation of Deissler and Eian (71) shown in Figure 3, and

$$h_r = 0.692\varepsilon T^3/10^8 \text{ Btu hr}^{-1} \text{ ft}^{-2} \text{ °F}^{-1} \qquad (14)$$

The correlation works best with regularly shaped and evenly sized particles and must be considered to give only approximate results for large particles of random shapes and sizes.

For nonstagnant conditions, Yagi, Kunii and Wakao (72) have proposed that the effective thermal conductivity can be calculated from

$$\left[\frac{K_s^E}{k_g}\right]_{\text{flowing}} = \left[\frac{K_s^E}{k_g}\right]_{\text{stagnant}} + 0.80\, N_{Re} N_{Pr} \qquad (15)$$

Equation (15) was determined from measurements of the steady-state axial temperature profile established under flowing conditions in a packed bed which was heated at one end. In the calculation used to determine the effective bed conductivity it was assumed that $T_g = T_s$ (i.e., the heat transfer coefficient $h_v = \infty$) and that the effective conductivity was not a function of temperature.

The above discussion has served to indicate that many of the published results depend on the models that the particular authors chose when calculating the physical property of interest. Over and above these problems are questions concerning the effective heat transfer area per unit volume of the bed and how this changes with void fraction, particle shape and size, and surface characteristics. There is no definitive answer to these problems and any estimates of the physical properties for a bed as heterogeneous as a refuse bed can only be considered approximate. For a burning bed the combustion process adds another degree of complexity and additional uncertainty into these estimates.

The conductive term in the gas phase equation for the conservation of heat is small under most practical conditions in comparison to the convective term, and therefore the methods

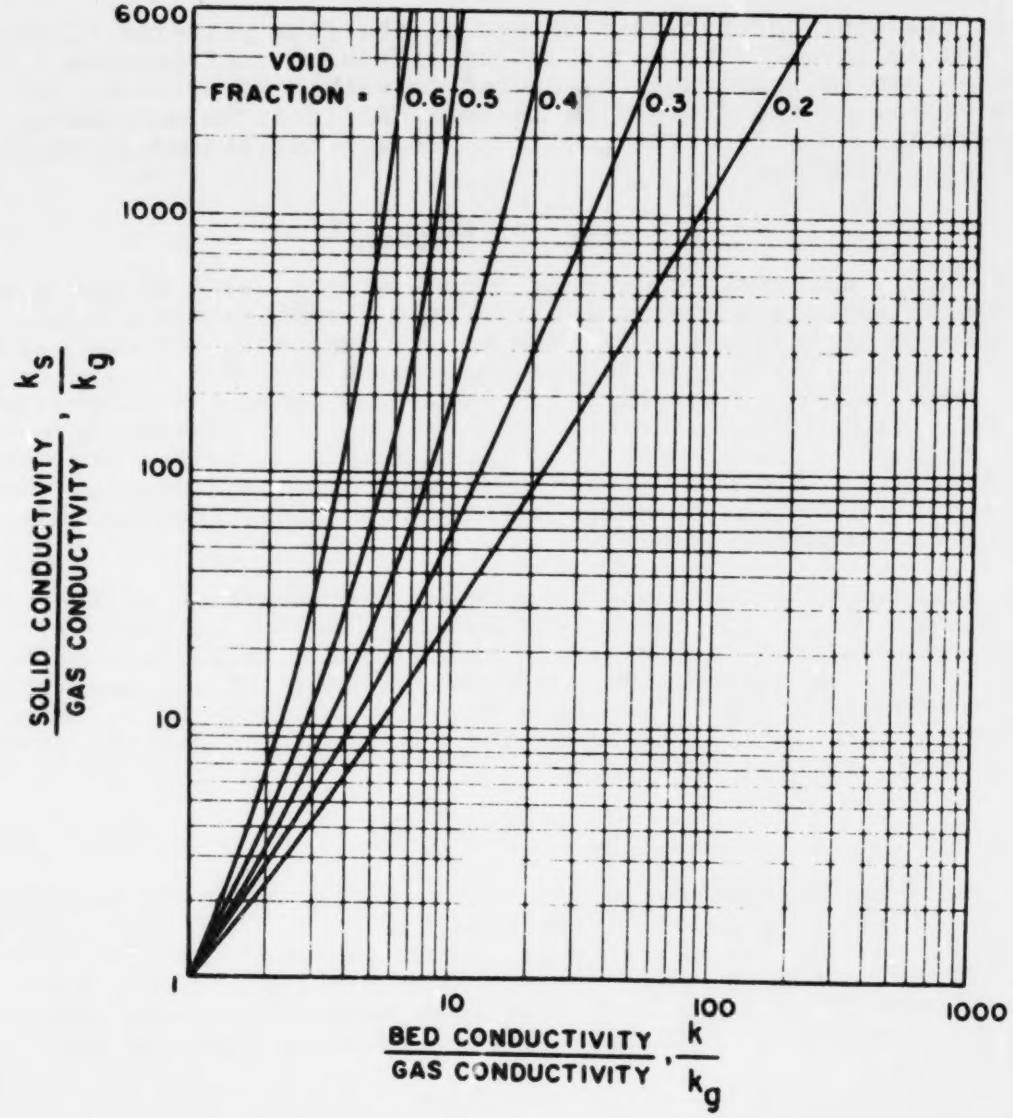

Fig. 3. Deissler-Eian Correlation for the Thermal Conductivity of Packed Beds (71)

for estimating the effective gas conductivity, previously cited, will not be elaborated upon. The last physical properties, therefore, that need to be estimated are the mass transfer coefficients for the various species undergoing heterogeneous reactions.

Mass transfer coefficients depend on the flow patterns close to the solid-gas interfaces and on diffusion coefficients. The latter can be reasonably predicted to within ∿5 percent, but the effect of the fluid flow is more difficult to determine. Generally, mass transfer coefficients are correlated in terms of the following:

$$N_{Sh} = aN_{Re}^{\alpha}N_{Sc}^{\beta} \tag{16}$$

Strictly, correlations of this form are only valid at low mass transfer rates and when the transferring species are present in low concentrations. If this is not the case, the concentration levels will appear in the functional dependence of the Sherwood number. High transfer rates and rapid gas temperature changes caused by exothermic reactions can conceivably affect the flow patterns close to the interphase boundaries, and this in turn will affect the functional form of equation (16). The calculation of mass transfer coefficients under these conditions is extremely complex.

The influence of the transfer rate on the magnitude of the mass transfer coefficient can be estimated following Spalding (73). For the idealized case of a constant property turbulent boundary layer, the relationship between the ratio of the mass transfer conductance (g) to the mass transfer conductance at zero transfer rate (g*) in terms of the mass transfer driving force B is given by Kays (74) as

$$\frac{g}{g^*} = \frac{\ln(1 + B)}{B} \tag{17}$$

For pure carbon burning in air, B is readily shown to be equal to 0.174 and therefore the ratio $g/g^* \cong 0.92$. The small change in g is typical for solid fuels, where the mass transfer driving force is always low. However, the ratio g/g* for actual fuels will be somewhat less than that calculated above because of the presence of volatile matter distilling from the fuel particles.

This section has served to point out the difficulties inherent in selecting good physical properties for use in any mathematical model and provides a rationale for simplifying the general conservation equations formulated in the previous section. In addition, although the methods outlined above will provide useful guidelines, the above discussion clearly shows the need for determining these physical properties from in situ tests using representative bed materials.

Criteria for Particle Isothermality. Equations (1) and (4) are written under the assumption that there is no variation in temperature within the fuel particles; for large particles of finite conductivity, this may not be true. (In this case, a rigorous analysis is still possible, following Amundsen (75), but analytical solutions are only possible when the reaction rate is considered to have a simple linear dependence on temperature. Even with this major simplification, the solutions are very complex and require tabulations of special functions.) The extent to which temperature gradients will be present within a particle will depend on the Biot number $(N_{Bi} \equiv h_s D_p / k_s)$. Chukhanov (77) has shown, using a simple theoretical model, that particles can be considered isothermal if

$$\frac{1}{N_{Bi}} > 2 \qquad (18)$$

Saunders and Ford (76) have shown experimentally that temperature gradients within particles may be neglected if the following condition is met:

$$(\dot{G} C_{p_s} D_p / k_s) < 4 \qquad (19)$$

This condition is similar in form to equation (18) but the term GC_{p_g} gives only an approximate measure of the heat transfer coefficient. Saunders and Ford worked with relatively small particles (the maximum diameter of particles used was 0.25 in.) and as the criterion has a poor theoretical basis it must be regarded as only approximate for larger particles.

Handley and Heggs (78) have suggested that the particles can be considered isothermal if

$$\frac{3k_s L(1-\delta)}{GC_{p_g} D_p^2} > 60 \qquad (20)$$

where L is the bed depth and the other symbols have the meanings given to them in the Nomenclature (Appendix I). It should be noted that the group on the left-hand side does not contain the heat transfer coefficient and therefore this criterion has the same shortcoming as that of Saunders and Ford's.

These criteria are based on the convective heating or cooling of particles and do not consider the effect of radiant heat transfer to the particle or the effect of chemical reaction within the particle. As such, they must also be considered approximate for many fuel bed situations. It should be noted here that exothermic reactions within the particle would help lower the internal resistance to heat transfer, while endothermic reactions would have the opposite effect.

Simplification of the Conservation Equations. For the purposes of the following development, the bed particles are considered to be isothermal. Many systems can be suitably approximated as being one-dimensional and in this case equations (1) through (5) simplify to:

Gas Phase

$$K_g \frac{\partial^2 T_g}{\partial z^2} - \dot{G} C_{p_g} \frac{\partial T_g}{\partial z} + h_v (T_s - T_g) = \delta \rho_g C_{p_g} \frac{\partial T_g}{\partial t} \qquad (21)$$

$$D^E \frac{\partial^2 C_j^b}{\partial z^2} - \frac{\dot{G}}{\rho_g} \frac{\partial C_j^b}{\partial z} + k_c A_s (C_j^i - C_j^b) = \frac{\delta \partial C_j^b}{\partial t} \qquad (22)$$

Solid Phase

$$K_s^E \frac{\partial^2 T_s}{\partial z^2} - \dot{U} C_{p_s} \frac{\partial T_s}{\partial z} - h_v (T_s - T_g) + \sum_j R_j^* \Delta H_j$$

$$= (1-\delta) \rho_s C_{p_s} \frac{\partial T_s}{\partial t} \qquad (23)$$

$$-\sum R_j^* = (1-\delta) \frac{\partial \rho_s}{\partial t} \qquad (24)$$

if it is assumed that $\dot{U}$, $\dot{G}$, C_{p_g}, C_{p_s}, ρ_g, h_v, k_c, A_s and δ do not vary through the depth of the fuel bed and that average values of K_g, D^E and K_s^E can be used. In equations (23) and (24) the different reaction terms have been lumped together into the term R_j^*. In actual fuel beds all of the physical properties will vary through the bed -- the mass flow of gas ($\dot{G}$) and solid ($\dot{U}$) will vary as reaction occurs; the specific heat and density of both gas and solid will change with composition and temperature, and K_s^E will be a strong function of temperature. In all practical cases, the term $R_j^* \Delta H_j$, which represents the net heat liberated within the bed from the processes of drying, pyrolysis and combustion (radial heat losses can also be included) will not be a simple function of temperature and will obviously vary with temperature, reactant concentration and position within the bed. Further simplifying assumptions are thus needed to make the equations tractable.

Schumann (79) was the first to present a solution to the simplified equations of the conservation of heat. Schumann neglected the thermal conductivity of the solid and gas phases and assumed that there was no bulk flow of the solid and non-reacting conditions; equations (21) and (23) then reduce to:

$$-\dot{G}C_{p_g}\frac{\partial T_g}{\partial z} + h_v(T_s-T_g) = \delta\rho_g C_{p_g}\frac{\partial T_g}{\partial t} \tag{25}$$

$$-h_v(T_s-T_g) = (1-\delta)\rho_s C_{p_s}\frac{\partial T_s}{\partial t} \tag{26}$$

with the boundary conditions

$$T_g(0,0) = T_o \tag{27}$$

$$T_s(0,0) = 0 \tag{28}$$

$$T_g(0,t) = T_o \tag{29}$$

The formal solution to this set of simplified equations is relatively complex, involving sums of Bessel's series:

$$T_s/T_o = e^{-y-x}\sum_{n=1}^{\infty} x^n M_n(yx) \tag{30}$$

$$T_g/T_o = e^{-y-x}\sum_{n=0}^{\infty} x^n M_n(yx) \tag{31}$$

where,

$$M_o(yx) = J_o(2i\sqrt{yx}) \tag{32}$$

$$M_n(yx) = \frac{d^n M_o(y)}{d(yx)^n} \tag{33}$$

$$y = h_v z/\dot{G}C_{p_g} \tag{34}$$

$$x = \left[h_v/(1-\delta)\rho_s C_{p_s}\right]\left[t - \frac{z\delta\rho_g}{\dot{G}}\right] \tag{35}$$

The solution to this simplified problem is given for completeness, as it has been widely used in many studies on heat transfer within packed beds. Furnas (62) was the first to realize that Schumann's solution provided a new approach to calculating heat transfer coefficients rather than direct determination (see page 25).

Subsequent to Schumann's solution, a number of approximate solutions to the rigorous problem have been proposed and the reader is referred to Klinkenberg (80) for a further discussion. More complete analyses of the conservation of heat equations have been developed by Singer and Wilhelm (81), Brinkley (82), Wilhelm, Johnson and Acton (83) and Amundsen et al. (75, 84, 85, 86). All of these authors had to make some simplifications to the equations before they could develop analytical solutions, the most common assumptions being a linear variation of the reaction rate with temperature and negligible axial conduction through the solid. All of these solutions are not strictly applicable to fuel beds and a somewhat different approach was suggested by Stewart and Saville (87). This method suggests a way of determining the effective thermal conductivity of the fuel bed.

The development below follows Stewart and Saville (87), and only those equations dealing with the conservation of heat will be considered; it is therefore assumed that the reaction rate term $\sum_j R_j^*$ can be determined independently of the equations of conservation of mass. The two equations considered are:

$$-\dot{G}C_{p_g}\frac{\partial T_g}{\partial z} + h_v(T_s-T_g) = \delta\rho_g C_{p_g}\frac{\partial T_g}{\partial t} \tag{36}$$

$$K_s^E\frac{\partial^2 T_s}{\partial z^2} - \dot{U}C_{p_s}\frac{\partial T_s}{\partial z} - h_v(T_s-T_g) + \sum_j R_j^*\Delta H_j = (1-\delta)\rho_s C_{p_s}\frac{\partial T_s}{\partial t} \tag{37}$$

where the conductive term in the gas phase equation has been eliminated, as under most practical situations it is small in comparison with the convective term. The temperature of the gas T_g can be eliminated from these equations and the equations combined in a number of different ways, depending on the physical model selected. It is commonly assumed, particularly when catalytic reactors are being modeled, that the heat transfer rate is so high that $\frac{\partial T_s}{\partial z} = \frac{\partial T_g}{\partial z}$. Equations (36) and (37) then reduce to:

$$K_s^E\frac{\partial^2 T}{\partial z^2} - \left[\dot{G}C_{p_g} + \dot{U}C_{p_s}\right]\frac{\partial T}{\partial z} + \sum_j R_j^*\Delta H_j = \left[\delta\rho_g C_{p_g} + (1-\delta)\rho_s C_{p_s}\right]\frac{\partial T}{\partial t} \tag{38}$$

where, as suggested by Stewart and Saville (87), the subscript on the temperature has been dropped and now can be considered to represent the temperature measured in the bed with a thermocouple. As pointed out by Stewart and Saville (87), the above assumption can be a poor one under conditions where bed temperature gradients are large (e.g., near the ignition front of a fuel bed).

By assuming that all reactions take place on the solid and that $\frac{\partial^2 T_g}{\partial z^2} = \frac{\partial^2 T_s}{\partial z^2}$, a better approximation first proposed by Woods and Harris (88) is obtained. Equations (36) and (37) then can be combined to give:

$$\left[K_s^E + \frac{\dot{G}^2 C_{p_g}^2}{h_v}\right] \frac{\partial^2 T}{\partial z^2} - \left[\dot{G} C_{p_g} + U\dot{C}_{p_s}\right] \frac{\partial T}{\partial z} + \sum_j R_j^* \Delta H_j$$

$$= \left[\delta \rho_g \, C_{p_g} + (1-\delta) \rho_s C_{p_s}\right] \frac{\partial T}{\partial t} \tag{39}$$

Except near the ignition zone in the underfeed bed, where there will be large quantities of oxygen available to react in the gas phase with pyrolysis products and carbon monoxide, the assumption that reactions are confined to the solid phase is probably quite good. (There is strong evidence (89) suggesting that carbon monoxide is the primary product of the carbon-oxygen reaction at high temperatures.) Stewart and Saville propose that the second assumption may be abrogated by using a truncation factor, β, which compensates for any difference between the second derivatives of gas and solid temperature with respect to distance. The truncation factor was found as follows. Neglecting the heat capacity of the gas, rearrangement of equation (36) gives:

$$\frac{\partial T_g}{\partial z} = \frac{h_v}{\dot{G} C_{p_g}} (T_s - T_g) \tag{40}$$

Continuous differentiation of equation (40) gives $\frac{\partial T_g}{\partial z}$ in terms of a series expansion of derivatives of T_s with respect to distance.

$$\frac{\partial T_g}{\partial z} = \frac{dT_s}{dz} - \gamma \frac{d^2 T_s}{dz^2} + \gamma^2 \frac{d^3 T_s}{dz^3} - \gamma^3 \frac{d^4 T_s}{dz^4} + \gamma^4 \frac{d^5 T_s}{dz^5} - \ldots \tag{41}$$

where $\gamma = \dfrac{\dot{G}C_{p_g}}{h_v}$

Substituting (41) back into (40) gives

$$-h_v(T_s - T_g) = -\dot{G}C_{p_g}T_s^i + \frac{\dot{G}^2C^2_{p_g}}{h_v}\left[T_s^{ii} - \gamma T_s^{iii} + \gamma^2 T_s^{iv} - \gamma^3 T_s^v + \ldots\right] \tag{42}$$

where $T_s^i = \dfrac{\partial T_s}{\partial z}$. The series given in equation (42) can be shown to be equal to

$$T_s^i - \gamma T_s^{iii} + \gamma^2 T_s^{iv} - \gamma^3 T_s^v = \frac{1}{\gamma}\, e^{-z/\gamma} \int_{-\infty}^{z} e^{z/\gamma}\, T_s^{ii} dz \tag{43}$$

and, using this relationship, (42) can be rewritten as

$$-h_v(T_s - T_g) = -\dot{G}C_{p_g}\frac{dT_s}{dz} + \beta\left[\frac{\dot{G}C_{p_g}}{\sqrt{h_v}}\right]^2 \frac{d^2T_s}{dz^2} \tag{44}$$

where

$$\beta = \frac{e^{-z/\gamma}\int_{-\infty}^{z} e^{z/\gamma} T_s^{ii} dz}{T_s^{ii}} \tag{45}$$

Combining equation (44) with equation (37) gives the Stewart and Saville equation,

$$\left[K_s^E + \beta\left(\frac{\dot{G}C_{p_g}}{\overline{h_v}}\right)^2\right]\frac{\partial^2 T}{\partial z^2} + \left[\dot{G}C_{p_g} + \dot{U}C_{p_s}\right]\frac{\partial T_s}{\partial z} + \sum_j R_j^* \Delta H_j = \left[\delta\rho_g C_{p_g} + (1-\delta)\rho_s C_{p_s}\right]\frac{\partial T}{\partial t} \tag{46}$$

From the development, β must be a constant for equation (46) to hold. For a simple exponential dependence of temperature with distance such as $T = a + be^{cz}$ this is true, but for more complex relationships it would be purely fortuitous if β were found to be constant. Consequently, this modification of Stewart and Saville's must be used with caution. Developments along these lines can take us no further and it is suggested that under conditions where $\sum_j R_j^*$ is an unknown function of temperature that either equation (38) or equation (39) be used.

When $\sum_j R_j^*$ is a known function of distance, another method becomes aviable for eliminating T_g; this method also takes into account gas phase reaction. By differentiating equation (37), substituting $\frac{\partial T_g}{\partial z}$ from equation (36) and eliminating $h_v(T_s-T_g)$ from the resulting equation by using equation (37), the following is obtained:

$$\left[\frac{K_s^E \dot{G}C_{p_g}}{h_v}\right]\frac{d^3T}{dz^3} + \left[K_s^E - \frac{\dot{U}C_{p_s}\dot{G}C_{p_g}}{h_v}\right]\frac{d^2T}{dz^2} - \left[\dot{U}C_{p_s} + \dot{G}C_{p_g}\right]\frac{dT}{dz}$$

$$+ \sum_j R_j^* \Delta H_j + \frac{\dot{G}C_{p_g}}{h_v}\sum_j \frac{dR_j^*}{dz}\Delta H_j \tag{47}$$

It will be noted that this approach involves no approximations Mayers (90) used this method in his analysis, which will be discussed in a later section.

Equation (47) can also be readily solved using the method of variation of parameters to give

$$T_s = Ae^{m_1 z} + Be^{m_2 z} + \frac{1}{m_1-m_2}\left[e^{m_1 z}\int_0^z \sum_j R_j^* \Delta H_j\, dzdz - e^{m_2 z}\int_0^z e^{-m_2 z}\int_0^z \sum_j R_j^* \Delta H_j\, dzdz\right] + C \tag{48}$$

where

$$m_1 = \frac{1}{2}\left[-\left\{\frac{h_v}{\dot{G}C_{p_g}} - \frac{\dot{U}C_{p_s}}{K_s^E}\right\} + \sqrt{\left(\frac{h_v}{\dot{G}C_{p_g}} - \frac{\dot{U}C_{p_s}}{K_s^E}\right)^2 + 4\left(\frac{\dot{U}C_{p_s}h_v}{K_s^E\dot{G}C_{p_g}} + \frac{h_v}{K_s^E}\right)}\right] \tag{49}$$

$$m_2 = \frac{1}{2}\left[-\left\{\frac{h_v}{\dot{G}C_{p_g}} - \frac{\dot{U}C_{p_s}}{K_s^E}\right\} - \sqrt{\left(\frac{h_v}{\dot{G}C_{p_g}} - \frac{\dot{U}C_{p_s}}{K_s^E}\right)^2 + 4\left(\frac{\dot{U}C_{p_s}h_v}{K_s^E\dot{G}C_{p_g}} + \frac{h_v}{K_s^E}\right)}\right] \tag{50}$$

A, B and C are constants which must be determined from the boundary conditions (two on the solid phase and one on the gas phase). Even for the very simplest of reaction rate terms the evaluation of the integration constants presents a tedious algebraic task.

The approximate equations (38) and (39) can be written, for steady-state conditions, in the general form:

$$\frac{d^2T}{dz^2} + \gamma \frac{dT}{dz} + \bar{Q}(z) = 0 \tag{51}$$

which can be integrated directly to give:

$$T = -\frac{A}{\gamma} + Be^{-\gamma z} - e^{-\gamma z} \int_0^z e^{\gamma z} \int_0^z \bar{Q}(z)\,dz\,dz = 0 \tag{52}$$

where A and B are integration constants which can be determined from the appropriate boundary conditions.

Equation (52) may be used to determine the maximum temperature that will be reached in a fuel bed. With the boundary conditions,

$$\begin{aligned} &\text{at} \quad z = 0, \quad T = T_{max} \quad \text{and} \quad \frac{dT}{dz} = 0 \\ &\text{at} \quad z = \infty, \quad T = 0 \end{aligned} \tag{53}$$

both A and B can be found, the result being

$$T_{max} = \frac{Q_{net}}{(\hat{G}C_{p_g} + \hat{U}C_{p_s})} \tag{54}$$

where Q_{net} is the net total heat released from $z=\infty$ to $z=0$. Equation (54) is, of course, directly obtainable from a simple heat balance. The difficulty in applying equation (52) in a more general way lies in evaluating the double integral for which $\bar{Q}(z)$ must be known explicitly. Stewart and Saville (87) have used equation (52) along with some approximate methods of evaluating the double integral to obtain some interesting results for a sinter bed. The application of equation (52) to sinter beds is much easier than for a fuel bed, since in the former the separation of the exothermic and endothermic zones can be readily achieved and the total heat released, or absorbed, in each zone can be well-established; the picture is not so well-defined in a fuel bed.

For unsteady-state conditions such as experienced in a combustion pot, equations (38) and (39) may be written in the general form,

$$\frac{\bar{k}\partial^2 T}{\partial z^2} - V\frac{\partial T}{\partial z} + Q(z) = (\rho C_p)_{ave}\frac{\partial T}{\partial t} \tag{55}$$

If the temperature-time data from a combustion pot experiment are plotted up as temperature-distance curves at different times, it would be possible to evaluate $\frac{\partial^2 T}{\partial z^2}$, $\frac{\partial T}{\partial z}$ and $\frac{\partial T}{\partial t}$. For a region where thermal reactions are not important, the value of $\bar{k}$ could be estimated from

$$\bar{k} = \frac{(\rho C_p)_{ave}\frac{\partial T}{\partial t} + V\frac{\partial T}{\partial z}}{\frac{\partial^2 T}{\partial z^2}} \tag{56}$$

Similarly, the net reaction rate Q(z) could be determined from the same data obtained from a "reacting" zone using this value of $\bar{k}$. Admittedly this extrapolation of $\bar{k}$ to the higher temperature region contains some uncertainties, but a correction for the mean temperature difference in each zone could be crudely estimated using equation (13). Q(z) could then be calculated from

$$Q(z) = \frac{(\rho C_p)_{ave}\frac{\partial T}{\partial t} + V\frac{\partial T}{\partial z}}{\frac{\bar{k}\partial^2 T}{\partial z^2}} \tag{57}$$

Experimental Investigations of Combustion in Coal Beds

Overfeed Combustion: The Work of H. Kreisinger et al. (23) and K. I. Kolodtsev (91). The purpose of these investigations was to study the rate of combustion of an overfeed bed and to measure gas compositions and temperatures within the burning fuel bed. In both these works, water-cooled probes were used to collect the gas samples. Kreisinger et al. measured the concentrations of O_2, CO_2, CH_4, N_2, tar and soot, while Kolodtsev only measured CO, CO_2 and O_2. Kolodtsev used platinum/platinum-rhodium thermocouples and an optical pyrometer (for temperatures greater than 1500°C) for the temperature measurements, while Kreisinger et al. measured temperature only with an optical pyrometer. The apparatus used in these investigations were somewhat different in design and mode of operation.

Kreisinger et al. used the equipment shown in Figure 4, an arrangement that is commonly referred to as a combustion pot. Three different fuels were used -- Pittsburgh coal, anthracite and coke, with the Pittsburgh coal being the richest in volatile matter (34%), while the anthracite and coke had similar compositions and low volatile matter contents (5% for the anthracite and 1.5% for the coke). Another difference between the coke and the anthracite was the moisture content (2.8% for the anthracite and 0.7% for the coke). The moisture content of the Pittsburgh coal was around 2.3%. All the fuel was graded to the same size by passing it over 1 in. square-mesh screen and through 1 1/2 in. screen of the same type. Kreisinger et al. operated the fuel bed under "steady-state" conditions, adding fresh fuel, at regular intervals, to the top of the bed during the test to keep the depth of the fuel bed constant. Two different bed depths were studied -- 6 in. and 12 in. In this study, gas compositions were taken at a few fixed positions above the grate and temperature measurements were taken sequentially through the same holes that were used to introduce the gas sample probes into the bed. The temperatures were read immediately after the sample probe was pulled from the bed, the optical pyrometer being sighted down the tunnels left by the probe in the fuel bed.

In Kolodtsev's experiments a fixed amount of fuel was charged to the apparatus (see Figure 5) and the fuel bed was burnt in an unsteady-state mode; the ignition and burning "front" propagated down through the bed in the direction of the imposed gas flow. Because of the unsteady-state nature of the experiment and the fact that the gas samples were taken at a fixed location in the bed, the distance of the probe from the ignition front had to be calculated from knowledge of the prevailing ignition rate and the time the sample was taken. The temperature measurements were carried out in parallel with the gas sampling, but at a different position in the bed. Kolodtsev used electrode carbon of 98.6% purity with 0.01% ash and 0.05% moisture for his fuel. Experiments were conducted with fuel graded to four different sizes: 2.6 - 3.7 mm, 4.8 - 6.0 mm, 6.0 - 7.2 mm, 7.2 - 9.0 mm. In the majority of the experiments, the original height of the bed above the gas sampling port was 70 mm, while the total depth of the bed was 190 mm.

Kolodtsev's results will be discussed first because they represent the best data available on the most idealized fuel possible. Figure 6 shows the compositional change with particle size and air velocity. In Figure 6(a), (b) and (c), the particle size was held constant and the air velocity changed over more than an order of magnitude. The composition

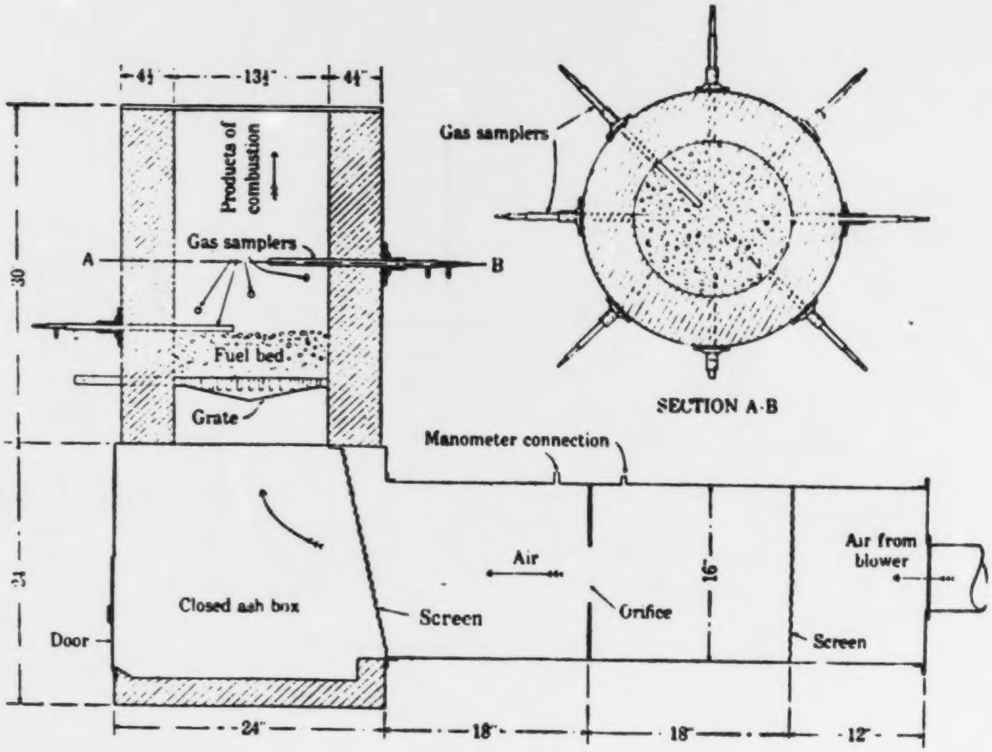
4½
13½"
4½"
30
Products of combustion
Gas samplers
A
B
Fuel bed
Grate
Closed ash box
Door
Screen
24"
18"
18"
12"
Manometer connection
Air
Orifice
16"
Air from blower
Screen
Gas samplers
SECTION A-B

Fig. 4. Schematic of Apparatus Used by Kreisinger et al. (23)

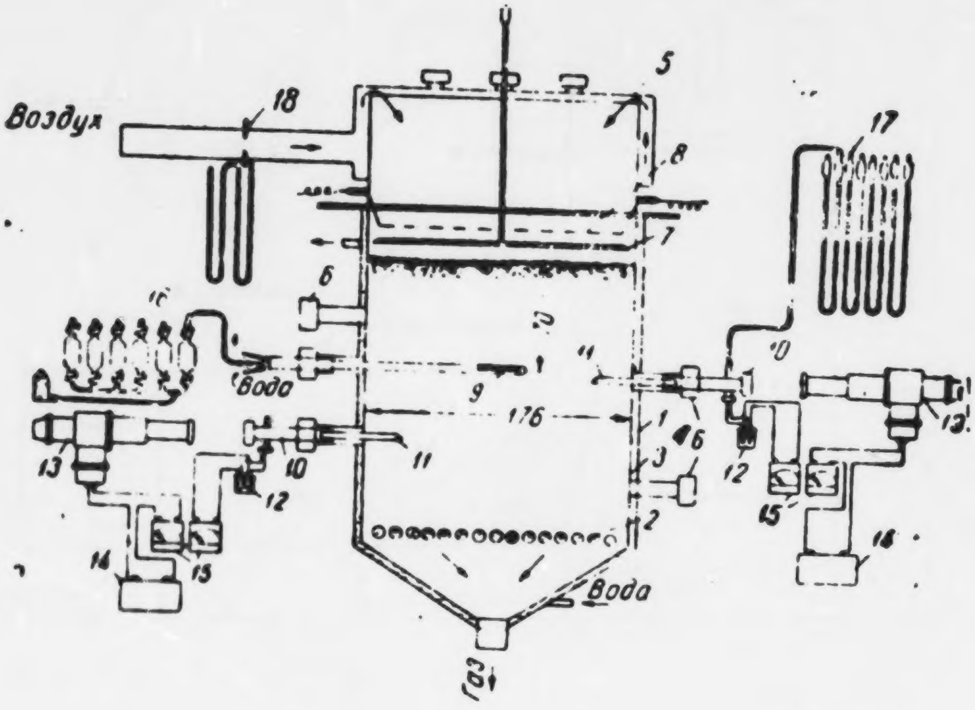
Воздух
18
5
8
17
7
6
16
Вода
9
176
10
11
1
4
6
3
2
13
12
14
15
Вода
Газ

Fig. 5. Equipment Used by Kolodtsev (91)
(1) Combustion chamber, (2) grate, (3) water jacket, (4) fuel bed, (5) blast compartment, (6) connecting pipes, (7) mixer, (8) electric furnace, (9) slit of gas sampling tube, (10) holder, (11) hot junction of thermocouple, (12) cold junction of thermocouple, (13) optical pyrometer, (14) accumulator, (15) galvanometers, (16) gas sampling battery, (17) manometers, (18) orifice

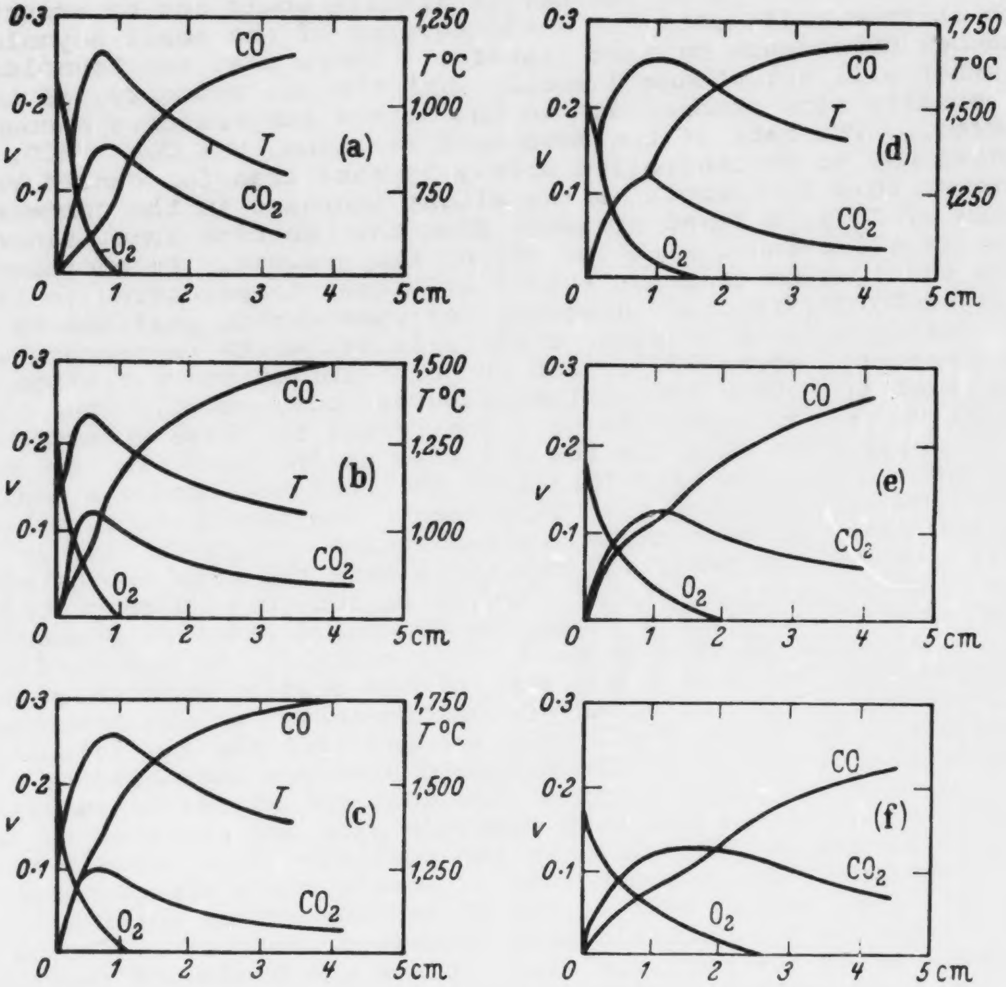

	a	b	c	d	e	f
Particle diameter cm	0·32	0·32	0·32	0·54	0·66	0·81
Air velocity cm/sec	11	49	150	150	150	150

Fig. 6. Gas Compositions and Temperature Profiles in an Overfeed Fuel Bed. Data of Kolodtsev (91)

profiles were only marginally affected by this change. The calculations of Yagi and Kunii (92), which are based on the experimental data of Parker and Hottel (93), show that the rate of the reaction $C + O_2 \rightarrow CO_2$, under the conditions of Kolodtsev's experiments, would be expected to be mass transfer controlled (see Figure 7). Thus the oxygen profile would not be expected to shift significantly as a consequence of the small Reynolds number dependence on mass transfer. (Note that the Reynolds number will not change directly with the gas velocity, as the viscosity also changes due to the higher temperatures encountered.) The rate of the Boudouard reaction, $C + CO_2 \rightarrow 2CO$, is known not to be controlled solely by mass transfer considerations; this fact explains the slight increase in the concentration of CO at a fixed distance from the ignition zone, since the rate increased with the higher temperature. In addition, the equilibrium constant shifts at higher temperatures to favor larger CO/CO_2 ratios. However, for pure carbon gasified by air, the maximum concentration of CO is 34.5%, which is reached at temperatures above 900°C, and the equilibrium concentration of CO is greater than 30% at temperatures above 800°C. Thus equilibrium did not appear to be a constraint in these experiments. The temperature level in the bed rose as the gas velocity increased, since the heat lost from the fuel bed became a smaller fraction of the total heat liberated. The temperature peaked at the plane of zero oxygen concentration. This was as expected since the oxidation reactions were the only exothermic ones taking place. After the point of zero oxygen concentration, the temperatures fell because the Boudouard reaction occurring in this region is endothermic. Presumably if the fuel bed was deep enough, the heat loss from the bed coupled with the endothermic reaction would lead to the "freezing" of the Boudouard reaction. In Figure 6(c), (d), (e) and (f), the air velocity was held constant while the particle size was increased by a factor of 2.5. These figures show that the oxygen consumption distance (z_0) increased with particle size and appeared to have scaled almost in proportion to the particle size. Mass transfer considerations suggest that z_0 should scale approximately as $D_p^{1.4}$ (see pages 75-82). The CO and CO_2 curves shifted to the right as the particle size increased, but not in direct proportion to the particle size. Since the Boudouard reaction is not truly mass transfer controlled, there is no simple scaling law which can be applied.

Kolodtsev's results show clearly that if a fuel bed is being operated for the purposes of heat generation, it should be kept thin (i.e., not much greater than the oxygen consumption distance). If it is not kept thin, then overfire air needs to be added to burn out the carbon monoxide issuing from the top of the bed. If, on the other hand, the fuel bed is being run to generate producer gas, which is rich in hydrogen and carbon monoxide, then the bed should be kept as deep as possible. Finally, Kolodtsev indicated that the ratio of particle size to

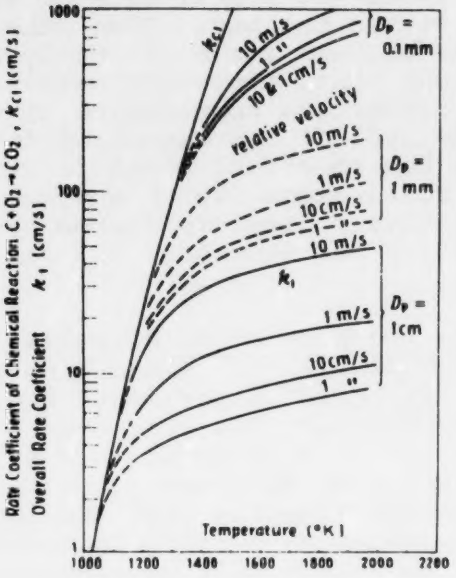

Fig. **7.** Overall Reaction Rate Coefficient for the Combustion of a Pure Carbon Particle (92). Data of A. S. Parker and H. C. Hottel (93) diameter of his combustion chamber had to be greater than 1:18 for his results not to be substantially affected by this ratio.

The results of Kreisinger et al. closely parallel those of Kolodtsev, even though the fuel type and size were quite different. These authors concluded that their fuel beds, which were quite deep, acted as gas producers with the flue gases being rich in hydrogen and carbon monoxide. They also found that the oxygen was rapidly consumed within approximately 2 to 4 particle diameters from the ignition zone. Kreisinger et al. varied the air flow rate through the bed over almost as wide a range as did Kolodtsev. They found that within wide limits of the air flow rate there was practically no effect on the composition of gases within the bed. Thus, the measured burning rate found by these authors scaled directly with the air rate. They also pointed out that, since the variation of the air flow rate did not affect the composition of the gas issuing from the top of the bed, it was essential for secondary air to be added above the bed to effect complete burnout of combustibles. The above conclusions, which appeared in 1916, seem to be the first definitive statements backed by experimental proof of the necessity for secondary air for complete combustion.

The Underfeed Bed: The Work of P. Nicholls (24) and W. C. Marskell and J. M. Miller (94). Along with the work of Kreisinger et al., Nicholls' experiments have become classic in the field of combustion. His experiments were the first to give combustion engineers a clear picture of the processes of ignition and combustion at different positions on a traveling-grate stoker. Although Nicholls also studied the effect of underfire air and preheat on overfeed combustion, only his work on underfeed combustion will be discussed here. To do justice to this excellent study taken as a whole would require more space than available here and so only those parts of direct relevance to this work will be covered.

The apparatus used by Nicholls in these tests is shown in Figure 8. The underfire air was supplied by a blower and the flow rate measured with an orifice plate. The apparatus is very similar to that of Kreisinger et al. and differs mainly in the water-cooled top, which was necessary so that the composition of the flue gas could be measured to determine the burning rates. As an underfeed burning mode was being studied, an unsteady-state experiment had to be performed. Despite the drawbacks to this method, it was preferred over the difficulties of a continuous feed system. Temperature measurements were made with nine bare Chromel-Alumel thermocouples placed on the center line of the combustion pot. The height of each thermocouple was recorded by measuring from a crossbar over the furnace. These thermocouples were not used to measure the

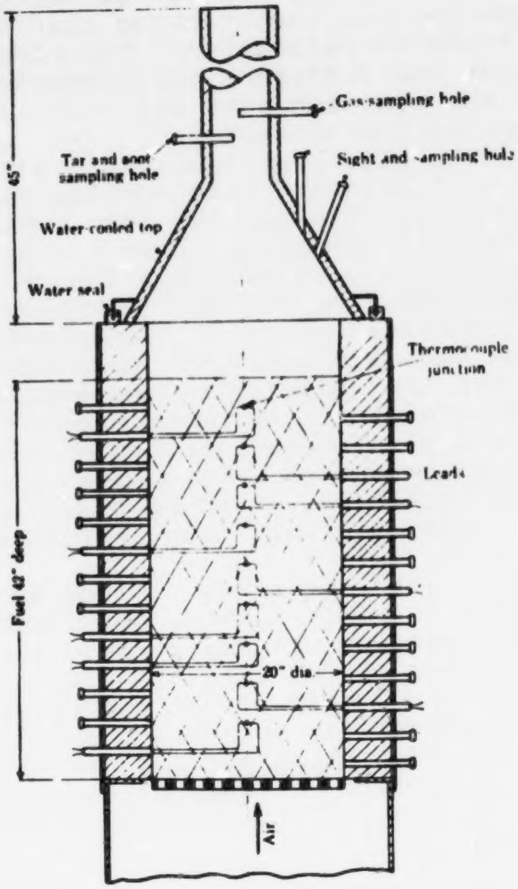
45"
Gas-sampling hole
Tar and soot sampling hole
Sight and sampling hole
Water-cooled top
Water seal
Thermocouple junction
Leads
Fuel 42" deep
20" dia.
Air

Fig. 8. Schematic of Nicholls' Apparatus for Underfeed Burning Tests (24)

temperature history at their respective positions within the bed, but rather for determining the rate of travel of the ignition front. For each test, the fuel was charged to the combustion pot and the thermocouples placed in position. The fuel was ignited with a fixed weight of charcoal and petroleum coke wetted with kerosene and spread over the top of the fuel bed. After the fuel was observed to have been ignited satisfactorily, the water-cooled top was put on and gas samples were taken continuously from the stack so that the instantaneous burning rates could be calculated. The time at which the ignition plane passed the different thermocouples was noted and from this data the ignition rate was calculated. Only for a few tests were detailed measurements of gas compositions and temperatures within the bed made. In these tests, the gas samples were taken with standard water-cooled gas probes and analyzed for CO, CO_2, CH_4, H_2, tar and soot. Nicholls tested for channeling of the underfire air close to the side walls by comparing gas compositions obtained from the center of the bed with average compositions from the stack. There was strong evidence that a large amount of the underfire air flowed preferentially up the side walls but probably not enough to seriously detract from the validity of the general trend of the results. Guarding against the occurrence of channeling is almost impossible, but this channeling could have been kept to a minimum, by Nicholls, by using a grate with a high pressure drop instead of the simple bar grate he employed. In any case, the very deep beds used certainly aggravated the problem.

Nicholls studied four different sizes of fuel (2 - 2 1/2 in., 1 - 1 1/2 in., and 1/2 - 1 in.) of different fuel types (coke, both high and low temperature; anthracite; petroleum coke, an ashless fuel; and four different bituminous coals). This array of fuels covered most of the different fuel types with respect to volatile matter, moisture content, and the fuels' proclivity to cake and form solid barriers to the flow of underfire air. The proximate analyses of the fuels can be considered to be close to those for similar fuel types in the study of Kreisinger et al.

Some typcial data obtained by Nicholls on the underfeed combustion of high temperature coke are shown in Figure 9. These results will be discussed in detail and the results on the other fuels referred to only as necessary. Figure 9 indicates that at low underfire air flow rates the rate of ignition was greater than the burning rate and consequently the depth of the live fuel bed continuously increased until the ignition plane reached the grate. As the underfire air flow rate increased, the rate of burning increased more rapidly than the rate of ignition and eventually the two rates became equal (point c for the 1 1/2 - 2 in. size coke). At air flows higher than this critical air flow rate, the rate of burning was

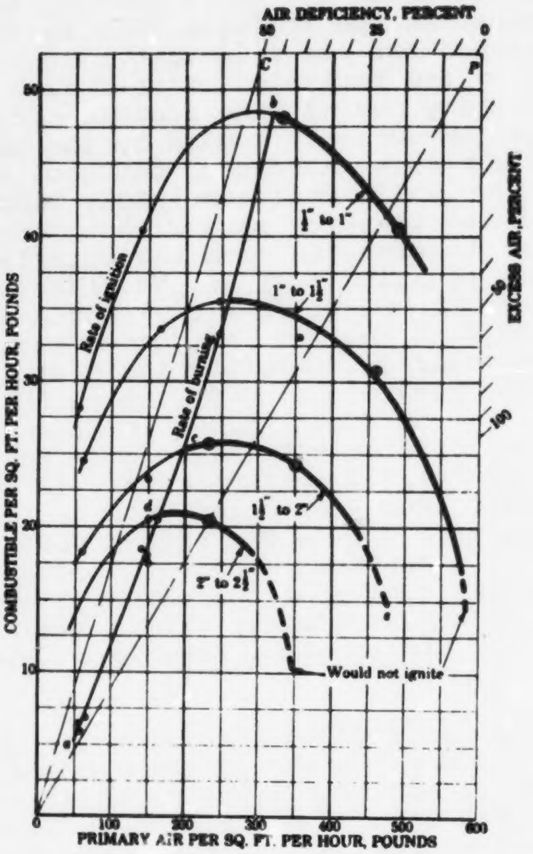

Fig. 9. Underfeed Burning, High-Temperature Coke: rate of ignition and rate of burning with rate of primary air and size of coke as variables. Data of P. Nicholls (24)

controlled by the rate of ignition, since the fuel could obviously not burn faster than it was ignited. The heavy solid lines define the region in which there was, to use Nicholls' term, equilibrium burning, under which condition the depth of the live fuel bed remains constant. As the underfire air was increased further, the ignition rate started to decrease and eventually a point was reached where ignition could not be sustained. The results on the different fuel sizes show that the ignition rate increased as the particle size decreased, increasing by a factor of about 1.5 for a halving in the particle size. The decrease in the ignition rate at the higher air flow rates is expected for the following reason. The fuel is ignited by conduction and radiation of heat from the hot combustion zone immediately behind the ignition front, while at the same time it is convectively cooled by the underfire air; as the underfire air flow increases, the cooling effect becomes dominant and eventually will completely hinder ignition. The increase in the ignition rate with a decrease in the fuel size would not be expected from the correlation of the dependence given in equation (13) of the effective thermal conductivity of a bed on the particle size. For smaller particles, it would be expected that the effective thermal conductivity would decrease and likewise the ignition rate. This was not observed and the reason probably lies in the criterion necessary for the ignition of a particle. It is common knowledge that it is far more difficult to light a large log of wood than a small one principally because there is less thermal inertial to overcome. For a piece of wood to ignite, it needs to have been heated to the extent that the rate of generation of pyrolysis products is great enough to provide a combustible gas in the vicinity of the particle surface. This condition is achieved more quickly with a small particle than a large one with the time scaling roughly as the square of characteristic radius.

The above discussion has centered on the situation observed in a fuel bed with no restriction to the ignition plane. The curves shown are, however, not restricted to this sole condition and in fact for the case of restricted ignition the fuel bed can be operated at any point within the envelope of the burning and ignition curves (i.e., anywhere inside curve ace for the 1 1/2 - 2 in. size fuel particle). An equilibrium bed will result at any point in this envelope. An increase or decrease in the feed rate, provided it does not cross ab, will result in a gradual change in the fuel bed thickness corresponding to the new feed rate. If the increase in feed rate crosses ab the thickness of the live fuel bed will increase continuously; if it crosses bd the thickness will not increase and the ignition plane will slowly be forced up by the fresh fuel below.

Changes in fuel bed thickness at different underfire air rates are reflected in the position of the burning rate with respect to the air deficiency or air excess lines. When the burning rate is not restricted by the ignition rate, Figure 9 shows that the burning rate is almost at a maximum. Following curve ce it can be seen that the thickness of the bed must have become less as the air flow rate was increased, and for burning rates to the right of line OP, oxygen had penetrated through the bed. For the 1 1/2 - 2 in. size particles the thickness of the bed at an air flow rate of 350 lb $hr^{-1}ft^{-2}$ was about 10 in. and it is therefore surprising to find oxygen breaking through the bed at this point. It is possible that the lower bed temperatures probably associated with this point caused a significant shift in the controlling mechanism of the carbon-oxygen reaction, causing the oxygen consumption distance to increase markedly over that predicted from mass transfer theory. It will be shown later that it is probably not possible for fuel bed temperatures to drop low enough for this to happen without having the fire die out and it is more likely that this is a manifestation of the degree of channeling that occurred near the side walls.

Figure 9 brings out the fundamental differences between the underfeed and overfeed modes of operation. For the underfeed mode, the maximum burning rate of any particular size of fuel is fixed, while for the overfeed mode any size of fuel can be burnt at almost any rate desired by adjusting the air rate and the bed depth.

The ignition rates for all the fuels studied by Nicholls at various air flow rates are presented in Figure 10. All the fuels were of the 1 - 1 1/2 in. size and the underfire air was kept at 80°F (the degree of preheat of the underfire air was found to markedly affect the rate of ignition). The dotted portions for the bituminous coals are extrapolations, since these fuels did not burn satisfactorily at these low air rates due to serious caking. All of the fuels, except the low temperature coke and the petroleum coke, reached a maximum rate of ignition; it can be presumed that for these cases further increases in the underfire air rate would have eventully caused the fire to be blown out. The situation with the petroleum coke and low temperature coke is not so clear, but, from the nature of the ignition process discussed above, it is likely that they would follow the same behavior.

Nicholls also presented a series of smoothed and averaged plots for the temperature profiles below the plane of ignition for various fuels of the 1 - 1 1/2 in. size and at a fixed underfire air rate. These profiles are depicted in Figure 11. The shape of the profile depends in a complex way on the effective thermal conductivity of the bed, the heat transfer coefficient

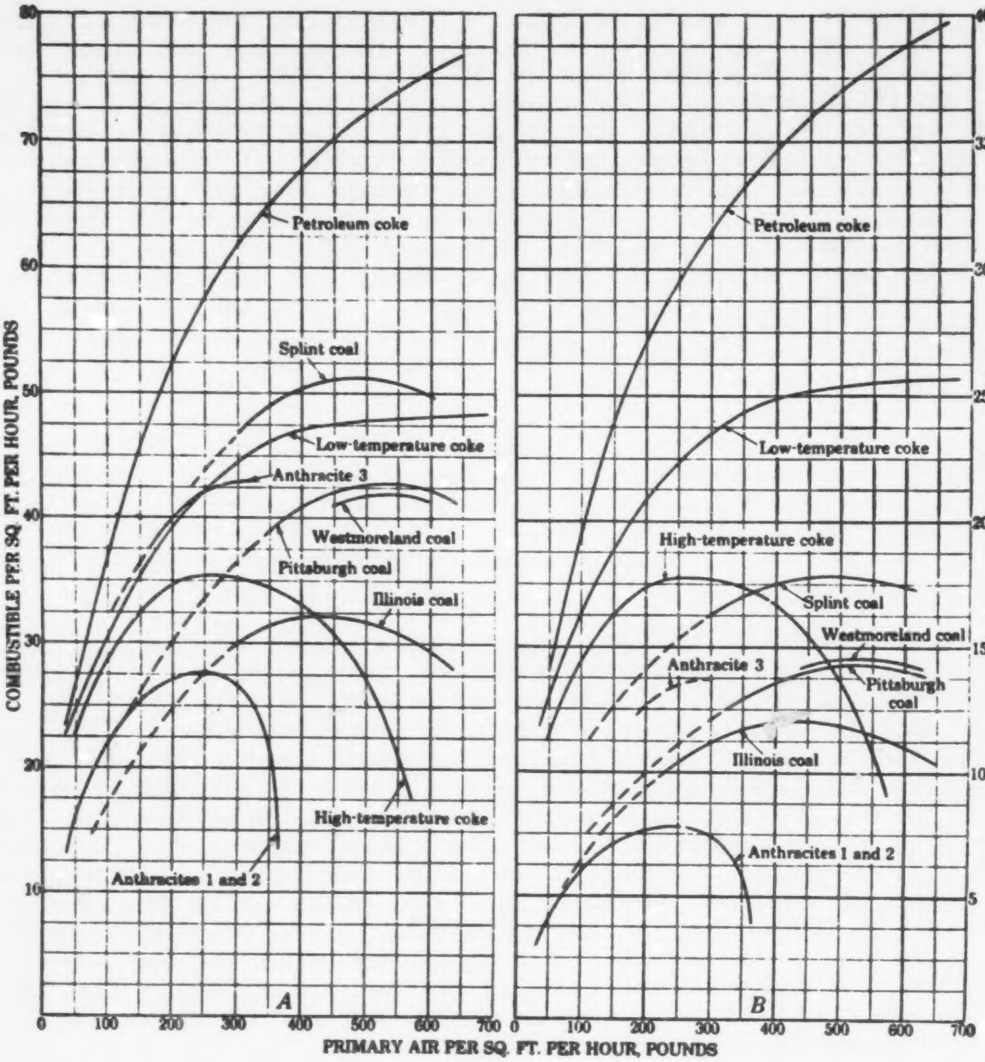

Fig. 10. Rate of Ignition of Different Fuels, 1 - 1½ in. size, 80°F air temperature. Data of P. Nicholls (24)

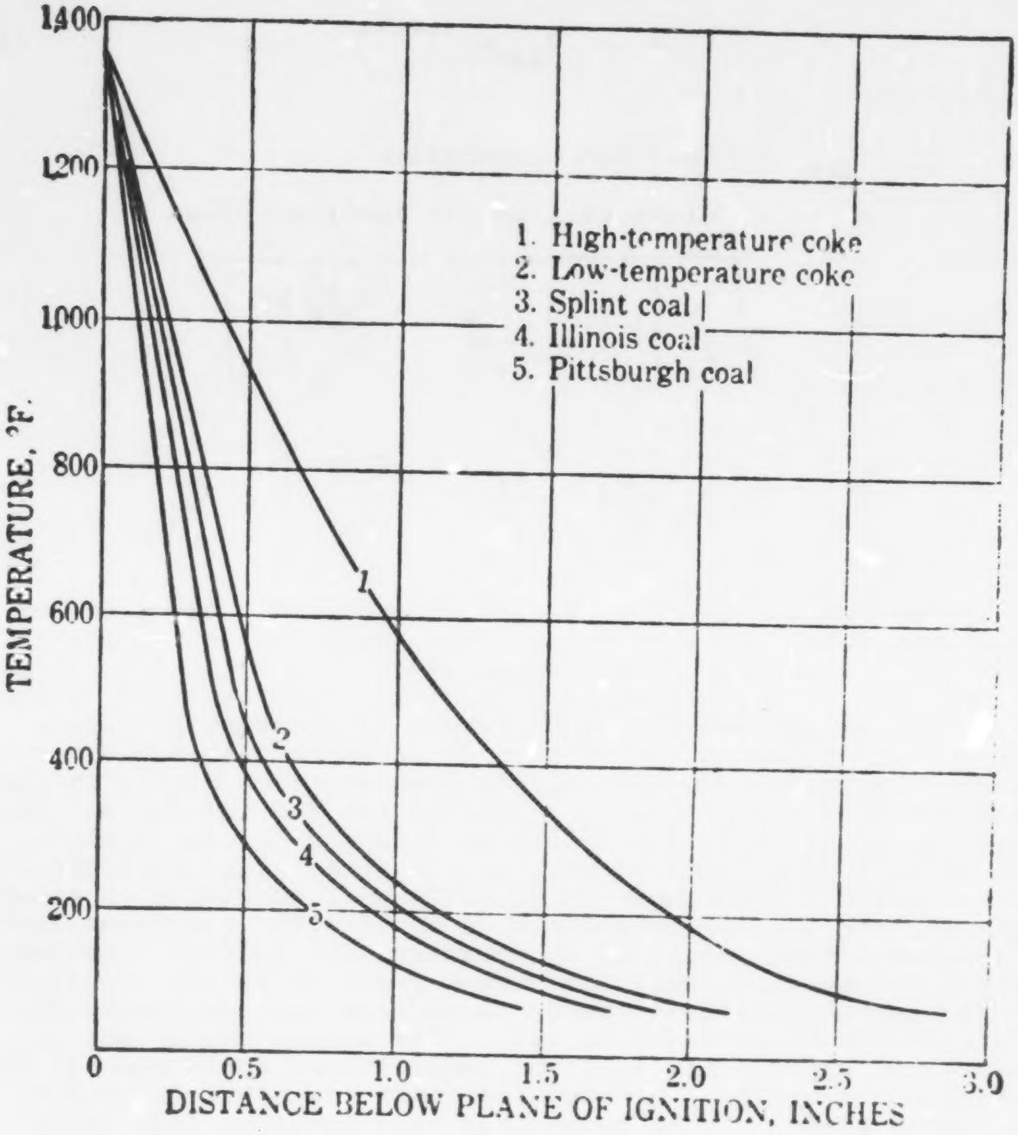

Fig. 11 Temperature Below Ignition Plane for Different Fuels. Data of P. Nicholls (24)

and the sensible heat fluxes of the air and fuel. The relationship, using equation (48) with the reaction terms set to zero and the boundary conditions $T=T_{ign}$ at $z=0$ and $T=0$ at $z=\infty$, is

$$T = T_{ign}e^{-(\alpha+\beta)z} \qquad (58)$$

where

T_{ign} = ignition temperature

z = distance from the ignition plane

$$\alpha = \sqrt{\frac{h_v}{K_s^E}\left[1 + \frac{1}{4}\left\{\frac{\dot{U}C_{p_s}}{\sqrt{h_vK_s^E}} + \frac{h_vK_s^E}{\dot{G}C_{p_g}}\right\}^2\right]}$$

$$\beta = \frac{1}{2}\sqrt{\frac{h_v}{K_s^E}}\left[\frac{\dot{U}C_{p_s}}{\sqrt{h_vK_s^E}} - \frac{\sqrt{h_vK_s^E}}{\dot{G}C_{p_g}}\right]$$

On the assumption that Nicholls' study (24) the ignition temperature was the same for all the fuels, all the terms in equation (58) except U were approximately constant for the different tests. On this basis, the higher ignition rates should have been associated with the steeper temperature profiles. Comparison of the data of Figure 10 shows that this was not always the case. The discrepancy probably lies mainly in the assumption of equal ignition temperatures for the fuels. The ignition temperature for a fuel will depend on its chemical and thermal properties as well as its size. Ignition temperatures were not determined by Nicholls and, as Figure 10 shows, were all arbitrarily considered to be 1378°F. For those fuels which had a lower ignition temperature than 1378°F, a certain amount of reaction would have taken place below the "ignition" front; these additional energy terms were not considered in the development of equation (58). For a true comparison of theory and experiment, ignition temperatures would need to be determined and T/T_{ign} plotted (ordinate against z (abscissa). It should also be recognized that equation (58) holds only for isothermal particles, and that in this region of the bed the shallower the temperature profile shown in Figure 11 the more closely this stipulation will be met.

The final piece of Nicholls' experimental work to be covered is his study of the temperature and gas composition profiles within an underfeed bed of high temperature coke. These are shown in Figure 12. The underfeed bed profiles were much the

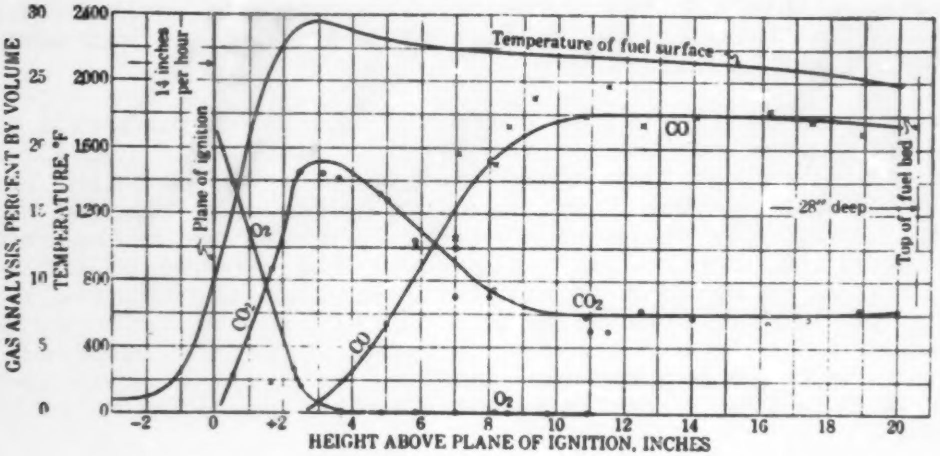

Fig. 12. Gas Compositions and Temperature Profile within an Underfeed Fuel Bed. High-temperature coke, 1 - 1¼ in. size, underfire air 160 lb $hr^{-1}ft^{-2}$. Data of P. Nicholls (24)

same as those for the overfeed bed, but the former were more spread out near the ignition front. In this experiment, the bed was deep enough for the CO/CO_2 ratio to reach equilibrium, as shown by the almost constant CO and CO_2 compositions. A similar test was performed for Illinois coal (Figure 13), which is rich in volatile matter (35%). In this test, the oxygen was much more rapidly consumed than in the test with high temperature coke and disappeared in a distance of about 1 1/2 in. from the ignition plane. This was presumably due to the greater possibility of reaction of oxygen with the larger amount of pyrolysis products generated by the fuel. Despite the large volatile content of the fuel, the concentrations of tars, soot and methane are quite small and appear mainly near the ignition zone. It is interesting to note that in this experiment only one third of the total heat of combustion was released within the bed. The other two thirds would have been released in the overfire section if the off-gases had been combusted with overfire air.

Marskell and Miller (94) studied the change in structure of a coal bed during combustion for varying combustion rates. The data were obtained from a modified underfeed combustion pot segmented into layers 1 in. deep which could be removed separately, allowing the coal contained therein to be analyzed. For the tests, the combustion process was stopped by cutting off the air at various intervals after lighting the fuel; the layers of burning coal were then quickly removed and quenched by placing the live coals into a metal container immersed in water. In these experiments the fuel used was a bituminous type of size 1/2 - 1/4 in. and the underfire air was preheated to 200°F.

Figure 14 shows the volatile and ash content of the six layers of the bed (the bottom layer is numbered "1") for two different air flow rates (190 and 750 lb $hr^{-1}ft^{-2}$). For both air rates, the volatile content fell from the initial value of 36% to zero, with the top layer being devolatized first. For the low flow rate (190 lb $hr^{-1}ft^{-2}$), the ash compositions in the layers rose to a steady content until all the volatile matter was driven off. At this stage, the ash content in the bottom layer started to rise and only after this layer was almost burnt away did the higher layers commence to burn out in quick succession from the bottom upwards. For the high air flow rate (750 lb $hr^{-1}ft^{-2}$), the picture was different. In this case, the ash content in each layer rose as the volatile content fell; thus the bed burnt out from the top down.

No burning or ignition rates were quoted by Marskell and Miller for these tests. However, for the degree of underfire air preheat (200°F) and the type and size of fuel used, Nicholls' (24) experiments suggest that for the low underfire air rate the ignition rate was greater than the burning rate; and for the

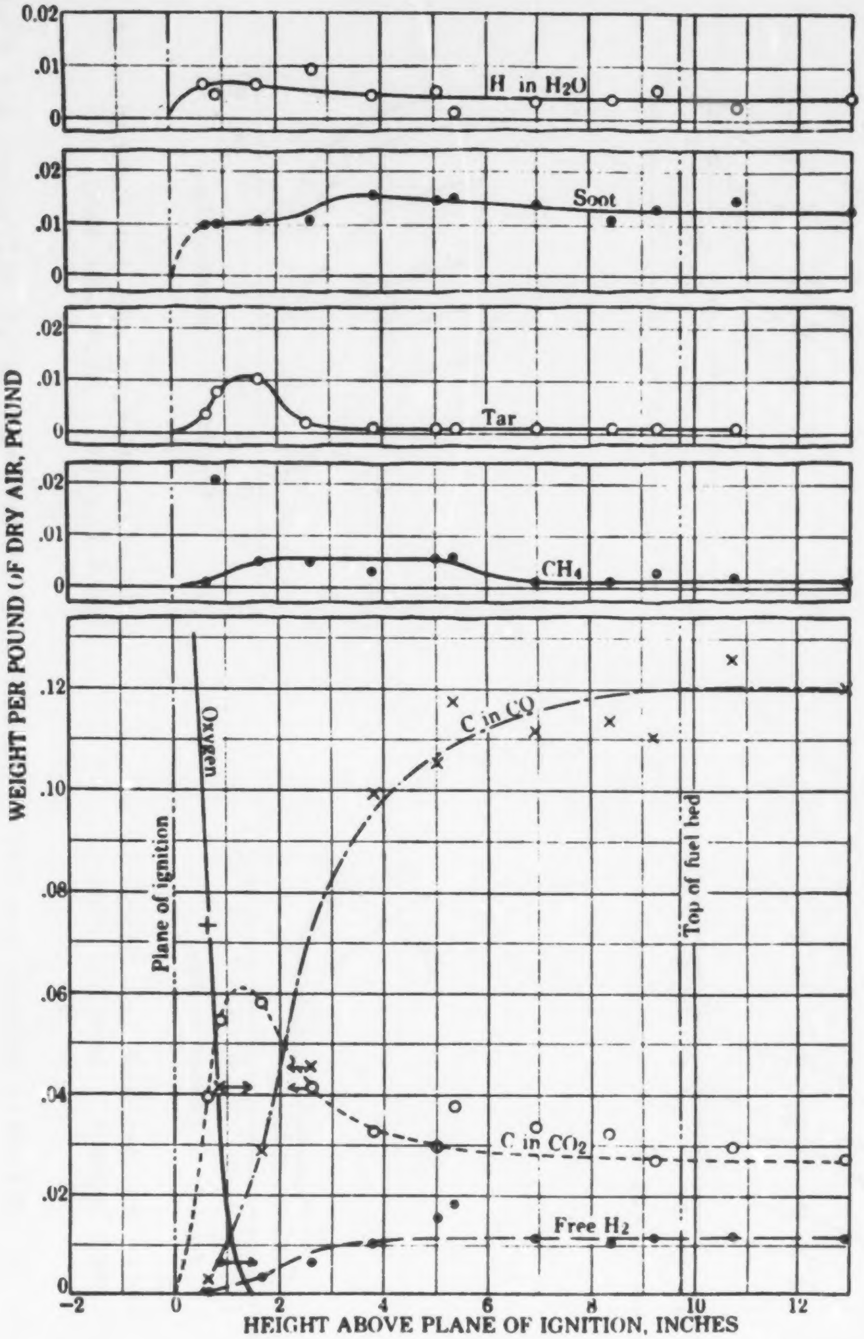

Fig. 13. Underfeed Burning, Action through Fuel Bed Expressed as Weight of Fuel Products Carried Per Pound of Dry Air Supplied, 3/4 - 1 in. Illinois Coal. Data of P. Nicholls (24)

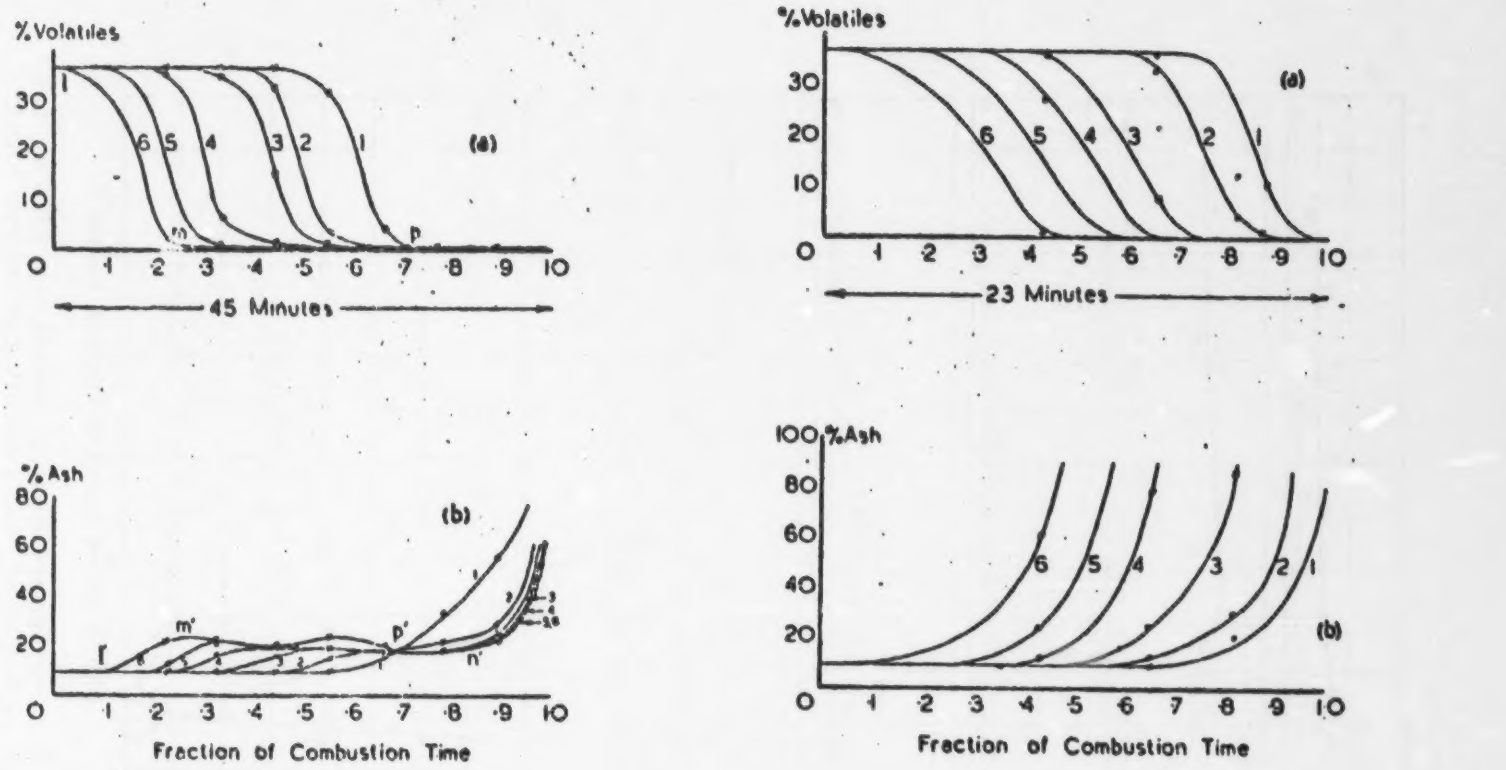

Volatile Matter and Ash Contents of Fuel Bed Layers. Low Air Rate

Volatile Matter and Ash Contents of Fuel Bed Layers. High Air Rate

Fig. 14 Volatile Matter and Ash Contents of Fuel Bed Layers at Different Air Flow Rates. Data of Marskell a[illegible] Miller (94)

high underfire air rate equilibrium burning (equal ignition and burning rates) was achieved. If this is correct, the burning zone depth increased with time in the low underfire air experiments while it remained of constant thickness for the high underfire air rate experiments. This hypothesis is consistent with the experimental observation that, at the low underfire air rates, active burning continued for some time after the volatile content had fallen to zero at the bottom of the bed, while for the high underfire air rate this condition was only achieved close to the end of active combustion. Using the experimental observations of Nicholls (24) and Marskell and Miller (94) it seems reasonable to conclude the following: (a) For low underfire air rates where the ignition rate is greater than the burning rate the burning depth will increase up to the point that the ignition front reaches the grate. From this time until the end of the run the bed will "burn out" from the bottom (where the oxygen concentration is the greatest) upwards, with the bed slowly settling towards the grate; (b) For high underfire air rates where equilibrium burning is achieved the burning will take place in a zone of constant thickness which moves slowly through the bed; there will be a gradual increase in the ash content of this zone as it moves towards the grate. It should be pointed out that although coal beds exhibit different behavior at these extremes of underfire air rate, for refuse burning high underfire air rates would be unacceptable because of the possibility of excessive particulate entrainment.

This discussion concludes the survey on the experimental work with coal, the purpose of which was to provide the necessary background for the following discourse on the various theoretical treatments of coal bed combustions. Although there is as yet no direct evidence to say that refuse beds will behave in a similar way to coal beds, the work of Kreisinger, Augustine and Harpster (95) with lignite, which contained 40% moisture and only 25% fixed carbon, showed results closely parallel to those for coal and suggests that this may well be the case.

Theoretical Treatment of Fuel Bed Combustion

Background Information. There have been very few papers (notably the work of Mayers (90, 96, 97), Thring (98, 99) and Silver (100, 101) concerned with developing theoretical treatments of fuel bed combustion. This situation is partly due to the extremely complex nature of the process and partly due to lack of real interest. The impetus for the first theoretical treatments came from attempts to improve the operation of the chain grate stokers which were used for power generation up until the 1940's, when the larger units began to be superseded by pulverized coal-fired plants. The gas producer is the only other process using solid fuel combustion or gasification in which there has been a theoretical interest; however, this process is not widely used. Incineration, then, has been the main unit operation over the past forty or fifty years in which solid fuel bed combustion is used. For many years, there was no incentive to improve incineration, but the realization that it will provide an important platform in the solid waste program and that effective design and control criteria are required in view of increasingly more stringent environmental constraints has caused a renaissance of interest in this field.

The development of fuel bed combustion models can start with three separate objectives: (a) a description of the burning rates; (b) a description of the ignition rates, or (c) a combination of both. Concern over the description of ignition rates is confined to the underfeed bed, where, as previously discussed, the ignition process may limit burning rates. Strictly, therefore, it is not possible to separate the burning and ignition rates in an underfeed system. In general, the ignition rate will be partly dependent on the relative position of various exothermic and endothermic reactions taking place within the fuel bed which must be determined by burning rate models. The processes are often separated, however, to make the problem more tractable.

Almost all of the fuel bed models presented in the literature to date can be placed in two general classes: those based in part on empirical relationships concerning the gross fuel bed behavior and those based on a description of the rates of material and energy transfer and of the fundamental reaction rates. Both classes have their drawbacks. The former suffers from the paucity of empirical information on fuel beds and the uncertainty associated with using these relationships in situations different from those under which they were derived. The latter, although a more rigorous approach despite the many simplifications which need to be invoked, depends heavily on an accurate knowledge of the physical and chemical properties of the fuel bed and of the chemical kinetics of the reactions involved. In addition, realistic boundary conditions need to be selected for the governing differential equations. The discussion on pages 25 - 30 has highlighted the difficulty of obtaining accurate data on the physical properties of fuel beds. The extreme difficulty in obtaining the requisite information on kinetics and the chemical and physical properties of fuel beds has forced the proponents of this type of model to select the values of these model parameters that make their calculated theoretical results fit particular experimental results. This approach obviously reduces the generality of the model and severely limits its applicability in systems other than the one to which it was originally fitted.

The fuel bed combustion models that have been presented in the literature and that are most applicable to this study will be discussed below, and some of their advantages and shortcomings pointed out. The work of Mayers (90, 96, 97) will be discussed, first, as illustrative of those models which utilize a fairly rigorous description of the material and energy transport within the fuel bed, coupled with kinetics to predict ignition and burning rates, fuel bed temperatures and gas compositions. Following this, the work of Thring (98, 99) and Silver (100, 101) will be covered. Thring's paper is limited to an attempt to calculate gas composition profiles in a fuel bed and the distance required for complete oxygen consumption in an underfeed coal bed from a knowledge of mass transfer rates in packed beds. Silver proposed that the concentrations of oxygen, carbon dioxide and carbon monoxide at different depths through the fuel bed could be calculated from a knowledge of the pressure drop across the fuel bed and argued that this pressure drop could be used to determine a friction factor which in turn could be related to the rate of mass transfer. In addition to his work on predicting gas composition within a fuel bed, Silver developed a criterion for the combustion stability of a fuel bed. Thring and Silver both attempted in their work to avoid the semi-empirical nature of Mayers' approach by relying on correlations of mass and momentum transfer within packed beds.

The M. A. Mayers Theory (90, 96, 97). The first attempt to develop a theoretical model of a fuel bed, to explain and complement the experimental investigations of Kreisinger, Augustine and Ovitz (23) and P. Nicholls (24), was by M. A. Mayers (90). The simplified fuel bed proposed by Mayers, shown in Figure 15, was thought of as a continuous solid, of a porous nature such that air could be blown through it. Thus, the bed was considered as a whole rather than as a collection of discrete pieces, an assumption that eliminated the necessity of dealing with temperature variations in the lumps of fuel. Variation of the properties of the bed was only considered for the vertical (z) direction; radial and angular variations were neglected. There was a flow of fuel in the bed, taken as positive in the z direction, and ignition was supposed to take place at some plane $z=z_1$ which could have any value from $z=0$ to $z=\ell$ (the depth of the bed). The differential equation, developed from an energy balance on a differential element of the fuel bed, describing the temperature of the bed as a function of z was stated as:

$$\frac{\partial}{\partial z}\left(K_s^E\frac{\partial T_s}{\partial z}\right) - \frac{\partial}{\partial z}\left(\dot{U}C_{p_s}T_s\right) - h_v(T_s-T_g) + \sum_{i=1}^{3} r_i^{eff}\Delta H_i - \phi(T_s) = \rho_s C_{p_s}\frac{\partial T_s}{\partial t} \tag{59}$$

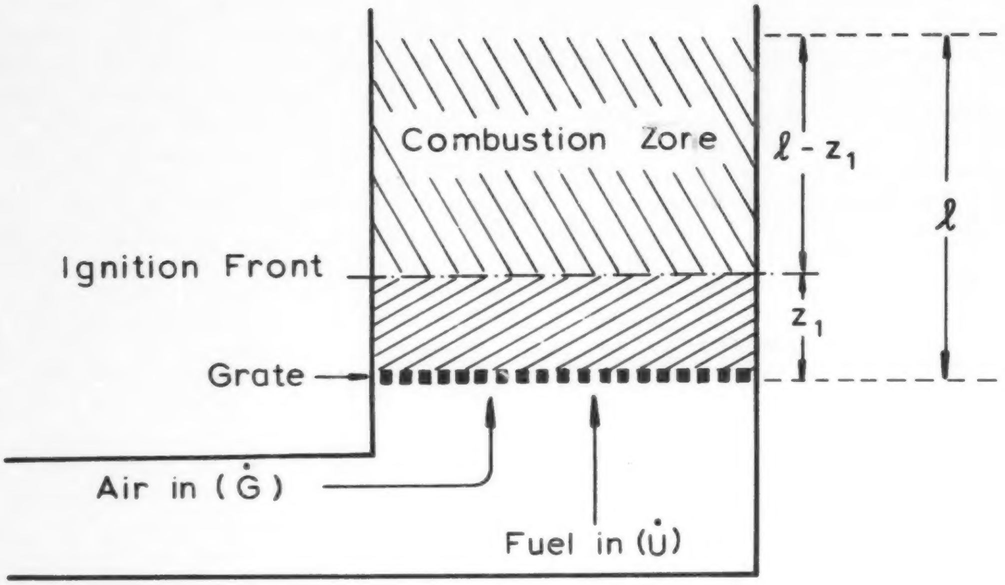
Combustion Zone
Ignition Front
Grate
Air in ($\dot{G}$)
Fuel in ($\dot{U}$)
$\ell - z_1$
z_1
ℓ

Fig. 15. Representation of Mayers' (90) Simplified Fuel Bed

As written, equation (59) rigorously describes the various modes of energy transfer within the bed given the three assumptions used. However, the equation had to be substantially simplified in order to obtain an analytical solution. The assumptions necessary were: steady-state operation; heat effects of all endothermic reactions were small; the solid was uniform and isotropic allowing constancy of C_{p_s} and h_v; the mass flow of fuel was constant throughout the depth of the fuel bed; a suitable average value of K_s^E , the effective bed thermal conductivity, could be found. Equation (59) then simplified to

$$K_s^E \frac{d^2T_s}{dz^2} - C_{p_s}\dot{U}\frac{dT_s}{dz} - h_v(T_s - T_g) + \sum_{i=1}^{2} r_i^{eff}\Delta H_i = 0 \qquad (60)$$

with $\sum_{i=1}^{2} r^{eff}\Delta H_i$ given by

$$\sum_{i=1}^{2} r_i^{eff}\Delta H_i = \begin{cases} 0 \text{ when } 0 \leq z \leq z_1 \\ \mu_1\Delta H_1 p_1(z, z_1) - \mu_2\Delta H_2 p_2(z, z_1) \text{ when } z_1 \leq z \leq \ell \end{cases} \qquad (61)$$

where μ_1 and μ_2 represent the rates of reaction $C + O_2 \rightarrow CO_2$ and $C + CO_2 \rightarrow 2CO$ respectively, at unit concentration of the reacting gases and on the basis of a unit volume of fuel bed; ΔH_1 and ΔH_2 are the quantities of heat liberated or absorbed in the two reactions, referred to unit weight of reacting gas, and p_1 and p_2 represent the fractional concentrations of O_2 and CO_2 respectively. Representing the function $\sum_{i=1}^{2} r_i^{eff}\Delta H_i$ in this way introduces two further assumptions: the two reactions $C + O_2 \rightarrow CO_2$ and $C + CO_2 \rightarrow 2CO$ are the only ones occurring within the fuel bed; and all the reactions take place in the solid phase.

Four additional equations plus suitable boundary conditions were required to specify Mayers' problem. A differential energy balance on the gas phase, excluding the contribution of axial conduction and assuming no gas phase reactions and steady-state operation, gave the following equation for the gas temperature:

$$\dot{G}C_{p_g}\frac{dT_g}{dz} - h_v(T_s - T_g) = 0$$

where $\dot{G}$ is the mass rate of gas flow per unit area of bed, assumed constant throughout the depth of the fuel bed, and C_{p_g} its mean specific heat. The equations describing the change in concentration with fuel bed depth of the various constituents in the gas phase were given by Mayers as

$$O_2 \quad : \quad \dot{G}\frac{dp_1}{dz} + \mu_1 p_1 = 0$$

$$CO_2 \quad : \quad \dot{G}\frac{dp_2}{dz} + \mu_2 p_2 = \mu_1 p_1 \quad \text{when } z_1 \leq z \leq \lambda \tag{63}$$

$$CO \quad : \quad \dot{G}\frac{dp_3}{dz} = 2\mu_2 p_2$$

where p_3 is the mass fraction of CO in the combustion gases. These equations assume that each reaction is mass transfer controlled or first order with respect to the reactant with a suitable average rate constant and that they are not constrained by equilibrium. In addition to the assumption about the rate controlling mechanism of the two reactions, these equations neglect any axial diffusion of the three species. The equations are formulated for steady-state operation and imply constancy of the gas flow rate.

Mayers was able to solve the above equations analytically with the boundary conditions described below. In setting up these boundary conditions the ambient temperature was taken as zero, and thus the calculated values of T_s represented temperature elevations above ambient conditions. The boundary conditions for equation (60) were given as

$$\frac{dT_s}{dz} - \left[\frac{\beta + \dot{U}C_{p_s}}{K_s^E}\right] T_s = 0 \qquad \text{at } z = 0 \tag{64}$$

$$\frac{dT_s}{dz} + \left[\frac{\gamma}{K_s^E}\right] T_s = 0 \qquad \text{at } z = \ell \tag{65}$$

where β and γ are equivalent radiation heat-transfer coefficients at the bottom and top of the bed, respectively. The quantity $\frac{\dot{U}C_{p_s}}{K_s^E}$ was included as a coefficient in equation (64) because of the necessity of providing sufficient heat at the bottom of the bed to raise the temperature of the incoming fresh fuel from the ambient temperature to that of the bed at z=0. These boundary conditions introduce further assumptions as they are not exact, since radiant heat losses are proportional to the fourth power of the absolute temperature. Mayers compensated for this error through the appropriate choice of the heat transfer coefficient. Although Mayers did not explicitly state that the values of K_s^E in equations (64) and (65) were different, it must be assumed that values were chosen which were representative of conditions at the top and bottom of the bed. In addition, the value of K_s^E for the bottom boundary condition would be expected to be a function of the position of the ignition front when the ignition front is close to the bottom of the fuel bed.

Only one boundary condition was needed for equation (62) and Mayers chose

$$T_g = 0 \quad \text{at} \quad z = 0 \qquad (66)$$

Finally, the three boundary conditions needed for equation set (63) were

$$\begin{aligned} p_1 &= p_1^* \quad \text{for} \quad z \le z_1 \\ p_2 &= 0 \quad \text{for} \quad z \le z_1 \qquad (67) \\ p_3 &= 0 \quad \text{for} \quad z \le z_1 \end{aligned}$$

where p_1^* is the mass fraction of oxygen in the underfeed air.

The gas temperature was eliminated from equations (60) and (62), as described on pages 32-39, to give a third order inhomogeneous differential equation (with constant coefficients); equation (63) was readily solved permitting $\sum r_i^{eff} \Delta H_i$ to be evaluated. Mayers' solution to the third order inhomogeneous equation is algebraically very complex and the interested reader is referred to the original paper (90).

Figures 16 and 17 show how the gas compositions calculated from the solution of equation set (63) and how the temperature of the solid phase of the fuel bed, calculated from the solution of the third order differential equation, compare to the experimental data of Nicholls (24). Considering the complex nature of a fuel bed, the agreement, at least superficially, is quite good. However, a few points need to be raised as to how the agreement was achieved.

The experimental temperature profile shown in Figure 17 (solid line) is for an underfeed bed with unrestricted ignition for high temperature coke of size 1 - 1 1/2 in. with an underfire air rate of 160 lb $hr^{-1}ft^{-2}$. The gas compositions of Figure 16 shown by the solid and dashed lines are taken from Mayers'

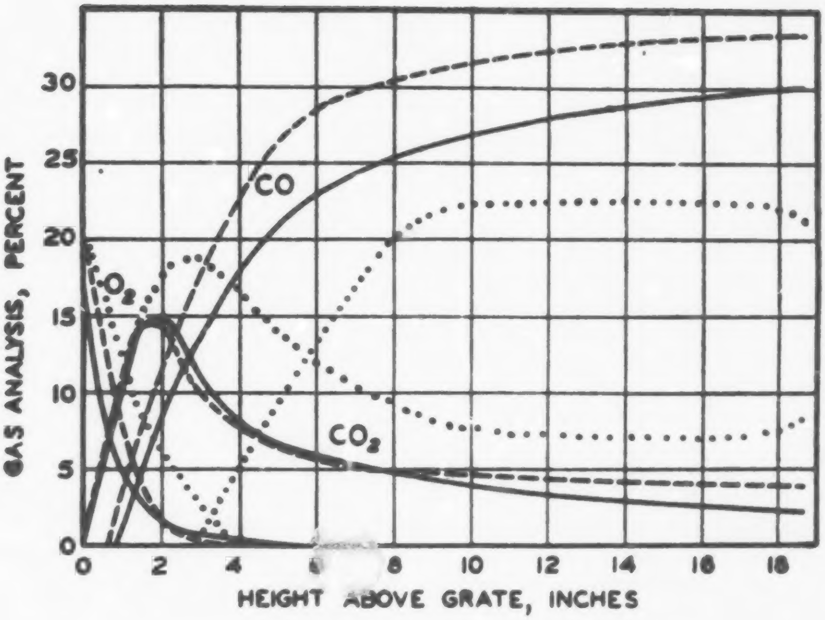

Fig. 16. Gas Analysis in a Fuel Bed. Solid curve plotted from experimental values for overfeed combustion of coke (24). Dotted curve plotted from experimental values for underfeed combustion of coke (24)· dashed curve plotted from calculated values (90).

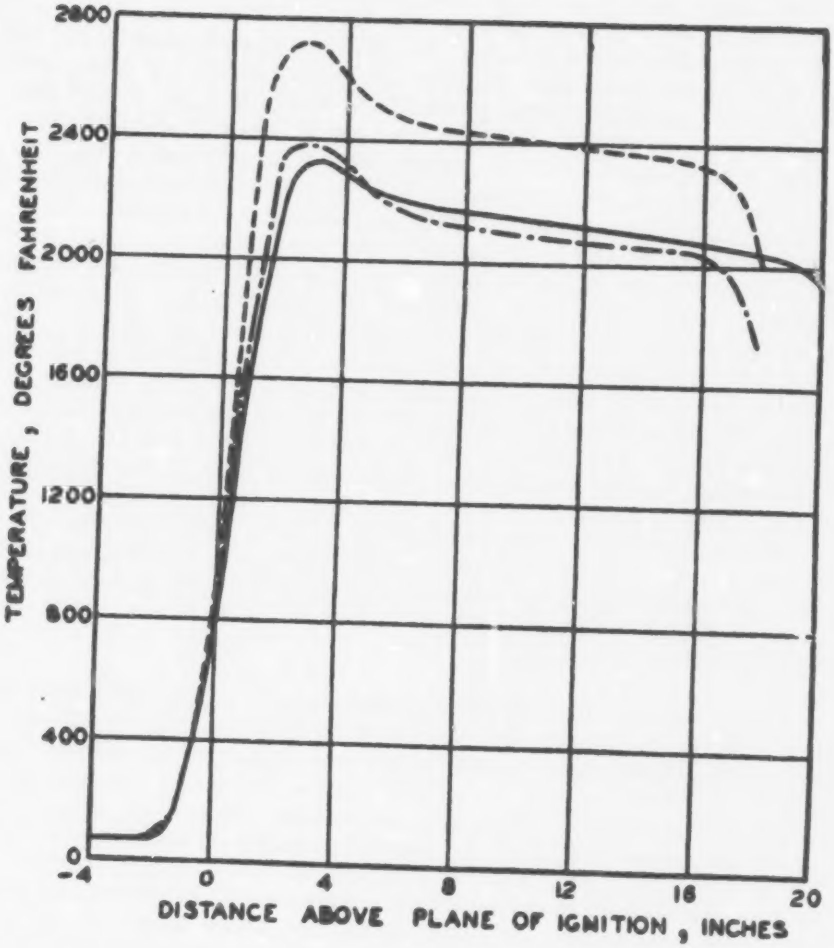

Fig. 17. Temperature in Underfeed Fuel Bed. Solid curve plotted from experimental values (24). Dashed curve plotted from values calculated for unrestricted ignition (90). Dot and dash curve plotted from values calculated for restricted ignition (90). Air flow rate = 160 lb $hr^{-1} ft^{-2}$, combustion rate = 25 lb $hr^{-1} ft^{-2}$, and rate of advance of ignition zone = 26.1 lb $hr^{-1} ft^{-2}$.

original paper (90), which implies that they were used to calculate the temperature profiles of Figure 17. The experimental gas compositions shown by the solid line in Figure 16 were, in fact, taken from Nicholls' data (24) for an overfeed bed of 1 - 1 1/2 in. coke with an underfire air rate of 149 lb $hr^{-1}ft^{-2}$ and preheated to 80°F. Nicholls (24) points out, in his study of underfeed combustion, that the gas composition profiles through the fuel bed are more spread out in this mode of burning than in the overfeed mode (see pages 46-59). The gas compositions taken from the same experiment as the temperature profile of Figure 17 was obtained are shown in Figure 16 by the dotted lines. The gas composition profiles define the function $\sum_i r_i^{eff} \Delta H_i$, which gives the heat release rates within the bed. Using the gas compositions from one set of data to calculate temperature profiles for comparison with another set of data is therefore not justified. The agreement between the theoretical and experimental temperature profiles is not particularly good (for most of the bed the theoretical temperatures are at least 20 percent too high); in addition, the heat losses from the top of the bed were over-estimated, probably in an attempt to try to lower the profiles. Any one-dimensional theory would be expected to predict temperatures that are higher than experimental because it would not take into account radial heat losses from the bed. The author feels that temperature measurements taken in the center of a combustion pot and near the ignition zone are to a certain extent insulated from side wall losses as a result of the larger quantities of air flowing up near the walls. The greater mass flux of oxygen at the walls causes higher temperatures at this location than at the center of the bed and helps minimize heat losses to the cold refractory walls.

For the calculation of the gas composition profiles Mayers needed to have estimates of the two quantities, $\mu_1/\dot{G}$ and $\mu_2/\dot{G}$. **He found calculated** values of $\mu_1/\dot{G}$ at different underfire air flow rates from the data of Kreisinger et al. (23) on overfeed beds. The results are shown in Figure 18. The scatter in the results is appreciable but this must be expected from the complexity of the processes occurring. However, there are some fundamental erroneous assumptions lying behind the presentation of the data in this way.

The two-zone theory of Mayers suggests that $\frac{\mu_1}{G}$ can be related to a mass transfer coefficient if it is assumed that the reaction is very fast at the fuel bed temperatures encountered. The two assumptions necessary for this relationship to hold for all fuel beds are that there is no other sink for oxygen consumption other than reaction at the fuel surface (i.e., combustion with CO or pyrolysis products) and that the effective surface area for mass transfer per unit volume of bed for all fuel beds of the same particle size is the same. The first assumption is more nearly correct for an overfeed bed than for an underfeed bed, except that there will always be CO present, which is a primary product of the carbon-oxygen reaction at high temperatures (89). A third assumption necessary for the relationship Mayers presented is that the reaction is not hindered by ash. In the data of Kreisinger et al., a plot of the log of oxygen concentration within the bed as a function of distance from the ignition front (suggested by equation (63)) often deviates from a straight line, indicating that there was in fact ash build-up at the bottom of the grate, against which insufficient precaution was taken. This fact probably accounts for some of the scatter in Figure 18.

Recognizing the assumptions above, another attempt was made, by this author, to recalculate the data of Kreisinger et al. (23) using a form more appropriate to calculating mass transfer data in packed beds than that suggested by Mayers (97). The results of this study are shown in Figure 19. The same difficulty with the nonlinear semilog plot of oxygen concentration versus distance as experienced by Mayers was found when analyzing the data. The problem of selecting a best straight line through the points plotted in the manner above accounts for much of the scatter in Figure 19.

Figure 19 stresses some of the inherent difficulties in analyzing any fuel bed data: namely, (a) the selection of an appropriate Reynolds Number complicated by the ambiguities associated with the values of D_p and μ; (b) the evaluation of the effective mass transfer area per unit volume of the bed, A_s; and (c) the determination of an average ρ_g to use in calculating the j_D factor. Figure 19 shows that the effective mass transfer rate for O_2 is considerably higher than that predicted by a typical mass transfer correlation, but somewhat lower than the line suggested by Mayers (97). From the earlier discussion, it would be expected that, because of the lesser possibility of oxygen reacting with pyrolysis products, the oxygen consumption rates in coke beds would be lower than those in bituminous coal beds. This was not observed under all circumstances, although the coke data on the average fell below the bituminous coal data. The pattern was different when comparison of the anthracite and bituminous coal was made; the anthracite data appeared to lie, on the average, above that of the bituminous coal. There could be a number of plausible reasons for this discrepancy, a likely one being varying CO/CO_2 ratios at the surface of the different fuels.

Returning to Mayers' work, the disturbing feature of Figure 18 is that the line Mayers drew through the data is weighted heavily in favor of data taken in situations where the oxygen concentration might be expected to fall much faster than predicted from mass transfer theory because of secondary gas phase reactions (the circles shown in Figure 18). The squares

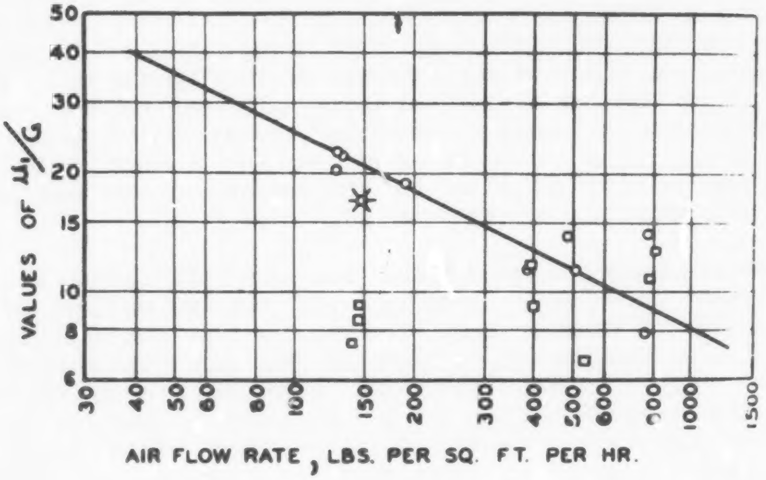

Fig. 18. Mayers' (97) Correlation of $\mu_1/\dot{G}$ [see equation (III-62)] as a Function of the Underfire Air Flow Rate. Circles indicate data for coal (23); squares indicate data for coke (23); star indicates data for coke (24).

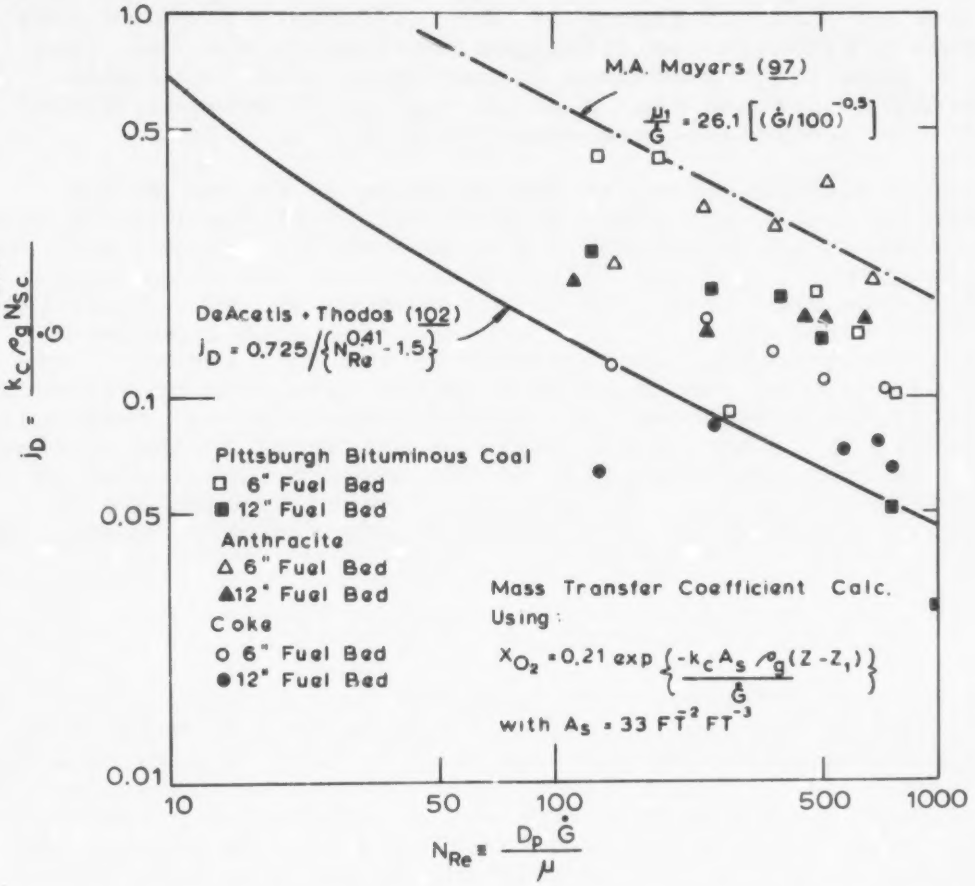

Fig. 19. Comparison of Mass Transfer Correlation and Data of Kreisinger, Ovitz and Augustine (123) for Oxygen Consumption in a Fuel Bed. (Analysis of Fuel: Pitt. Bituminous, 2.28% moist., 34.27% volat., 52.63% fixed C, 10.82% ash; Anthracite, 2.76% moist., 5.28% volat., 81.62% fixed C, 10.34% ash; Coke, 0.71% moist., 1.42% volat., 81.26% fixed C, 16.61% ash. Mean particle diameter = 1.25 in.)

on the plot shown at a value of $\dot{G}$ about 150 lb $hr^{-1}ft^{-2}$ are for coke, while the starred point is taken from Nicholls' (24) data from an overfeed bed, depicted as the solid line in Figure 16, which are, of course, the results Mayers' theory is attempting to predict. In the calculation of the parameter $\mu_2/\dot{G}$ similar fitting techniques were used. For the CO and CO_2 concentration curves shown in Figure 16, two different values of this parameter, effective in different portions of the bed, were used to make the theoretical curves agree with experiment. It is hardly surprising then that the agreement between experimental and theoretical gas composition was so close.

The above discussion raises the question as to how Mayers elected to select the other average values of the various coefficients in his equations. The methods he employed will be briefly covered. Mayers (97) discussed how the other model coefficients were estimated in a second paper and pointed out that they were chosen to make theory agree with experiment. The effective thermal conductivity of the fuel bed was estimated using an extension of an equation developed by Terres et al. (103) which proposed that the effective thermal conductivity across any plane in the fuel bed was equal to the average of the thermal conductivities of the air and fuel, weighted in proportion to the part of the plane covered by each and an equivalent conductivity due to black body radiation across the voids.

$$K_s^E = (1 - \delta)k_s + \delta k_g + 4\sigma T_s^3 d \times 10^{-8} \qquad (68)$$

where d is an effective mean radiation beam length. Terres et al. developed an experimental correlation of d with the bulk and true density of the particle and the bulk density of a dust that showed no increment in conductivity due to radiation. This correlation developed by Terres was a function of particle size. Terres et al. only worked with particles of 6 mm in size and Mayers had to extend the correlation of the mean beam length so that he could estimate d for the size coke particles that were used by Nicholls, which ranged from 1/2 in. to 2 1/2 in. diameter. Mayers used the correlation he developed and equation (68) to obtain an estimate of the bed thermal conductivity for the different size particles at different temperatures. Comparison between his results and those predicted from equation (13) shows that the two estimates differ by upwards of 50 percent and could both be quite badly in error because of the rather scanty data on the thermal conductivity of coke and coal particles. Mayers appears to have used a value of k_s of around 0.1 Btu $hr^{-1}ft^{-1}\,°F^{-1}$, while the author favors a value of at least an order of magnitude greater. Short of a detailed experimental investigation, there is no answer to this problem and the discussion serves only to point out the difficulties always encountered in trying to model fuel bed combustion.

For K_s^E to be a constant in Mayers' energy balance equation, he had to select an average value of T_s that would give a value applicable throughout the fuel bed; the value to pick is not intuitively obvious particularly as the fuel bed temperature rises sharply after the ignition front. Mayers circumvented this problem by balancing the average effective thermal conductivity and the average value for the solid-gas heat transfer coefficient. For his solution to fit Nicholls' data, he found that two quantities, each a function of K_s^E , h_v and the ratio of the specific rate (μ_1) of the reaction $C + O_2 - CO_2$ to the rate of flow of gas (G) through the fuel bed, had to assume certain values. The ratio μ_1/G was assumed to be accurately known from measurements of the rate of decay of the oxygen concentration in fuel beds. From these two independent expressions he was able to determine K_s^E and h_v. The value of K_s^E chosen in this manner provided the clue to the temperature level that should be selected in evaluating the mean bed conductivity; this temperature, around 1800°F, is somewhat lower than the peak bed temperature for restricted ignition (2300°F) or the temperature of most of the bed (2200°F). The heat transfer coefficient (h_v) calculated by this method was 6000 Btu $ft^{-3}hr^{-1}$ $°F^{-1}$; this appears very high, and on the basis of most heat transfer work, including that of Furnas (62), a value at least an order of magnitude lower would seem more appropriate. Mayers (97) points out this anomaly and suggests that gas radiation accounts for the difference. This is unlikely. Furnas' data were obtained by heating packed beds to temperatures up to 1100°C with combustion products having the approximate composition 5% CO_2, 10% H_2O, 10% O_2 and 75% N_2; the effect, therefore, on heat transfer by gas radiation would be expected to be about the same in both Furnas' experiments and a fuel bed. The high temperature data obtained by Furnas were for packed beds of iron ore. It could be argued that the external resistance to heat transfer of this material is different from that of coke. Recalculating Furnas' data using equation (6) still gives an estimated effective heat transfer coefficient for coke of around 200 Btu $hr^{-1}ft^{-3}$ $°F^{-1}$, well below the value of 6000 Btu $hr^{-1}ft^{-3}$ $°F^{-1}$ used by Mayers.

Mayers used his solution to calculate burning rates and ignition rates in fuel beds as a function of the underfire air rate. The results of these calculations are shown in Figure 20. The burning rates followed experimental results quite well because of the force-fitting of the theoretical and experimental gas composition profiles. As has been already mentioned, the calculation of the burning rate for a coal bed in a non-ignition controlled regime is relatively simple because equilibrium is often closely reached and variations in gas flow hardly affect the gas compositions. (In a refuse bed this is not so, a point which will be returned to later.) Mayers' ignition calculations were markedly different from Nicholls' results (see

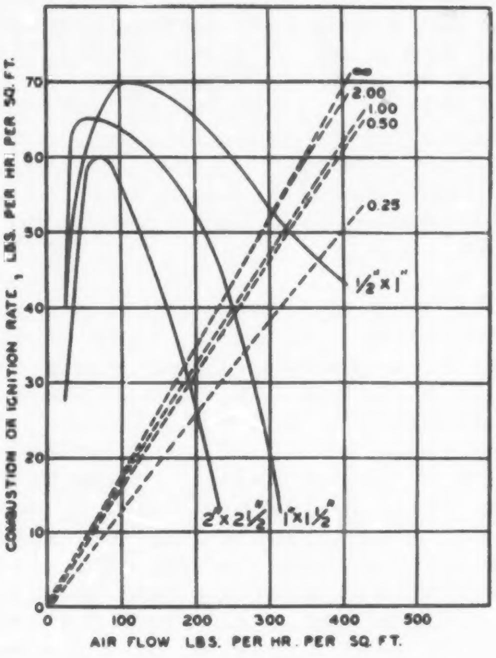

Fig. 20. Mayers' Theoretical Relationship between Combustion and Ignition Rates and Air Flow Rates (90). The solid curves give ignition rates for different particle sizes. The dashed curves give combustion rates for different bed depths in feet.

Figure 9) although they showed a similar trend with particle size. One reason the ignition rate showed a much sharper peak and a maximum at a lower air flow rate than observed experimentally was that in the formulation of the rate terms, no temperature dependence was considered. At both high and low air flow rates, the change in temperature level between the ignition plane and the plane of zero oxygen concentration will cause the average oxygen-carbon reaction rate to fall more into the chemical controlled regime, leading to a broadening of the exothermic reaction zone. This broadening will in turn lead to a lower ignition rate. Another reason may be that the ignition problem is an "internal" one, meaning that it may depend on the unsteady-state heating of the fuel particle. Such a phenomenon cannot be explained by an isothermal model. These points will be discussed in more detail on pages 94-106.

The M. W. Thring Theory (98, 99). Thring's theoretical work was concerned with calculating reaction rates in coal beds asasuming an idealized fuel comprising only carbon. Thring assumed that the physical processes of diffusion and mixing rather than chemical reaction were the rate-determining steps in the combustion process. The fuel bed was considered as a series of inter-connecting passages between particles through which the gas flowed and was rapidly mixed by turbulent eddies in the core of the void spaces. The chemical reactions taking place within the core of the voids were considered to occur at an infinite rate. Each particle was assumed to be surrounded by a boundary layer where the flow was laminar and through which the gases had to diffuse before they could react with the solid surface. The controlling resistance was therefore assumed to be the rate of diffusion across the boundary layer. The reactions, considered to be taking place as postulated by Bangham and Thring (104), were in three zones:

Zone I	Particle surface accessible to O_2	$C + 1/2O_2 \rightarrow CO$	(69)
Zone II	Gas phase region accessible to O_2	$CO + 1/2O_2 \rightarrow CO_2$	(70)
Zone III	Particle surface accessible to CO_2	$CO_2 + C \rightarrow 2CO$	(71)

This three-zone theory was in contrast to Mayers' two-zone theory, where, it will be recalled, the reactions were considered to be

$$C + O_2 \rightarrow CO_2 \tag{72}$$

$$CO_2 + C \rightarrow 2CO \tag{73}$$

The change in the molar flow rate of oxygen at any point within the bed from consideration of the reaction scheme stoichiometry is

$$0.034\dot{G}\,\frac{dP_{O_2}}{dz} = -\tfrac{1}{2}\,N_{CO} - N_{O_2} \quad \text{moles hr}^{-1}\text{ft}^{-2} \qquad (74)$$

where p_{O_2} is the partial pressure of oxygen, N_{CO} the number of moles of carbon monoxide diffusing away from the fuel surface, and $-N_{O_2}$ the number of moles of oxygen diffusing toward the fuel surface. The reaction scheme proposed implies that

$$N_{CO} = 2(N_{O_2} + N_{CO_2}) \qquad (75)$$

and that as long as any oxygen remains

$$p_{CO_2} = 0.21 - p_{O_2} \qquad (76)$$

The flux of A through the boundary layer is given approximately by

$$N_A = k_G(p_A^b - p_A^i) \quad \text{moles hr}^{-1}\text{ft}^{-2} \qquad (77)$$

where k_G is a suitable mass transfer coefficient. Using the fact that the concentration of the various reacting species at the solid interface is small in comparison with the bulk concentration, equation (74) can be rewritten as

$$0.034\dot{G}\,\frac{dp_{O_2}}{dz} = -k_G(p_{O_2} + 0.21) \qquad (78)$$

which on integration, using the boundary condition that at $z=0$, $p_{O_2} = 0.21$, gives

$$p_{O_2} = 0.42 \exp\left\{\frac{-k_G z}{0.034\dot{G}}\right\} - 0.21 \qquad (79)$$

Thus the oxygen concentration falls to zero in a finite distance z_0 and the rate of consumption of oxygen is greater than that predicted by the two-zone theory of Mayers (90) because of the allowance for the reaction of oxygen with carbon monoxide. The oxygen consumption distance from equation (79) is given by

$$z_0 = \frac{0.024\dot{G}}{k_G} \qquad (80)$$

Using reasoning similar to that above, Thring also developed equations for the changes in concentration of carbon dioxide and carbon monoxide after all the oxygen had disappeared. The results are shown in Figure 21, which also shows the rate of disappearance of oxygen calculated from the two-zone theory. The general shape of the gas composition curves followed that measured within fuel beds (see Figure 10), but there were obvious differences, namely that in the real bed some carbon monoxide appears before all the oxygen is consumed, showing that the mixing in the voids is not perfect, as assumed by Thring. However, this approach does have some merit in that the curves are calculated from basic principles and are not derived empirically from the data that the theory is required to explain, as was the case with Mayers.

Using the correlation of Gamson (105), which is similar to equation (13), for the rate of mass transfer within packed beds, Thring calculated the length z_0 of the oxygen consumption distance. This distance was found to be of the order of a few particle diameters, a situation which fits well with experimental observation. The variation of z_0 with gas velocity, particle diameter, void fraction and temperature can be found using equations (80) and (13) under the assumption that $j_D \approx j_H$. The result, with some approximation in the coefficient of the temperature dependence, is

$$z_0 \propto \frac{(\dot{G})^{0.41} \, (D_p)^{1.41}}{(1-\delta)^{1.41} T^{0.37}} \qquad (81)$$

Equation (81) shows the weak dependence of z_0 on the air rate and temperature and its somewhat larger dependence on the particle size; this result was anticipated in the discussion on pages 39-46.

Thring also presented a plot of various experimental relative carbon saturation factors (RCS factors) as a function of distance from the ignition front, normalized with particle size, and compared them to his theoretical calculations. These are shown in Figure 22.

The RCS factor was developed by Thring (109) as an aid in predicting coal bed gasification rates. The factor is the ratio of the amount of carbon gasified (as determined from the bed gas compositions) to the theoretical maximum amount that could be gasified per mole of underfire air. The maximum amount of carbon that can be gasified is limited by consideration of the carbon, carbon dioxide and carbon monoxide equilibrium at temperatures that can be practically achieved. At around 2000°F in an air-carbon combustion system, the equilibrium carbon monoxide content is approximately 34.6 percent, and does not increase significantly with further increases in temperature. On this basis, the RCS factor F_{RCS} can be readily shown to be

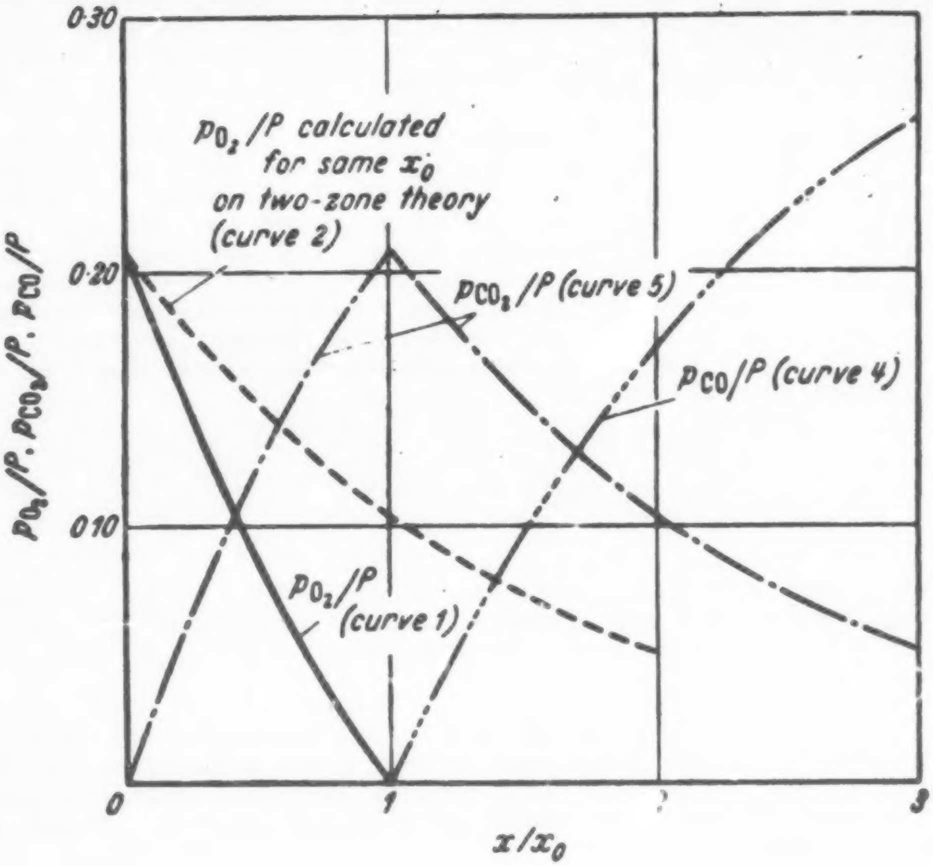

Fig. 21. Theoretical Gas Compositions Profiles Calculated Using the Three-Zone Theory of M.W. Thring (98). Also shown is the corresponding oxygen profile calculated using the two-zone theory of Mayers (90).

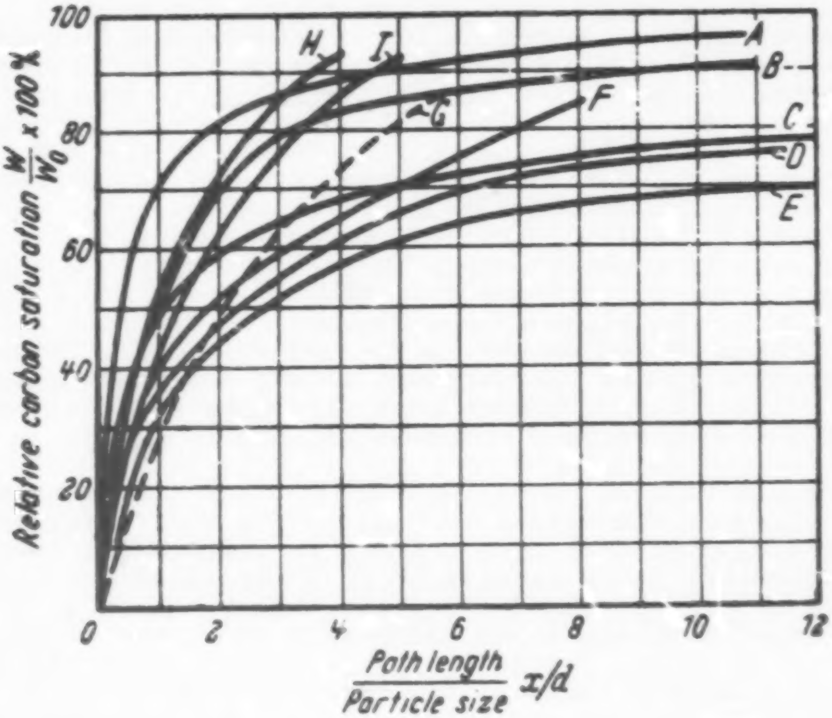

Fig. 22. Comparison between Theoretical and Experimental Relative Carbon Saturation Factors for Air-Coal Beds (98). Curve A, P. Nicholls, 600°F preheat (24); Curve B, P. Nicholls, 80°F preheat (24) Curve C, L.H.F. NIchols, 60 ft^3/min (106); Curve E, L.H.F. NIchols, 20 ft^3/min (106); Curve F, R.A. Mott and R.V. Wheeler (107); Curve G, M.W. Thring, theoretical curve for D_p = 3 cm, air flow rate, G = 20 lb hr^{-1} ft^{-2} using Löf and Hawley (108) mass transfer correlation; Curve H, same as G but based on Gamson (105) mass transfer correlation with fuel bed voidage, $\delta = 0.40$; Curve I, same as H but with $\delta = 0.50$.

given by

$$F_{RCS} = \frac{42}{41.9} \left\{ \frac{1 - 0.01881 \left[CO_2\right] - 0.04762 \left[O_2\right]}{1 + 0.01 \left\{ \left[CO_2\right] + \left[O_2\right] \right\}} \right\} \qquad (82)$$

where CO_2 and O_2 represent the measured concentrations of carbon dioxide and oxygen respectively in volume percent.

The RCS factor can be developed as a function of any two of the three combustion gases: Oxygen, carbon dioxide and carbon monoxide. The use of oxygen as one of the gases seems to be a general choice (36, 110) as it disappears rapidly within the fuel bed and makes computation of the RCS factor easier. The rapid disappearance of oxygen leads to uncertainty in the concentration profile within the bed and can cause some errors if the RCS factor is calculated for the gas close to the ignition front; however, the errors decrease once all of the oxygen has been consumed. Two points should be noted about the RCS factor. First, the convenience of casting the RCS factor into this particular form of equation (82) is only possible with a pure carbon-air combustion system. For a more typical incinerator fuel, such as wood or paper, it is not strictly possible to calculate a RCS factor from the carbon dioxide and oxygen concentrations because the excess hydrogen in the fuel will compete for part of the oxygen in the underfire air. Second, the RCS factor does not take account of any gas phase reactions (i.e., $CO + 1/2O_2 \rightarrow CO_2$) and as such cannot be used to give a measure of the heat release rates within the fuel bed.

Figure 22 shows that the experimental RCS factor increased initially at about the rate predicted by Thring's theory, but that at greater distances from the ignition front the theoretical RCS factor increased faster than the experimental curves. This is as expected since the theory, as shown above, fits experimental observations quite well up to the distance z_0. After this point, the discrepancy is readily explained, as the theory assumed that all the reactions taking place were mass transfer controlled and this is definitely not true for the $C + CO_2 \rightarrow 2CO$ reaction at fuel bed temperatures. Thus the CO concentration calculated under the assumption that the reaction was mass transfer controlled would increase more rapidly than if the reaction was partially kinetically controlled.

Some quite clear evidence, shown in Figure 23, that the $C + CO_2 \rightarrow 2CO$ reaction is not mass transfer controlled was supplied by Thring (99), who calculated CO_2 reduction rates from P. Nicholls' data (24). The dotted line ($R.R. \alpha T^2$) is shown for a typical increase in reaction rate with temperature under mass transfer controlled conditions. Obviously the actual temperature dependence of the Boudouard reaction shown by Figure 23 is more in line with a kinetics controlled reaction rate. The

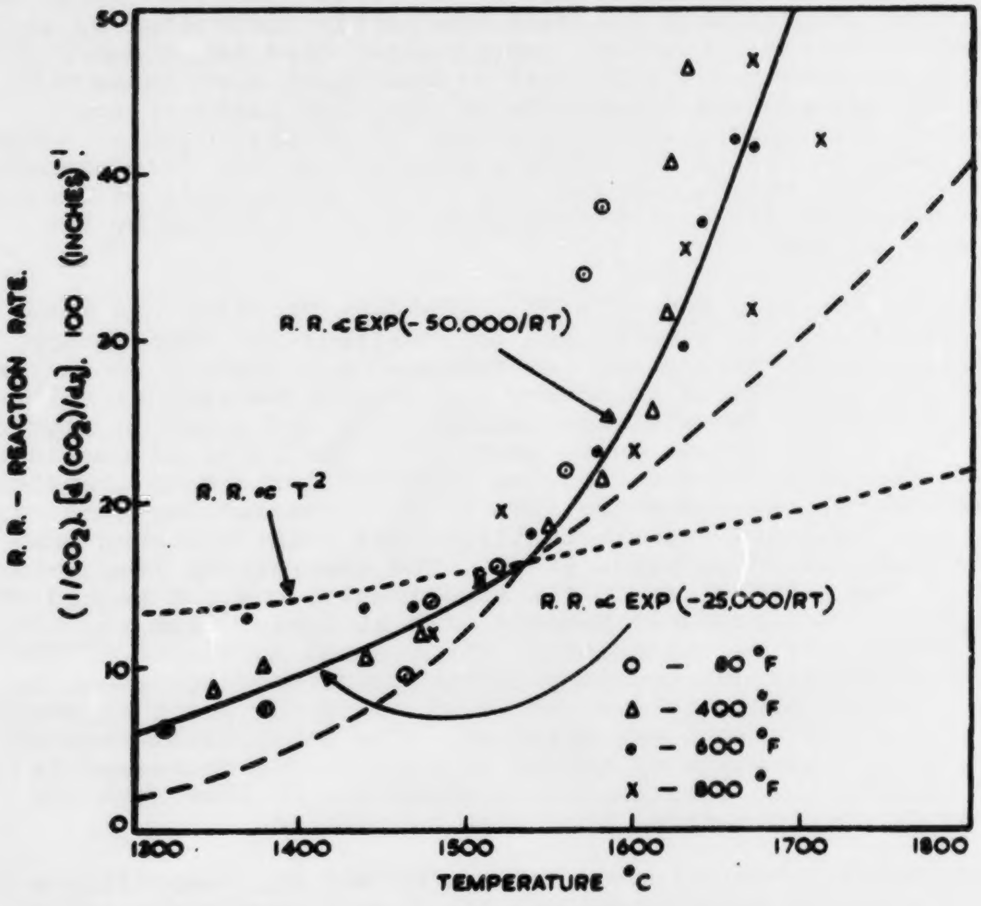

Fig. 23. CO_2 Reduction Rates in a Bed of 1 - 1-1/2 in. Coke Particles with Various Preheat Temperatures (99). Data of P. Nicholls (24).

experimentally observed jump in apparent activation energy at 1540°C has not been fully explained, but Essenhigh (110) has suggested that it was either a peculiarity of the experimental conditions or that large pores opened up, helping to lower any internal diffusional resistance that was present. Wheeler (141) and Weisz and Prater (142) have shown that the apparent activation energy under conditions where internal diffusion is important is one half that where these effects are absent. The jump in activation energy shown in Figure 23 follows this pattern and it is possible that, at the higher temperatures, the rate was controlled solely by chemical kinetics, while at the lower temperatures the rate was partly controlled by internal diffusion. However, experimental data taken under laboratory conditions with pure carbon (111) have indicated that the temperature dependence of reaction rates of the Boudouard reaction was even greater (50-58 kcal/g.mole^{-1}) than that shown in Figure 23. This suggests that the rate observed in a fuel bed may be controlled by physical as well as chemical considerations (i.e., the hindrance of the reaction by the presence of ash).

The D. B. Spalding Theory (73). Spalding utilized his mass transfer theory to predict gas compositions and temperature profiles within fuel beds. He compared his results to the experimental results of Kolodtsev (91). His theoretical calculations and Kolodtsev's experimental data are shown in Figure 24. The agreement was quite good up to the point of complete oxygen consumption, and then, as expected for a mass transfer based theory, the concentrations of CO increased far more rapidly than observed experimentally. This point has been adequately discussed on pages 75-82. The theoretical temperature profile was quite close to the experimental one but peaked at a higher value, probably because of heat losses from the bed unaccounted for by the theory. The general agreement of the temperatures was not too surprising, since good agreement between the gas compositions, at least up to the point of zero oxygen concentration, was obtained. The theoretical temperature, after the plane of oxygen concentration, decreased far more rapidly than experimentally observed, in line with the larger CO concentrations that were calculated.

Unfortunately, the agreement of the CO and CO_2 compositions up to the plane of zero oxygen was based on a completely arbitrary condition which arises in the following way. The Transfer number (B) can only be calculated from knowledge of the gas composition at the solid surface and in the bulk of the gas stream. In general, the solid surface composition is only easily calculated if it is assumed that the reaction is mass transfer controlled; the surface concentration is then close to zero. For carbon combustion, it can be postulated that the oxygen concentration at the surface is zero and that the CO_2

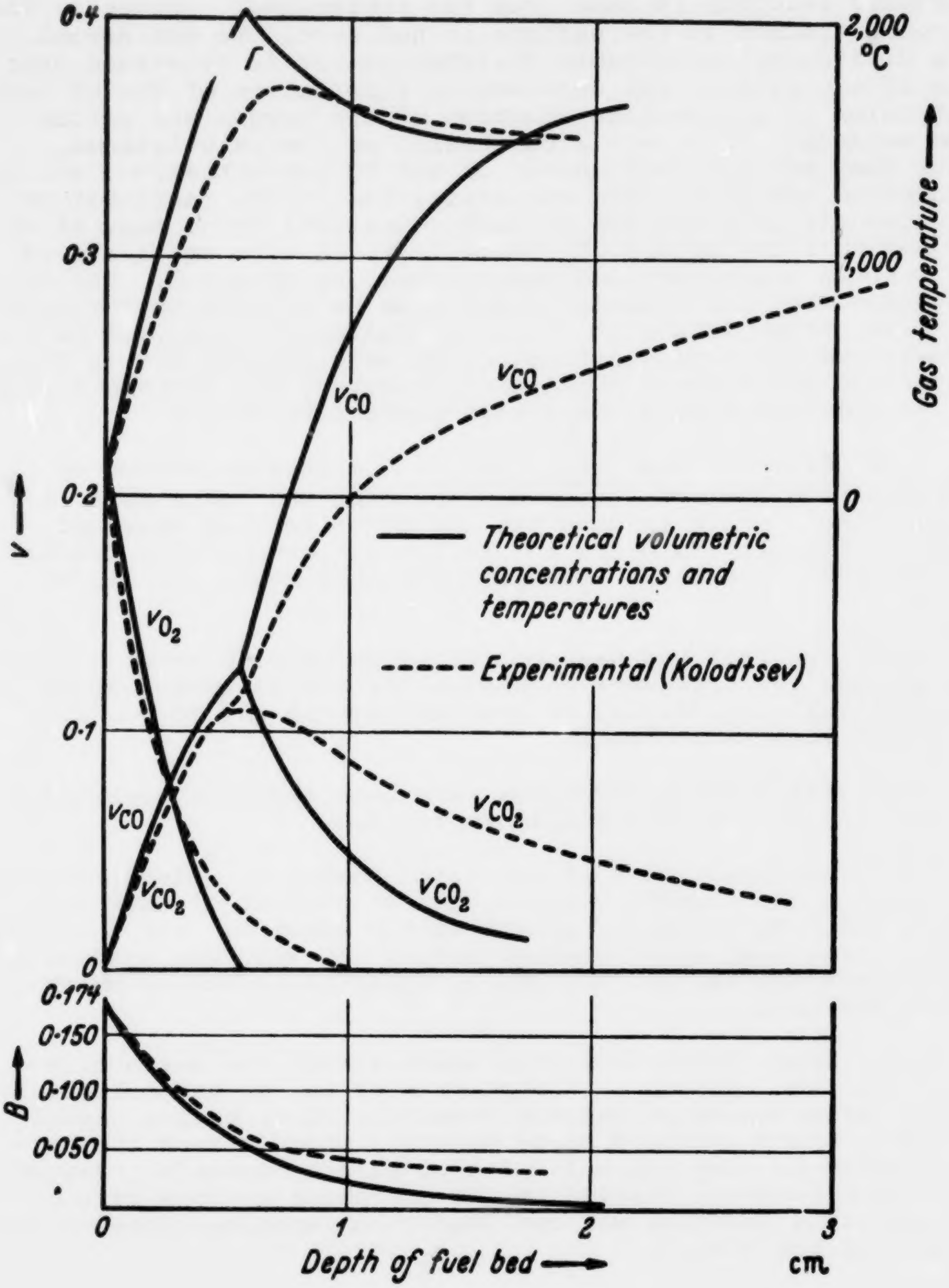

Fig. 24. Gas Compositions and Temperature in a Fuel Bed (73). Experimental data for bed of particles of diameter 0.32 cm, air velocity 150 cm/sec. Solid curves, theoretical volumetric concentrations and temperatures; dashed curves, experimental, from Kolodtsev (91).

concentration is close to zero (if it is assumed that the Boudouard reaction is mass transfer controlled). However, the CO concentration at the surface is not zero. To get around this difficulty, a suitable Transfer number (a conserved property of the system) can be found by elimination of the CO concentration by appropriate addition of the oxygen and carbon atom balance. This puts a constraint on the calculations, since they are now independent of the CO concentration, and an assumption has to be made concerning the CO/CO_2 ratio before gas composition plots can be made. Spalding found that if he assumed that the CO and CO_2 concentrations were equal, a good fit between experiment and theory could be obtained. Spalding has shown that the Transfer number can be related to Thring's relative carbon saturation factor. Spalding's analysis obviously has the same shortcomings as were pointed out in the discussion of Thring's RCS factor, however, and therefore cannot be considered as a completely predictive theory.

The R. S. Silver Theory (100, 101). A different method of approach from that of Thring and Spalding was taken by R. S. Silver (100), which invoked the analogies between mass and momentum transfer in order to predict gas composition throughout the bed. The basic assumptions of the model are listed below:

(i) The fuel bed was considered to be made up of a number of parallel irregular channels. It was assumed that it was legitimate to discuss an average channel and to consider it a tube with carbon walls.

(ii) All surface reactions were mass transfer controlled and gas phase reactions mixing controlled.

(iii) The fraction β of the total number of molecules flowing through the channel which struck an element of wall was proportional to the axial length of the element. The fraction of any particular species which struck the wall was assumed to be the same fraction of the local number of molecules which struck the wall.

(iv) Every oxygen molecule which struck the surface reacted with the carbon, a portion x of the oxygen molecules giving carbon monoxide and the remainder (1-x) giving carbon dioxide. Every carbon dioxide molecule which struck the carbon reacted to give two molecules of carbon monoxide. Oxygen and carbon monoxide reacted in the gas phase to form carbon dioxide; this reaction was confined to an annulus close to the surface of the channel.

There are two distinctions between Thring's model and Silver's model. First, the introduction of the variable x generalizes

Thring's model to fit the experimental picture of the carbon-oxygen reaction for which Arthur (112) and others have shown that the primary CO/CO_2 ratio can be expressed approximately by

$$\frac{CO}{CO_2} = 10^{3.4} e^{-12,000/RT} \tag{83}$$

Second, Silver's model utilized all possible reactions at all possible positions in the bed and did not restrict itself to the two-zone burning model of Thring. It will be recalled that in Thring's development CO_2 was assumed not to react with the carbon until all the O_2 was consumed.

If N_{O_2}, N_{CO} and N_{CO_2} are the molar fluxes of oxygen, carbon monoxide and carbon dioxide, and y_{O_2}, y_{CO} and y_{CO_2} their respective concentrations at any point l in a channel, then the assumptions above, coupled with the reaction stoichiometry, gives the following differential equations:

$$\frac{dN_{O_2}}{dl} = -\beta N_{O_2} \tag{84}$$

$$\frac{dN_{CO_2}}{dl} = -\beta N_{CO_2} + \beta N_{O_2}\left[1 - x + \frac{1}{2} y_{CO}(1 + x)\right] \tag{85}$$

$$\frac{dN_{CO}}{dl} = 2\beta N_{CO_2} - \beta N_{O_2} y_{CO}(1 + x) + 2\beta x N_{O_2} \tag{86}$$

Now, since the overall reaction scheme is not mole-conserving,

$$y_a = \frac{N_a}{N^i + 1/2N_{CO}} \tag{87}$$

where N^i is the initial number of moles present. Equations (84, 85, 86) can then be rewritten in terms of y'_{CO}, y'_{CO_2}, and y'_{O_2}, where

$$y'_a = \frac{y_a}{N^i} \tag{88}$$

The resulting equations are intractable as they stand, but by making an approximation that $y'_{CO} = y_{CO}$ Silver obtained a rather algebraically complex solution; the interested reader is referred to the original paper (100). From his solution to these equations Silver calculated the gas composition profiles through a bed as a function of u = βl. These compositions, for the case x=0, are shown in Figure 25. Physically, u represents the fraction of the total number of molecules flowing through the channel that have struck the carbon surface by the time point l is reached. Figure 25 agrees in general shape with experimental observation, but the maximum CO_2 content appears to be rather low. For values of x greater than 0, the CO_2 curve is depressed and the carbon monoxide curve rises more steeply. The asymptotic value of the CO concentration is, of course, 35% since there was no equilibrium constraint in Silver's model; this value is theoretically only possible at high temperatures but is a good approximation for most fuel bed conditions. The other interesting feature of Figure 25 is the exponential decay with distance of the oxygen concentration resulting from the solution of equation (84). The oxygen concentration in this theory, like Mayers', will never reach zero in a finite distance. This arises in Silver's model as a consequence of the assumption that the reaction $CO + 1/2O_2 \rightarrow CO_2$ takes place in a thin shell close to the carbon surface and competes for the βN_{O_2} molecules of oxygen supposedly about to strike the carbon surface. This points out a flaw in the formulation of equation (84), for by definition βN_{O_2} is the number of moles of oxygen striking the carbon wall, not just passing into a boundary layer. The proper formulation of the oxygen balance equation (84) using β as defined by the list of assumptions would lead to a much more complex set of equations. If proper allowance had been made for reaction in the void spaces, the oxygen would have been consumed in a finite distance. Silver argues that the lack of agreement between Figure 25 and actual measurements might lie in poor sampling procedures which allow the reaction $CO + 1/2O_2 \rightarrow CO_2$ to occur in the probe. It is difficult, however, to debate this point without much more detailed knowledge of the sampling procedures used in the experimental study.

For Silver's theory to be truly predictive, a method of calculating β had to be bound. Silver showed that β could be related to the friction factor for the bed in the form

$$\beta = \frac{2f}{d} \qquad (89)$$

where f is the friction factor and d is the diameter of an average pore in the bed. This result obviously applies best for N_{Sc} close to unity and is strictly only acceptable for a smooth tube. The friction factor can be found by experimentally measuring the pressure drop across a nonburning bed, but the question then arises as to which portion of the pressure drop is attributable to form drag (i.e., at corners, edges, etc.) and which portions to frictional drag. The momentum transfer that is involved with form drag is in no way connected with

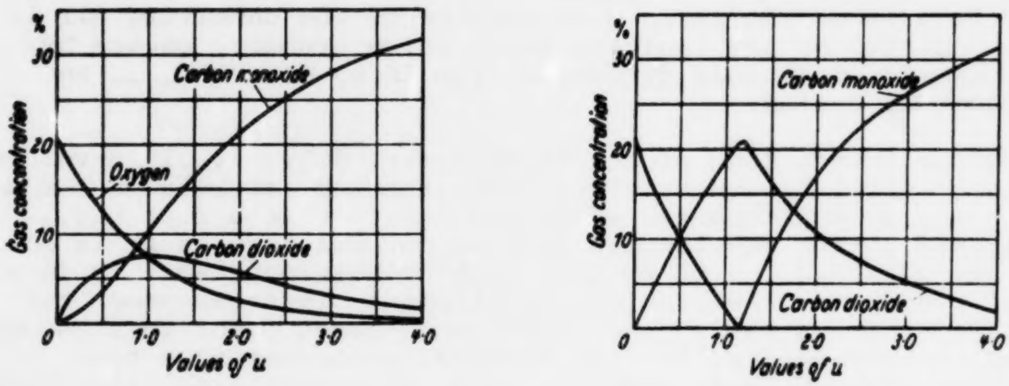

Figure 1a **Figure 1b**

Fig. 25. Gas Composition within a Fuel Bed Calculated by Silver (100).

mass transfer, which takes place at surfaces. Silver attempts to make some implicit correlation for the amount of form drag but the correction is only very approximate. When values of β where calculated from experimental results on pressure drops across a cold simulated fuel bed, the depth of the bed required to give a value of u=1 was found to be 4 1/2 in. for a fuel of the 1 - 1 1/2 in. size. This distance doubled for a fuel of 1 1/2 - 2 in. size, an increase far greater than that experimentally observed. The gas compositions of Figure 25 at u=1 are approximately correct for this depth from the ignition zone for a fuel of the 1 - 1 1/2 in. size, but the oxygen concentration is much higher than typically observed. The calculation of β, based on a correlation of mass transfer in packed beds as a function of pressure drop, is a weak link in this theory because of the difficulty of adequately correcting for form drag. Even the usual j_D correlations of mass transfer in packed beds are rather suspect when applied directly to a fuel bed because of the rapid acceleration of the underfire air in the vicinity of the ignition zone, which probably causes hydrodynamic conditions different from those occurring in an isothermal system.

From the foundations of his first paper, Silver (101) developed a theoretical treatment of the temperatures attained in combustion and a condition for sustained ignition in a fuel bed. Only the latter development will be covered here as it is one of the few theories which deal with combustion stability in a fuel bed. From the previous development, it as assumed that all molecules striking the carbon wall react. For this assumption to have been valid, the chemical rate must have been greater than the mass transfer rate; on a unit area basis this can be expressed as

$$r \cong A Y_{O_2}^{n} e^{-E/RT} > \frac{\beta Y_{O_2} N^{i}}{\Pi d} \qquad (90)$$

Equation (90) is written for a region close to the ignition plane where $Y_{O_2} = Y_{O_2} = 0.21$. Assuming that the reaction of O_2 with CO produces a thin flame zone close to the wall of the channel, the heat loss from this zone can be written as

$$Q^{loss} = \Pi d h_s (T_f - T_s) + \Pi d h_s (T_f - T_g) \qquad (91)$$

where

T_f = flame temperature

T_s = solids temperature

T_g = gas temperature

h_s = heat transfer coefficient, assumed equal to both gas and solid

The rate of heat generated by reaction, assuming chemical kinetics control, is,

$$Q^{gen} \cong \Pi d A y_{O_2}^{n} e^{-E/RT} \Delta H_{O_2} \qquad (92)$$

where ΔH_{O_2} is the heat of reaction of oxygen with carbon monoxide per unit weight of O_2. For sustained combustion

$$Q^{gen} \geq Q^{loss} \qquad (93)$$

or

$$A y_{O_2}^{n} \Delta H_{O_2} e^{-E/RT} \geq h_s(T_f - T_g) + h_s(T_f - T_s) \qquad (94)$$

Silver showed that the term on the right-hand side of equation (94) was in fact equal to $\frac{\beta Y_{O_2} N^1}{\Pi d}$ and concluded that for a fire to exist the temperatures had to be great enough for the chemical kinetics not to be a controlling factor. This appears to have been the first quantitative statement that has been published concerning the phenomenon of combustion stability in a fuel bed. Silver's development will not be covered in detail here as a discussion (which is somewhat more general than this approach) on fuel bed combustion stability will follow on pages 113-118. Briefly, the development required that h_s be related to β using the Reynolds analogy for the relationship between h_s and the friction factor, and that T_g could be approximated as a linear function of T_s.

Experimental and Theoretical Work on Refuse Combustion

The Experimental Studies at the Bureau of Mines (26, 27, 28). The Bureau of Mines pioneered some of the first small-scale experimental work in incineration about fifteen years ago. Their work has been concerned primarily with the testing and development of the vortex incinerator (27, 28), so called because the combustion air (almost all supplied above the bed) is fed tangentially into the overfire region. The main concern of the Bureau of Mines was the complete combustion of the volatiles distilling off the bed, and thus the major experimental effort was concentrated in the gas phase overfire region. From their most recent data (28), it appears that burning rates of 16 - 30 lb $hr^{-1}ft^{-2}$ of bed area are achievable with this system when using a standard synthetic refuse containing 29% moisture, 56% volatile matter and 12% fixed carbon. Burning rates at the lower end of this range were those most commonly reported. In these tests a very small fraction of the total air requirements for combustion (approximately 5%) was supplied as underfire air, but from the composition and temperature profiles above the bed it was likely that a portion of the cold overfire air, still with some oxygen content, spiralled down the side of the unit and then flowed back up through the center of the bed. The extent to which this will occur can be determined from a momentum and buoyancy force balance and is roughly proportional to $L^{1/2}$ and to $1 - \frac{T_c}{T_h}^{\,1/2}$ where T_c is the cold gas temperature at the walls, T_h is the hot gas temperature at the center of the unit, and L is a characteristic height.

The only work that the Bureau of Mines has done on fuel bed combustion has been with the equipment shown in Figure 26. The unit was divided into two sections which were joined together with a water seal. The bottom section, which contained the fuel bed, could be weighed throughout the course of combustion with the scale. The temperature profiles throughout the bed were measured with Chromel-Alumel thermocouples inserted through the insulating walls at regular intervals above the grate. The underfire air (sometimes not used) was supplied by a blower through the grate supporting the fuel bed. The overfire air was supplied tangentially from ports at a fixed height above the bed. To perform a test, the two sections were separated; the bottom section was charged with fuel and the thermocouples inserted into the bed. During this time, the top section was preheated with the gas burners. When the temperatures in the top section refractories had stabilized, the two sections were joined together and the progress of combustion was monitored by noting the change in weight of the bottom section and taking gas samples from the stack. No auxiliary fuel was used in any of the tests.

The fuel used in these experiments was composed of wood chips (3/4 in. square), newspaper, corrugated carboard (1/4 - 2 in. strips), and leafy vegetables such as lettuce and cabbage (3/4 in. square). The moisture content of the fuel was adjusted to either 25 or 50 percent moisture by varying the proportion of leafy vegetables.

Typical temperature-time profiles from one of their tests are illustrated in Figure 27, which shows distinct plateaus when the temperature at each thermocouple reached 212°F, corresponding to the vaporization of the moisture. When vaporization was nearly completed, the temperature rose quickly and the fuel ignited rapidly. From this type of data the rate of travel of the evaporation front and the ignition could be calculated; a typical result is shown in Figure 28, along with the corresponding weight loss. For these calculations, the rate of travel of the drying front was determined from the position of the leading edge of the drying front and the rate of travel of

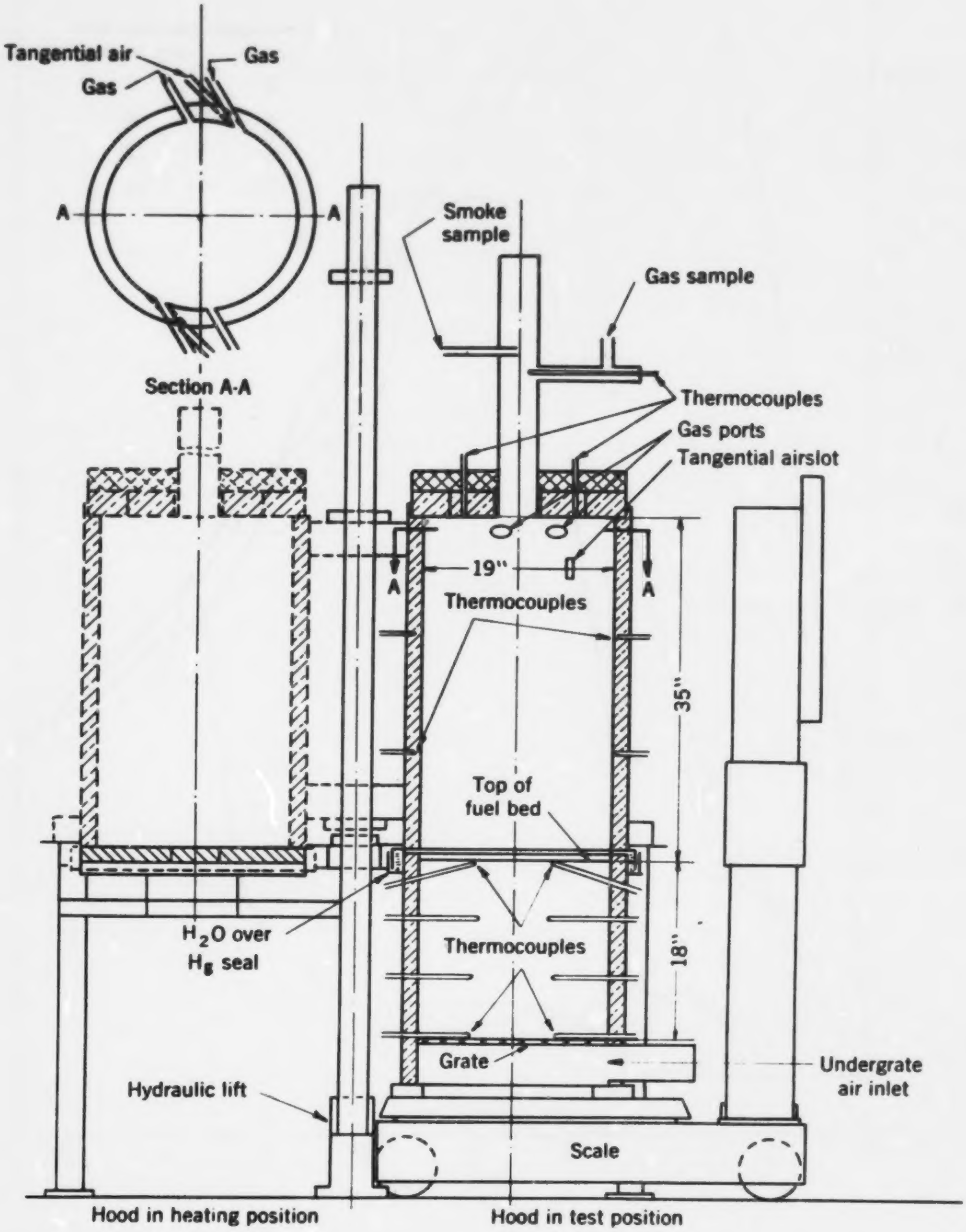
Tangential air
Gas
Gas
A
A
Section A-A
Smoke sample
Gas sample
Thermocouples
Gas ports
Tangential airslot
A
A
19"
Thermocouples
35"
Top of fuel bed
H_2O over H_g seal
Thermocouples
18"
Grate
Undergrate air inlet
Hydraulic lift
Scale
Hood in heating position
Hood in test position

Fig. 26. Apparatus Used by the U.S. Bureau of Mines (26) for Studying Combustion Characteristics of Refuse.

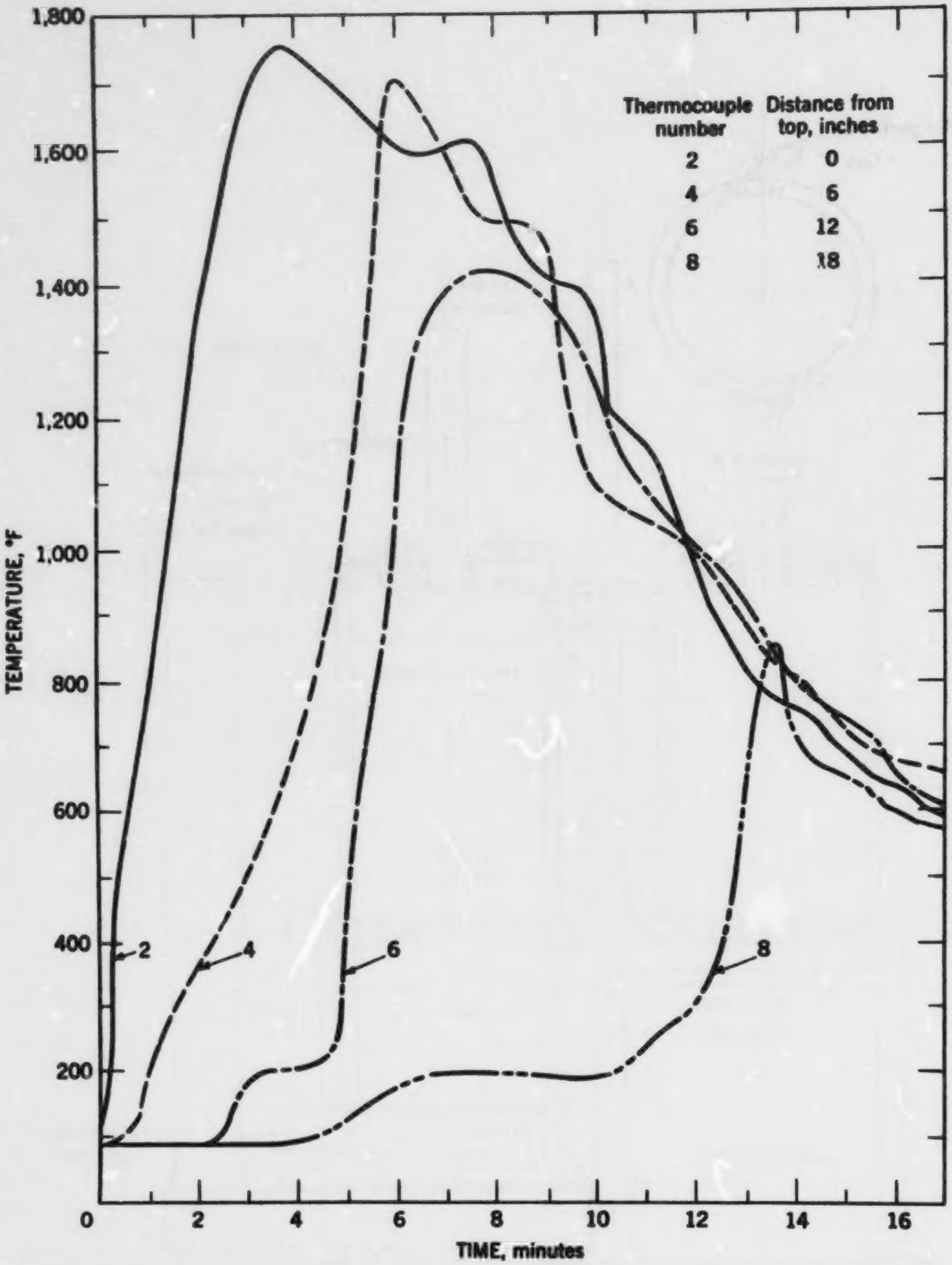

Fig. 27. Bed Thermocouple History, Incineration of Synthetic Feed with 50 percent moisture, total air rate 61 cfm, roof temperature 1800°F, (27).

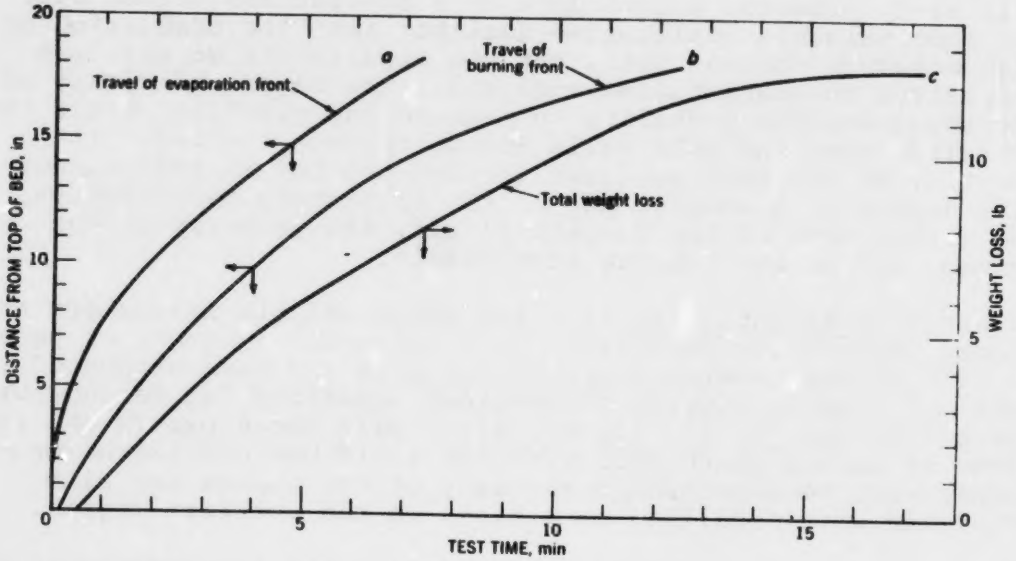

Fig. 28. Travel of Evaporation and Burning Fronts and Total Weight Loss as Functions of Test Time in a Typical Bed of Synthetic Refuse Having a Moisture Content of 50 Percent and a Bed Depth of 18 Inches (27).

the ignition front from the propagation rate of the 500°F plane through the bed. From Figure 28, it appears that the burning rate was at a maximum at the beginning of the experiment and continuously decreased throughout the duration of the run. However, this high initial burning rate is not possible on a physical basis, for the thermal wave could not have penetrated very deeply into the bed initially and thus pyrolysis and burning could not have occurred to any appreciable extent. The data show that the distance between the drying and ignition fronts increased initially and then remained almost constant. This is roughly consistent with a drying limited combustion process.

This study provided useful data on a specialized vortex unit and some valuable qualitative insights into the combustion of a high moisture content fuel, but the experiments do not lend themselves to quantitative analysis. The major deficiency of the study was the inability to measure the quantity of air that spiralled down the cold walls and up through the bed. The quantity of air that is drawn through the bed in this manner will depend in a complex way on the refractory temperatures, the firing rate of the tangential air, the geometry of the system, and on the burning rate itself.

Research of Essenhigh et al. Essenhigh and his co-workers at Pennsylvania State University have presented a number of papers (30-47) in the general incineration area and have attempted in some of them to develop theoretical equations for design purposes (32, 36, 37, 38, 41, 43, 47). Only those papers and sections of papers which deal with the solid bed combustion processes will be discussed here; many of the papers are also concerned with modelling conditions in the overfire region.

Some of the papers (37, 38) which dealt with the combustion of the solid fuel developed a simplified Mayers-type model for the rate of propagation of the ignition wave through a fuel bed simulated by a set of dowel rods placed vertically in a combustion pot. The analysis encountered the same problems as Mayers' did in estimating the physical properties of the fuel bed and was essentially a semi-empirical approach. The authors concluded, as did Mayers, that radiation played an important part in the ignition process, since the observed ignition rates were much higher than those predicted from their theory on the assumption that all of the heat fed forward for ignition was by conduction alone. When a contribution for radiation was added into the thermal conductivity term using a mean radiating length of a reasonable magnitude, the theory could be made to fit the experimental results adequately. The results from such experiments must be taken as being only qualitative as this analysis has even less merit than Mayers', since the experimental set-up could not be considered a model of any real system.

The other papers by Essenhigh et al. that deal with solid bed combustion attempt to develop theory directed towards predicting burning rates and maximum temperature levels in beds as well as the effect of inert content on the burning rates. Shieh and Essenhigh (47) tried to unify much of the previous theoretical work of the group and tested the theory against experimental data taken on their test incinerator. As this paper covered nearly all the group's work connected with the fuel bed combustion processes, it will be the only one discussed here in detail.

Shieh and Essenhigh (47) proposed that the burning rate of a fuel bed per unit area (F_A) could be given by an expression of the form

$$F_A = (0.75F_{RCS})\, m_{O_2} \frac{\dot{G}}{(1-V)\,(1-A-M)} \qquad (95)$$

where F_{RCS} is the relative carbon saturation factor (see pages 75-82), m_{O_2} the mass fraction of air in the underfire air, $\dot{G}$ the air supply rate per unit area, V the volatile fraction of the fuel on a dry-ash-free basis, and A and M the ash and moisture fractions of the fuel, respectively. The derivation of this equation was based on the simplified physical model of an incinerator shown in Figure 29. It was assumed that the fuel was fed in an over-feed mode and that the material was fully pyrolyzed (i.e., it consisted only of carbon) before it entered the combustion and gasification zone. The rate of supply of oxygen to the combustion zone by the underfire air was $m_{O_2}\dot{G}$ lb $hr^{-1}ft^{-2}$. Assuming all the carbon dioxide formed in the combustion zone is reduced to carbon monoxide by the time the gases reach the top of zone I(A) of Figure 29, the carbon burning rate will be $\frac{(2M_C)\,m_{O_2}\dot{G}}{M_{O_2}}$ where M_C and M_{O_2} are the molecular weights of carbon and oxygen, respectively. If the bed is not deep enough to permit complete reduction of carbon dioxide to carbon monoxide, the carbon burning rate becomes $0.75m_{O_2}\dot{G}F_{RCS}$ lb hr^{-1} ft^{-2}. To calculate the total fuel burning rate from this carbon burning rate, the volatile, moisture and ash content of the fuel must be considered. If the volatile fraction of the fuel on a dry-ash-free basis is V, each pound of carbon is produced from $\frac{1}{(1-V)}$ pounds of dry and inert-free fuel; and one pound of char is produced from $\frac{1}{(1-V)(1-A-M)}$ pounds of as-fired fuel.

Essenhigh and Shieh related the RCS factor to the combustion bed depth L_C by the equation

$$L_C = L_O \ln\left[\frac{K}{(1-F_{RCS})}\right] \qquad (96)$$

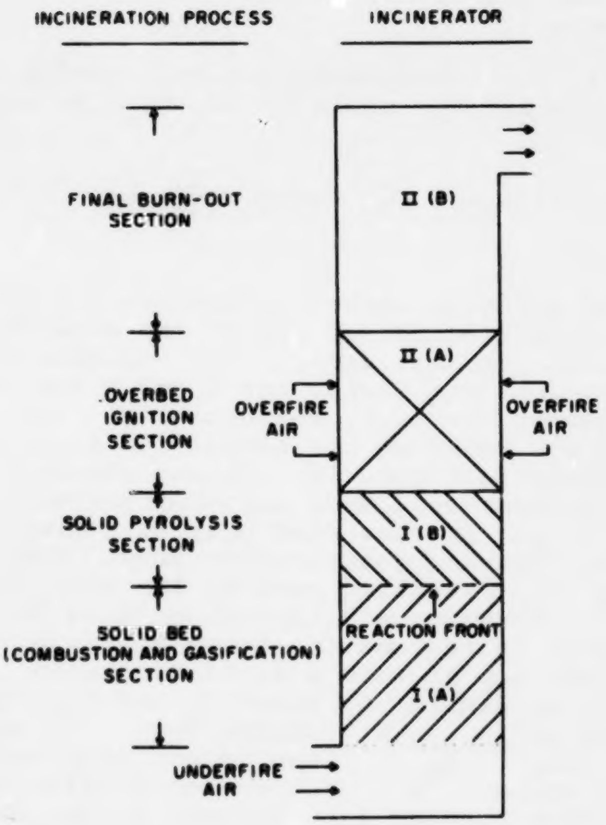
INCINERATION PROCESS
INCINERATOR
FINAL BURN-OUT SECTION
II (B)
OVERBED IGNITION SECTION
II (A)
OVERFIRE AIR
OVERFIRE AIR
SOLID PYROLYSIS SECTION
I (B)
SOLID BED (COMBUSTION AND GASIFICATION) SECTION
REACTION FRONT
I (A)
UNDERFIRE AIR

Fig. 29. Schematic of Test Incinerator Used by Essenhigh et al. (47)

where L_O was defined by the authors as being a characteristic reaction depth and K a semi-empirical constant of approximately 1.10. Equation (96) was derived in an earlier paper by Kuwata, Kuo and Essenhigh (37), where the RCS factor was related to depth assuming that the rates of the two reactions $C + O_2 \rightarrow 2CO$ and $C + CO_2 \rightarrow 2CO$ were controlled by the diffusion of reactants to the solid char surface and that the diffusivities of the reactants and the temperature dependence of the diffusivities were the same. In the case of the carbon-oxygen reaction, there is a good body of evidence to suggest that it is diffusion controlled under the conditions in a fuel bed; but there is strong evidence to suggest that the Boudouard reaction is kinetically controlled under fuel bed conditions unless ash build-up hinders the reaction. These points have been fully discussed earlier on pages 75-82. The form of equation (96) is very similar to the empirical expression suggested by Thring (110), namely

$$F_{RCS} = A(1-e^{\alpha L/D}) \qquad (97)$$

where A and α are empirical constants, L the fuel bed height at which the RCS factor is required and D the mean diameter of the particles in the fuel bed. The RCS factor calculated from equation (97) with suitable values of A and α increases far more rapidly with depth than that experimentally observed, as discussed on pages . Equation (96) would be expected to have the same deficiency as it is not materially different from equation (97). The simple exponential dependence of the RCS factor can only be obtained using the above assumptions of Essenhigh and Shieh and, as it is established that the Boudouard reaction is much slower (about five orders of magnitude) than the carbon-oxygen reaction at the same temperature and reactant concentration, it is not surprising to find that the calculated RCS factor increases more rapidly with depth than that experimentally observed.

The Kuwata, Kuo and Essenhigh development of the variation of the RCS factor with fuel bed depth does suggest bounds that can be placed on the constant K but it provides very little insight into the selection of L_O, which, although it has some theoretical basis (given the assumptions involved), cannot be confidently calculated from first principles. Although L_O can be estimated from experimental data, the underlying assumptions of the theory are unsound and the use of a value of L_O determined from one set of experimental results in another system would be unwise. In addition to the fuel bed material balance, the authors wrote a simple energy balance for a differential element of the fuel bed and used the equation so developed to predict the temperature profile within the fuel bed. This energy balance was decoupled from the mass balance equation because the RCS factor could not be used to give an indication of the heat release rate in the fuel bed as a function of height. The equation used to describe the temperature variation within the fuel bed was stated as

$$K_s^E \frac{d^2T}{dz^2} - \left\{ \dot{G} - F_A(1-V) \right\} \bar{C}_p \frac{dT}{dz} + Q_R = 0 \qquad (98)$$

where for zone I(A) of Figure 29

$$Q_R = \frac{3}{4} \dot{G}m_{O_2}(1 - 0.72r) \frac{\Delta H^c \delta}{L_O} \exp\left[\frac{-z}{L_O} \right] \qquad (99)$$

and from zone I(B)

$$Q_R = - Q_p \qquad (100)$$

where K_s^E is the sum of the coefficients of conduction (including radiant conduction) through both the gas and the solid per unit area of bed cross-section (i.e., taking account of porosity); T the temperature (of solid and gas assumed equal), at height z above the grate; $\bar{C}_p$ the average specific heat of both solid and gas (also assumed equal); r the ratio $\frac{(CO\%)}{(CO\%) + (CO_2\%)}$; ΔH^c the calorific value of the fuel; and Q_p the heat of pyrolysis of the fuel. The boundary conditions were stated as

$$T = T_O \quad \text{at} \quad z = 0 \qquad (101)$$

$$\frac{dT}{dz} = 0 \quad \text{at} \quad z = L_c \qquad (102)$$

and

$$F_A\bar{C}_p(T_L - T_O) = Q_r \qquad (103)$$

where Q_r is the net radiant flux from the overfire combustion region, T_L the temperature at the top of the bed and T_O the ambient temperature.

Equation (98) is a very simplified heat balance since it assumed equality of temperature between the gas and solid as well as equality in their specific heats. The ratio of the specific heat of the fuel used in their experiments (computer cards) to that of the combustion gases lay approximately in the range 1.3 to 1.5. In general the assumption of equality of gas and solid temperatures can be very erroneous where temperature gradients in the fuel bed are high (see pages 32-39).

Equation (99), which gives the heat release rate as a function of height throughout the zone I(A), includes a number of major assumptions. First, the authors assumed that all reactions in this zone were exothermic; this is not strictly correct, as near the top of this zone carbon monoxide would be produced via the endothermic Boudouard reaction. Second, no account was taken of changes in gas composition (given by r) with depth as r was assumed to be a constant. Obviously the heat release at different points within the bed was fixed by the local gas composition and temperature. The authors have completely neglected this and have essentially assumed a fixed heat release rate scaled with depth by the factor $\frac{1}{L}\exp(-z/L_O)$. There is no physical significance to this approach. Equation (99) can be broken down into three parts: (a) $3/4\dot{G}m_{O_2}$, which, as shown before, gives the pounds of carbon carried by the combustion gases assuming carbon monoxide is the only product of combustion; (b) $(1-0.72r)\Delta H^c$ represents the proportion of char which reacted to give carbon monoxide. The net heat release is then given by

$$\Delta H = \frac{r\Delta H^c}{n} + (1 - r)\Delta H^c \tag{104}$$

where ΔH^c is the heat of combustion of carbon to carbon dioxide, and n is the ratio of the heats of combustion of carbon to carbon dioxide and to carbon monoxide (approximately 94/26.4 = 3.55). Part (c), $\frac{\delta\exp(-z/L_O)}{L_O}$, is the factor that scales the heat release rate with depth; it is highest when $z=0$ and decays exponentially with height up to $z=L_c$. This term gives only a crude approximation to the heat release as it is based neither on the appropriate kinetics of the reactions involved, nor on any experimental gas composition profiles within the bed.

Equation (100) may be considered reasonably valid for the simplified sequential pyrolysis-combustion system of Figure 29. However, in the experimental set-up used in this research, considerable quantities of oxygen were known to have spiralled down into the fuel bed from the overfire region (46) and it must be concluded that some exothermic reactions did take place in zone I(B).

The three boundary conditions used are open to serious criticism. The first boundary condition states that the temperature of the fuel bed at $z=0$ is the same as the ambient, yet the heat release as given from equation (99) is at a maximum; it was physically impossible for the temperature at $z=0$ to be held at T_O in the experimental apparatus employed. Using the boundary condition that $\frac{dT}{dz} = 0$ at $z=L_c$ forces the temperature profile to peak at $z=L_c$ and in essence also forces the profile to fit the experimentally observed form, once a suitable temperature at the top of the bed is specified. The temperature at the top of the bed was calculated from the remaining boundary condition given in equation (103). This equation is a heat balance taken on a differential section at the top of the fuel bed; the effect of convective heating of the incoming fuel by the combustion gases has been neglected and nowhere in the paper do the authors say how Q_r, the net radiant heat flux to the top of the bed, was obtained.

The experimental results, against which the above theory was tested, were obtained on a batch incinerator fully discussed in another paper by Shieh and Essenhigh (46) and Figure 29 will suffice as a rough schematic of the apparatus. Briefly, the unit consists of a refractory box of 2-ft-square cross-section standing about 10 ft high with 9-in. heavy-duty refractory walls. Computer cards were used as the fuel and were fed from an aperture in one wall near the top of the unit so that they fell onto the grate, which was made of a perforated steel plate. The bed was normally maintained about 10 in. deep with a fuel feed rate of 120 lb hr^{-1} (30 lb $hr^{-1}ft^{-2}$). Air was divided between overfire air and underfire air in varying proportions, with the total air running from deficient to excess. When overfire air was used, it was injected through two sets of four nozzles located so that two vortices rotating in opposite senses were produced above the bed. This produced a stirred section -- zone I(A) -- roughly 10 in. to 20 in. above the top of the fuel bed. Above that, another 50 in. was available for the (plug flow) burn-out region -- zone II(B). Experimental data included temperature and oxygen measurements in the fuel bed; wall temperatures; gas temperatures, and measurements of CO, CO_2, O_2 and H_2O in the overbed region. The procedure adopted for comparing theory and experiment was by way of the temperature profile through the bed. As indicated earlier, the bed temperatures were found to increase to a peak, T_{max}, at a height above the grate designated by the authors as L_c. Normalization of the temperature profile was based on these two parameters which were obtained both experimentally and through calculations based on the theory previously discussed. Table 7 shows the comparison of predicted and experimental values of T_{max} and L_c and Figure 30 shows the theoretical and experimental normalized temperature through the fuel bed. The calculations were performed for a value of L_0 = 0.5 ft. No values of the other model parameters $\bar{C}_p$, r, B_0E, Q_p and Q_r were given. The theoretical value of L_c was calculated using equations (95) and (96) as F_A was known from the rate of fuel addition to the test apparatus that was required to keep the bed depth constant during an experiment.

The variation of L_c with underfire air rate, as calculated by Shieh and Essenhigh and reproduced in Table 7, is unusal. As the underfire air rate increased (runs 1 to 4) the calculated value of L_c decreased, as expected from the equations. However, with the underfire air flow rate still increasing, but

Table 7

Comparison of Predicted and Experimental Values of Maximum Bed Temperature (T_{max}) and Combustion Zone Depth (L_c) in the Solid Bed (47)

	Air Supply Data cfm			T_{max} °C		L_c (ft)	
Run No.	Over-fire Air	Under-fire Air	Excess Air %	Pre-dicted	Experi-mental	Pre-dicted	Experi-mental
1	80	10	29	1230	900	0.67	0.58
2	80	15	36	1101	950	0.63	0.58
3	80	20	43	1040	980	0.59	0.58
4	80	25	50	1007	1000	0.56	0.58
5	40	30	0	1035	940	0.90	0.60
6	40	40	14	998	950	0.76	0.60
7	40	50	29	973	960	0.67	0.73
8	40	60	43	953	980	0.60	0.73

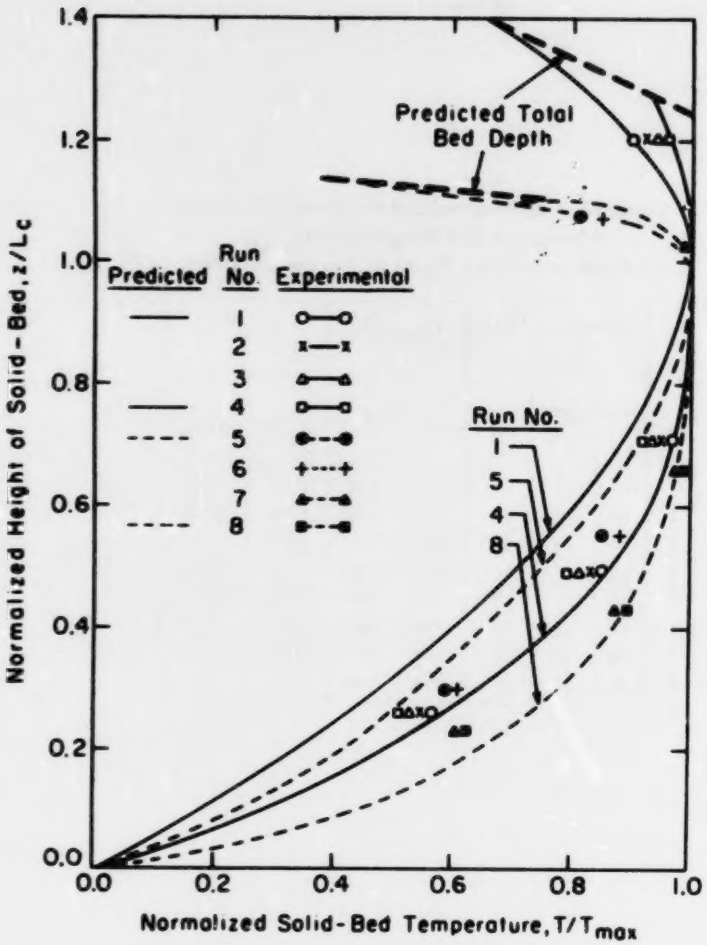

Fig. 30. Comparison of Predicted and Experimental Profiles through the Solid Bed (normalized axes). From Essenhigh and Shieh (47)

this time coupled with a step decrease in the overfire air rate, the calculated value of L_c was reported to rise suddenly (the overfire air rate was not considered in developing either equation (95) or (96). This effect can be seen by comparing the values of L_c calculated for runs 4 and 5. With the overfire air maintained at the higher value, the value of L_c again decreased with an increasing underfire air rate. This jump in the calculated value of L_c is anomalous, because equations (95) and (96) do not take into account the effect of the overfire air flow rate since they constitute only a simple material balance on the fuel bed; the authors offer no explanation for this behavior. The experimental values of L_c were found to be approximately constant at 0.58 ft for the high overfire air rate and did not depend on the underfire air rate. For the low overfire air rate the value of L_c increased with underfire air rate, contrary to the theory presented by the authors.

Another astonishing result emerges from the air supply data of Table 7. The burning rate of the cards was not increased by augmenting the underfire air rate. On the assumption that the composition of the computer cards used was approximately the same as cellulose, the burning rate for runs 1 through 8 can be calculated; the calculations show that the burning rate for all the runs was the same, about 16.5 lb $hr^{-1}ft^{-2}$. This value is much lower than the value of 30 lb $hr^{-1}ft^{-2}$, which the authors quoted as being typical. Previous experience with coal beds burning in the overfeed mode has shown (23) that the burning rate should be roughly proportional to the underfire air rate. Departures from strict proportionality are caused by changes of the RCS factor; but over a wide range of conditions it was found that the higher fuel bed temperatures, and therefore the greater reaction rates associated with increased underfire air flow rates, compensated for the shorter residence time of the gases in the fuel bed.

The major reason the theory predicts the opposite effect of underfire air rate on the value of L_c from that experimentally observed stems from the fact that the area firing rate, F_A, appears to have remained constant with increasing underfire air; this forced the value of L_c, as predicted from equations (95) and (96), to decrease. Physically, this means that a given value of the RCS factor was reached in a progressively shorter distance as the underfire air was increased. This is completely contrary to all other experiences with overfeed fuel beds, as well as to the authors' own theory. Shieh and Essenhigh state that the characteristic depth L_O can be given as

$$L_O = v\delta d/4D_{O_2-N_2} \qquad (105)$$

where v is the average gas velocity through the bed, d is the average pore or channel diameter in the bed, D is the coefficient of oxygen diffusing through nitrogen, and δ is an effective diffusion path length or diffusion-layer thickness. The analysis leading to equation (105) is discussed by Kuwata, Kuo and Essenhigh (37) and contains, like the development of equation (96), a number of approximations. However, given that equation (105) is valid, it would follow that L_O would increase as the underfire air flow rate increased for the ensuing reasons. The film thickness δ can be expressed as (113)

$$\delta \; \alpha \; \left[\frac{\mu D_p}{\rho_g v}\right]^{0.5} \qquad (106)$$

where D_p is the diameter of the fuel particle and μ and ρ the viscosity and density of the combustion gases. Assuming that d and D_p do not vary with underfire air rate

$$L_0 \; \alpha \left[\frac{\mu}{\rho_g D}\right]^{0.5} v^{0.5} \sqrt{\frac{d^2 D_p}{D}} \qquad (107)$$

Equation (107) indicates that L_O should increase slowly with the underfire air rate. An offsetting factor is the rise in temperature associated with the increase of underfire air. The Schmidt number $\left[\frac{\mu}{\rho_g D}\right]$ is a weak function of temperature since $\mu \; \alpha \; \sqrt{T}$, $\rho \; \alpha \; \frac{1}{T}$, and $D \; \alpha \; T^{1.75}$; hence

$$N_{Sc} \equiv \frac{\mu}{\rho_g D} \; \alpha T^{-0.25} \qquad (108)$$

so that $L_O \; \alpha \sqrt{\frac{G}{T}}$. Using the data from runs 1 and 4 on the maximum bed temperature and the amount of underfire air, L_O would be expected, on the basis of equations (107) and (108), to increase about 70% from run 1 to run 4; thus the depth required to reach a given value of the RCS factor would increase, a result compatible with experiment.

In summary, the two problems with the Essenhigh and Shieh theory rest with the unvarying firing rate F_A with underfire air and the assumed constancy of L_O. It is likely that channeling may have caused the burning rate not to increase with underfire air. The method used in this study, of feeding the computer cards onto the fuel bed, and the low pressure drop grate, almost definitely would lead to bad channeling, especially near the walls. The problem was probably aggravated by the use as a fuel of computer cards, which would tend to pack together in layers inaccessible to the underfire air.

Another point which can be raised in discussing the material balance equations is the validity of comparing the calculated value of L_c with the value found from experiment. First, it will be recalled that the experimental L_c was taken as the depth where the fuel bed temperature peaked; this was also the point where the oxygen concentration reached its minimum. This point does not compare physically with the value of L_c as calculated in the theory. The experimental value of L_c reflects the degree of back-mixing of the overfire air into the fuel bed and the rate of reaction of the oxygen in this air with the pyrolysis products in zone I(B) of Figure 29. The amount of back-mixing will decrease as the underfire air rate is increased and therefore L_c will increase, a conclusion in accord with the experimental observations. L_c as used in equation (96) has a different physical significance, namely the depth of fuel bed required to reach a given RCS factor. As shown earlier, L_c will be expected to increase as the underfire air increases, but not for the same reasons that the experimental values increased. Second, it was assumed that there was substantially no net hydrogen in the char throughout the entire depth of the so-called combustion zone. This assumes that char combustion is the controlling step in the burning process; this may not be correct as the pyrolysis and drying stages may be much slower than the combustion stage, being heat transfer limited in many cases. It is possible that the computer cards are thin enough for this assumption to hold, but this assumption would need to be abrogated for a fuel with a larger characteristic dimension.

The heat balance results, for the value of T_{max}, exhibit the same anomalous results as those for L_c, as they also show a dependence on the overfire air rate (compare the calculated values of T_{max} for runs 4 and 5 in Table 7). It is possible that the overfire air rate has some effect on Q_r, the net radiant heat flux to the top of the bed, but as the authors do not state how this value was calculated it is impossible to comment on it. However, if one assumes that Q_r is dependent on the amount of excess air, runs 1 and 7 and 3 and 8 would have equivalent heat fluxes to the top of the fuel bed and hence equal temperatures T_L, since F_A is a constant. The temperature at the top of the bed will directly influence T_{max} but as can be seen from Table 7 the values of T_{max} for runs 1 and 7 and 3 and 8 are very different. In addition to this anomalous behavior, the calculated value of T_{max} progressively decreased with increasing underfire air rate (at constant overfire air rate). This is in direct contrast to the experimental values, which increased, in agreement with other experimental evidence (23).

Table 7 also shows that the experimental values of T_{max} were affected by the overfire air rate and decreased by 60°C between runs 4 and 5. It is felt that this reflects the quantity of air that back-mixed into the fuel bed, which would diminish as the overfire air was decreased and with increasing underfire air. The reason that the predicted values of T_{max} exhibited the opposite behavior to the experimental values probably lay with the unchanging burning rate with underfire air rate. Increases in $\dot{G}$ would on the basis of equation (99) increase the heat release within the bed (Q_r), but the major effect will be felt near the grate at z=0 where the boundary condition of equation (101) forced the temperature to T_O. At the same time, increases in $\dot{G}$ will increase convective heat losses without compensation from the convective heating of the fuel flow, and thus the predicted T_{max} will drop with increases in $\dot{G}$. In short, despite the superficially good agreement between theory and experiment, as shown in Figure 30, the heat balance has many shortcomings and it can only be assumed that the theory was forced to fit experiment.

The authors conclude in their paper that their theory has been adequately substantiated by experiment and needs minor refinements for it to have a broader range of applicability. The above discussion has highlighted the shortcomings of the theory and suggests that the authors' conclusion is perhaps premature. In addition, it may be questioned if this theory will be valid for fuel bed conditions where large diffusional resistances to heat transfer are encountered within the fuel elements.

The Theory of W. R. Niessen, A. F. Sarofim et al. (19). The authors have presented a simplified global picture of refuse pyrolysis and gasification on the assumption that the water gas shift reaction ($CO_2 + H_2 \rightleftarrows CO + H_2O$) is equilibrated at the top of the fuel bed. This assumption was based on Kaiser's data (114) from the Oceanside Incinerator on Long Island, New York. The assumption of the equilibration of the water gas shift reaction is often made in calculations on coal gasification (115) when temperatures above 2000°F are encountered. The water gas shift reaction is primarily considered as a heterogeneous phenomenon, although it can also take place in the gas spaces in the fuel bed via a free radical mechanism,

$$H_2O + H \rightleftarrows H_2 + OH \qquad (109)$$

$$CO + OH \rightleftarrows CO_2 + H \qquad (110)$$

There is no direct experimental evidence concerning the rate of the water gas shift reaction, but it will obviously depend on temperature and may well be strongly affected by fuel reactivity and catalytic effects of the fuel ash. There is, however, a good body of experimental evidence (115) which suggests that the reaction is rapidly equilibrated above 2000°F. The authors assume that the gasification reactions occurring within the bed produce mainly CO, CO_2, H_2, and H_2O with only small quantities of CH_4, tars and soot. Nicholls' (24) results show that this is a reasonable assumption (see Figure 13) and Kaiser's data (114) also substantiate this assumption.

The refuse was assumed, on a dry, inert and ash free basis, to have the composition of cellulose. The composition could then be represented by $C(H_2O)_n$ where n had the value 5/6 for dry cellulose. The following overall material balance, which assumes no ignition restrictions, was written for the gasification of the process

$$O_2 + 3.76N_2 + xC(H_2O)_n \rightarrow aCO + bCO_2 + cH_2 + dH_2O + eC + 3.76N_2 \qquad (111)$$

where x is the number of moles of $C(H_2O)_n$ gasified per mole of oxygen in the underfire air. Equation (111) contains six unknowns. Five relationships between these unknowns can be found from consideration of the three element balances, an overall energy balance, and by assuming that the water gas shift reaction is equilibrated. The energy balance, of course, introduces one more unknown T, the temperature of the gases leaving the bed. These relationships are:

Element Balances

Carbon: $a + b + e = x$ (112)

Hydrogen: $c + d = nx$ (113)

Oxygen: $b + (a+d)/2 = 1 + nx/2$ (114)

Water Gas Shift Equilibrium

$$\frac{[CO_2][H_2]}{[H_2O][CO]} = \frac{bc}{da} = K_{WGS} \qquad (115)$$

The amount of energy released in the bed per lb mole of oxygen (Q_R) is given by the difference between the heats of formation of the products and reactants

$$Q_R = \overbrace{\underset{(CO)}{47,560a} + \underset{(CO_2)}{169,290b} + \underset{(H_2O)}{140,240d}}^{\text{products}} - \overbrace{\underset{(C_6(H_2O)_5)}{320,940\left(\frac{x}{6}\right)}}^{\text{reactant}} - \overbrace{\underset{(H_2O)}{104,240\left(\frac{n-5}{6}\right)x}}^{\text{moisture vaporization}} \qquad (116)$$

where the last term represents the endothermic vaporization of the moisture in the fuel exclusive of the 5/6 mole per C atom that is chemically bound. The energy lost from the bed in the sensible heat of the off gases (Q_P) assuming that the temperature of these gases is 2000°F is given by

$$Q_P = (a\bar{C}_{P_{CO}} + b\bar{C}_{P_{CO_2}} + c\bar{C}_{P_{H_2}} + d\bar{C}_{P_{H_2O}} + 3.76\bar{C}_{P_{N_2}})(1940) + (18{,}000)(n - \tfrac{5}{6}) \tag{117}$$

where the average heat capacities (Btu $\text{mole}^{-1}\,{}^{\circ}\text{F}^{-1}$) between 60°F and 2000°F are $\bar{C}_{P_{CO_2}} = 13.8$, $\bar{C}_{P_{CO}} = 8.3$, $\bar{C}_{pH_2O} = 11.0$, $\bar{C}_{P_{H_2}} = 7.6$ and $\bar{C}_{P_{N_2}} = 8.2$.

With the rate of heat loss from the bed through side-wall and radiant-heat losses being Q_L, the following balance is obtained

$$Q_R = Q_P + Q_L \tag{118}$$

which provides the fifth independent equation relating the six unknowns. The temperature of 2000°F was chosen by Niessen et al. (19) as it was representative of the data of Nicholls' (24) and Kaiser's (114) results on the Oceanside Incinerator. Although a somewhat arbitrary temperature, the 2000°F figure may not be unreasonable, as the endothermic reactions which occur after all the oxygen has been consumed may well be effectively quenched at temperatures below this value. The only other way the temperatures in the bed could drop below this level would be through radiative and side-wall losses.

Another assumption had to be made in order for the set of equations (112) and (118) to be solved. This assumption concerned the amount of char produced per mole of oxygen (e), which will be a function of the rates of ignition and burning and as such will depend on the underfire air rate. From the previous discussion on pages 46-59, it can be concluded that at high air rates, e will be zero and will increase as the air rate is decreased.

Results were calculated for different moisture contents of the fuel, fraction carbon gasified and heat lost or gained by the bed. With all other parameters held constant, increases in moisture content were shown to decrease the amount of CO and H_2 formed; this resulted in a decrease in the percentage of the total energy release that was given off above the bed (for

0% moisture, 74% of total heat release occurred above the bed, while for 33% moisture this value dropped to 44%). The same trend was observed when the amount of heat lost by the bed increased (all other parameters being held constant). The explanation of these results is evident when gasification is considered to proceed via a net exothermic step (reaction of the cellulose to give char, CO_2 and H_2O and the vaporization of any free moisture) followed by an endothermic step consisting of the reactions $C + H_2O \rightarrow CO + H_2$ and $C + CO_2 \rightarrow 2CO$. With the assumption of a fixed final gas temperature the smaller the quantity of heat that is available for the endothermic reactions, the lower the concentrations of CO and H_2 above the bed. The amount of heat available for these reactions depends on the moisture content of the fuel and the heat lost from the bed. Heat losses from the bed will depend in part on the furnace configuration and would be greater with a water-walled unit than with a conventional refractory-lined furnace.

This simple model showed the necessity of overfire air for the burn-out of the combustibles issuing from the bed and how the air requirements would vary with changes in the feed moisture content and heat loss from the bed. Much of the combustible would be expected to be mainly CO and H_2, with tar and soot and CH_4 only present in any quantity near the inlet of the furnace where ignition was achieved. The model further showed that for conditions where the fuel moisture content increased the burning rate could be kept up if the underfire air rate was increased; the air helps provide more energy for water vaporization. This function would obviously be helped if the air was preheated. This result concurs with what is often done in practice and gives a quantitative basis for a guideline which has been disputed by some incinerator operators.

The major shortcoming of the model is the simple one-step char production assumption of equation (111) and the somewhat arbitrary assumption about the magnitude of e. Obviously in a fuel bed there will be major diffusional resistances to heat transfer in many particles and therefore pyrolysis will continue long after the ignition front has passed over the particle. The modification of this model, to take into account events in a real bed, will have to await a better understanding of the bed burning processes if the model is to be truly predictive. The development of a more realistic model, followed by a set of arbitrary assumptions that would have to be made, at this stage of our understanding of bed-burning processes, concerning the varying C/H/O ratios in the fuel as a function of combustion extent would negate the attractive features of the model as it now stands.

It is possible, on an order-of-magnitude basis, to check the validity of the 2000°F quench temperature by considering the rates of the two reactions $C + H_2O \rightarrow CO + H_2$ and $C + CO_2 \rightarrow CO_2$ which are the predominant reactions taking place in the endothermic region of the fuel bed. A simple heat balance on a differential section of the bed, assuming equality of the gas and solid temperatures and negligible heat capacity of the solid phase, gives,

$$\dot{G}C_{p_g}\frac{dT}{dz} + \frac{(\Delta H_A)\dot{G}}{\rho_g}\frac{dc_A^*}{dz} = 0 \qquad (119)$$

where c_A^* is the molar concentration of A(lb mole ft^{-3}) and ΔH_A the heat of reaction (Btu lb mole^{-1}). Equation (119) can be conveniently changed to a time base by substituting $t = z\rho_g/G$, giving,

$$\frac{\Delta T}{\Delta t} \approx \frac{dT}{dt} = -\frac{\Delta H_A}{C_{p_g}\rho_g}\frac{dc_A^*}{dt} \qquad (120)$$

For the reaction $C + CO_2 \rightarrow 2CO$, the data of Wu (111) and Lewis, Gilliland and McBride (116) for electrode carbon of 30 - 40 mesh size, as indicated by von Fredersdorff and Elliott (115), suggest a reaction rate of the form

$$r_{CO_2} = \frac{6.9 \times 10^5 \exp\left[\frac{-47,600}{RT}\right] p_{CO_2}}{1 + 0.014\exp\left[\frac{15,000}{RT}\right] p_{CO} + 0.21\exp\left[\frac{6300}{RT}\right] p_{CO_2}} \quad \frac{\text{g mole}}{(\text{g})(\text{min})(\text{atm})}$$

For the reaction $C + H_2O \rightarrow CO_2 + H_2$, the rate and mechanism of which is understood less well than the Boudouard reaction, the rate is given by von Fredersdorff and Elliott (115) for coconut shell charcoal as,

$$r_{H_2O} = \frac{1.58 \times 10^{10} \exp\left[\frac{-62,300}{RT}\right] p_{H_2O}}{1 + 33p_{H_2} + 3.16 \times 10^4 \exp\left[\frac{-21,100}{RT}\right] p_{H_2O}} \quad \text{g mole g}^{-1}\text{min}^{-1}\text{atm}^{-1} \qquad (122)$$

This rate is exclusive of the water gas shift reaction, $CO + H_2O \rightleftarrows CO_2 + H_2$.

The rates given in equations (121) and (122) are on the basis of unit weight of carbon and it is necessary to convert these rates into rates based on a unit volume of bed for use in equation (120). There is no exact way of doing this as there is no experimental evidence given by von Fredersdorff and Elliott as to the effective surface areas of the different carbon types used. For simplicity the weight to unit volume of bed ratio will be taken as $(1 - \delta)\rho_s$ although the treatment of the data in this manner may grossly misrepresent the kinetics under fuel bed conditions. The rate can then be given by

$$\frac{dc_A^*}{dt} = -r_A \times 60 \times (1-\delta)\rho_s \text{ lb mole ft}^{-3}\text{hr}^{-1}\text{atm}^{-1} \qquad (123)$$

Assuming $p_{CO} = p_{CO_2} = p_{H_2} = 0.1$ atm, $p_{H_2O} = 0.15$ atm, $\delta = 0.4$ and $\rho_s = 30$ lb ft^{-3}, for temperatures of 2500°F and 2000° F the rates of the two reactions are found to be

$$\begin{aligned}
-\frac{dc_{CO_2}}{dt} \quad & T=2500^{\circ}F \quad \cong 39 \text{ lb mole hr}^{-1}\text{ft}^{-3} \\
-\frac{dc_{CO_2}}{dt} \quad & T=2000^{\circ}F \quad \cong 2 \text{ lb mole hr}^{-1}\text{ft}^{-3} \\
-\frac{dc_{H_2O}}{dt} \quad & T=2500^{\circ}F \quad \cong 1300 \text{ lb mole hr}^{-1}\text{ft}^{-3} \\
-\frac{dc_{H_2O}}{dt} \quad & T=2000^{\circ}F \quad \cong 42 \text{ lb mole hr}^{-1}\text{ft}^{-3}
\end{aligned} \qquad (124)$$

Equation (124) indicates that the rates of both reactions drop by more than an order of magnitude from the maximum expected rate at the end of the exothermic zone to the 2000°F temperature level. At temperatures a little below 2000°F the reactions will be slow enough that they can be considered quenched. Moreover, the above calculations show that at temperatures above 2000°F the steam-carbon reaction may well be mass transfer controlled.

The rate at which the temperature of the gases falls can be calculated using equations (120) and (124). As the steam-carbon reaction is very fast at 2500°F, it will be assumed that it is mass transfer controlled and that the rate of steam conversion is 40 lb mole $hr^{-1}ft^{-3}$. On this basis, a rough estimate of the possible rate of change of temperature is

$$\frac{\Delta T}{\Delta t}_{\max} \cong \frac{39 \times 74{,}000 + 40 \times 56{,}500}{3600 \times 0.02 \times 0.4} \cong 4500^{\circ}\mathrm{F}\ \mathrm{sec}^{-1} \quad (125)$$

This calculation has neglected the heat effects associated with the solid; but since generally $UC_{Ps} < GC_{Pg}$, the order of magnitude of $(\Delta T/\Delta t)_{max}$ will not be greatly affected. This result suggests that the temperature drop in the endothermic zone will be quite rapid even if the reaction rates are very much slower than calculated here. Nicholls' (24) data show that the temperature in a fuel bed initially drops quite sharply with distance from the end of the exothermic zone (300° - 350°F/sec), confirming that the rates of the endothermic reactions at this point in the bed are indeed quite high.

Ignition and Combustion Stability of a Fuel Bed

Background. The problem of ignition and combustion stability of a fuel bed can be conveniently divided into three parts: the ignition of the top layers of fuel in the virgin bed by radiation received from the hot combustion gases and the refractory lining of the furnace; the propagation of the ignition wave down into the fuel; and the stability of the fully ignited bed. The first of these problems has been extensively studied in the literature on fire research and flame spread. Under most operating conditions incipient ignition will cause little difficulty in an incinerator as long as the underfire air rate at the front of the grate, where the fuel is ignited, is kept low enough. The reason for this is covered below. Simms and Law (117) have shown that radiation densities of the order of 1 - 1.7 cal cm^{-2} sec^{-1} (13 - 22 x 10^3 Btu hr^{-1} ft^{-2}) are sufficient for the spontaneous ignition of typical woods (≈ 1 1/2 cm in thickness) containing 20 to 60 percent weight of moisture. An ignition criterion based solely on a flux density must be used with discretion, as other factors (thermal properties of the material and size, for example) can markedly affect the amount of heat that must be transferred to the specimen to achieve ignition. However, the ignition of the types of material used by Simms and Law would probably be more difficult than that of most objects in refuse because of their high moisture contents and thickness. Radiant flux densities under most conditions within an incinerator would be in excess of 50,000 Btu hr^{-1} ft^{-2}, showing that incipient ignition is not likely to be a problem unless the convective cooling of the fuel by the underfire air is excessive.

The remainder of this section will be devoted to studying the process of ignition through the bed and the stability of the fully ignited bed. The latter problem will be discussed first, as it is the less complicated of the two and more studies have been addressed to it. These studies have been concerned with the stability of catalytic packed-bed reactors but the basic principles developed can be expected to apply to a fuel bed; a catalytic packed-bed reactor can be considered to be a highly idealized refuse bed. The literature in this field (e.g., 143, 144, 145, 146, 147 and references contained therein) has shown that a multiplicity of steady states can be achieved in a reactor. Two different physical phenomena are apparently responsible for this multiplicity of steady states. First, the fact that the heat must be conducted in the opposite direction to the fluid flow gives rise to multiple steady states for the reactor system, and second, because reaction takes place on the surface of or inside a catalyst pellet (fuel element) each pellet may be in one of two steady states. For a fuel bed, at least two steady states are immediately recognizable: (a) the virgin fuel bed at ambient temperature, (b) active combustion; (c) in addition, a third stable state corresponding to smoldering may be hypothesized.

Combustion Stability of a Fully Ignited Bed. The ensuing discussion will focus on conditions in a bed after it has been fully ignited. For both the underfeed bed and traveling grate this would occur after the ignition front had reached the grate; at this point it will be assumed that the fuel has been fully pyrolyzed and consists only of char. The discussion has been applied frequently to the combustion behavior of a single particle surrounded by an infinite combustion medium and is well known. The discussion will be extended here to cover fuel bed conditions but it must be considered only approximate because of the difficulty of adequately taking into account changes in oxygen concentration and gas temperature and modes of heat transfer other than convection.

Assuming that the bed loses the major portion of the heat generated within it by convective cooling to the gases flowing through it, the following balance can be established between the heat generation rate to the heat loss rate

$$Q^{gen} = \frac{m_{O_2}\Delta H^{c}}{\frac{1}{k_m} + \frac{1}{\rho_g K \exp(-E/RT_s)}} = Q^{loss} = h_s(T_s - T_g) \qquad (126)$$

where it has been assumed that all the heat is generated within the solid and that the rate of heat generation may be controlled by both mass transfer and kinetic factors. Equation (126) may be made dimensionless by dividing through by the maximum possible heat generation rate giving

$$\frac{1}{1 + \frac{k_m}{\rho_g K \exp(-E/RT)}} = \frac{h_s(T_s - T_g)}{k_m m_{O_2} \Delta H^c} \tag{127}$$

A simple heat balance, on an element of the fuel bed considered as a tube with carbon walls for adiabatic steady-state operation, gives

$$T_g - T_O = \left[1 - \frac{m_{O_2}}{m^O_{O_2}}\right] (T_{ad} - T_O) \tag{128}$$

where T_O is the entering air temperature, $m^O_{O_2}$ the mass fraction of oxygen in the entering air and T_{ad} is given by

$$T_{ad} = T_O + \frac{m^O_{O_2} \Delta H^c}{C_{p_g}} \tag{129}$$

Using equations (128) and (129) and assuming that $j_D = j_H$, equation (128) may be rewritten as

$$\frac{1}{1 + \frac{k_m}{\rho_g K \exp(-E/RT)}} = N_{Le}^{2/3} \frac{T_s - T_g}{T_{ad} - T_g} \tag{130}$$

where $N_{Le} = N_{Pr}/N_{Sc}$. The right-hand side of equation (130) represents a dimensionless heat generation term while the left-hand side represents a dimensionless heat loss term. A sketch of these two functions is shown in Figure 31. The intersections of the two lines represent solutions to equation (130) and only those where the slope of the heat generation curve is less than the slope of the heat loss curve are stable. The active burning of coal is represented by the upper stable point, which can be seen to be in the mass transfer controlled regime. It can also be readily seen that if the reaction ever moves away from the mass transfer regime it will be quenched; this result concurs with Silver's analysis

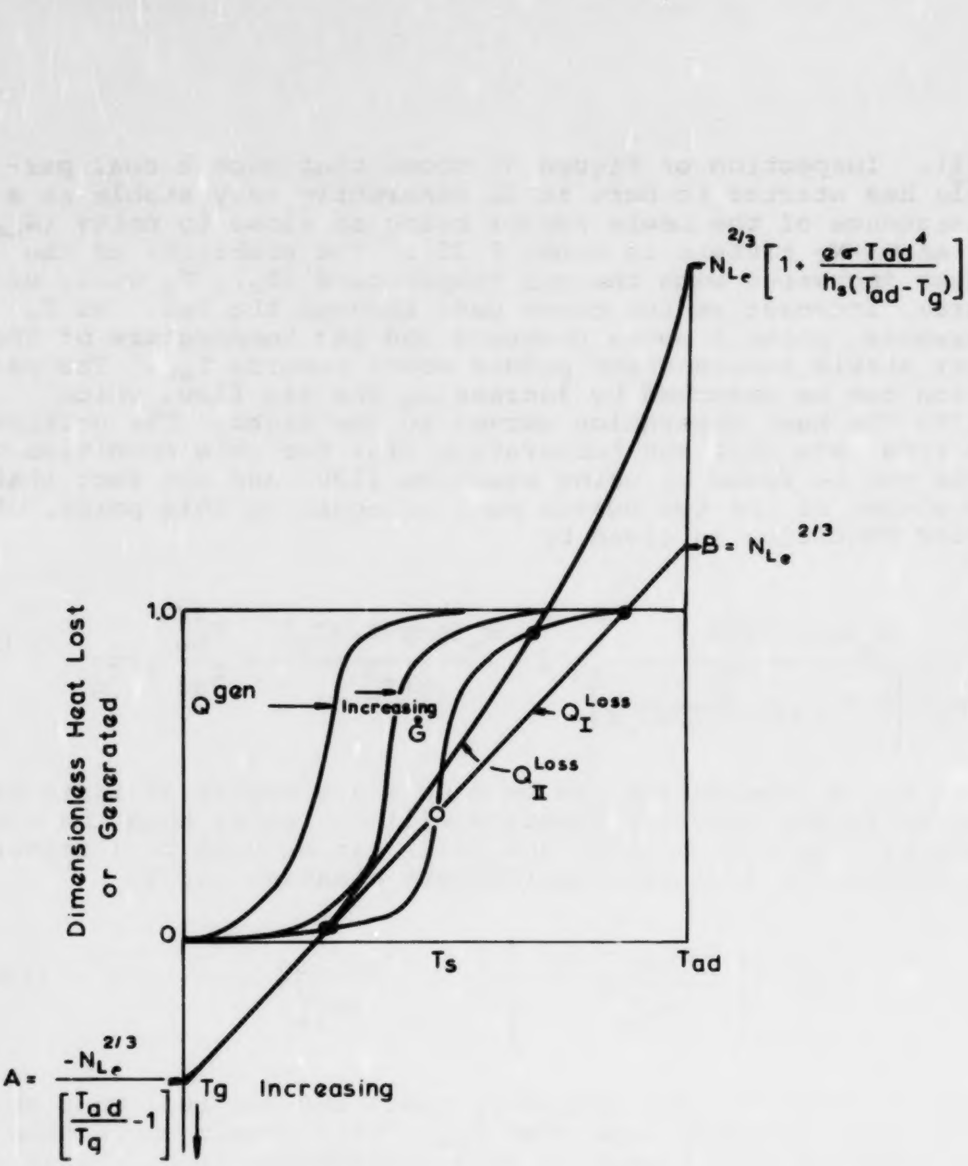

Fig. 31. Sketch of Dimensionless Heat Generation and Heat Lost Curves Q^{loss} represents heat lost curve for no radiative losses. Q_{II}^{loss} represents heat lost curve with radiative losses. Points (●) are stable points; points (0) are unstable).

(101). Inspection of Figure 31 shows that once a coal particle has started to burn it is inherently very stable as a consequence of the Lewis number being so close to unity (N_{Le} for an O_2-N_2 mixture is about 1.15). The stability of the system increases with the gas temperature (T_g); T_g will, of course, increase as the gases pass through the bed. As T_g increases, point A moves downward and the temperature of the upper stable intersection points moves towards T_{ad}. The reaction can be quenched by increasing the gas flow, which shifts the heat generation curves to the right. The critical gas flow rate (G_c) and temperature (T_c) for this condition to occur can be found by using equation (130) and the fact that the slopes of the two curves must be equal at this point, the latter condition is given by

$$\frac{k_m E\exp(E/RT_c)}{\rho KRT_c^2\left[1 + \frac{k_m}{\rho K\exp(-E/RT_c)}\right]^2} \cong \frac{k_m E\exp(E/RT_c)}{\rho KRT_c^2} = \frac{N_{Le}^{2/3}}{T_{ad} - T_g} \qquad (131)$$

where the approximation can be made since Figure 31 indicates that at T_c the chemical kinetics will be faster than the mass transfer. Equations (130) and (131) can be used to eliminate k_m, giving the following approximate equation for T_c

$$T_c^3 - T_gT_c^2 + \left[\frac{E(T_{ad} - T_g)}{RN_{Le}^{2/3}}\right]T_c - \frac{ET_{ad}(T_{ad} - T_g)}{RN_{Le}^{2/3}} = 0 \qquad (132)$$

Equation (132) has two imaginary roots and one real root at a value of T_c slightly less than T_{ad}. This result could have been foretold from Figure 31 as a consequence of N_{Le} being so close to unity. Using this value of T_c, it is possible to calculate the value of G at which the reaction would be quenched (G_c). The calculated value of G_c is very much higher than any reasonable value ever reached in a fuel bed showing that quenching of the fire by too high an underfire air rate is a theoretical abstraction which would never be reached in practice. This result has been dealt with in detail as it differs from a result previously obtained by Spalding (118) for the quench temperature T_c, namely,

$$T_c = \frac{E}{2R}\left[\sqrt{1 + \frac{4R}{E}\left\{ \frac{12\Delta H^c}{16C_{p_g}} m_{O_2} + T_g \right\}} - 1 \right] \tag{133}$$

in which $12\Delta H^c/16C_{p_g}\ m_{O_2} + T_g$ was quoted to be of the order of $1720^{\circ}K$. Spalding's analysis, although based on a different approach, uses much the same reasoning given above. The author feels that although Spalding reaches the same general conclusion as above, he overstated the importance of possible quenching of the reaction by high gas flow rates as a consequence of a poor assumption used in deriving equation (133); the value of T_c calculated using this equation is too low. Employing a value of T_c calculated from equation (133) Spalding suggested that the minimum diameter particle which could burn in air was 0.256 cm; and as this phenomenon is never observed experimentally he suggested that some of the chemical and physical constants used in deriving this figure were probably wrong. The result derived above, that T_c is of the order of T_{ad}, indicates that the decrease in size is not nearly so important as Spalding's analysis claims.

The treatment given here covers a very restricted case where no radiant heat losses are taken into account. The effect of considering radiant heat losses is shown in Figure 31 with the heat loss curve Q_{II}^{loss}. For this case, point A is the same as before but point B has moved up to $B^{I} = N_{Le}^{2/3}\left\{1 + \delta\sigma T_{ad}^{4}/h_s(T_{ad} - T_g)\right\}$. The slope of the line, instead of being linear, is now proportional to T_s^3. Without resorting to working out the mathematics, it can be readily deduced that heat losses by radiation tend to make the fuel bed less stable and the bed could be quenched with a somewhat lower $\dot{G}$ than that required in the absence of radiation heat losses. Radiant heat and side-wall losses account for the quenching of fuel beds at low values of air rate; this behavior cannot be explained solely on the basis of convective heat losses.

In concluding this section, it will be shown that the solid temperature, in the case where convection heat losses dominate, is handly affected by the degree of conversion, and is not dependent on the gas flow rate $\dot{G}$. Since the combustion rate is entirely controlled by mass transfer and assuming $j_D = j_H$

$$T_s - T_g = \frac{k_m}{h_s} m_{O_2} \Delta H^c \tag{134}$$

$$T_s - T_g = \frac{m_{O_2}\Delta H^c}{C_{p_g} N_{Le}^{2/3}} \qquad (134)$$

Eliminating T_g from equation (134), using equation (128) gives

$$T_s - T_O = (T_{ad} - T_O)\left[1 - \frac{m_{O_2}}{m_{O_2}^{O}}\left(1 - N_{Le}^{2/3}\right)\right] \qquad (135)$$

which shows that (T_s-T_O) is hardly affected by the degree of conversion and is of the order (T_{ad}-T_O) since N_{Le} is close to unity. Thus the maximum temperature is fixed by the specific heat of the air and combustion products and the heat of reaction; it will not change with underfire air rate $\dot{G}$. The results of Kreisinger et al. (23) support this claim, the slight increase in temperature observed at higher air flow rates probably resulting from a smaller portion of the total heat liberated within the bed being lost to the side walls.

Propagation of an Ignition Wave through a Fuel Bed. Other than Mayers' original work (90), this problem has been studied in the literature relatively recently in a few papers on the propagation of an "ignition" plane through a catalyst bed (119, 120, 121, 148). The theoretical development of Vortmeyer (119) will be covered here. The simplified conditions within the bed are shown in Figure 32 and, following the development (see pages 32-39), the heat balance for the bed can be written for steady-state conditions

$$K_s^E \frac{d^2T}{dz^2} - (\dot{G}C_{p_g} + \dot{U}C_{p_s})\frac{dT}{dz} + r_{O_2}^{eff}\Delta H^c = 0 \qquad (136)$$

where only one exothermic reaction is assumed to take place, the reaction $C + O_2 \rightarrow CO_2$. However, the heat of reaction ΔH^c may be adjusted to compensate for endothermic effects. An assumption has to be made concerning the functional dependence of the reaction term $r_{O_2}^{eff}$ on distance and of the oxygen consumption distance z_O on the imposed gas flow rate ($\dot{G}$).

Vortmeyer assumed that z_O could be given by an equation developed by Wicke (122) for mass transfer controlled conditions,

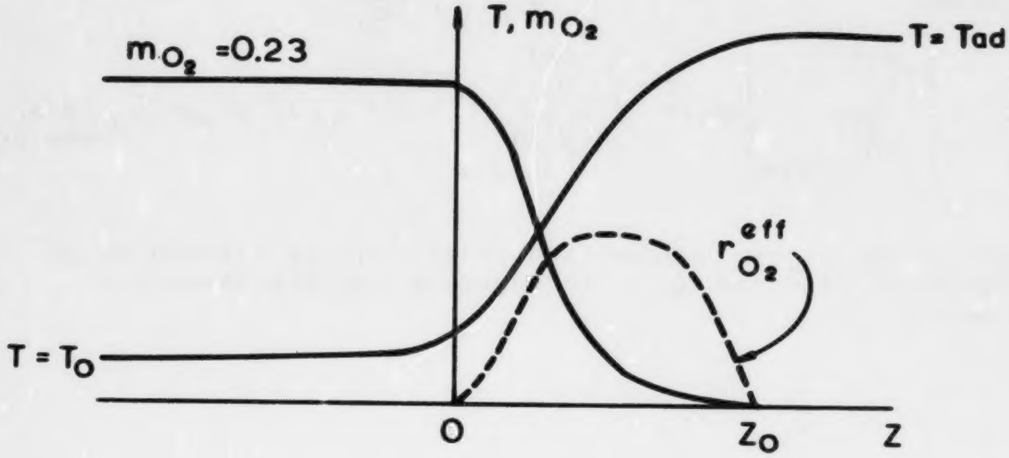

Fig. 32. Variation of Gas Composition, Temperature and Reaction Rate in the Vicinity of Ignition Front. After Vortmeyer (119).

$$z_0 \simeq \Lambda \simeq 0.185\, N_{Re}^{0.45}\, D_p \qquad (137)$$

where Λ is the distance that the oxygen concentration has dropped by a factor of e (called "Abklinglange" by Wicke). The development by Wicke for Λ follows Mayer's two-zone theory discussed on pages 61-75 and results in an infinite depth being required for complete oxygen consumption. As shown on pages 75-82, the three-zone theory is required to predict the correct order of z_0, but Vortmeyer (119) implicitly corrected for this by assuming $z_0 \simeq \Lambda$.

To obtain a reaction term insensitive to changes in gas flow rate and oxygen concentration, Vortmeyer took an average heat generation rate defined by $(r_{O_2}^{eff})_{ave} \;\; \frac{Gm_{O_2}^0}{z_0}$ and defined the function

$$f(z) = \left[\frac{r_{O_2}^{eff}}{(r_{O_2}^{eff})_{ave}}\right] \text{where} \int_0^\infty \frac{r_{O_2}^{eff}}{(r_{O_2}^{eff})_{ave}}\, dz = \bar{z}_0 \text{ in which } \bar{z}_0 \text{ is an average}$$

value of the oxygen consumption length and is assumed to be independent of G and $m_{O_2}^0$. Introducing the dimensionless variables

$$\theta = \frac{T - T_0}{T_{ign} - T_0}$$

$$\zeta = \sqrt{\frac{(r_{O_2}^{eff})_{ave} \Delta H^c}{K_s^E\, (T_{ign} - T_0)}} \qquad (138)$$

$$\lambda = (\dot{G}C_{p_g} + \dot{U}C_{p_s}) \sqrt{\frac{(T_{ign} - T_0)}{K_s^E (r_{O_2}^{eff})_{ave} \Delta H^c}}$$

into equation (136) gives,

$$\frac{d^2\theta}{d\zeta^2} - \frac{\lambda d\theta}{d\zeta} + f(\zeta) = 0 \qquad (139)$$

The appropriate boundary conditions are,

$$\theta = 0 \text{ at } \zeta = -\infty$$

$$\frac{d\theta}{d\zeta} \rightarrow 0 \text{ as } \zeta \rightarrow \zeta_0 \qquad (140)$$

where ζ_0 is defined as

$$\int_0^\infty \frac{r_{O_2}^{eff}}{(r_{O_2}^{eff})_{ave}} (\zeta) d\zeta = \zeta_0 \qquad (141)$$

This is an eigenvalue problem, but, with the transformation given above, ζ is now dependent on $\dot{G}$ and D_p as well as the initial mass fraction of oxygen in the air $(m_{O_2}^0)$. Using the relationships for K_s^E proposed on pages 25-31, the dependence of ζ on G and D_p is found to be very weak $[\zeta \propto (D_p G)^{-0.225}]$. Assuming that $m_{O_2}^0$ does not change, and that only small variations in G and D_p are considered, for a given $f(\zeta)$

$$\dot{G}C_{p_g} + \dot{U}C_{p_s} \simeq \lambda(m_{O_2}^0) \sqrt{\frac{K_s^E (r_{O_2}^{eff})_{ave} \quad \Delta H^c}{(T_{ign} - T_0)}} \qquad (142)$$

Using the relationships for K_s^E, equation (142) may be written approximately as

$$\dot{G} + \frac{C_{p_s}}{C_{p_g}} \dot{U} \simeq A(m_{O_2}^0) \sqrt{\frac{\dot{G}^{1.55}}{D_p^{0.45}} \left\{ \frac{\mu_g \delta h_r}{0.8 N_{Pr} k_g \dot{G}} + 1 \right\}} \qquad (143)$$

where A is a constant, dependent upon $m_{O_2}^0$.

A plot of $\left[G + \frac{C_{p_s}}{C_{p_g}} \dot{U} \right]$ as a function of $\sqrt{\frac{G^{1.55}}{D_p^{0.45}} \left\{ \frac{\mu_g \delta h_r}{0.8 N_{Pr} k_g \dot{G}} + 1 \right\}}$

is shown in Figure 33 for the data of P. Nicholls (24) on the underfeed combustion and ignition of different sizes of high temperature coke. The expected linear behavior is quite closely followed, but the effect of particle size is not fully taken into account by the theory. It should be noticed that this method of plotting the data is not very sensitive to values of $\dot{U}$ but the deviations from linearity shown for any particle size in Figure 33 can probably be attributed more to experimental error than to insensitivity of the plot.

Given the many assumptions that went into the development of equation (143), the general agreement between theory and experiment shown by Figure 33 is quite good; but a major shortcoming is the inability of the theory to predict the upper and lower ignition extinction limits. The theory suggests that there is no upper limit to extinction, for it is possible to have the ignition zone travel in the same direction as G (i.e., negative values of $\dot{U}$). The only limit would be reached when the ignition zone was blown out of the reactor or fuel bed. This type of behavior was noticed by Vortmeyer (119) in his experiments. This behavior has never been observed in a fuel bed and points to an essential difference between the two systems.

Vortmeyer's experiments were conducted with 0.4 cm diameter activated charcoal particles burning in O_2-N_2 mixtures; the oxygen concentration of the mixing was kept in the range 5% - 9% to minimize the amount of combustion that occurred. The particles were contained in a quartz tube which was surrounded by a heating mantle to keep heat losses from the burning zone small. The particles were ignited in an underfeed mode. The low oxygen concentrations used in this study explain why it was possible to observe the ignition front traveling with the gas flow; at high gas velocities, there was enough fuel remaining in the "burnt" bed to sustain ignition as the ignition front reversed direction and traveled back up the bed. This behavior would not be expected to be observed in a fuel bed because there would be very little fuel left behind the ignition plane.

An attempt was made in this study to develop an ignition criterion that circumvented some of the shortcomings of the Vortmeyer approach, following the developments of laminar flame propagation theory. There is no direct analogy between laminar flame propagation through gas mixtures and ignition in fuel beds because of the two-phase separation of the fuel and oxidant in the latter case and the different convective fluxes associated with each of these components. Mathematically, this means that the reaction rate term in a fuel bed

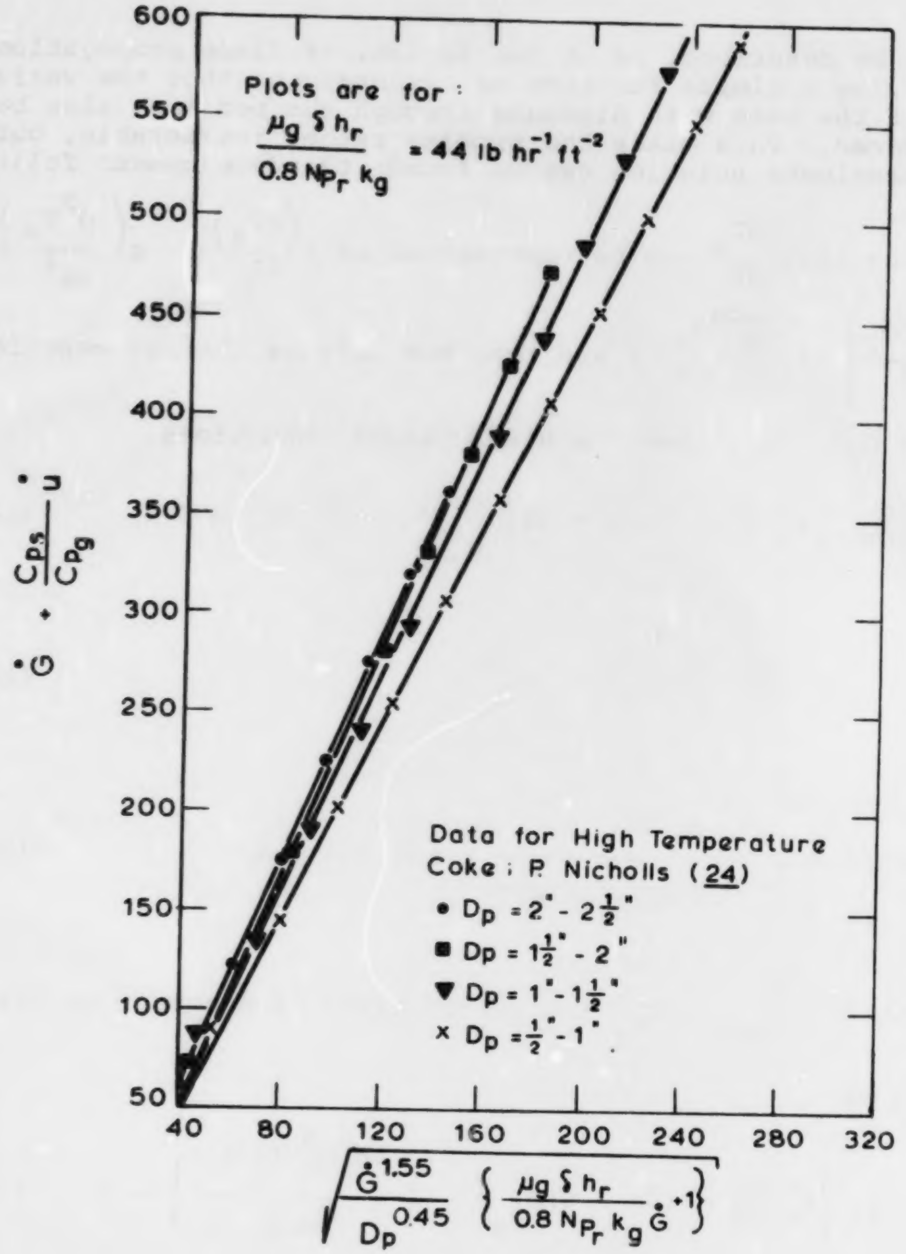

Fig. 33. Comparison of Vortmeyer's (119) Ignition Theory with the Experimental Data of P. Nicholls (24).

cannot be described, as it can in laminar flame propagation theory, by a simple function of temperature; thus the variation of the rate with distance through the bed must also be considered. This makes the problem rather intractable, but an approximate solution can be found; the development follows.

Assuming that $\frac{dT_g}{dz}$ can be represented as $f\left(\frac{dT_s}{dz}\right)$ or $g\left(\frac{d^2T_s}{dz^2}\right)$,

$D^E\left\{\frac{d^2m_{O_2}}{dz^2}\right\} << \frac{\dot{G}}{\rho_g}\frac{dm_{O_2}}{dz}$, and that the only exothermic reaction

is $C + O_2 \rightarrow CO_2$, then for steady-state conditions,

$$\frac{d}{dz}\left\{K_s^E\frac{dT}{dz}\right\} - (a\dot{U} + \dot{G})C_{p_g}\frac{dT}{dz} + r_{O_2}^{eff}\Delta H^c = 0 \qquad (144)$$

and

$$\dot{G}\frac{dm_{O_2}}{dz} = -r_{O_2}^{eff} \qquad (145)$$

where

$$r_{O_2}^{eff} = \frac{A_s m_{O_2}}{\frac{1}{k_m} + \frac{1}{\rho K\exp(-E/RT)}}, \text{ and } a = \frac{C_{p_s}}{C_{p_g}} \qquad (146)$$

Putting $\theta = \frac{T}{T_{max}}$, $m_{O_2} = m_{O_2}^o(1-\zeta)$ gives from equations (144)

and (145)

$$\frac{d}{dz}\left\{K_s^E\frac{d\theta}{dz} - (\dot{U}a + \dot{G})C_{p_g}\theta - \dot{G}\frac{\Delta H^c m_{O_2}^o(1-\zeta)}{T_{max}}\right\} = 0 \qquad (147)$$

and

$$\frac{d\zeta}{dz} = \frac{\bar{K}}{\dot{G}}(1-\zeta) \qquad (148)$$

where

$$\bar{k} = \frac{A_s}{\frac{1}{k_m} + \frac{1}{\rho K \exp(-E/RT_{max}\theta)}} \qquad (149)$$

Using the boundary condition that

$$\frac{d\theta}{dz} \to 0 \text{ as } \theta \to 1 \text{ and } \zeta \to 1 \qquad (150)$$

gives

$$\frac{d\theta}{dz} = \frac{(\dot{U}a + \dot{G})C_{p_g}(\theta - 1) + \dot{G}\Delta H^c m^O_{O_2}(1-\zeta)/T_{max}}{K^E_s} \qquad (151)$$

Equation (151) cannot be integrated directly as $\zeta = f(\theta,z)$. But

$$\frac{d\zeta}{d\theta} = \frac{d\zeta}{dz} \cdot \frac{dz}{d\theta} = \frac{K^E_s \bar{k} (1 - \zeta)}{\dot{G}^2 \left\{ C_{p_g} \frac{(\dot{U}a + 1)}{\dot{G}} (\theta - 1) + \frac{\Delta H^c}{T_{max}} m^O_{O_2} (1 - \zeta) \right\}} \qquad (152)$$

which can be integrated if a mean value of the product $K^E_s\bar{k}$ is taken. Putting,

$$w = 1 - \zeta \qquad (153)$$

and

$$y = - \frac{C_{p_g} T_{max}}{\Delta H^c m^O_{O_2}} \left\{ \frac{aU}{\dot{G}} + 1 \right\} (\theta - 1) \qquad (154)$$

and taking $K^E_s\bar{k}$ at its maximum value, when $\theta = 1$ gives

$$\frac{dw}{dy} = \frac{(K^E_s \bar{k})_{max}}{G^2 C_{p_g} (\frac{a\dot{U}}{\dot{G}} + 1)} \left\{ \frac{w}{w-y} \right\} \qquad (155)$$

The solution to equation (155), which passes through $w = y = 0$, is given by

$$w = \left\{ 1 + \frac{(K_s^E \bar{k})_{\max}}{G^2 C_{p_g} \frac{a\dot{U}}{\dot{G}} + 1} \right\} y \tag{156}$$

Using equation (156) in equation (152) gives, upon integrating the resulting expression for $d\zeta/d\theta$ from 0 to 1, the following result for the ignition velocity ($\dot{U}$)

$$\dot{U} = \frac{\dot{G}}{a} \left[\frac{(K_s^E \bar{k})_{\max}}{\dot{G}^2 C_{p_g} \left\{ \frac{1}{\int_0^1 R d\theta} - 1 \right\}} - 1 \right] \tag{157}$$

where

$$\int_0^1 R d\theta = \int_0^1 \frac{K_s^E(\theta)\bar{k}(\theta)}{(K_s^E \bar{k})_{\max}} d\theta \tag{158}$$

Unfortunately the evaluation of the integral given in equation (158) is not possible analytically. The values of $\dot{U}$ for different values of $\dot{G}$, therefore, have to be calculated using a suitable integration formula to evaluate the integral term. The results of some calculations performed to test equation (157) against the experimental data of P. Nicholls (24) on high temperature coke are shown in Figure 34. For these calculations the data of Parker and Hottel (93) were used to obtain the pre-exponential factor and the activation energy of the chemical reaction. The maximum value of the temperature (T_{max}) was calculated using the simple heat balance relationship

$$T_{max} = \frac{\Delta H^c m^0_{O_2}}{C_{p_g} \frac{a\dot{U}}{\dot{G}} + 1} \tag{159}$$

Since the development of the theory assumed a simple exponential decay of the oxygen concentration with distance (Mayers' (90) two-zone theory), the error this introduced was

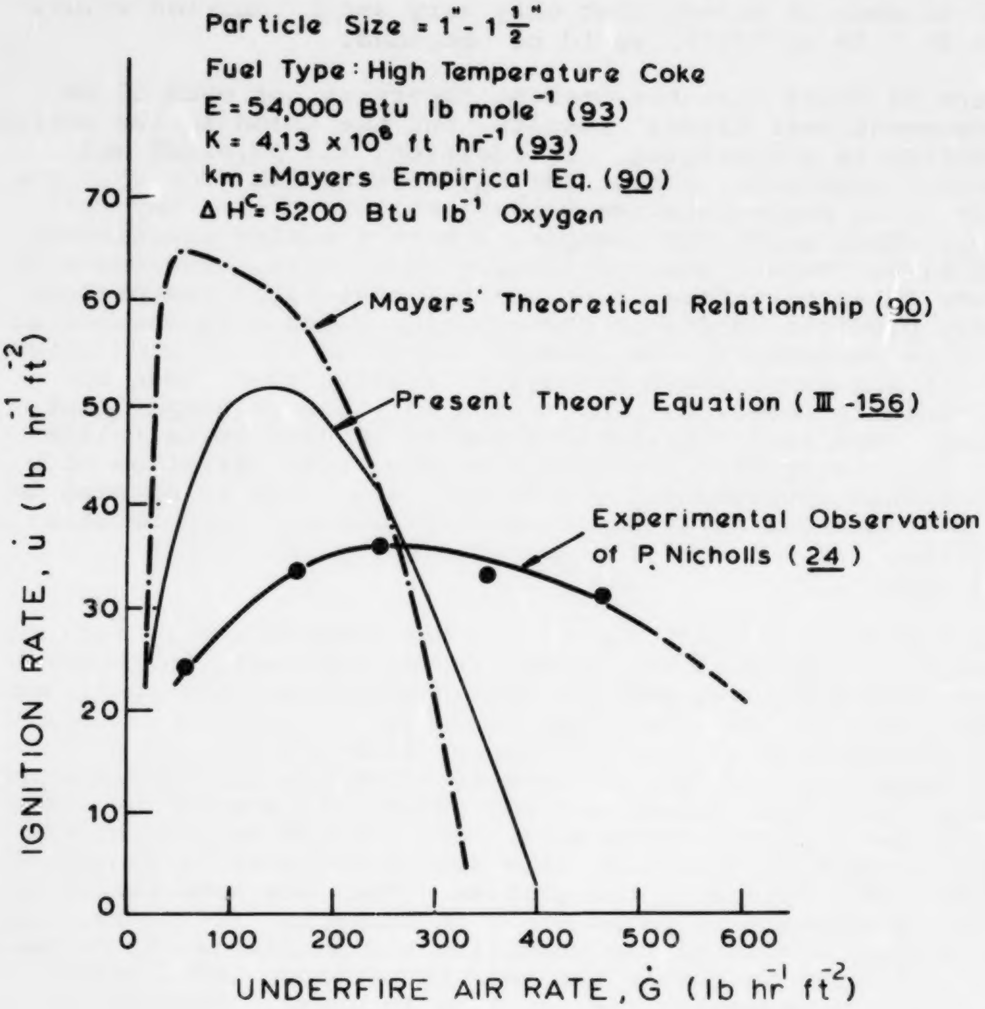

Fig. 34. Comparison of Ignition Theories with Experimental Data of P. Nicholls (24).

implicitly corrected by the use of Mayers' empirical relationships; this forced the reaction zone length to be of the right order of magnitude. Using a standard mass transfer correlation would, with this two-zone theory, broaden the reaction zone to such an extent that only very small ignition velocities ($\approx$ 5 lb $hr^{-1}ft^{-2}$) would be obtained.

Figure 34 shows that the present theory is not much of an improvement over Mayers' results, but the trend in the correct direction is encouraging. In addition, all physical and chemical constants, except for k_m, were chosen from what are known to be representative values; this is unlike Mayers' theory which used, for example, a heat transfer coefficient many times greater than physically reasonable. The curve in Figure 34 is therefore in no sense a best fit. The present theory predicts shifts in the ignition rates with changes in particle diameter in the correct direction but of a magnitude more of the order shown by Mayers' results than those experimentally observed. The reason for this is simply that Mayers' empirical correlations had to be used to calculate k_m. The theory also predicts a much sharper variation of $\mathring{U}$ with G than experimentally observed, and there is nothing in the mathematical development which prevents $\mathring{U}$ from becoming negative. This is, of course, physically impossible in a fuel bed.

Both Vortmeyer's (119) theory and the present theory fail to predict for the fuel bed (although, in fairness, Vortmeyer's theory was not developed for this application) the upper and lower limit to ignition. The lower limit probably depends on the magnitude of the heat losses from the bed and as such will depend on the type of apparatus used in the experimental study. Such heat losses are not taken into account by either of the theories presented here. The failure to predict the upper extinction point is, this author believes, a result of the internal nature of the problem. This has been hinted at in the discussion on pages 46-59 on Nicholls' (24) work. As the cooling effect of the underfire air increases, it becomes more difficult to obtain the mean temperature level within the particle necessary for ignition to occur. Presumably, for coke or coal particles, ignition is quantized to each particle because of the large thermal sink of the particle and its good thermal conductivity. Thus it is postulated that the localized ignition of one spot on the particle is an inherently unstable condition. For ignition to proceed, the whole layer of virgin fuel particles must ignite and this condition will only be reached when the whole layer reaches a mean temperature level high enough for this to occur. Once the cooling effect of the underfire air reaches a level where this mean temperature cannot be reached, ignition stops. The ignition plane cannot now be driven backwards and the fuel that has been ignited simply burns away and eventually dies out.

For the case of refuse, similar trends would be expected even though the characteristic dimension of the fuel elements will vary greatly and thus the amount of heat that is required to be transferred to each element for it to reach an ignition temperature will also vary. Those elements (i.e., paper, cardboard, etc.) which ignite easily will tend to propagate flame ahead of the main ignition plane. It is likely that the effect of the thermal sinks for both conductive and radiative heat transfer surrounding these tongues of flame will cause them to be damped out and the ignition front will in all likelihood propagate relatively evenly. The effect of tumbling the refuse (which has not been considered in this discussion up to now, although it commonly occurs in practice) will help the ignition processes if the tumbling is mild enough to prevent ignited material being plunged into an environment where it can lose enough heat to colder materials to quench active burning. The tumbling action can be considered an effective way of increasing the heat transfer in the bed to the cold unignited parts from the active burning part.

If, as suggested above, the ignition problem is an internal one, the simple theories presented here will not be able to adequately predict ignition behavior. A far more complex model would have to be developed, taking into account the thermal history of each layer of particles. In a simplistic way, some progress may be made by considering the unsteady-state heat transfer into semi-infinite slabs of material with suitable boundary conditions.

PROCESSES OCCURRING WITHIN A FUEL BED

Introduction

The conditions within the bed of a traveling grate have been qualitatively determined for coal-firing furnaces (123, 124, 94). The processes within a refuse bed are markedly more complex than those in a coal or coke bed because of the higher moisture and volatile content, as well as the greater heterogeneity, of the fuel; the various processes occurring at different positions on the traveling grate of an incinerator have not been adequately described. The purpose of this section is to provide a description of these processes as a reference frame for the discussion of the experimental results which will be presented on pages 184-261. The discussion given here will draw heavily on the results of the survey on pages 21-130.

The one area of refuse combustion not covered in the survey on pages 21-130 is that concerning the role of drying and pyrolysis of the fuel; to date there has been no work in this field of direct application to incinerator conditions. This section will therefore begin with a description of the effect of moisture content on the time required for ignition and on the rate of combustion of the fuel particles.

Effect of Moisture on Ignition and Combustion Times

Outline of Problem Considered. The heat effects associated with drying are greater than those associated with pyrolysis and, therefore, for a high moisture content fuel such as refuse, the drying heat load will be assumed to be the only one of importance. The moisture content of a fuel particle can obviously affect the time required for the particle to ignite, and the drying of the particle may provide the limiting step in the overall combustion process. The drying behavior of a particular particle will depend on many factors (amount of moisture, both free and bound; micro- and macroscopic structure of the particle; its diathermicity; and the heating rate itself). None of these factors has been studied in enough detail to permit anything but a crude picture to be established for a "typical" refuse particle. There will, naturally, be a wide range of behavior in the drying characteristics of refuse components; only the two extremes of this range will be discussed here. These limits correspond to the cases where (1) the rate of heat transfer to the particle is much higher than the rate of internal diffusion of water and (2) the rate of internal diffusion of water is high enough for the surface temperature to remain in the vicinity of the vaporization temperature of water (212°F).

For the first case it is assumed that, at the high heating rates associated with a fuel bed, the solid exhibits drying characteristics that resemble the "falling rate period" in drying operations, and that a vaporization plane will retreat into the material as it is heated. This model, at least for wet wood irradiated with intensities from 2.0 to 3.1 cal cm^{-2} sec^{-1} (2.7 to 4.2 x 10^4 Btu $hr^{-1}ft^{-2}$), has been observed to fit experimental results reasonably well (125, 126). The progress of the drying front is controlled by the conduction of heat to the vaporization plane, and other mechanisms of moisture transport (diffusion of bound water through cell walls and the migration of free water under capillary effects) are slow in comparison to the rate of travel of the vaporization plane. The effect of the intertracheid motion of the steam has been shown by both Williams (125) and Gardon (126) to have little effect on the drying process. This model of the drying behavior of the fuel particle reduces mathematically to the so-called Stefan problem, which despite its conceptual simplicity is mathematically complex because of the nonlinearity introduced by the boundary condition at the vaporization plane.

For the second extreme of behavior, it is assumed that the internal diffusion of water is very rapid. In this case, the drying time can be calculated from the amount of heat that must be transferred to the particle to supply all the heat for drying under the assumption that the surface remains at 212°F. This type of behavior might be exhibited by, for example, oranges and watermelons.

Development of Drying Models. For the first type of limiting behavior, the ignition time may be calculated using the following mathematical description of the drying process. The particle is considered semi-infinite, and initially at the vaporization temperature of the liquid (T_s^v); all thermal properties of the material are uniform and constant. The equations describing the process of vaporization, assuming that the convective flow of the steam has a negligible effect on the temperature distribution within the solid, are then as follows. Within the dry phase, the temperature is determined by

$$\nabla^2 T_s = \frac{1}{\alpha_s^d} \frac{\partial T_s}{\partial t} \qquad (160)$$

where α_s^d is the thermal diffusivity of the dry solid. The required boundary conditions are

$$
\begin{aligned}
&\text{(i)} && T_s = T_s^v \ \text{ at } x = X, \text{ the dry-wet interface} \\
&\text{(ii)} && -k_s^d \left.\frac{\partial T_s}{\partial x}\right|_{x = X} = \rho_s^d\, \overline{\Delta H_v}\, \frac{dX}{dt} \\
&\text{(iii)} && -k_s^d \left.\frac{dT_s}{dx}\right|_{x = 0} = h_s(T_s - T_\infty) \\
\text{or}\ &\text{(iv)} && -k_s^d \left.\frac{dT_s}{dx}\right|_{x = 0} = Q
\end{aligned}
\qquad (161)
$$

where T_s^v is the temperature at the drying front; k_s^d the thermal conductivity of the dry solid; h_s the gas-solid heat transfer coefficient per unit area of solid surface; T_∞ the temperature of the gases flowing past the solid (assumed constant); Q the net heat flux per unit area of solid surface; and $\overline{\Delta H_v} = \Delta H_v\left(\frac{\rho_s^w}{\rho_s^d} - 1\right)$, where ΔH_v is the latent heat of vaporization of water and ρ_s^d and ρ_s^w the dry and wet density of the solid. The boundary condition at the dry-wet interface is obtained by a heat balance which equates the rate at which heat is absorbed at the interphase by vaporization of the water to the rate at which heat is transferred to the interface by conduction. The boundary condition at the surface can be expressed in two forms, by postulating either radiant heat flux or convective heating of the solid. Kreith and Romie (127) and Goodman (128) have presented graphical results of the solution to the above set of equations. These are shown in Figures 35 and 36.

A rough check on this model may be made by calculating ignition times for different moisture contents and comparing them to the data of Simms and Law (117). Using Q = 0.5 cal cm^{-2} sec^{-1} (6.6×10^3 Btu $hr^{-1}ft^{-2}$), $\rho_s^d \approx 50$ lb ft^{-3}, $C_{Ps} \approx 0.5$ Btu lb^{-1} $°F^{-1}$, $k_s^d \approx 0.2$ Btu $hr^{-1}ft^{-2}$ $°F^{-1}$, and an ignition temperature suitable for piloted ignition, $(T_s^\circ)_{ign} = 644°F$ gives, from Figure 36, the time required for ignition of wood with a moisture content of 20% as 2.5 min. The data of Simms and Law show that, for the above conditions, times of between 4-5 min were needed for the piloted ignition of European

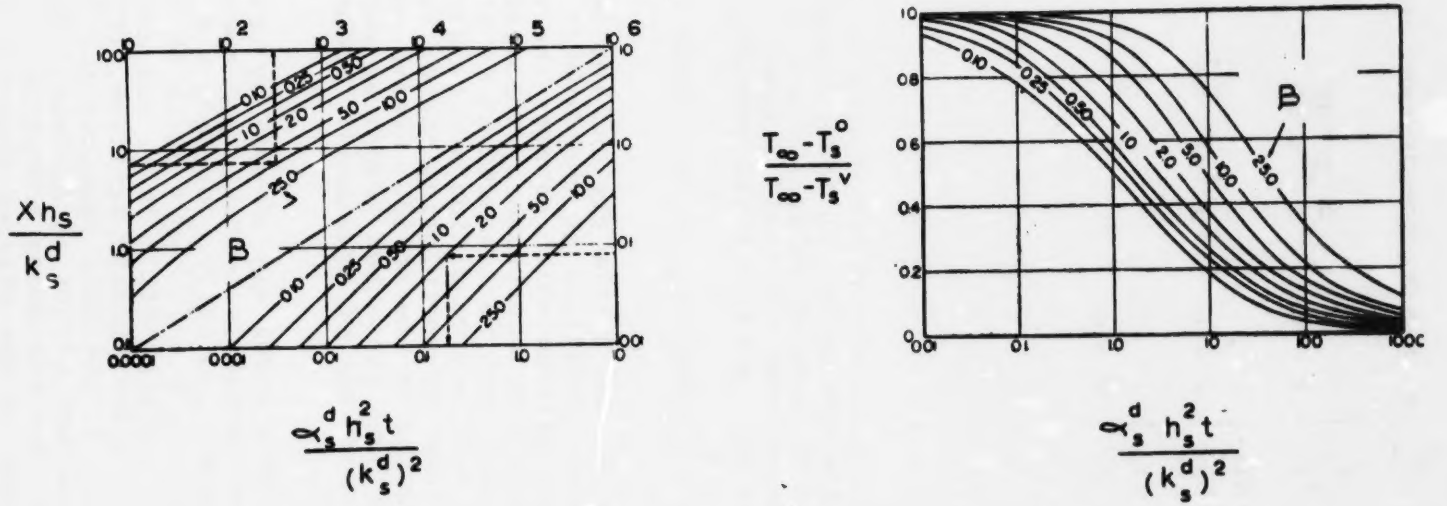

Fig. 35. Surface Temperature ($T_s^{\,o}$) and Depth of Penetration (x) of the Vaporization Plane in a Semi-infinite Slab for Convective Heating of Surface by Gas at T_∞.

Results of Kreith and Romie (127), $\beta = \dfrac{\Delta H_v}{C_{p_s}(T_s^v + T_\infty)}$

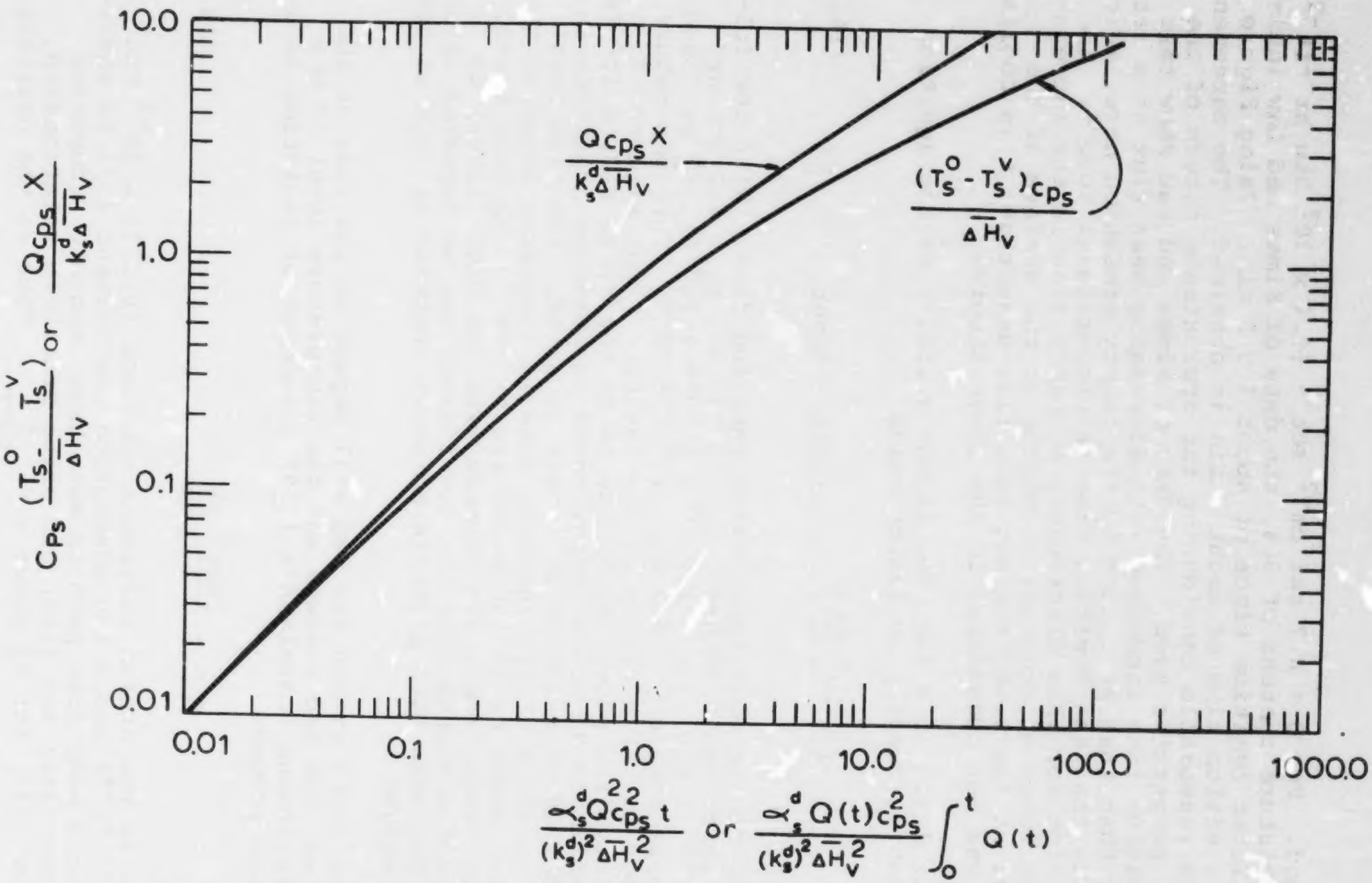

Fig. 36. Surface Temperature (T_s^o) and Depth of Penetration (X) of the Vaporization Plane in Semi-infinite Slab for Constant Heat Flux (Q) Surface Condition. Results of Kreith and Romie (127) and Goodman (128).

whitewood. For $Q = 0.7$ cal cm^{-2} sec^{-1} (9.4×10^3 Btu hr^{-1}ft^{-2}) and a moisture content of 60%, the data of Simms and Law indicate piloted ignition times of about 4.5-5 min. Using Figure 36, an ignition time of about 3 min is obtained. The agreement is quite reasonable considering the approximate nature of the thermal properties used. The data of Simms and Law show that the ignition time increased with decreasing heat flux at a rate greater than that predicted by the theory presented here, which indicates that the ignition time is proportional to Q^{-2}. The explanation for this discrepancy probably lies in the increasing importance of convective cooling of the surface of the material at the lower radiant heat flux densities; this cooling effect was not considered in the above theory.

The flux level in a fuel bed in the vicinity of the ignition plane can be readily evaluated using

$$q = -K_s^E \frac{dT}{dx}\Big|_{x\,=\,\text{ignition front}} \qquad (162)$$

where K_s^E can be calculated using equation (13). With the following approximate values: $D_p = 0.125$ ft, $k_s = 0.2$ Btu hr^{-1} ft^{-1} °F^{-1}, $\delta = 0.4$, $\epsilon = 1.0$, $T = 1800$°F (2260°R), K_s^E is found to be approximately ≈ 4.2 Btu hr^{-1}ft^{-1} °F^{-1}. The temperature gradients in the vicinity of the ignition front were found in this study (see pages 206-208) to be in the range 6-20 x 10^3 °F ft^{-1}, while in Nicholls' experiments temperature gradients in the range 10-30 x 10^3 °F ft^{-1} were observed. The flux level in the vicinity of the ignition zone is therefore expected to be of the order of 25-100 x 10^3 Btu hr^{-1}ft^{-2}. On this basis, ignition times from a few seconds (for the high fluxes) to about half a minute (for the low fluxes) can be expected within a fuel bed even with particle moisture contents as high as 60%-70% by weight.

The flux level within the bed will depend on the size of the particles, the bed voidage and the temperature level of the bed. Following Rosseland's (129) treatment of radiation as a diffusion process

$$q = -\frac{16\sigma T^3}{3\lambda}\frac{dT}{dx} \qquad (163)$$

where σ is the Stefan Boltzmann constant (0.1713×10^{-8} Btu ft^{-2}hr^{-1} °R^{-4}) and λ the absorption coefficient ($1/\lambda$ is equivalent to a mean free path or mean beam length). Comparing equations (162) and (163) and using Schotte's relationship, equation (13), for K_s^E gives $\lambda = \dfrac{3}{4D_p\delta}$. Thus as the particle size (D_p) or the voidage (δ) increases, the mean beam length ($1/\lambda$) will increase and the unignited fuel will be exposed to a greater heat flux as it will "see" more of the hot combustion zone.

The most important dependence of K_s^E will be on the temperature, but the results of this study (see pages 204-206) and Nicholls' (24) data show that the peak temperature at the ignition front is not strongly affected either by changes in underfire air rate or by fairly wide variations of bed composition. For fuels which approximate refuse, temperatures of the order of 1800°F are typically observed near the ignition front (26, 27, 47) and this finding has been substantiated by this study. Evaluating the thermal conductivity on the basis of a temperature of 1800°F therefore appears reasonable for incinerator fuel bed conditions.

The next consideration is how the moisture content of the fuel hinders the combustion rate. This may be estimated as follows. Assuming a fixed surface temperature (T_s^o) and a linear temperature distribution in the particle (which will be valid for high moisture contents), the progress of the drying front can be readily shown to be given by

$$\frac{dX}{dt} = \sqrt{\frac{k_s^d (T_s^o - T_s^v)}{2\overline{\Delta H}_v \rho_s^d \, t}} \tag{164}$$

Equation (164) shows that the rate of propagation of the vaporization plane decreases as $t^{-0.5}$, as expected, since the potential for heat transfer (dT/dx) decreases as $t^{0.5}$. Further assuming that the pyrolysis reactions occur instantaneously above a critical temperature T_s^c, the rate of generation of pyrolysis products is

$$\dot{R}_p = \frac{w_p (T_s^o - T_s^c)}{2\,(T_s^o - T_s^v)} \sqrt{\frac{k_s^d (T_s^o - T_s^v)}{2\overline{\Delta H}_v \rho_s^d \, t}} \tag{165}$$

where w_p is the mass of pyrolysis products per unit volume of fuel. Bamford, Crank and Malan (130) indicated that a pyrolysis product generation rate greater than 1.84 lb $hr^{-1} ft^{-2}$ is necessary for spontaneous combustion to occur. For the conditions in a fuel bed, where some flame is present, this pyrolysis product generation rate should provide an upper bound for the rate required to sustain combustion. Inserting typical values into equation (174) -- $\rho_s^d \approx 50$ lb ft^{-3}, $k_s^d \approx 0.2$ Btu hr^{-1}ft^{-1} ^{o}F^{-1}, $T_s^o \approx 1800^{o}$F, $T_s^v \approx 212^{o}$F, $T_s^c \approx 600^{o}$F, $w_p \approx 30$ lb ft^{-3}, $\overline{\Delta H}_v \approx 600$ Btu lb^{-1} (for 60% moisture content) -- gives $\dot{R}_p \approx \frac{0.85}{\sqrt{t}}$. Using the Bamford, Crank and Malan criteria for sustaining combustion, the rate of pyrolysis product generation would fall below the threshold level only after a period of 0.2 hr. It can be hypothesized, therefore, that drying may limit the pyrolysis rate to the extent that it will hinder active flaming. Some further elementary calculations show that the heat load associated with the movement of the drying wave will not act as a severe local heat sink, as the enthalpy required can be readily supplied by convective transfer from the combustion gas and radiative heat transfer from surrounding elements.

For elements whose drying characteristics are of the first limiting type, the time required to dry a particle of known moisture content and size can be estimated following Tao (131). The equations solved in this case are the same as equations (160) and (161), except they are written for spherical geometry and for a constant surface temperature, so that

$$\nabla^2 T = \frac{1}{\alpha_s^d} \frac{\partial T}{\partial t} \qquad (166)$$

becomes

$$\frac{2}{r} \frac{\partial T}{\partial r} + \frac{\partial^2 T}{\partial r^2} = \frac{1}{\alpha_s^d} \frac{\partial T}{\partial t} \qquad (167)$$

and

$$T_s^o = a \quad \text{at} \quad r = r_o \qquad (168)$$

This model assumes that there are no reactions taking place within the solid. Near the ignition zone the reaction of oxygen on the surface of the particle will have a strong exothermic effect while, when all the oxygen has been depleted, the reactions $C + CO_2 \rightarrow 2CO$ and $C + H_2O \rightarrow H_2 + CO$ will give moderate endothermic effects. It will be assumed here that radiative exchange will minimize the effects of these reactions.

Tao presented the results of a numerical solution to the equations (166) and (161). These are shown in Figure 37,

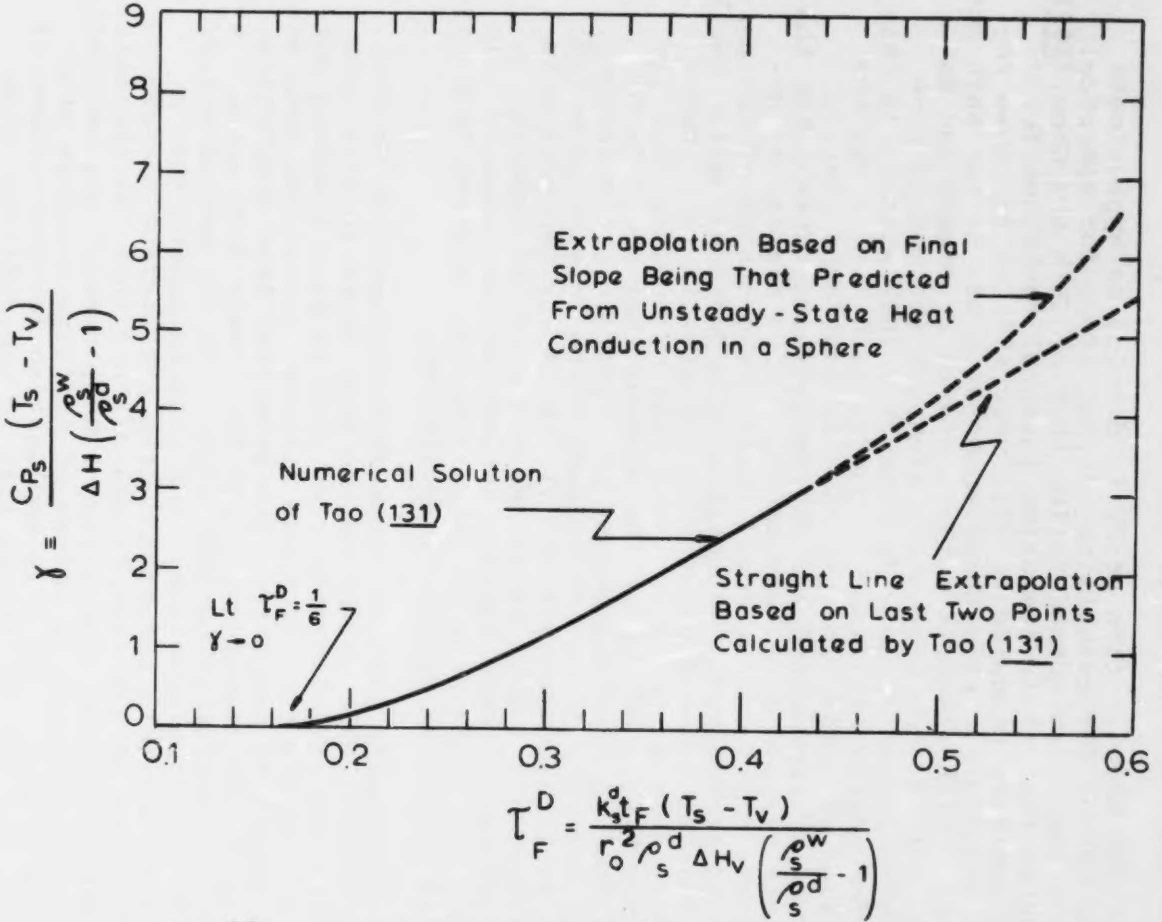

Fig. 37. Drying Times for Spherical Particles of Different Moisture Content. Numerical results of Tao (131)

where τ_F^D is the final dyring time (dimensionless) and γ the dimensionless moisture loading. Tao's results for the rate of propagation of the drying wave appear to agree (within 5%) with the analytical solution to equations (160) and (161) for short times, but there is no known analytical solution that can be used to check his numerical values of τ_F^D.

As attempt was made in this study to develop an approximate analytical method for calculating drying times for spherical particles. The first method follow that of Shih and Chou (132), who indicated that their iterative integral technique for spherical geometry produced results very similar to those reported by Tao (131). From these authors' study of the Shih and Chou method, which was originally proposed by Siegel and Savino (133), it is concluded that, although the method gave results which agreed closely (within 5% - 10%) with Tao's calculation for nearly all times in the range $0 < \tau^D < \tau_F^D$, the method failed at times close to τ_F^D. It was found that, in the limit as τ^D approached τ_F^D, the method gave times, when the drying front reached a certain radius, which started to decrease as the drying front moved towards the center of the particle. This is obviously impossible on a physical basis. Shih and Chou made no comment about this behavior in their paper. Furthermore, this author also found that even after four iterations had been used (about the maximum that could be obtained without an enormous amount of algebraic manipulation), the solution gave a linear dependence of the drying time (τ_F^D) on the initial moisture content (γ). A linear dependence is not shown by Tao's calculations and would not be expected on physical grounds. These authors suggest on the basis of this study, that the usefulness of this iterative integral technique, at least in spherical geometry, is limited.

A second approximate integral technique suggested by Goodman (128) was tried. This technique has been shown to give good results with the semi-infinite slab with various boundary conditions, but it has not, to these authors' knowledge, been used before in spherical geometry. The spherical heat conduction equation (167) was transformed into the linear form using θ = Tr, on the suggestion of Goodman (134) that the method worked best for the Laplace equation. The results showed that at zero moisture content, the method gave the correct dimensionless drying time of 1/6 (see Figure 37) but that, as the moisture content increased, the drying time increased exponentially and approached infinite at values of the dimensionless heat load greater than 5. The only explanation for the failure of this method that can be offered lies in the different form of the boundary conditions at the interface, which results when the transformation θ = Tr is used, to that form for the semi-infinite slab given in equation (161). On the basis of this study and a brief literature review it appears that at present there are no approximate analytical techniques suitable for the Stefan problem in spherical geometry.

Tao's calculations therefore represent the only generalized method of caluclating drying times for spherical particles. Using his results, the drying time for a 3-in.-diameter sphere of wood containing 60% moisture is found to be about 25-30 min. The drying time scales as the radius squared (r^2) so that for a particle of 6 in. diameter containing 60% moisture the drying time would be greater than a typical residence time for traveling-grate incinerators, which is about one hour.

On the basis of the foregoing discussion the following conclusions can be drawn for combustible elements which exhibit the first type of drying behavior (i.e., where the rate of heat transfer to the particle is much higher than the rate of internal diffusion of water). The presence of moisture increases the time required for ignition over that required for a dry element; however, at the flux levels typically obtained within a fuel bed, the ignition delay is not expected to be more than about half a minute even for particles containing 60-70% by weight of water. From Tao's generalized calculation of drying times, active drying and pyrolysis will, for large particles, continue for extended periods after the particles have been ignited. Using equation (165) and typical values of the physical properties of wood, it may be hypothesized that the drying rate may, with high moisture content fuel elements, provide the rate-limiting step for combustion. Finally, the heat load associated with the propagation of the drying wave is not expected to act as a severe local heat sink, and therefore the drying process will not affect the combustion behavior of the drying particles' neighbors.

For the other case of limiting behavior, where the internal diffusion of moisture is high, the calculation of an ignition time is somewhat more complex because of the effect of the local heat sink on the fuel bed surrounding the particle. A simple calculation shows that, at the heat transfer rates expected in a fuel bed, particles of up to a few inches (say, the size of an orange) would be expected to dry in times well under one minute. However, it is common experience that materials of this type can remain uncharred in a fuel bed for much longer periods. The explanation lies in the strong local heat sink created by this type of particle because of its low surface temperature. It can easily be shown that the strength of this heat sink can be expected to be far greater than any possible local heat generation (except very close to the ignition front), and it can therefore be concluded that these particles essentially quench all the surrounding materials (see pages 113-118 and the discussion of radiant heat loss on ignition stability). Fuel elements of this type are dried mainly by the convective heating of the hot gases flowing past them. The drying time, based on the convective heating of the particle with gases at 2000°F, is about 10-15 min. for a particle the size of an orange.

The conclusion that, for refuse materials which exhibit this type of drying behavior, the fuel bed is locally quenched is a strong argument for effecting some tumbling action on the grate so that these particles will be exposed to the flame and refractory above the bed. For this type of refuse particle, the drying time plays the dominant role in the overall combustion time, as the combustion of the fully dried material (which will only be a small fraction of the original weight of the particle) will be a very small fraction of the total "combustion" time.

Description of Fuel Bed Conditions on a Traveling Grate

Ignition of the Fuel Bed. Traveling grates are used in many incinerators, and therefore the ensuing discussion will focus mainly on conditions in the fuel bed of such a system. Despite the heterogeneity of the bed and the different drying and combustion characteristics of the various fuel elements, it is convenient forpurposes of discussion to subdivide the burning fuel bed on the traveling grate into well-defined zones as shown in Figure 38.

A combustible element in a fuel bed may receive the thermal energy required for drying, pyrolysis and ignition via a number of different mechanisms. In the overfeed bed the thermal energy is supplied by radiation from the overfire region (from both the hot combustion gases and the refractory walls) by the convective heating of the combustion gases flowing up through the fuel bed and by radiative heating from the combustion zone of the fuel bed. In the underfeed bed the major portion of the thermal energy is supplied via radiation from the combustion zone directly behind the ignition front, while the remainder is supplied by conduction through the fuel (97). In the case of the traveling-grate stoker the fuel at the top of the bed near the feed end of the grate is heated solely by radiation from the overfire region. Once the ignition plane progresses down into the fuel bed, as shown in Figure 1(c), the thermal energy

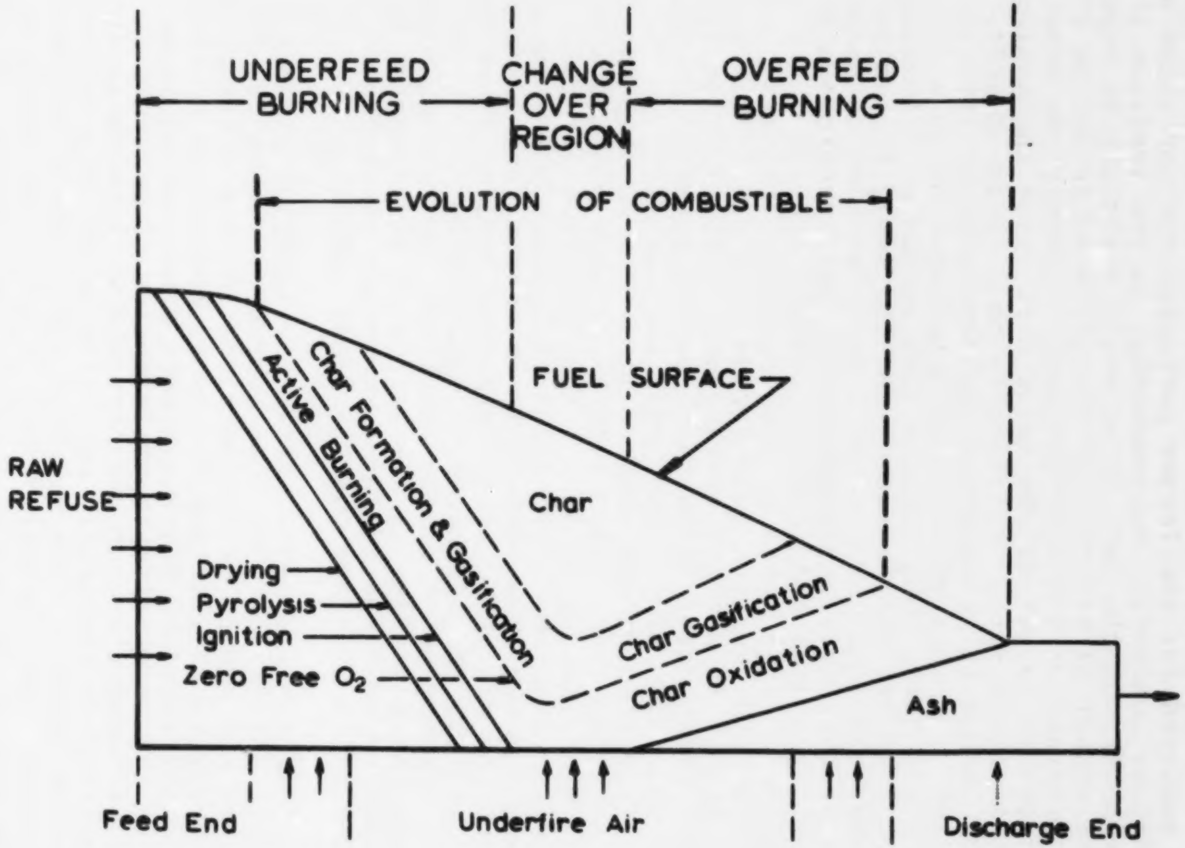
UNDERFEED BURNING
CHANGE OVER REGION
OVERFEED BURNING
EVOLUTION OF COMBUSTIBLE
FUEL SURFACE
RAW REFUSE
Char Formation & Gasification
Active Burning
Char
Char Gasification
Char Oxidation
Ash
Drying
Pyrolysis
Ignition
Zero Free O2
Feed End
Underfire Air
Discharge End

Fig. 38. Simplified Schematic of Processes Occurring in the Fuel Bed on a Traveling Grate

required is transferred to the virgin fuel in a manner analogous to the underfeed case.

As discussed on pages 112-113 and pages 118-129 , it is important to keep the underfire air rate low at the entrance to the traveling-grate stoker in order to insure that ignition is achieved for the larger particles and for those with high moisture contents. Subsequently, as the ignition plane propagates through the bed, it is again necessary to supply the right amount of air through the grate so as not to hinder the progress of the ignition wave. Ideally the underfire air should be set at the value that gives the maximum possible ignition rate. Practically this is impossible, because not enough is known about the processes of ignition propagation for this value to be determined on an a priori basis. Field tests would be the only method of selecting the correct underfire air rate. Qualitatively it can be expected that the ignition rate will be a function of underfire air preheat (24) and supply rate (24), particle size (24), fuel type (24) and moisture content (26,27). For refuse, Kaiser's (114) tests on the Oceanside Incinerator indicated that the ignition rate varied from 0.3 ft/min for wet material to 0.5 ft/min for average material. The ignition rate would be expected to decrease as the moisture content of the fuel increased since there will be a decrease in the total heat liberated within the bed that is available for heating up fresh fuel (see pages 118-129). Present theories do not give an indication of how the underfire air rate should be varied to take into account the different fuel moisture contents; it would seem reasonable to expect that lower air rates might be necessary with increasing fuel moisture contents. Finally, the hindrance of ignition by having too little underfire air may be of little practical importance, since in reality the underfire air is likely to be augmented by air induced through the bed by temperature gradients between the center of the furnace and the "cold" walls.

Combustion of the Fuel Bed. After the ignition plane has passed over a fuel particle, the course of combustion will be dictated by the nature of the particle and its moisture content. Two types of limiting behavior, controlled by the drying characteristics of the fuel, were discussed on pages 131-141. When the internal rate of diffusion of moisture is low, the surface temperature of the particle will increase slowly until ignition is achieved. Depending on the particle's size and moisutre content, this may take place over a period of a few minutes after the main ignition front has passed by. After the surface reaches an ignition temperature, the particle will continue to pyrolyze and burn until either all the oxygen surrounding the element is consumed or the rate of generation of pyrolysis products falls below the level required to sustain ignition; the latter condition would be achieved if the heat supplied to the fuel element was not great enough to drive the vaporization plane at a rate sufficient to supply the required amount of dry pyrolyzable material. This point was discussed on pages 131-141 . The surface of a fuel element, shortly after the ignition plane has passed it, will begin to char; it will then be oxidized by any available O_2 or will react with CO_2 and H_2O, according to the reactions $C + CO_2 \rightarrow 2CO$ and $C + H_2O \rightarrow H_2 + CO$. Only the very small particles will burn out completely at this stage, and the larger ones will still be drying and pyrolyzing when all oxygen in the underfire air is consumed.

For fuel elements in which the rate of diffusion of moisture is rapid, the heat sink will cause, as discussed on pages 131-141 , local quenching of ignition and combustion; these particles and those surrounding them will then remain in this quenched state until all the moisture from the fuel element has been removed and there is enough oxygen and heat supplied to the element for it to ignite and burn. If the residence time in the furnace is not long enough, these elements will be discharged incompletely combusted and may cause some of the surrounding particles to be discharged in a similar state.

The important reactions occurring within the fuel bed, excluding pyrolysis reactions and the combustion of tarry pyrolysis products, are given in Table 8 along with their heats of reaction. The equilibrium constants of these reactions are plotted as a function of temperature in Figure 39 and their relative reaction rates are compared in Table 9. Table 8 shows that, except for the almost neutral water gas shift reaction (vi) and the slow and thermodynamically unfavorable reaction (vii), the only exothermic reactions taking place within the bed will consist of the reaction of oxygen with char and pyrolysis products. The very high rate of reaction of oxygen with both char and pyrolysis products, as indicated by Table 9 suggests that all the oxygen in the underfire air will be quickly consumed within a small zone just behind the ignition front; this behavior was observed in the coal bed studies of Nicholls (24) and Kreisinger *et al.* (23) -- see pages 9 - 14 and pages 18 - 21 . The heat released within this zone provides the only source of energy within the fuel bed to dry and pyrolyze the fuel and to sustain ignition.

Active burning will take place in a zone determined by the rate of consumption of underfire oxygen in both volatile and char combustion. Burning rates in coal beds were found by Nicholls (24) to be approximately proportional to underfire air supply rate, unless the burning rate

TABLE 8

Common Fuel Bed Reactions and Their Heats of Reaction (135)

	Reaction	Standard Heat of Reaction* (Btu lb $mole^{-1} \times 10^{-3}$)
(i)	$C_{(\beta)} + O_{2(g)} \rightarrow CO_{2(g)}$	-169.29
(ii)	$C_{(\beta)} + \frac{1}{2}O_{2(g)} \rightarrow CO_{(g)}$	-47.55
(iii)	$CO_{(g)} + \frac{1}{2}O_{2(g)} \rightarrow CO_{2(g)}$	-121.74
(iv)	$C_{(\beta)} + CO_{2(g)} \rightarrow 2\,CO_{(g)}$	74.19
(v)	$C_{(\beta)} + H_2O_{(g)} \rightarrow CO_{(g)} + H_{2(g)}$	56.48
(vi)	$CO_{(g)} + H_2O_{(g)} \rightarrow CO_{2(g)} + H_{2(g)}$	-17.71
(vii)	$C_{(\beta)} + 2\,H_{2(g)} \rightarrow CH_{4(g)}$	-32.20
(viii)	$H_{2(g)} + \frac{1}{2}O_{2(g)} \rightarrow H_2O_{(g)}$	-104.04
(ix)	$CH_4 + 2\,O_2 \rightarrow CO_2 + 2\,H_2O$	-345.17
(x)	$C_2H_4O_{2(g)} + 2\,O_{2(g)} \rightarrow 2\,H_2O_{(g)} + 2\,CO_{2(g)}$ (acetic acid)	-358.16

---

* Negative sign indicates exothermicity. β-graphite assumed to have zero heat of formation; various types of amorphous carbon are reported to have positive heats of formation ranging from 3.06 to 4.68 Btu lb $mole^{-1}$ (136)

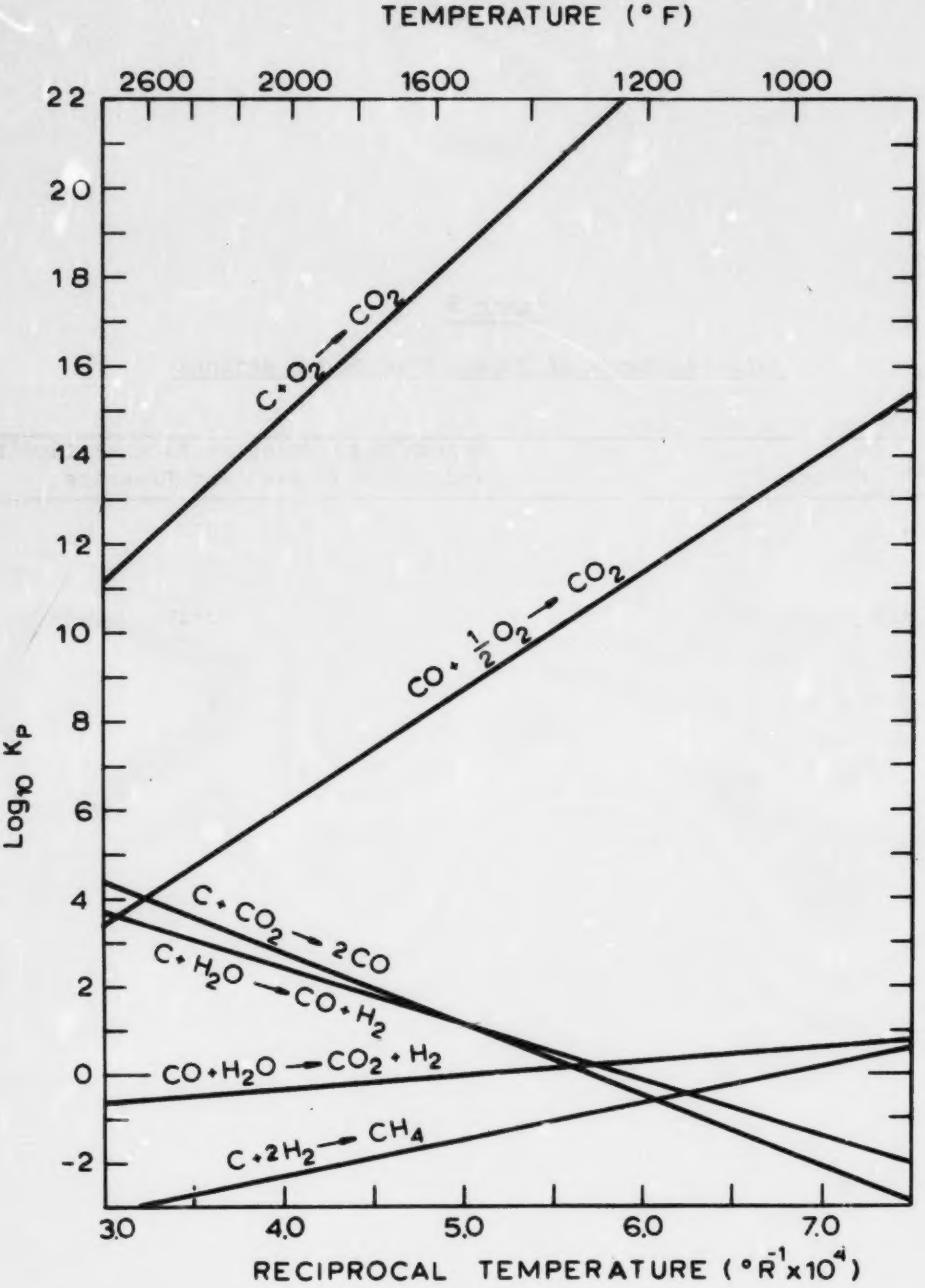

Fig. 39. Equilibrium Constants of Common Fuel Bed Reactions (92). (All compounds as gases; carbon as β-graphite.)

TABLE 9

Relative Rates of Common Fuel Bed Reactions

Reaction	Approximate Relative Rate at 1800°F and 0.1 Atm. Reactant Pressure
$C + O_2 \rightarrow CO_2$	10^5
$C + H_2O \rightarrow CO + H_2$	3-10
$C + CO_2 \rightarrow 2\ CO$	1
$C + 2\ H_2 \rightarrow CH_4$	10^{-3}

was restricted by the ignition rate (see pages 46 - 59). Roughly the same behavior can be expected in a refuse bed if the model of Niessen et al. (19) is correct (see pages 106-112). Beyond the point of oxygen depletion, additional release of volatiles will occur from the larger particles and the char will be gasified by the CO_2 and H_2O rising from the burning zone. Up to the point where the ignition wave reaches the grate, the burning action will be of the unrestricted underfeed type. After the ignition plane has reached the grate, combustion of the residual char will be limited by the supply of oxygen; the CO_2 released on combustion in this region will partially react with the remaining char to yield CO.

Burning rates may be estimated from the results of Niessen et al. (19) or by considering that the reactions $C + CO_2 \rightarrow 2CO$, $C + H_2O \rightarrow H_2 + CO$ and $C + 2H_2 \rightarrow CH_4$ are all fast enough for them to equilibrate by the time the top of the fuel bed is reached. As discussed below, this concept of total equilibrium is a poor one for a refuse bed, as the energy requirements are too great, and fuel bed depths too shallow, for these reactions to be equilibrated.

Figure 40 shows equilibrium gas concentrations, for different fuel compositions, calculated under the assumption that the above three reactions are equilibrated. These gasification calculations were performed using values of the equilibrium constants at chosen temperatures; hence, no energy constraints were imposed upon the system. For typical fuel bed temperatures (1600°F-2000°F), it is common to observe the following ranges of gas compositions at the top of the bed (assuming no bypass oxygen): CO, 10%-20%; CO_2, 10%-20%; H_2, 5%-10%; H_2O, 10%-15%; and traces of methane and pyrolysis products. These values are quite different from those expected on the basis of total equilibration, where the equilibrium constants for the reactions indicate that mainly CO and H_2 should be observed at temperatures above 1600°F. This discrepancy can readily be explained since, for the complete conversion of CO_2 and H_2O to CO and H_2 more energy would be required than could be supplied by the exothermic reactions taking place within the bed, and therefore in an incinerator the degree of approach to equilibrium will be constrained by energy considerations (see pages 106-112).

Figure 41 shows the amount of fuel gasified per lb mole of underfire air as a function of fuel bed temperature and fuel composition on the assumption of total equilibration and no energy constraints. The caluclated gasification rates (at typical refuse bed temperatures) are very much higher than those observed in practice (about 60 lb $hr^{-1} ft^{-2}$), reflecting

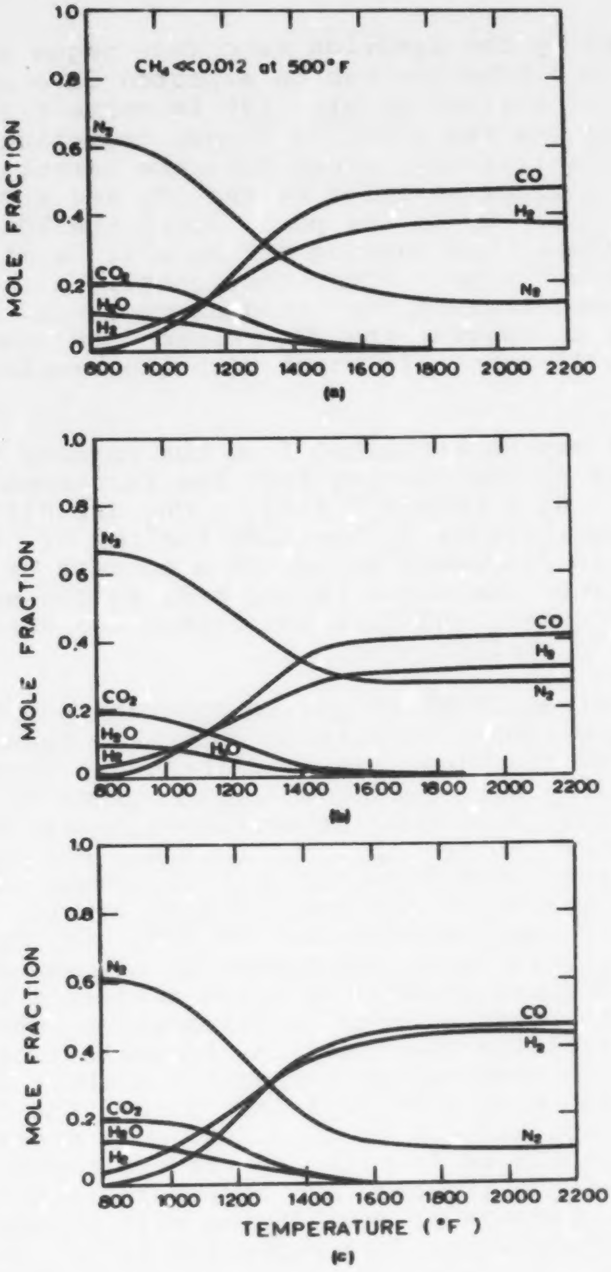

Fig. 40. Equilibrium Gas Compositions at Various Assumed Fuel Bed Temperatures. Different fuels gasified with air at 1 atm pressure: (a) pure cellulose, (b) Kaiser's (49) approximate composition (dry), (c) Kaiser's (49) approximate composition (15% moisture).

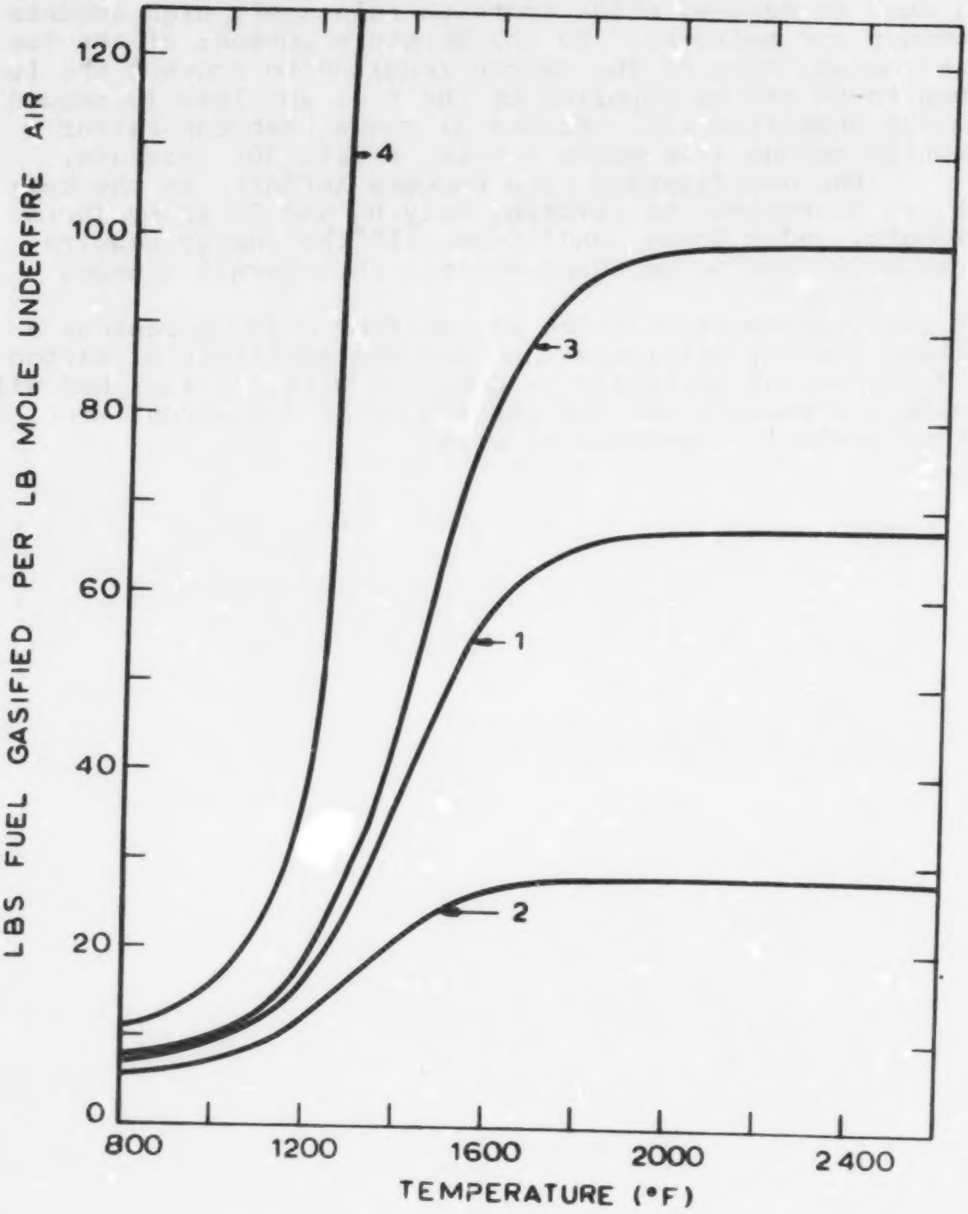

Fig. 41. Variation of Burning Rates with Temperature for Different Fuels. 1 - dry cellulose; 2 - Kaiser's composite, dry ash sulphur and nitrogen free; 3 - Kaiser's composite, 15% moisture; 4 - Kaiser's composite, 30% moisture.

the greater "saturation" of the underfire air with respect to carbon and hydrogen when enough energy can be supplied to the bed so that H_2 and CO are the only products of combustion. Figure 41 shows an interesting characteristic of a fuel such as refuse, which contains relatively high amounts of oxygen and hydrogen. As the moisture content of the fuel is increased, more of the oxygen required to convert the fuel carbon to CO can be supplied by the fuel and less is needed from the underfire air. Figure 41 shows that for Kaiser's composite refuse (see pages 9 - 14) with 30% moisture, the gasification rate becomes infinite as the temperature increases, so favoring only H_2 and CO as products; obviously, under these conditions, all the energy requirements would have to be supplied from an external source.

This qualitative description of the four major processes -- heating, drying, pyrolysis, and the gas reactions of carbon and carbonaceous materials -- occuring within a fuel bed will provide a framework for the discussion in subsequent sections of this author's experimental work.

EXPERIMENTAL EQUIPMENT AND PROCEDURE

Choice of Experimental Equipment

Brief Outline of Equipment Selected. The experimental equipment chosen for this study was an extension of the underfeed combustion pot equipment used by the early workers [e.g., Kreisinger et al. (23) and Nicholls (24)] in the field of solid fuel bed combustion. The simple combustion pot was modified so that the radiant heat flux condition which would be experienced by the top of the fuel bed in a traveling grate unit could be simulated under these batch conditions and so that burning rates could be determined by measuring the weight loss of the fuel bed as a function of time. In principle an instantaneous fuel bed burning rate can be calculated if it is possible to close a complete material balance around the unit at any particular time. However, the cumulative errors associated with this approach are greater than those connected with a weighing technique and the latter method is therefore preferable.

The modification adoped here follows the approach used by Weintraub et al. (26), in which the apparatus is constructed in two sections, the overfire combustion region, or top section, and the fuel bed section, or bottom section. Overfire air was supplied at a number of different positions in the top section, while the underfire air was fed through a grate which supported the fuel bed in the bottom section. The design allowed the top section to be isolated from the bottom section and then preheated with gas burners. When the temperature gradients in the top section refractories had stabilized, the two sections were joined together and the fuel bed was ignited by exposure to the radiant heat flux from the hot brickwork of the top section. The initial radiant heat flux density used to ignite the fuel was controlled by the final temperature level of the refractories in the top section at the end of the preheat stage. During a run the radiant heat flux to the top of the fuel bed could be roughly controlled by adjusting the overfire air flow rate, which in turn changed the temperature level of the refractories. The course of combustion was followed as a function of time by measuring the change in weight of the bottom section.

This type of apparatus provided a satisfactory model of the conditions in the fuel bed on a traveling grate, in that time in this batch-type experiment was equivalent to position on a traveling grate (94, 137, 138). The major criterion that needed to be satisfied for adequancy of this model was the similarity of the fuels in the two systems. This analogy has had certain limitations which are discussed below.

Discussion on Limitations of Batch Systems. In the moving-grate system a continuous belt carries the burning bed in one direction. The bed is ignited at the feed end of the grate by the absorption of radiant heat and the ignition zone gradually penetrates the bed until it reaches the grate further towards the discharge end of the grate. Referring back to Figure 1(c), it will be recalled that H is the length of the fuel bed burning on what Nicholls (24) called "the unrestricted ignition underfeed principle," and 0 is the length of the fuel bed burning in a manner similar to the overfeed principle. It should again be stressed that length 0 of the fuel bed is burning only in a way similar to the overfeed principle. The burning rate in this section will increase roughly in proportion to the quantity of underfire air, but there will be no pyrolysis products issuing from the top of the bed, unlike a continuous overfeed operation. The actual process of combustion can be further complicated since the bed is in many cases agitated by a reciprocating grate. This has the advantageous effect of mixing and breaking up agglomerates in the bed, but the back-mixing can also lead to increased losses in unburnt material to the ash pit and in increased fly-ash carry-over.

The development of methematical and experimental models of the combustion processes within the fuel bed can proceed from the stand-point of an external or internal observer. From any external position, the conditions on a grate would appear to be steady-state, resulting in a steady-state, two-dimensional (length and depth) problem. The justification for only considering two of the spatial directions in any mathematical representation lies in the fact that many traveling grates are wider than 6 feet and therefore property variations across the width of the grate can be ignored. From any fixed position on the grate the conditions in the fuel bed would be changing with time, and, if one were to model a small section of this fuel bed as it traveled across the grate at the prevailing grate speed, an unsteady-state, one-dimensional (depth) problem would result. The property variations across the width of the grate can also be ignored in this formulation for the same reason as stated above. In this model, the time coordinate is proportional to distance traveled across the grate, the proportionality constant being the grate speed. These considerations indicate that a small batch incinerator with no property variations in either the length or breadth (or radial or angular) directions (i.e., one-dimensional in depth) could be used to simulate a small section of the bed as it travels across the length of the incinerator. A criticism of this formulation is that the inclination of the ignition zone in the traveling grate creates both horizontal and vertical components for the ignition wave propagation velocity as indicated in Figure 42. The angle of inclination of the ignition zone to the grate will be a function of both the grate velocity, V_G, the underfeed ignition propagation velocity, V_N, and the crossfeed ignition propagation velocity, V_P. The relationship being

$$\tan \beta = V_N/(V_G - V_p) \qquad (168)$$

or

$$\tan \beta = V_N/V_G \text{ for } V_G >> V_P \qquad (169)$$

where β is the angle of inclination of the ignition front to the grate. Typical values of V_N and V_P (4 in/min) and V_G (1 ft/min) indicate that β will in general be a small angle (< 20°) and suggest that under normal operating conditions a small segment of the bed, taken perpendicular to the grate, could be adequately treated as being one-dimensional in depth.

Further complications with this model formulation ensue, since, during the course of conbustion, the resistance of the bed varies and as a result, on a traveling grate, there will be a tendency for greater underfire air flow through the portions of the bed with low resistance (i.e., near the discharge end). This problem is partly circumvented in practice by dividing the wind box into compartments and controlling the flow of air to each compartment. In the batch system this effect can be simulated by varying the underfire air as a function of time. A drawback with the batch mode of operation is that, as the fuel bed burns down, cold walls are constantly being uncovered in the bottom section and thus the isotherms in this type of bed cannot be expected to follow those in a traveling grate. This cooling effect can be minimized in the experimental model by carefully insulating the bottom section, or by providing a movable grate which can be used to hold the ignition front at the same relative position in the apparatus. The latter expedient is difficult to accomplish experimentally and all investigators using the combustion pot type of apparatus have opted for the former approach. A somewhat simplified analysis of the cooling effect expected when using carefully insulated side walls is given in Appendix B and shows

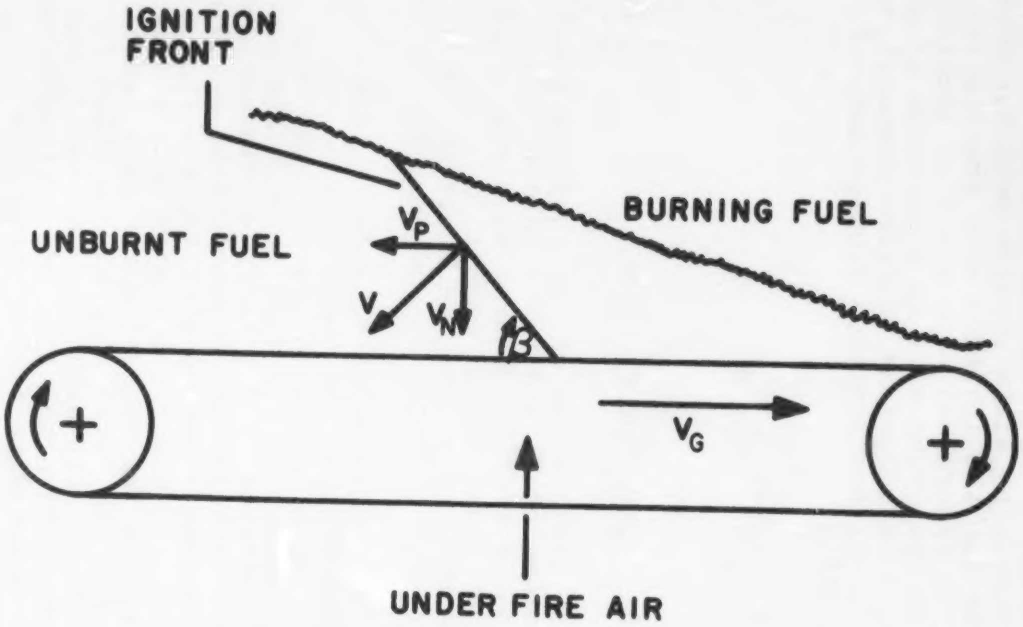
IGNITION FRONT
BURNING FUEL
UNBURNT FUEL
V_P
V
V_N
β
V_G
UNDER FIRE AIR

Fig. 42. Diagrammatic Representation of Direction of Ignition Wave Propagation Relative to Directions of Grate Travel and Underfire Air Flow. V_P = ignition velocity parallel to grate; V_N = ignition velocity normal to grate; V = resulting ignition velocity; V_G = grate velocity; = angle of ignition front to grate

that the heat losses are small compared with the heat generated during combustion.

Up to this point the discussion has focused on the modeling of the fuel bed itself, but it is also necessary to consider the similarities and dissimilarities in the processes occurring in the overfire region of the continuous and batch systems and any advantages or disadvantages that the batch system might have. Generally, the flue gas compositions in batch experiments would not be expected to compare with those found in continuous units, unless a period of "pseudo steady-state" operation were achieved. In fact, the gas composition from a continuous unit would more closely agree with the gas composition found from a batch experiment if all the flue gases from such an experiment were collected and mixed together. Further difficulties are also apparent, since it would be very unlikely that the degree of mixing of the overfire air and combustion products would be alike in the two types of experiments, as the geometry of the system plays an important role in this process. The gas temperatures in the batch system would tend to be lower than those in a continuous system, since the latter would be physically larger and heat losses less significant. Consequently, it is impossible to match weight-averaged temperature histories of the gas in the different apparatus, and thus difficult to develop quantitative theories which would be equally applicable to both. However, as serious as these shortcomings appear, the batch system provides a very convenient and compact way of studying the qualitative effects of overfire mixing and its effect on the burnout of soot particles, smoke and carbon monoxide. Further, in a batch system, the changes in composition of the flue gases may be studied during the different burning regimes of the fuel bed, and effects detected which may well be disguised by gross mixing in a continuous unit.

The above discussion has shown that many of the shortcomings of this approach at simulating a traveling grate can be overcome by careful design of the experiment. The advantages of using a batch system over a scaled-down traveling grate far override the disadvantages for the following reasons:

(a) The distribution of air, both above and below the bed, can be closely controlled in a small experiment by the use of a high-pressure drop grid below the bed and by careful selection of jet size and air momentum above the bed.

(b) A unidimensional system is approached so that a fairly complete map of temperature and composition distribution may be obtained both within and above the fuel bed. The problem of obtaining gas and temperature profiles is greatly reduced.

(c) Instantaneous values of the rate of incineration may be obtained. The measurement of a burning rate at a particular time corresponds to that at a given position on a grate; the start of a run corresponds to the discharge from the feed-hopper, and the end of a run to the point of discharge into the ash-quench tank.

Description of Experimental Apparatus and Peripheral Support Equipment

Incinerator Hardware. A brief description of the apparatus is given in this section, a fuller description with complete engineering drawings being left to Appendix A. The description given here covers all the modifications that have been made to the equipment since it was first completed in May 1971. Many of the experimental runs were not performed with all the system modifications described below; the evolutionary development will be fully covered in the section on Results and Discussion (see pages 184-261).

A sketch of the apparatus indicating all the salient features is shown in Figure 43. Figures 44 and 45 are photographs of, respectively, the apparatus with some of its peripheral equipment and the interior of the fuel bed section. The principle of design for the apparatus closely followed that used by Weintraub et al. (26), the top section (overfire region) was joined to the bottom section (fuel bed region) so that the bottom section could be weighted independently. A flexible steel diaphragm, mounted in the "no flex" position (which exerted the minimum drag on the bottom section), provided a seal between the two sections. The top section was suspended from the ceiling of the test cell, while the fuel bed section was supported on a load cell which measured this section's weight using the strain gauge principle. As shown in Figure 43, the fuel bed section was mounted on a base plate which had a central shaft protruding from the undersurface. This shaft, made from special case hardened steel, passed through two linear ball bushings and rested on the load cell.

There were a number of possible arrangements for weighing the fuel bed section using load cell techniques, but the above method was considered the most satisfactory as it eliminated the effect of eccentric loads and kept inherent load cell errors to a minimum. A more detailed discussion of this

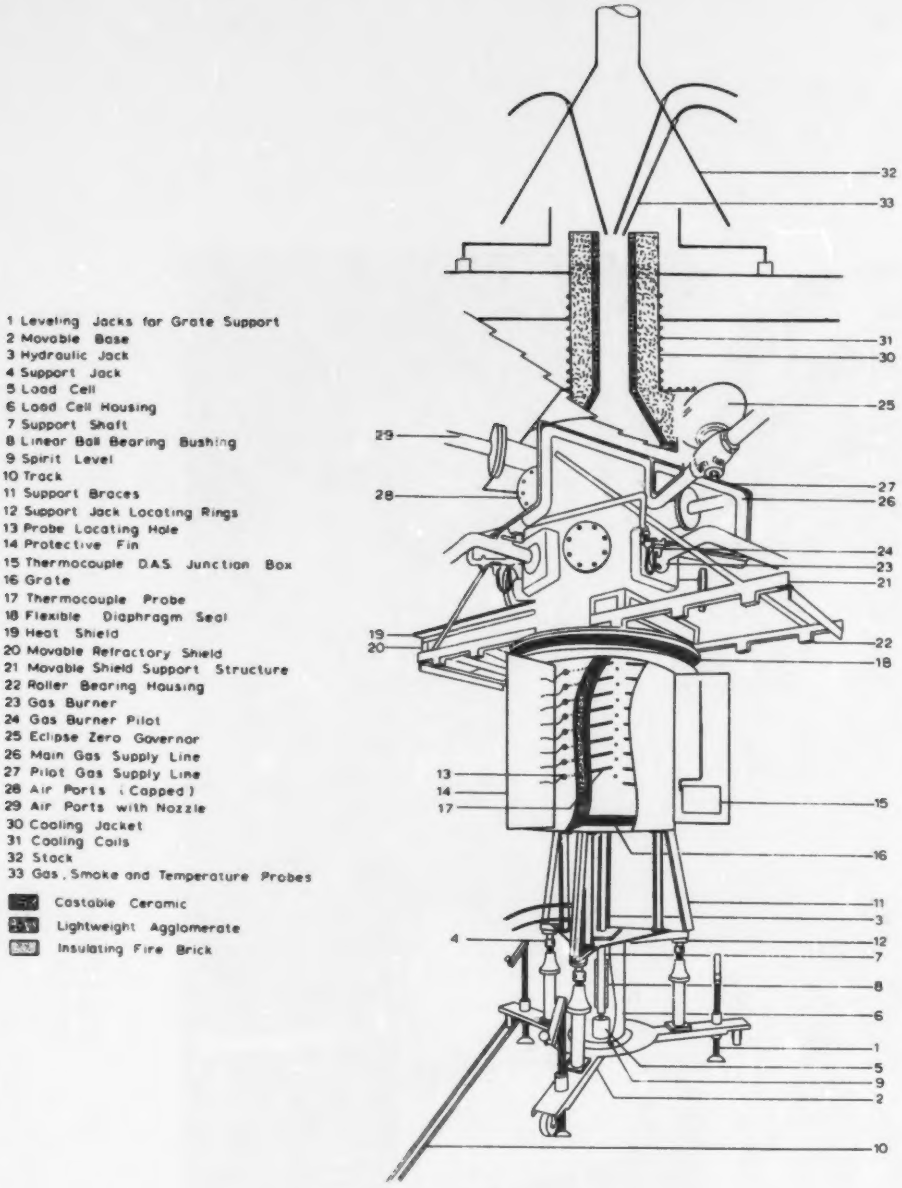
1 Leveling Jacks for Grate Support
2 Movable Base
3 Hydraulic Jack
4 Support Jack
5 Load Cell
6 Load Cell Housing
7 Support Shaft
8 Linear Ball Bearing Bushing
9 Spirit Level
10 Track
11 Support Braces
12 Support Jack Locating Rings
13 Probe Locating Hole
14 Protective Fin
15 Thermocouple D.A.S. Junction Box
16 Grate
17 Thermocouple Probe
18 Flexible Diaphragm Seal
19 Heat Shield
20 Movable Refractory Shield
21 Movable Shield Support Structure
22 Roller Bearing Housing
23 Gas Burner
24 Gas Burner Pilot
25 Eclipse Zero Governor
26 Main Gas Supply Line
27 Pilot Gas Supply Line
28 Air Ports (Capped)
29 Air Ports with Nozzle
30 Cooling Jacket
31 Cooling Coils
32 Stack
33 Gas, Smoke and Temperature Probes
▨ Castable Ceramic
▨ Lightweight Agglomerate
▨ Insulating Fire Brick

Fig. 43. Sketch of Experimental Incinerator.

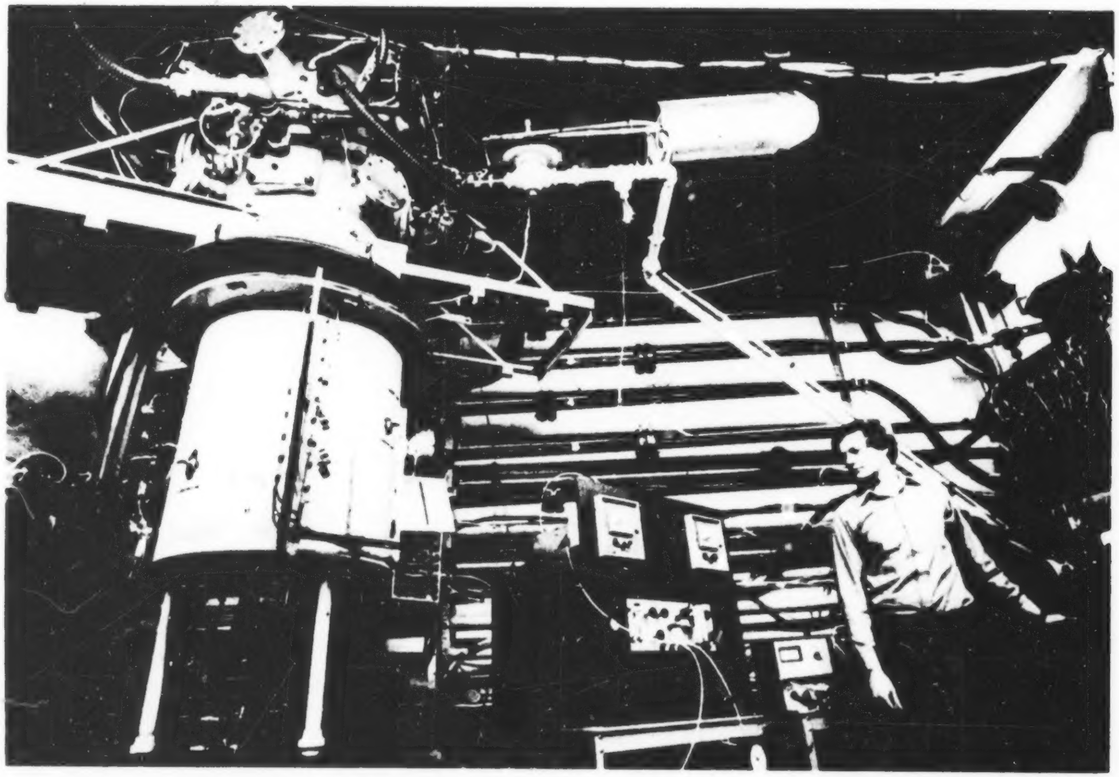

Fig. 44. Experimental Incinerator, Gas Analysis Train and Peripheral Equipment.

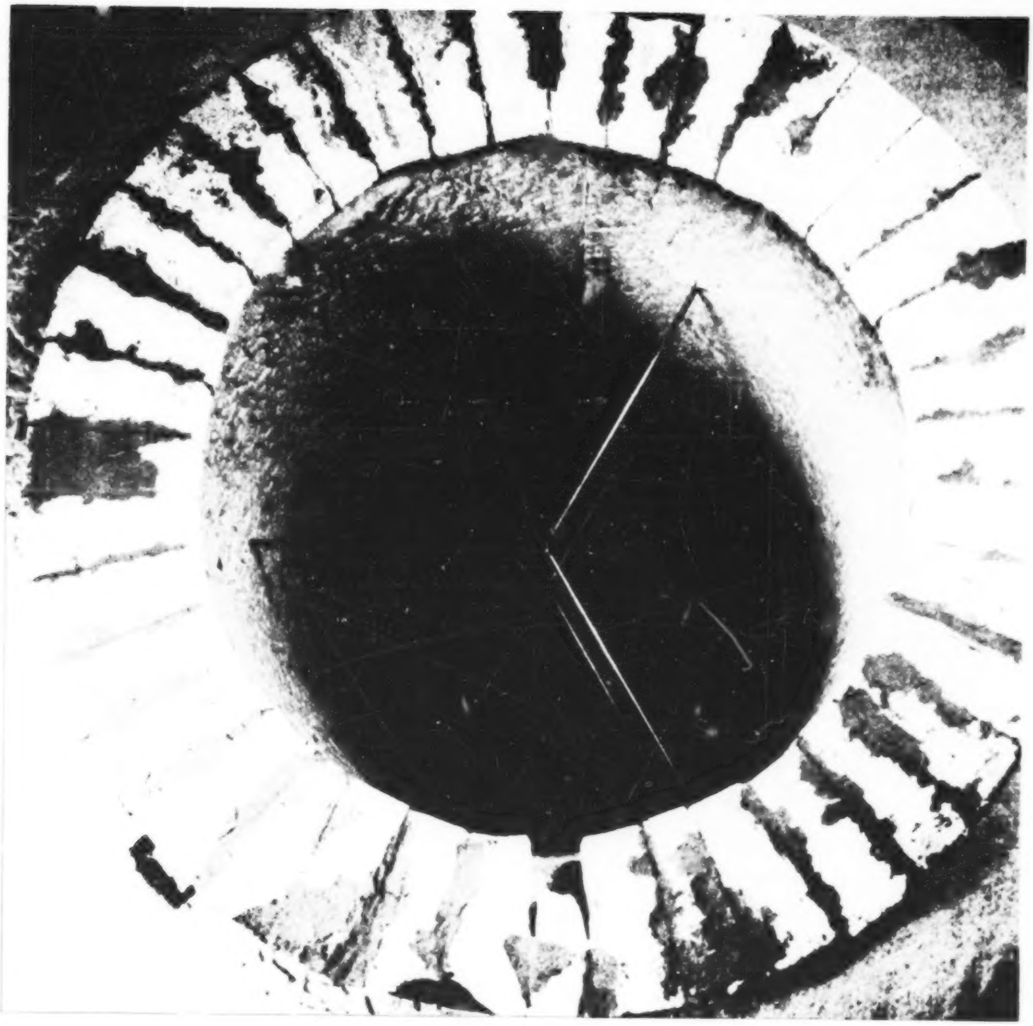

Fig. 45. Interior of Fuel Bed Section with Thermocouple Probes Installed.

point and details of the load cell are given in Appendix C.

When the apparatus was not in use, the dead load of the fuel bed section was lifted off the load cell using the support jacks. Before using the weighing system the bottom section was accurately leveled with the leveling jacks and the fuel bed section was then lowered onto the load cell.

The two sections of the incinerator were separated by a sliding refractory shield which was mounted just above the diaphragm seal. The shield moved in a plane perpendicular to the rest of the incinerator and was constructed in two refractory-lined sections. One half had a cooling coil set into its base while the other half had an 18-inch-diameter hole cut through the middle of the refractory lining. When the shield was in the "off" or closed position, the section containing the cooling coils sealed the top section from the bottom section and thus permitted the top section to be preheated without any excess heat leakage to the bottom section. In the "on" or open position, the hole in the shield aligned with the top and bottom section combustion areas, thus connecting the two sections and permitting the radiant heat flux from the top section to ignite the fuel bed.

Overfire air was supplied to the top section via any combination of twelve nozzles at various vertical and radial positions. The nozzle ports permitted the installation of a wide range of nozzle configurations. The fuel bed was built on a grate supported by a hydraulic jack which was used to set the grate at different vertical positions so that the burning characteristics of beds of different depths could be studied. The underfire air was supplied through the grate, the design of which insured an even air distribution. The pressure drop across the grate was kept large in comparison to the pressure drop across the fuel bed, thus minimizing the probability of having the underfire air channel through the fuel bed.

The bottom section of the apparatus had three sets of nine sample ports spaced at 120-degree intervals around its circumference. The vertical arrangement of the twenty-seven sample locations allowed measurements to be made at one-inch intervals throughout the bed. The maximum bed depth that could be studied was thirty inches, equivalent to a fuel bed volume of 4.2 ft^3. The thermocouples (Chromel-Alumel) and the gas probes were designed so that they were mutually compatible with the sample port fittings. Three "heat loss" probes, each consisting of three thermocouples at different radial positions, were located at different vertical and angular positions within the insulating walls of the fuel bed section. The temperature histories of the three thermocouples in each probe gave an indication of the rate of heat leakage through the insulating walls of the fule bed. The top section had eight thermocouples imbedded in the refractory lining near the surface and three thermocouples on the outside steel shell. These were used to monitor the temperature and temperature gradients of the rafractory, both during the preheat stage and during an experimental test. Gas and smoke samples were taken from the flue gases in the stack, and the temperature of the flue gas was recorded using a shielded Chromel-Alumel thermocouple.

For the purposes of calculating material balances, it was essential to know all air flow rates into the equipment. Since it was very difficult to seal the whole unit against air leaks, perticularly around the sliding refractory shield, the leakage rate was determined by feeding a known flow rate of helium into the overfire air. Batch samples were taken during a run from the stack gas probe and the helium concentration in the sample subsequently measured using a Beckman gas chromatograph.

The measurements taken during a typical experiment are discussed below. Twelve thermocouples were used within the fuel bed, ten located at the center, the other two near the edges of the fuel bed. The thermocouples were roughly evenly distributed throughout the depth of the fuel bed. Two gas probes were used in the bed, one 20 inches and the other 12 inches above the grate. These probes were used to analyze for oxygen, carbon monoxide, carbon dioxide, nitrogen, methane and hydrogen. All three fuel bed heat loss probes were employed, as were all the thermocouples in the top section. The flue gas temperature and its water, carbon dioxide, carbon monoxide and oxygen content were recorded, and the concentration of the helium leak tracer was measured. The fuel bed weight loss was followed by recording the load cell output, and the overfire and underfire air flow rates were measured at frequent intervals. The ambient conditions of temperature, pressure and relative humidity were noted both prior to and immediately following the experiment. Fuller details of the measurements and the measurement techniques are given in subsequent sections and appendices. All of the measurements made with equipment and instruments that gave response signals in a voltage form were recorded on punched paper tape using a Hewlett-Packard 2014B Data Acquisition System. The data collection and analysis procedures are covered fully in a later section.

Air Supply. The overfire and underfire air, as well as the air necessary for running the gas burners and pilots, was supplied by a Hoffman blower capable of delivering 470 cfm at 2 psig. A back-up air supply was available from an Ingersoll-Rand 125 psig oil-free compressor capable of delivering up to 450 cfm. The air supply system is shown schematically in Figure 46. The air from the Hoffman blower and the 125 psig compressor was fed to a distribution plenum 18 inches in diameter and 8 feet high, the air pressure from the compressor having been previously reduced to 2 psig by a large capacity pressure regulator. The air from the above blower was introduced into the plenum, a filter screen which helped eliminate extraneous matter. The air flow rate to the plenum from the compressor was controlled by globe valve v_1, while that from the flower was controlled pneumatically by valve v_2. From the plenum, the air was distributed to the gas burners and the lines supplying the overfire and underfire air.

For general operation, the air for the gas burners and their pilots was taken from the plenum below the filter screen; it was then fed to the two burners via two 2-inch flexible hoses and to the pilots via one 1-inch flexible hose. The two globe valves, v_3 and v_4, provided an air shut-off for the gas burners in addition to the butterfly valves on the gas burners. An air shut-off for the pilots was supplied at the pilots with a gas cock. In special situations, when it was imperative to have detiled knowledge of the air flow rates to the two burners, the air was fed through one of the lines available for supplying the overfire and underfire air, and the flow rate was measured using an orifice plate.

Six lines were available for supplying the overfire and underfire air,the flow rates being measured with orifice plates. The orifice plates were mounted between 300-lb flanges at the ends of two lengths of nominal 2-inch-diameter shcedule-40 mild steel pipe that were mounted horizontally along one wall of the test cell. The pipes extended six feet upstream of the orifices, with four feet of pipe downstream of the orifice plates before the flow control valves, v_5 to v_{10}, as shown in Figure 46. Downstream of each flow control valve there was a short length of pipe followed by an elbow and nipple. Flexible hose was used as a connector between these nipples and the overfire air nozzles and the grate. At the far upstream end of each 6-foot length of pipe, a 6-inch section of honeycomb was placed inside the mild steel pipe to help straighten and calm the air flow. The pipes were connected to suitable 2-inch mild steel nipples at different vertical and radial positions in the distribution plenum with flexible hoses.

Flange taps, set in the 300-lb flanges, were employed for measuring the pressure drop across the orifice plates. The pressure drops (inches of H_2O) were measured on a bank of manometers while the upstream static pressures were recorded in mm of Hg on another manometer bank. The temperature of the

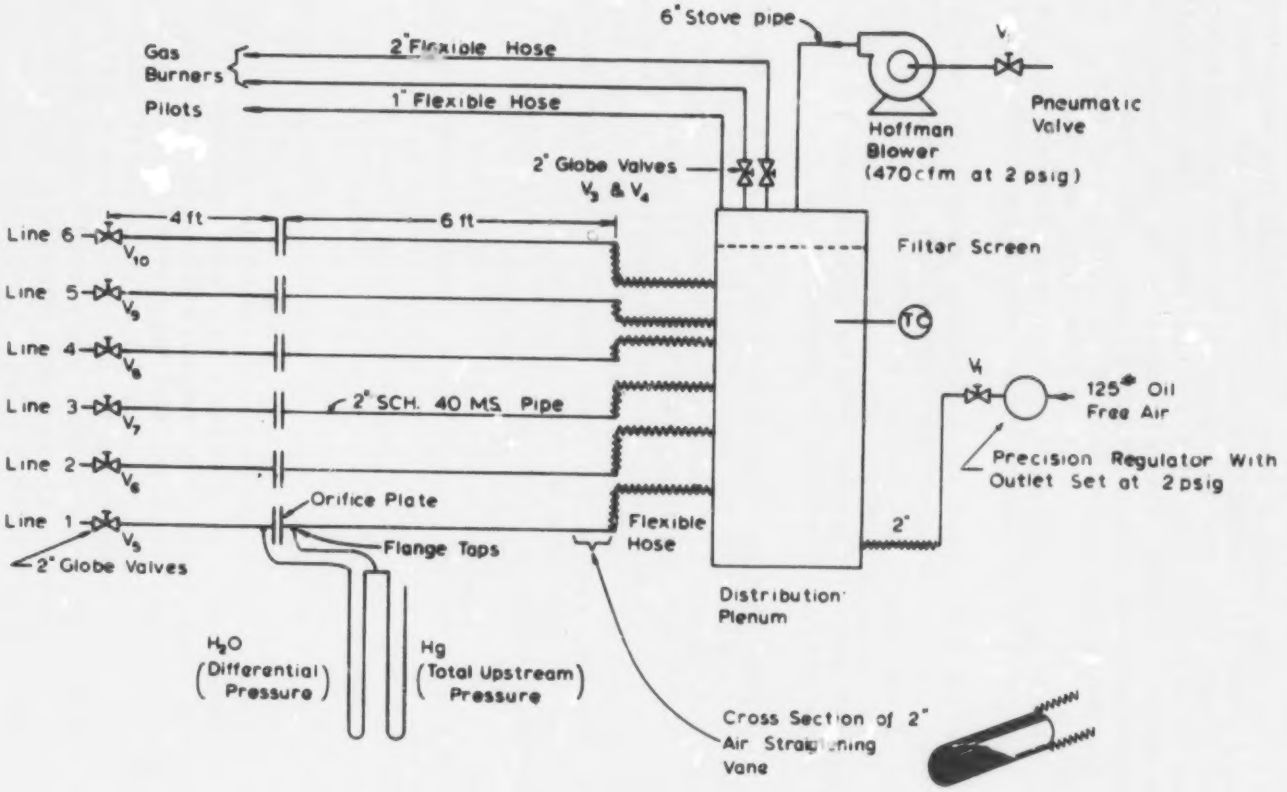
6" Stove pipe
Gas
Burners
2" Flexible Hose
1" Flexible Hose
Pilots
Hoffman
Blower
(470cfm at 2 psig)
V_1
Pneumatic
Valve
2" Globe Valves
V_3 & V_4
4 ft
6 ft
Line 6
V_{10}
Line 5
V_9
Line 4
V_8
Line 3
V_7
Line 2
V_6
Line 1
V_5
2" Globe Valves
2" SCH. 40 MS. Pipe
Orifice Plate
Flange Taps
Flexible
Hose
Filter Screen
TC
V_2
125# Oil
Free Air
Precision Regulator With
Outlet Set at 2 psig
2"
Distribution
Plenum
H_2O
(Differential
Pressure)
Hg
(Total Upstream
Pressure)
Cross Section of 2"
Air Straightening
Vane

Fig. 46. Schematic of Overfire and Underfire Air Supply

air inside the plenum was measured with a Chromel-Alumel thermocouple.

Two orifice sizes were employed. The smaller size (0.8535-inch diameter orifice) was used for measuring the overfire air rates and the underfire air rate when it was set below 100 lb hr^{-1} ft^{-2}. The larger size (1.312-inch diameter orifice) was used when the underfire air rate was set above this value and for measuring the air supply to the two burners, when this was necessary. In the latter case, the one orifice sufficed for both burners, the air supply to the burners being split downstream of the orifice plate. The smaller orifice gave a pressure differential of 24 inches of H_2O for a flow of 50 cfm of air measured at 14.70 psia and 60 °F, while the larger orifice gave the same pressure differential for a flow of 120 cfm of air measured under the same conditions.

The orifice plates were used as a primary measuring device and therefore great care was taken in installing them in hydrodynamic conditions which met American Gas Association Standards (139). A fuller description of the orifice plate installation and of the procedures and computations undertaken to calculate the air flow rates is given in Appendix D.

Gas Burners and Gas Supply. The overfire combustion section was preheated with the two Eclipse 838-36 PMP sealed tunnel burners shown in Figure 43; they were located 90 degrees apart and just above the sliding refractory shield. The burners consisted of a combustion block cemented to a flanged cast-iron block holder, and were mounted to the outer shell of the overfire section using the four corner mounting holes in the block holder. Each burner had its own gas-air mixing system and was supplied with low pressure air from the distribution plenum and city gas at atmospheric pressure from an Eclipse Zero Governor. The low pressure air was directed into a venturi-shaped burner throat producing a pressure low enough to draw in the gas from the Zero Governor. The gas-air ratio could be varied, using the adjustable gas orifice located in the mixing tee. Each burner was provided with a peep sight and a high-pressure, manually ignited blast pilot. The air for the pilots was taken from the air distribution plenum. The gas line to the Zero Governor had an emergency "quick shut-off" gate valve installed in it so that both burners could be rapidly shut down in case of a flame-out. A pressure tap was located at the air entrance side of each burner to measure the air delivery pressure. The pressure was read on the manometer bank in inches of H_2O. This allowed both burners to be run under balanced conditions (i.e., the heat output from both were equal). The burners had a dual purpose in that they could also have been used as after-burners when it was not possible to burn out the smoke using overfire air alone.

Cooling Water Supply. Cooling water was used for the top section cooling coils shown in Figure 43, the cooling coils in the sliding refractory shield, the stack gas sample probe, and the fuel bed gas sampling probes. Each cooling circuit, except for the fuel line probes, had a mercury pressure switch installed in it to indicate when water was flowing through the circuit and as a warning system to indicate a loss of water main pressure. Visual checks were used to verify water flow through the fuel bed probes. Provision was made for flowing the water out of the top section cooling coils and the stack gas probe after an experiment. This prevented the lines from rupturing during winter months.

Fuel Bed Grate and Support System. The grate measured approximately 8 inches deep and 17.5 inches on its outside diameter at the top. The side walls were conical in shape and narrowed down the cross section of the grate to roughly 15 inches OD at its base. This method of construction minimized the chance of binding between the grate and the fuel bed walls.

The inside of the grate was divided into two layers, each 4 inches deep. The first layer acted as a distribution plenum for the air that was supplied through the base of the grate. A baffle was placed over the entry port to the plenum to help distribution. The upper layer consisted of a 1/2 inch-thick piece of high-temperature felt placed across the entire diameter of the grate and carefully sealed at the edges, with the remaining depth of the layer filled with small granite stones. The stones prevented the felt, which supplied the major pressure drop, from being blown out of the grate and were an effective packing for good air distribution. Under typical operating conditions, the pressure drop across the grate was approximately 5 inches H_2O, while that through the bed was of the order of 0.1 inch H_2O. The high pressure drop across the grate relative to that across the fuel bed gave (at lease in the lower portions of the fuel bed) good air distribution across the entire fuel bed. The grate was mounted on a hydraulic jack. An automobile power-steering pump utilizing a 3/4-horsepower, 1750 rpm electric motor was the driving source. A four-way valve controlled the direction of the flow of the hydraulic fluid to the jack, allowing the grate to be either raised or lowered. A pump bypass regulated the flow of fluid to the jack and was used to control the speed at which the jack was moved.

Miscellaneous Equipment. Two audio warning systems helped to provide ease and safety in operating the equipment. One indicated when the Data Acquisition System was about to run out of paper tape while the other registered a low air pressure in the large air distribution plenum. All the thermocouples located in the top section of the apparatus were wired in parallel with a Honeywell Electronik 16 recorder and the Data

Acquisition System. The visual display of the recorder was useful in controlling the refractory temperatures.

One of the channels through to the Data Acquisition System was reserved as an "event indication" channel. By connecting this channel to different known voltage sources, the time and duration of a particular event (such as the start of a run or when the underfire air was set at its final value) could be accurately recorded.

Gas Analysis System

Previous Experimental Techniques. Apart from the notable early work of Kreisinger *et al.* (23) in 1916, Nicholls (24) in 1934, and the later work of Kolodtsev (91) in 1945, there have been relatively few studies reported in the literature of experimental measurements of gas concentrations within a solid fuel bed. The three studies cited dealt with fairly homogeneous fuel beds of coke, coal or carbon particles of well-defined sizes and attempted to measure the oxygen, carbon dioxide, carbon monoxide and, in the case of Nicholls and Kreisinger *et al.*, hydrogen, methane, tar and soot composition at different depths throughout the bed. The samples were collected on a batch basis during an experimental run by drawing samples under vacuum with water-cooled probes from different positions in the fuel bed into collection vessels. The samples were analyzed using wet chemistry techniques. The probes used were of large (approximately 0.3 inch) internal bore, which helped prevent problems of clogging with tarry pyrolysis products.

Analysis of the data obtained from these fuel beds indicates that there was a fair degree of error associated with them, a shortcoming which is understandable, considering the experimental difficulties inherent in this type of study and the pioneering aspects of these investigations. For example, the oxygen concentration fell off very rapidly through the fuel bed and once the ignition plane was reached it was difficult to locate accurately the point of oxygen extinction; difficulties were also encountered in freezing the $CO + 1/2\ O_2 \rightarrow CO_2$ reaction in the probes. Even in these relatively well defined systems, the experimental difficulties associated with obtaining good data were great. The experimental challenge offered in the study of a heterogeneous refuse bed where the fuel is undergoing drying, pyrolysis and combustion, and where relatively large concentrations of tarry pyrolysis products may be expected, is enormous. Only one previous investigation (46) has been reported on gas compositions with a simulated refuse bed, all other investigations on refuse systems having been concerned exclusively with the gas-phase combustion regime, where experimental techniques have been developed.

Gas Sample Train. Figures 47 and 48 show, schematically, the arrangement used for gas sampling and analysis. Gas samples were taken from three positions in the apparatus; two water-cooled probes were employed in the fuel bed section and one water-cooled probe in the stack. Figure 48(b) shows the method of construction of the water-cooled probes. The gas sample was drawn through the center tube while water passed down the inside annulus formed by the other two tubes and out through the outer annulus. The plug at the top of the probe between the center and outside tubes was made with silver solder. The fittings at the other end were made from 1/4-inch Sawgelok elbows.

The samples from the fuel bed were analyzed for oxygen, carbon monoxide and carbon dioxide at frequent intervals throughout the run with on-line instruments. Batch samples were also taken from the fuel bed frequently during the run and analyzed afterwards using a gas chromatograph for hydrogen, oxygen, nitrogen, carbon dioxide, carbon monoxide and methane. The samples from the water-cooled probe in the stack were also analyzed with the on-line instruments at frequent intervals for oxygen, carbon dioxide and carbon monoxide; in addition, batch samples were taken regularly for the helium tracer analysis (see Figure 47). The sample from this probe, which was made from a 1/4-inch stainless-steel tube, was split into two portions. One portion was cooled, the condensate removed, and the dry gas tested with a Von Brank filtering recorder to obtain a rough estimate of the amount of particulate and smoke emissions. At regular intervals throughout a run, a known volume of the second portion was drawn through a steam-traced line to a U-tube trap placed in an acetone-Dry Ice mixture where the water content was removed by freezing. The U-tubes used for these measurements were made from 6 mm Pyrex tubing and measured about six inches from the top of the legs to the bottom of the U. The volume of gas drawn through the U-tube was measured with a wet test meter, and the amount of condensate was found from the difference between the initial and final weights of the U-tube. The weighings were performed only after the U-tubes had equilibrated with the ambient conditions in the balance room. The details of the computational procedure used to calculate the water content of the stack gases from the above measurements are given in Appendix F.

The on-line instrument tain was set up to measure carbon

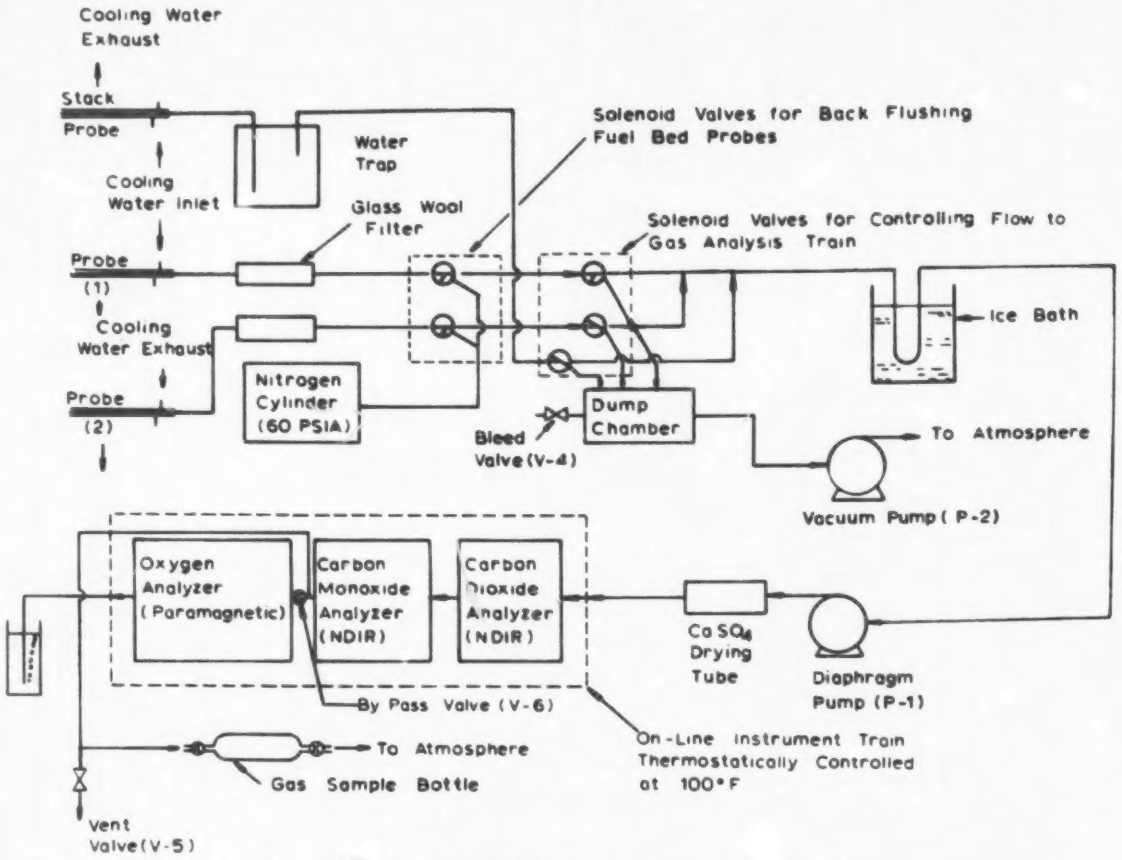
Cooling Water Exhaust
Stack Probe
Water Trap
Cooling Water Inlet
Glass Wool Filter
Solenoid Valves for Back Flushing Fuel Bed Probes
Solenoid Valves for Controlling Flow to Gas Analysis Train
Probe (1)
Cooling Water Exhaust
Ice Bath
Nitrogen Cylinder (60 PSIA)
Probe (2)
Bleed Valve (V-4)
Dump Chamber
To Atmosphere
Vacuum Pump (P-2)
Oxygen Analyzer (Paramagnetic)
Carbon Monoxide Analyzer (NDIR)
Carbon Dioxide Analyzer (NDIR)
CaSO4 Drying Tube
Diaphragm Pump (P-1)
By Pass Valve (V-6)
To Atmosphere
Gas Sample Bottle
On-Line Instrument Train Thermostatically Controlled at 100°F
Vent Valve (V-5)

Fig. 47 Gas Sampling and Analysis Train

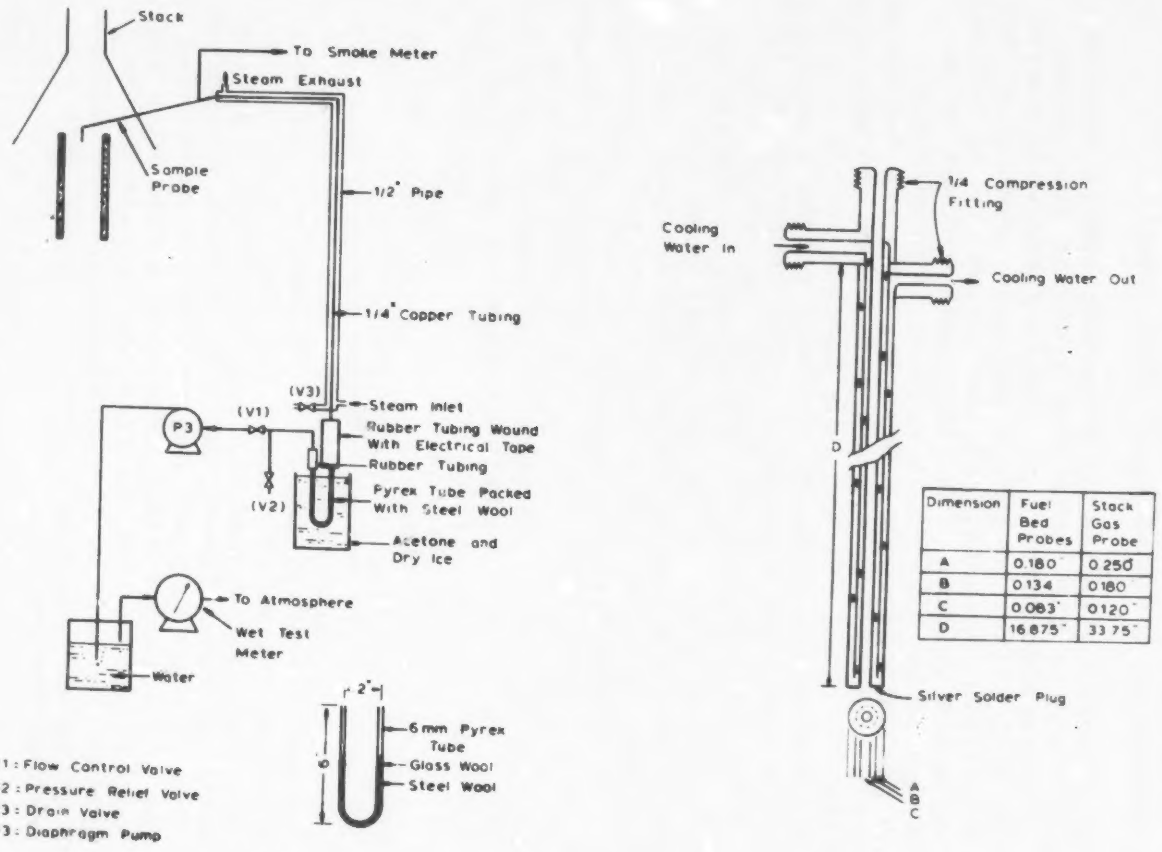
Stack
To Smoke Meter
Steam Exhaust
Sample Probe
1/2" Pipe
1/4" Copper Tubing
(V3)
(V1)
P3
Steam Inlet
Rubber Tubing Wound With Electrical Tape
Rubber Tubing
(V2)
Pyrex Tube Packed With Steel Wool
Acetone and Dry Ice
To Atmosphere
Wet Test Meter
Water
2"
6"
6 mm Pyrex Tube
Glass Wool
Steel Wool
V1: Flow Control Valve
V2: Pressure Relief Valve
V3: Drain Valve
P3: Diaphragm Pump
(a)
1/4 Compression Fitting
Cooling Water In
Cooling Water Out
D
Silver Solder Plug
A
B
C
(b)

Dimension	Fuel Bed Probes	Stack Gas Probe
A	0.180"	0.250"
B	0.134"	0.180"
C	0.083"	0.120"
D	16.875"	33.75"

Fig. 48 (a) Stack Gas Moisture Content Measurement;
(b) Details of Sampling Probe

monoxide (0-50%), carbon dioxide (0-30%) using nondispersive infrared analyzers, and oxygen (0-21%), using a paramagnetic analyzer. The analyzer sections of the oxygen, carbon monoxide and carbon dioxide units were situated in a closed box in a 100°F thermostated environment. The temperature was held constant in order to minimize errors in the temperature-compensating systems of the analytical instruments.

The batch samples were collected by attaching sample bottles to the downstream end of the instrument train on the oxygen bypass line. The samples taken from the fuel bed were passed through a glass wool filter to remove the major portion of the high boiling pyrolysis products, and then passed on to two banks of three-way solenoid valves. The first bank was set up so that the probes could be cleaned at regular intervals with pulses of high pressure nitrogen. When a button was depressed on the operator's control box, one solenoid valve was activated; the valve would shut off the line leading to the instrument train and open up the probe to the high pressure nitrogen line. Under most operating situations, this technique of backflushing the probe was adequate in keeping the probes clean if performed at regular intervals. On release of the button, the solenoid valve would return to its normal open position. After the first bank of solenoid valves, the fuel bed probe sample lines joined the stack probe sample line and the three lines entered the second bank of solenoid valves. These valves were situated as close as possible to the instruments and were activated from the operator's box. In the closed position, the gas sample flow was directed to a "dump chamber" connected to a vacuum pump. The dump chamber pressure was controlled by adjusting a bleed valve leading into it. In the open position, the valve directed the flow through to the instrument train and under operation conditions, therefore, only one valve was open at a time. As a safeguard against opening two valves simultaneously, a light next to the control switch for each valve was activated whenever the valve was opened. From the opened solenoid valve, the gas stream passed first through a water trap placed in a freezing ice-water mixture and then through a small diaphragm pump. The pump pushed the sample through a drying tube filled with calcium sulphate and then through the instrument train. Two calcium sulphate drying tubes were mounted in parallel in the instrument train, permitting a tube with expended calcium sulphate to be removed from the circuit and refilled without disrupting the flow to the instruments. The bypass to the oxygen meter was manually controlled to give the required flow through the sensor.

The pressure inside the instrument train (generally around 5 to 6 inches of H_2O) was recorded on a manometer. The manometer had a dual purpose: to indicate blockage of a probe and to act as a warning device when the batch samples were being taken. The latter purpose needs some explanation. When the sample bottles were attached to the end of the instrument train, sloppy operation could result in a pressure surge through the train. All the instruments measured the absolute number of molecules in a sample cell and pressure fluctuations could cause spurious results. The most critical instrument in this respect is the oxygen meter, where a surge in pressure in the bypass line could send too much of the sample gas through the sensor, causing erratic swinging of the delicately suspended magnetic dumbbells.

The length of line between the solenoid valve and the outlet of the last instrument was kept as short as possible to minimize the "dead volume" that had to be swept out every time a different probe was switched through to the instrument train. Operating experience showed that it usually took about 45 seconds to flush out this "dead volume" adequately.

Data Collection

Almost all of the data taken during a run was collected on punched paper tape with a Data Acquisition System, the only data not being recorded this way being the stack gas water concentrations and, of course, the gas compositions determined by gas chromatography. The Data Acquisition System (Hewlett-Packard System model 2014B) had 1µV resolution and an input impedance of 10 megohms. Eight readings could be recorded per second and the system provided five voltage ranges from 100 µV through 1000V with five significant figures recorded on each range. The paper tape was punched in standard IBM 8 level code. Some data, for which a visual display was required for control purposes, were collected on a Honeywell Electronik 16 multichannel recorder. These data consisted of the top section temperatures, stack gas temperatures, inlet air temperature in the distribution plenum, and inlet and outlet cooling water temperatures.

Figure 49 shows, schematically, the connections from the various recording devices to the Data Acquisition System; Appendix E contains a table that shows the order in which the instruments were connected to the Data Acquisition System and the multichannel recorder. The switchboard shown in the

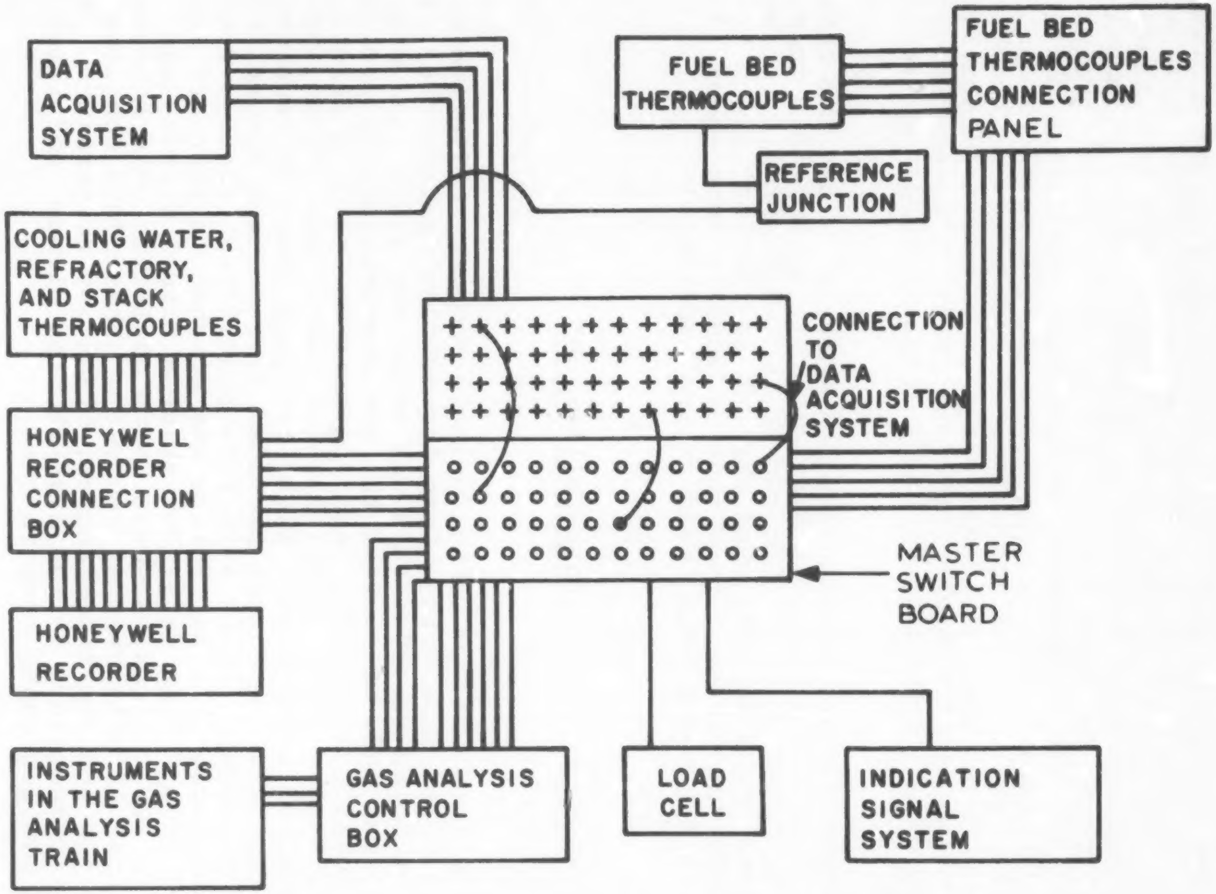
DATA ACQUISITION SYSTEM
FUEL BED THERMOCOUPLES
FUEL BED THERMOCOUPLES CONNECTION PANEL
REFERENCE JUNCTION
COOLING WATER, REFRACTORY, AND STACK THERMOCOUPLES
CONNECTION TO DATA ACQUISITION SYSTEM
HONEYWELL RECORDER CONNECTION BOX
MASTER SWITCH BOARD
HONEYWELL RECORDER
INSTRUMENTS IN THE GAS ANALYSIS TRAIN
GAS ANALYSIS CONTROL BOX
LOAD CELL
INDICATION SIGNAL SYSTEM

Fig. 49. Instrument to Data Acquisition System Connections

center of Figure 49 provided a useful device for grouping sets of data together. The top section, or upper switchboard, contained sixty permanent connections to the Data Acquisition System storage registers 140 through 199. The bottom section, or lower switchboard, held lengths of cable with appropriate electrical connections which were wired to the various recording devices. This arrangement allowed the output from any instrument or thermocouple to be connected to any of the sixty storage locations available on the Data Acquisition System. About forty separate thermocouple and instrument outputs were monitored during any one run and measurements of these outputs were taken at ten-second intervals during the course of the experiment.

The primary reason for taking readings so frequently was to permit the recording of an adequate number of readings of the gas compositions at the different probe locations. As indicated in the previous section, it was only possible to analyze the oxygen, carbon monoxide and carbon dioxide compositions at one probe at a time with the on-line instrument train, and the operator, therefore, had to switch each probe through to the instrument train in sequence. After switching the sample flow from a new probe to the train there was a period of approximately 45 seconds before a "pseudo steadystate" sample concentration was achieved. The pseudo steady-state condition applied after the instrument train had been adequately flushed off the gas from the previous probe; true steady-state conditions were never achieved in this type of batch operation. To check the pseudo steady-state condition it was necessary to obtain at least three readings of the sample oxygen, carbon monoxide and carbon dioxide concentrations before switching onto the next probe. With the Data Acquisition System taking readings every ten seconds, the complete oepration of recording the sample composition from one probe required seventy to ninety seconds. This was about the maximum time permitted if one were to map out a semicontineous plot of gas compositions as a function of time throughout a run.

It was desirable to store the three sets of data (oxygen, carbon dioxide and carbon monoxide compositions) obtained from each gas probe in separate storage registers in the Data Acquisition System. A control box performed the task of directing the three outputs of the on-line instruments to three sets of separate storage locations allocated. Each probe was assigned one set of three storage locations. For example, the lower switchboard addresses 50, 51 and 52 held the outputs from the oxygen, carbon dioxide and carbon monoxide analyzers for samples taken from the probe located in the stack; addresses 53, 54 and 55 held the oxygen, carbon dioxide and carbon monoxide outputs for samples taken from fuel bed probe number one, et cetera. It was of course still possible to store the information held in the lower switchboard addresses 50 through 55 on any of the Data Acquisition System channels, simply by making the appropriate connections through the upper switchboard.

The control box had one master switch for each probe. When the switch was in the "on" position, the signal from the online gas analyzers was switched to the Data Acquisition System; in the "off" position the switch short-circuited the signal to the Data Acquisition System. At any particular time during a run only the switch that was associated with the probe being sampled was in the "on" position. This arrangement made it very easy to tell from the data which probe was being used during any time period.

One channel through to the Data Acquisition System was kept as an "indication channel" and was used to indicate the start of various events. For example, when the sliding refractory shield was opened at the start of an experimental run, a switch was closed, completing an electrical circuit which sent a four-volt signal through the indication channel. Voltages of different magnitudes were used to signify the beginning of other operations.

Sequence of Operations During an Experimental Run

The sequence of operations undertaken in preparing for, and during, an actual test is outlined below. Full details on the operation of all the equipment are presented in Appendix E.

Feedstock Preparation. The feedstock was made up to the specifications required on moisture and inert content by combining the necessary weights of wet and air-dried wood and tin cans. The moisture content of the air-dried wood was typically around 7 percent, while that of the wet wood was around 50 to 60 percent. The individual constituents of the feedstock were weighed and stored in separate containers, care being taken to cover the wet blocks so that they did not lose any moisture content during the period prior to the fuel bed being charged. A priori it was difficult to determine what the bulk density of the feedstock would be. Experience showed that roughly 60 pounds of material were required for filling the fuel bed section when the maximum fuel bed depth of 30 inches was used. This corresponded to a bulk density of approximately 14 to 15 lb ft^{-3}.

Top Section Preheat. After the feedstock had been weighed, the overfire section was prepared for preheating. The fuel bed section was pulled out along its tracks from underneath the top section; this facilitated working on both sections and was essential for charging the fuel. The four overfire jets were then installed in their required positions. For all the runs, four overfire jets in the second level of ports were used. This configuration proved very satisfactory and the jets were therefore installed semipermanently in these positions. With the jets installed, the sliding refractory shield was pushed closed and the counterweight placed on the hook of the draw wire used to pull open the refractory shield at the start of the run.

The cooling water for the refractory shield, the top section and the stack gas probe was then turned on. The overfire and underfire air line valves were shut off, as were the butterfly valves to the burners and the pneumatic valve on the inlet to the Hoffman blower; this procedure minimized the load on the blower motor during start-up. The oil level in the two bearings on the blower were checked before the blower was started and, once the impeller had reached its operating rpm, the pneumatic valve was opened slightly. The control valves on the overfire air lines in use were opened and the air flow rates through the jets were set at the approximate values to be used during the run. The valves for one of the burners and its pilot burner were opened slightly and the gas line valves on both the main supply line and the pilot line were opened. The pilot burner was then ignited. After the pilot flame had stabilized, the main burner was ignited, the heat output being kept low until the combustion block warmed up. Once this stage was reached, the major work in the preheat stage had been done and the top section was slowly heated over a period of four to five hours by increasing the heat output of the one burner until the refractories had attained a temperature of around 1000°F, and then by using the other burner to help boost the temperature to 2000°-2200°F. The refractories were maintained at this temperature for at least half an hour before the run was started so that temperature gradients within the refractories would have stabilized.

Fuel Bed Section Preparation. While the top section was being preheated, the fuel bed section was prepared. The section was first cleaned by removing any unburnt remains from the previous run with a vacuum cleaner. Concurrently, the condition of the fuel bed thermocouples was checked, badly corroded ones removed, new ones installed, and bent ones straightened.

If possible, the thermocouples were pulled out so that just the tips were protuding into the fuel bed; this facilitated charging the feedstock. Sometimes extensive carburization of the sheath over the thermocouple did not permit the thermocouple to be pulled out. In this case, the thermocouple was left in place and care was taken in loading the fuel bed not to bend it out of position.

After the thermocouples had been checked out, the fuel bed gas probes were removed and disconnected from the water-cooling lines and sample lines; they were then thoroughly cleaned, both inside and out. The cleaning of the probe sample tubes reduced the chance of blocking during a run and was performed by drawing a thin wire back and forth through each probe and flushing it out, at frequent intervals, with acetone. The outside of the probe was easily cleaned with a wire brush. After cleaning, the probes were reconnected to their associated cooling-water and gas sample lines.

At this stage the grate was set at the required height using the hydraulic pump, and a seal was made between the bottom of the grate and the fuel bed section to prevent air leakage between the grate and the containing walls of the fuel bed. The seal was made from suitable pieces of heavy-duty alumunum foil held in place with electrical tape.

Gas Analysis Train Preparation. Following the preparation of the fuel bed section, the instruments in the gas analysis train were checked out and calibrated using the manufacturer's standard procedures. In addition to following the manufacturer's procedures, each on-line instrument was checked against at least one other gas of known concentration; this provided a useful double check on instrument operation. THe procedure adopted for these checks was as follows. The tip of one of the fuel bed probes was pushed through one hole of a two-hole rubber stopper placed in the mouth of a side-arm flask. A 1/4-inch line from the requisite gas source was pushed through the other hole in the stopper and a hose from the side arm dipped into a few inches of water. The calibration gas supply was opened; the solenoid valve which directed the flow from the probe being used to the instrument train was opened; and the gas sample pump turned on. The gas supply rate was adjusted and balanced against the sampling rate so that just a small gas flow was seen to bubble through the water trap. The procedure insured that only the desire gas was sampled, that a minimum of the gas sample was used in the process, and that thte pressure in the system was as close as possible to that found under actual operating conditions.

Miscellaneous Equipment Preparation. Once the instrument train was checked, the cold junctions for the thermocouples--five cold junctions were used for the fuel bed thermocouples and one for all the other thermocouples--were placed in Dewar flasks filled with ice-water mixtures. The final step before the fuel bed section was charged with fuel was the preparation of the stack gas water determination equipment and the connections to the Data Acquisition System. For the water determination the dry U-tube traps were weighed (they were dried in a vacuum over night) with rubber stoppers covering each arm of the U's. The weights were noted and the tubes numbered and laid out in order next to the cold trap, which was a large vacuum flask filled with a Dry Ice -- acetone mixture. The wet test meter was then leveled and zeroes and the steam to the sample line was turned on.

The connections for the Data Acquisition System were made after the number of fuel bed thermocouples to be used had been decided. The connections were made using the switchboard arrangement shown in Figure 49 so that sets of data were conveniently grouped together on adjacent registers on the Data Acquisition System. The only guideline for this process was that all the thermocouple registers had to be grouped together, as the computer programs developed for analyzing the data were written on this basis. The switchboard set-up typically used was as follows: event indication channel, fuel bed thermocouples arranged so that the thermocouple that was closest to the top of the bed was first and the lowest one last, heat loss probes, top section thermocouples, other thermocouple outputs, load cell output and input, and finally gas analysis outputs. Once the connections were made, the Data Acquisition System clock was synchronized with the clock in the test cell and the Data Acquisition System was set up to take readings every ten seconds through all the registers in use. The data Acquisition System was then left in a stand-by mode of operation.

Loading the Feedstock. The first step in loading the fuel was to obtain a reading of the weight of the fuel bed section without the fuel and with all thermocouple and gas probe connections made. To do this, the section was leveled with the appropriate jacks and then the support jacks were slowly lowered until the full weight of the fuel bed section was on the load cell.

A two-volt signal was switched to the event indication channel and nitrogen zero gas was passed through the oxygen meter. When the zero of the oxygen meter had been adjusted and stabilized, five to ten readings were taken with the Data Acquisition System. The support jacks were raised until the

the bottom section weight was completely off the load cell, and the fuel was loaded into the fuel bed section. The fuel bed was loaded in a pseudo-random fashion with care taken to distribute the wet and dry blocks of wood and tin cans evenly throughout the depth of the fuel bed. The various thermocouple and gas probes were pulled into place as the fuel bed was built up, care again taken to spread the fuel evenly across the fuel bed, as otherwise large gaps tended to develop at the sides. The fuel bed was charged so that the top of the bed was even with the top fo the brick doughnut of the bottom section; fuel was added or subtracted in order to do this and these additions or subtractions were carefully weighted and taken into account in determining the final weight and composition of the fuel.

With all the fuel charged, the support jacks were again lowered carefully and a five-volt signal was switched to the event indication channel. Air was passed through the oxygen meter and the up-scale reading adjusted; five to ten more readings were taken with the Data Acquisition System. The weight differential betwen the empty and full weights of the fuel bed section was calculated from the load cell outputs recorded by the Data Acquisition System and compared with the known weight of fuel added. The largest error between the calculated and actual weight of the fuel was always less than one pound.

The support jacks were then raised and the bottom section moved into place underneath the top section. The bottom section was carefully leveled with the leveling jacks and then raised using these jacks until the flange on the fuel bed section just mated with the flexible diaphragm; the mating was indicated by locating probes positioned on the fuel bed section flange (see Appendix A). The section was raised by rotating all three leveling jacks simultaneously one half-turn at a time. The close fit between the two mating doughnuts of the top and bottom sections (see Appendix A) made it imperative that the bottom section be raised in this manner, as the doughnuts would have bound together if the bottom section were not vertical. Once this operation was performed all electrical connections from the fuel bed thermocouples to the control switchboard were made. The support jacks were lowered and the weight taken on the load cell. At this point nothing was allowed to touch or bump the bottom section, as spurious readings from the load cell would have resulted.

At this juncture, another set of readings of all instrument outputs was taken with the Data Acquisition System. The weight of the fuel bed was computed from the load cell output obtained from this set of readings and compared with the previous value. This gave a good check that there was no binding between the top and bottom sections. This set of readings was also used to check the outputs of all the thermocouples to make sure that they were all operating correctly. Once all systems were operating properly, the run could be started.

The Start and Operation of a Run. A run was commenced by switching the solenoid valves for the gas analysis train so that a gas sample stream was taken from the stack gas probe. The Data Acquisition System was then switched on to a mode where it took readings through the total set of inputs every 10 seconds. The underfire air flow was turned on slightly (about 1/10 its final value) and the gas and air supply to the gas burners and pilots was shut off. Immediately after the burners were shut off, the sliding refractory shield was gently pulled open using the draw wire. This latter operation needed to be done carefully as the shield could cause considerable vibrations (with subsequent load cell errors) if it hit the restraining stops too hard. The shield was pulled out far enough to activate a switch which sent a six-volt signal into the event indication channel and activated a light on the instrument panel. This signal indicated the start of the run.

Shortly after the run had begun, stack gas water concentration measurements were begun and the underfire air rate was slowly raised to its final value. About three to four minutes were taken to raise the underfire air to the desired level, at which time a twelve-volt signal was sent to the event indication channel. Readings were taken of the orifice-plate pressure drops and upstream air pressure on all the overfire air lines and on the underfire air line every time they were changed. The times at which these changes occurred were noted on a log sheet.

Samples were taken from the three gas probes in a cyclic fashion. However, samples were not taken from the fuel bed until the ignition front had reached the first gas probe. Up to that time, samples were taken continuously from the stack with only brief breaks to check conditions at the first fuel bed probe. Once the ignition front reached the first fuel bed probe, as indicated by a dramatic increase in carbon dioxide level, a sampling sequence of gas probe /fuel bed probe was followed as rapidly as this operation permitted. Typically it took one and a half minutes to obtain a sample, as it took 45 seconds to attain a steady-state reading after switching over the probes and at least three readings were taken before making the next switch. Every so often, the second fuel bed probe was tested and once active burning was detected at this level a sampling sequence of stack/fuel bed probe one/stack/fuel bed probe two/stack was followed. Near the end of the run, when the carbon monoxide concentration in the fuel bed began to decay and the oxygen content started to increase, samples were again taken solely from the stack. During these sampling operations batch samples were taken from all the probes at those intervals throughout the run when the probes were switched to the gas analysis train. The probe location and the time at which the sample was taken were noted on the sample bottles which were analyzed after th run (hydrogen, oxygen, carbon monoxide, carbon dioxide, methane and nitrogen for the stack samples).

Stack gas water determinations were performed at regular intervals throughout the run, about every three to four minutes. The procedure for this was as follows. One of the U-tubes was connected between the two lengths of rubber hose shown in Figure 48(a) and then the vacuum flask filled with the Dry Ice -- acetone mixture was raised so that the top level of the liquid was as close as possible to the rubber/glass joint. After a period of a few seconds to let the glass and steel-wool packing cool, the valve v_1 of Figure 48(a) was opened slightly (the pump had been switched on and left running before the run was started) and a low flow rate of air was drawn from the probe. After 0.3 cubic feet of air had been pulled through the U-tube (three revolutions in the dial of the wet test meter) valve v_1 was rapidly closed and valve v_2 quickly opened to equalize the pressure on both sides of the U-tube. This procedure prevented the partial vacuum created on the pump side by the high pressure drop across the ice-packed U-tube from allowing any unaccounted-for air to be pulled through the U-tube. Once the pressure had equalized, the vacuum flask was lowered, the U-tube rapidly removed and both ends stoppered. The time of the sample, U-tube number and exact volume of gas passed through the U-tube were noted, as well as the time taken to collect the sample, generally one to two minutes. A new tube was mounted in position as soon as possible and the process repeated. Water determinations were started as soon as the run had begun and were continued until the end of the run.

Other than working the gas analysis train, taking batch gas samples, doing the water determination and changing the punch paper tape on the Data Acquisition System, the only additional operation necessary during a run was adjusting the overfire air rates in an attempt to keep the top section refractory temperatures around 1400°-1500°F. This method of operation was necessary in this batch system if the net heat flux to the top of the fuel bed was to be kept approximately constant. In practice, it had been found that the best way to achieve this goal was to keep the oxygen content in the stack gases around 10 to 15 percent. The large thermal sink effect of the refractories and the slow recording speed of the multipoint recorder meant that there was a large response time associated with any control system based on the refractory temperatures.

The runs was ended when the concentration of oxygen in the stack gases reached around 20,5 percent. At this stage the Data Acquisition System was switched off, the support jacks were raised until all weight was off the load cell and the load cell power supply was shut off. The Hoffman blower was switched off, all city gas lines closed at the main valves, the instrument train and control system switched off and the fuel bed probes removed. All cooling water circuits were turned off except those for the roof and for the stack gas probe. The cooling water circuits to these sections were left on for a period of at least four to six hours.

Data Processing

Three computer programs were used to process the raw data, which had been stored on punched paper tape. The first step in the data processing was to transfer the Data Acquisition System output from paper tape to magnetic tape. The first program then read the magnetic tape data and decoded the IBM 8 level code format to give an output in punched card form. This output deck could be checked for any errors which might have been caused by malfunctions of the high-speed punch on the Data Acquisition System. The deck also provided a convenient form for storing the raw data. The card output from the first progra, coupled with a few control cards, was used as input for the second program, which performed the task of converting the voltage readings into corresponding temperatures, gas compositions, and weight loss using conversion tables and calibration curves. The card output from the second program, which contained arrays of temperature, gas composition, probe number, and weight loss at the corresponding elapsed time from the start of a run formed the input data to the third program. This program plotted the data as a function of elapsed time using a Stromberg Carlson 4020 plotter. Complete details of the three programs are given in Appendix G and sample outputs from the programs are included in Appendix H.

In addition to the programs for handling and processing the raw data a program was developed for calculating instantaneous material balances around the unit. This program used the stack gas measurements, the overfire and underfire air flow rates and the helium tracer flow rate as input data. The development of the equations used for this program and a listing are given in Appendix F.

RESULTS AND DISCUSSION

Introduction

Summary of Experiments Performed. The experiments that were conducted can be conveniently divided into four groups of runs: Runs 1-2, Runs 3-10, Runs 11-16, Runs 17-18. A breakdown of the fuel type and composition used in all the tests is given in Table 10; the conditions used in the experiments and the measurements taken are summarized in Table 11. Runs 1 and 2 were of a preliminary nature, designed to check the overall operation of the test incinerator. The fuel bed grate used in these tests consisted of an 18-in.-diameter piece of sheet metal drilled with 1/8-in.-diameter holes on 3/16in. centers. No effort was made to control the underfire air, the air supply being set by the prevailing natural draft. The results from these two experiments showed that the overall operation of the equipment was satisfactory, but that in order to obtain the detailed information desired, a number of changes would have to be made. These improvements included removing intermittent short circuits in the fuel bed thermocouple electrical system and improving the method of joining the two sections of the apparatus in the interest of minimizing drag on the weighing system.

For Runs 3 through 10, an improved grate was added to the system, which permitted a controlled amount of underfire air to be introduced through the fuel bed. In these experiments, the fuel composition was maintained approximately constant (17-15% inerts, 28-33% moisture, and the remainder combustible) and the underfire air was varied from 127 to 275 lb hr^{-1} ft^{-2}.

In most of this second group of experiments, difficulty was encountered in igniting the fuel bed properly, although for the majority of experiments the underfire air was slowly increased to its final level over a period of a few minutes after the start of the run. Under these circumstances, the bed initially burnt vigorously but then slowly died down; this resulted in a severe decrease in the temperature level of the refractory lining of the overfire section and consequently a decrease in the radiant heat flux to the top surface of the bed. The fuel bed temperatures showed that in the experiments where ignition was not properly achieved, the temperatures rose above the ignition temperature in the first few inches ($\sim$5-7 in.) of the bed and then the ignition process stagnated. The

TABLE 10

Synthetic Fuel Composition and Analysis

Run No.	Wood Analysis				Sizes of Fuel Constituents (Dimensions in Inches)				Composition of Fuel (Percent by Weight)				Ultimate Analysis[2] of Fuel (Percent by Weight)		
	Ultimate Analysis (Percent by Weight -Bone Dry Wood)			As-Received Moisture Content of Wood			Metal Cans	Glass Jars[3]	Moisture	Combustible		Inert			
	%H	%C	%O		Wood	Paper[1]	h=height;	d=diameter		Wood (Bone Dry)	Paper		%C	%H	%O
1					2¼x1¼ x1 3/8	-	-	-	≃8	≃92	-	-	-	-	-
2	NOT ANALYZED			≃8	"	-	-	-	≃17	≃83	-	-	-	-	-
3					"	-	-	-	-	-	-	-	-	-	-
4									27.0	48.4	8.8	15.8	29.2	6.5	48.5
5									33.0	41.9	7.3	17.8	25.2	6.6	50.4
6					2¼x1¼ x3/4	5¼x2	h=4, d=3 5/8	h=1 7/8, d=2 1/8	29.9	46.5	8.4	15.2	28.0	6.7	50.1
7	6.08	52.24	41.68	7.96	2¼x1¼ x1 3/8	6x3	h=3, d=2 3/8	h=4, d=2¼	27.8	47.9	8.7	15.6	28.9	6.5	49.0
8					1 3/4 x1x3/4	4¼x6	h=5, d=4		31.2	44.9	8.5	15.4	27.2	6.7	50.7
9									30.7	46.0	8.3	15.0	27.7	6.7	50.6
10									31.8	47.6	3.6	17.1	26.4	6.6	49.9
11									24.0	60.5	-	15.5	31.0	6.3	47.2
12					2¼x1¼ x1¼				25.9	61.3	-	12.8	31.5	6.5	49.2
13									23.9	62.3	-	13.8	32.0	6.4	47.8
14					1¼x1¼ x1¼	NOT USED	h=3 1/8, d=2 3/4	NOT USED	14.7	70.2	-	15.1	36.0	5.8	43.1
15	5.96	51.30	42.74	6.90					26.4	73.6	-	0.0	37.8	7.3	54.9
16									24.9	58.9	-	16..	30.2	6.6	47.0
17									25.4	59.4	-	15.2	30.5	6.3	48.0
18									25.1	59.9	-	15.0	30.7	6.4	47.9

[1] Random configurations -- cut up, crumpled and twisted

[2] Assuming analysis for paper was the same as for cellulose, which from Kaiser's data (49) was a good approximation of the average composition of the mixture of papers used

[3] When glass was used the inert was made up of approximately 55% glass and 45% tin cans.

TABLE 11

Summary of Experimental Conditions[a]

Run No.	Fuel Analysis (% by weight)			Actual Amount of Fuel Charged (lb)	Amount of Fuel Charged, from Load Cell Reading (lb)	Underfire Air Rate(lb $hr^{-1}ft^{-2}$) at (elapsed time, sec)	Burning Rate(lb $hr^{-1}ft^{-2}$) at (elapsed time, sec)	Ignition Rate(lb $hr^{-1}ft^{-2}$) at (elapsed time, sec)	Max. Temp. Observed (^{o}F)	Comments
	Combustible	Inert	Moisture							
$1^{b,p}_{q,r}$	-92	-	-8	Not Determined		Natural Draft	68^{c} (960)	110^{c} (960)	e	Exploratory experiments. Data Acquisition System malfunction in Run 2 prevented detailed analysis of data.
$2^{b,p}_{q,r}$	-83	-	-17				$57^{c,d}$ (1200)	e	e	
$3^{b,f,p}_{q,r}$	-75	-	-25	60.0	o	137^{c}	d	e	e	Demonstration experiment.
$4^{b,f}_{r,q}$	57.2	15.8	27.0	57.0	53.0	146^{c}	35^{g}(1000) 64 (1900)	m	m	Burning appeared normal.
$5^{b,f}_{r,q}$	49.2	17.8	33.0	68.3	69.9	93(1600-2200) 145(2200-4000) 127(4000-)	62(3800)	125^{h}(3800)	1900^{i}	Bed initially ignited,then smoldered for first 2/3 of run. At 2600 sec burning began to improve. At 3600 sec active burning started and bed burnt rapidly for 800 sec until all fuel was consumed.
$6^{b,f}_{r,q}$	54.9	15.2	29.9	59.4	x	x	x	x	x	Bed ignited but could not sustain burning,despite varying underfire air and reigniting gas burners. Bed smoldered for 5 hr and almost complete combustion achieved. No data taken after first 20-25 min of run.
$7^{b,f,r}_{q,s}$	56.6	15.6	27.8	57.6	58.0	146^{c}	28^{g}(2000) 67 (2750)	79^{h}(1200)	2300^{i}	Behavior of bed similar to that observed in Run 5. Data indicated probability that bed had not been allowed to ignite properly before underfire air was raised to final level.
$8^{b,f}_{r,q}$	53.4	15.4	31.2	58.6	61.5	210(0-120) 130(3400-5260) 150(5260-6220) 210(6220-)	d	y	y	Bed did not ignite properly using underfir air at 210 $lbhr^{-1}ft^{-2}$. Air rate lowered and then increased slowly back to 210 $lbhr^{-1}ft^{-2}$ over 5 min period. Fire still did not improve and underfire air rate again decreased. Bed eventually started to burn.

Table 11 (Cont'd)

$9^{h,f}_{r,q}$	54.3	15.0	30.7	60.0	58.4	275(180-900) 88(900-1020) 175(2400-4200) 175(5000-)	5(1250) 27(3200) 27(5200)	64^{m}(4600)	1800^{i}	Underfire air raised over 180 sec to 275 $lbhr^{-1}ft^{-2}$. Fire died down, underfire air was decreased, then fire caught and underfire air increased back to 175 $lbhr^{-1}ft^{-2}$. Again fire died down, air was lowered, and, when fire caught again, raised to 175 $lbhr^{-1}ft^{-2}$ for rest of run. Data only taken during later stages of run when active burning was visually observed.
$10^{b,f,r}_{q,s}$	51.2	17.1	31.8	70.1	69.7	275(120-600) 175(600-)	22(2200) 35(3600)	34^{c}(2500)	2200^{i}	At high initial underfire air rate, fire began to go out; underfire air rate was decreased and burning improved.
$11^{j,k,l}_{q,t,s}$	60.5	15.5	24.0	69.3	70.8	155^{c}	40^{c}	50^{c}	2400^{i}	Gas probes plugged during test. Poor electrical connection between oxygen meter and D.A.S.
$12^{l,q}_{t,s}$	61.3	12.8	25.9	68.0	69.5	155^{c}(600-)	n	y	2000	Bed ignited but fire died down quickly. Underfire air decreased and then, after bed caught, was increased to final value.
$13^{l,q}_{t,s}$	62.3	13.8	23.9	64.9	65.6	240(0-900) varying (900-2400) 150(2400-4200) 175(4200-)	n	y	2200^{i}	Underfire air slowly raised to 240lb hr^{-1} ft^{-2} over 15 min period. Fire died down. Underfire air rate lowered and then, when fire had caught, raised to 210$lbhr^{-1}ft^{-2}$. Fire again died down. Underfire air rate decreased and, when fire caught, was set at constant level. Top of gas sampling probe blew off during run twice.
$14^{l,q}_{t,s}$	70.2	15.1	14.7	59.7	60.5	160^{c}	n	48^{c}	2400^{i}	Burning appeared normal.
$15^{l,q}_{t,s}$	73.6	0.0	26.4	82.3	81.7	156^{c}	n	54^{c}	2100^{i}	
$16^{l,q}_{t,s}$	58.9	16.2	24.9	61.6	63.1	118^{c}	n	41^{c}	2400^{i}	
$17^{l,u}_{v,w}$	59.4	15.2	25.4	62.6	62.7	140^{c}	39^{c}	38^{c}	2300^{i}	
$18^{l,u}_{v,w}$	59.9	15.0	25.1	66.5	67.2	86^{c}	30(0-1700) 41(1700-3200)	43^{c}	2350^{i}	

FOOTNOTES:

(a) All bed depths studied were 30 in. deep (4.2 ft^3).
(b) Operating difficulties with Nondispersive Infrared CO meter and Beckman 715 amperometric oxygen sensor.
(c) Rate constant over the major portion of test
(d) Considerable scatter in data because diaphragm tightened too much.
(e) Intermittent short circuits in the thermocouple electrical system gave poor fuel bed temperature data.
(f) Runs 3 through 10 inclusive were performed with the low pressure drop grate.
(g) Oxygen present at both fuel bed probe positions
(h) Ignition rate increased with time.
(i) Observed towards end of run
(j) Runs 11 through 18 inclusive were performed with the high pressure drop grate.
(k) From Run 11 through Run 18 two temperatures were recorded at the edge of the bed in addition to the ten measurements taken in the center.
(l) Paramagnetic oxygen analyzer used instead of amperometric sensor
(m) Problem with fuel bed thermocouple electrical system gave spurious results.
(n) Building vibrations and other difficulties with the load cell gave very poor weight loss data.
(o) Binding between top and bottom sections caused spurious results from weighing system.
(p) No fuel bed gas samples taken
(q) No air leakage rate measurements taken
(r) No measurements of moisture content in stack gas
(s) Some batch samples analyzed for CO, CO_2, O_2, CH_4, and N_2
(t) Measurement of moisture content in stack gas but readings all low because of poor water trap design
(u) Complete analysis made for fuel bed batch gas sample - CO, CO_2, H_2, O_2, CH_4, N_2
(w) Air leakage rate measurement satisfactory
(x) Incomplete data precluded analysis.
(y) Difficulties in igniting bed negated value of these measurements.

maximum bed temperature noted under these conditions (1000-1400°F) was very much less than the maximum observed when the bed was burning properly (1800°-2200°F). When this behavior was observed, the underfire air was decreased to around 60-70 lb hr^{-1}ft^{-2} and held at this level until the fire started to burn vigorously again. At this time the underfire air was raised back up to the desired level. On some occasions the underfire air was pulsed in an attempt to revive the fire, and the refractory brickwork reheated with the gas burners so that the heat flux to the top of the bed would be increased Runs 6,9 and 10). None of these methods proved to be very satisfactory, although they only failed once (Run 6) to revive the combustion process.

In this second group of experiments (Runs 3-10) data collection was extended to include gas samples from the fuel bed, as well as from the stack. These samples were taken from two positions in the bed and were analyzed using the on-line gas analysis train. Some batch samples were taken from the feul bed, and a limited analysis was performed on a gas chromatograph for O_2, CO, CO_2, N_2 and CH_4. A considerable amount of operational difficulty was encountered in this new procedure; most of the difficulty concerned the poor operation and response time of the Beckman 715 Amperometric Oxygen Analyzer originally used for the oxygen measurements. Additional equipment problems were related to the electrical circuitry of the non-dispersive infra-red CO analyzer. Finally, the distortion of the flexible diaphragm, where the top and bottom portion of the equipment were connected together, continued to cause weighing errors. The data from this group of runs are therefore rather sketchy, although they did provide some insights into the ignition behavior of the bed. These runs further showed (1) that the underfire air tended to channel through the fuel bed along the walls, (2) that the concept of drying and pyrolysis waves propagating through the fuel bed was unreasonable for the size and type of fuel used in the tests, and (3) that the closure of material balances coupled with the measurement of the concentration of water and hydrogen within the fuel bed would provide a valuable insight into the progress of drying and gasification.

For all experiments subsequent to Run 10, the glass content of the fuel was omitted. It was found that, when used, the glass readily melted at the high temperatures of the bed, coating the grate and insulating walls of the fuel bed. Great difficulty was encountered in cleaning out the fuel bed, because the solidified glass clogged the holes in the grate and covered the thermocouples. It was felt that, although removing the glass meant eliminating an element characteristic of refuse, the tin cans would suffice to simulate the inert content.

For the remainder of the experiments (Runs 11-18), a paramagnetic oxygen analyzer replaced the amperometric sensor and the gas analysis train was modified to decrease the time required to take a sample and to make its operation easier. The method previously used to join the two sections of the apparatus together (i.e., clamping the two sections together) was abandoned and the sections were joined by butting them together and relying on the rubber gasket between them to effect a seal. The rubber gaskets on the flange of the bottom section were built up so as to minimize gaps between the flange and the flexible diaphragm when two sections were butted together. For calculation of material balances,the stack-gas-water content had to be measured. The equipment necessary for this measurement was built and installed for Run 11. A description of this equipment is given (see pages 168-172).

Runs 11 through 16 attempted to fill the information gap suggested by Runs 3 through 10. For these runs (Runs 11-16), both the underfire air and fuel composition were varied around a base case. For the base case (Runs 11-12), the fuel composition was ≈ 25% moisture, 15% inert, and 60% combustible, and the underfire air was fixed at 155-160 lb hr^{-1}ft^{-2}. In Runs 13 and 16 the underfire air was varied from 118 to 240 lb hr^{-1}ft^{-2} while the fuel composition was held constant; in Runs 14 and 15 the fuel compositions were 0% inert, 25% moisture, 75% combustible and 15% inert, 15% moisutre, 70% combustible, respectively, and the underfire air was held to the base case value of 155-160 lb hr^{-1}ft^{-2}.

Problems were encountered in measuring the moisture content in the stack (from which the moisture content in the bed was calculated) and with the weighing system. The first problem was attributable to faulty design of the measuring system used and was readily corrected. The latter difficulty was caused by excessive vibrations set up by other operating equipment elsewhere in the building and could not be cured; however, by scheduling runs during relatively quiet times, the problem was largely circumvented.

Starting with Run 11, the grate design was modified so that the pressure drop across the grate was markedly higher than the drop in Runs 3 through 10; the modification appeared to decrease the amount of channeling that occurred through the fuel bed. Attempts to close material balances for Runs 11-16 showed that there was considerable air leakage into the test incinerator, probably through the spaces around the sliding refractory shield. This air leakage did not affect the measured burning rates because this air did not pass through the fuel bed. For material balance purposes, however, the air leak had to be measured and a helium tracer method, described on pages 168-172, was selected for this purpose.

The improved operation of the gas analysis train made it possible to obtain more gas samples from the fuel bed; in addition a greater number of batch samples were taken and analyzed more completely than previously (i.e., samples were analyzed for H_2 in addition to CO, CO_2, O_2, N_2, and CH_4). Although the additional measurement of hydrogen provided more detail of fuel bed conditions, it was not possible to check whether the water-gas-shift reaction was equilibrated at the top of the bed because of the poor stack-gas-water measurement and the unknown quantity of air leakage into the equipment. (The moisture content of the gases at the top of the bed could have been calculated from the known underfire and the overfire air flow rates and the stack gas moisture measurement.)

Before progressing with the final group of experiments (Runs 17 and 18), the apparatus, the gas measuring equipment, and the leak measuring technique were all thoroughly tested by closing material balances around the unit while burning a known amount of city gas. For these tests, the two sections of the apparatus were joined together in the manner used for a regular run, and overfire and underfire air was supplied at about the ratios and rates used in a typical test. The combustion air supplied to the gas burners was metered with a suitable orifice plate. The amount of city gas used was measured by a dry test meter specially installed in the main supply line to the Fuels Research Laboratory for this purpose.

Runs 17 and 18 provided the last set of results obtained and were the most complete runs performed. For both of these runs, all equipment worked well and good closure of material balances was achieved. The material balance gave an independent check on the load cell results and provided insight into the C/H and O/H ratios of the fuel that was being consumed. Using the material balances and the measurements of the concentration of hydrogen within the fuel bed made it possible to check the validity of the equilibrium of the water-gas-shift reaction at the top of the fuel bed. The base case fuel composition was used in both of these runs and the underfire air was varied from 140 lb $hr^{-1}ft^{-2}$ in Run 17 to 86 lb $hr^{-1}ft^{-2}$ in Run 18.

Outline of Discussion of Results. The ensuing discussion will be based primarily on the results obtained from Runs 5 through 18, as the results prior to Run 5 were of a preliminary nature and experimental conditions were ill-defined. The complete data set for one experiment (Run 17) is contained in Appendix H. It was not considered feasible for easons of space to include the complete data sets for all experiments; thus, the following discussion will be based on selected data from typical runs. Rather than dealing with the results from each of the experiments in sequence, the following sections will each be devoted to considering a different aspect of the results (for example, Bed Temperatures, Material Balances, Fuel Bed Gas Compositions, etc.).

Fuel Bed Temperatures

Fuel Bed Temperature Distributions for Active Burning Runs.

The temperature at the center of the fuel bed was measured at ten different vertical positions spaced, on the average, three inches apart. For the later runs (Runs 11 through 18) two thermocouples were used to measure the bed temperatures close to the side wall. The measurements taken in Run 10 at five positions in the bottom half of the bed are shown in Figure 50. It should be emphasized that these measurements were made with a thermocouple at the center of the bed, and that they represent a weighted mean of the temperature of the gas that flowed over the couple and the temperatures of the surfaces with which the couple was in radiative exchange. The recorded temperature therefore depended on the drying characteristics of the fuel surrounding the termocouple to the extent that these characteristics affected the surface temperature of the drying fuel element.

Despite the above qualifications, the temperatures in most runs showed, as in Run 10, a regular progression of the burning front from the top surface of the bed to the grate. In a few experiments the temperatures were observed to plateau at 212°F and about 500°F. Peak temperatures were typically around 2200°F. These maximum temperatures give a measure of the degree of melting, clinkering and ash fusion that could be expected on a traveling grate. The temperatures observed here, which appear typical for most refuse beds, are high enough for all soft glass to melt (as was experimentally observed) and were high enough to suggest that aluminum would also melt. The temperatures were never high enough to melt the tin cans, but the bright metal coating disappeared as a probable consequence of both vaporization and diffusion into the substrata; the steel was badly carburized. Figure 50 shows, from the temperature registered by thermocouple No. 5, that the ignition

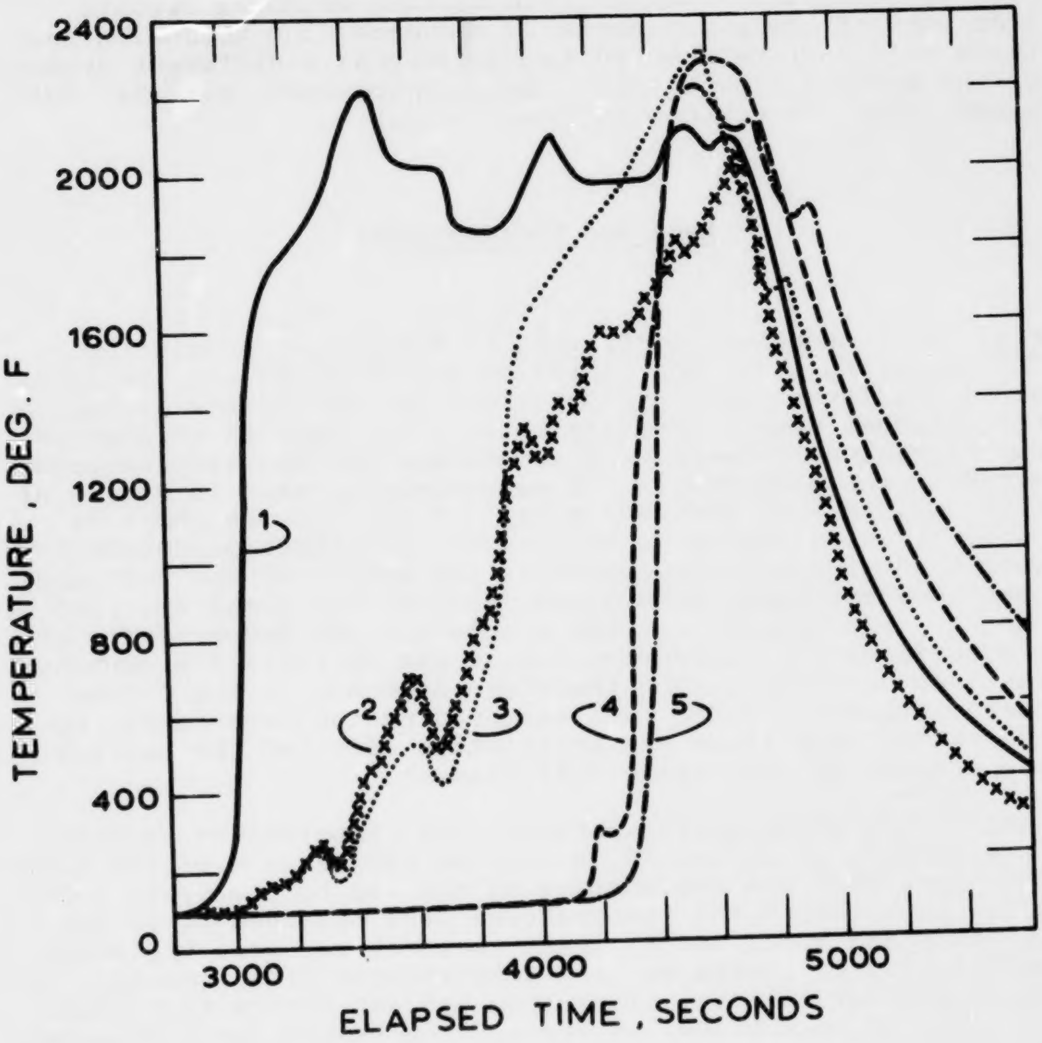

Fig. 50. Fuel Bed Temperatures (Run 10). Thermocouples 1, 2, 3, 4 and 5 were located 11, 9, 7, 2, 0 in. from the grate. Initial fuel bed depth 30 in.; underfire air rate 175 lb hr^{-1} ft^{-2}; bulk density of fuel 16.7 lb ft^{-3}

plane reached the grate 4400 sec after the start of the run. The temperature recorded by this thermocouple can be considered to be the grate temperature and as such gave a measure of the degree to which the grate was heated.

Care has to be taken when interpreting the fuel bed thermocouple data because of the continuously changing nature of the fuel bed. In this regard, two problems were encountered. First, at the end of a few runs, some thermocouples were found to be severely bent out of position. The following tentative explanation for this observation can be offered as no direct evidence was available from the data. The consumption of the combustible resulted in a continuous change in the density of fuel bed, and therefore the ash and inert content of the fuel had to settle slowly towards the grate over the course of an experiment. The mechanics of the settling of the bed would have depended on the difference between the ignition and burning rates. When the ignition rate was not much greater than the burning rate of the combustible content of the fuel, it can be hypothesized that the fuel was consumed in a thin reaction zone which moved through the bed. Under these circumstances, the inert and ash content of the fuel would have moved with the burning zone, and within this burning zone the inert and ash content would have increased with time. The settling of the bed in this fashion would have caused little drag on the fuel bed thermocouples. When the ignition rate was much faster than the burning rate, it can be conjectured that most of the fuel was consumed after the ignition front reached the grate; after this time, the major portion of the remaining fuel would have been consumed by the oxygen in the underfire air in the space of a few in. above the grate. Under these conditions, it can be expected that the whole of the remaining bed would have slowly settled towards the grate as the combustible was consumed; the resulting drag on the fuel bed thermocouples under these conditions would have been considerable.

An attempt was made to minimize the effect of the settling fuel bed on the thermocouples by supporting the thermocouples inside quartz tubing held in place by metal sheaths cemented into the side wall of the fuel bed. These efforts were largely successful but there were occasions when the quartz tubing broke and the thermocouple casing was rapidly carburized and weakened, allowing the thermocouple to be dragged down by the settling bed. (The rapid carburization of steel within a fuel bed is one of the primary difficulties associated with obtaining good fuel bed temperature data with thermocouples. It was found that 304 Stainless was rapidly carburized at the temperature levels of the bed; and of the more common high nickel content alloys only Inconcl 600 appeared to have a a reasonable lifetime.) A further difficulty raised by the consumption of the fuel was the relative position of the thermocouples within the bed as a function of time. As the bed burned down, the thermocouples were, since their position with respect to the apparatus was fixed, eventually exposed above the bed. At this point, the thermocouples were no longer recording bed temperatures but instead recorded a weighted mean of the temperatures of the refractory lining, the overfire combustion gases, and the gases issuing from the top of the bed.

The second problem assumed to have been encountered, but never proved explicitly, concerned the shielding of the thermocouples by the inert material (tin cans). It was possible that some of the thermocouples were covered by the inert material when the bed was being built up prior to the start of the run; in this case, it is conceivable that the affected thermocouples did not respond as rapidly as the unscreened thermocouples when the ignition front passed over them. In addition, it was likely that some thermocouples were shielded during the run as the inert material settled towards the grate. (This may, in part, be the reason for the erratic behavior of thermocouple No. 2 in Figure 50).

The thermocouple history can, on the basis of the above discussion, be expected to give a reasonable representation of the temperatures within the fuel bed up to the point when the ignition plane reached the grate. After this time, the interpretation of the temperatures becomes difficult because of the uncertainty introduced by the bed movement.

From the temperature histories of the twelve fuel bed thermocouples, bed temperature profiles were constructed. Figure 51 shows the temperature profiles throughout the bed at different times during Run 18. The plot is typical of the results of those runs in which sustained active burning was achieved. The heterogeneous nature of the fuel bed created a rather poorly defined ignition front, but this restriction aside, Figure 51 shows that an ignition front of approximately constant shape propagated through the bed from top to bottom. Near the end of the run, the bed temperatures increased (typically by 400°-500°F). It is thought that this increase in temperature occurred subsequent to the drying and pyrolysis of the major portion of the bed (all but the last layer or so of fuel particles), and did so because at this late stage of the run more of the energy liberated by chemical reaction was available to raise the sensible heat of the bed and less was required to provide the energy requirements of drying and pyrolysis. This result indicates that the grate links of a traveling-grate stoker could receive their major punishment towards the discharge end of the furnace; in practice the underfire air rate to the last grate is high and provides the necessary convective cooling of the links. Some care needs to be exercised in interpreting the profiles shown in Figure 51, as the location of the top of the fuel bed at different times was not determined experimentally. The profiles indicated are strictly, therefore, composite profiles of the entire fuel bed section measuring temperature both in and above the bed. The initial and final depths of the fuel bed are indicated in Figure 51; the final depth is based on measurement of the volume occupied by the quantity of inert material present at the end of the experiment. The rate of recession of the top of the bed was not measured experimentally and any theoretical estimate would have to depend on a somewhat crude model of the mechanics of fuel burn-out. This question will be reconsidered on pages 213-230. This drawback affects neither the above discussion of the temperature profiles at the ignition front nor that concerning the temperature increase at the end of the run; however, the shortcoming does not permit any reasonable estimate of the heat lost or gained by the bed to be obtained from the profiles of Figure 51. From the earlier discussion of the mechanics of the settling of the bed as it burnt out, it may be hypothesized that under the conditions of Run 18 (approximately equal burning and ignition rates) the inert content probably accumulated above the burning zone as it moved through the bed, insulating the bed from radiative heating from the overfire section.

The slight temperature decline from the peak temperature at the ignition front to that measured at the top of the bed observed in this study over most of the duration of the runs parallels the results of Nicholls (24). Nicholls' results also indicated that the temperature decline in an underfeed bed was rather less than observed in an overfeed bed. The decrease in temperature can be explained by the occurence of the endothermic reactions $C + CO_2 \rightarrow 2CO$ and $C + H_2O \rightarrow H_2 + CO$ in in this region of the bed. Figure 51 shows that the temperature drop through the bed increased near the end of the run, probably due to the augmented rates of the endothermic reactions as a consequence of the general temperature increase through the bed at this time.

In the early experiments (Runs 1-10) it was noticed that the temperatures at the side wall appeared to be higher than at the center of the fuel bed. Although side wall temperatures were not measured directly, this trend was deduced from the discoloration of the thermocouple sheaths extending for about two inches from the side wall towards the center of the bed. The higher side wall temperatures were attributed to channeling of the underfire air, resulting in a localized heat release. For the later runs (Runs 11-18),

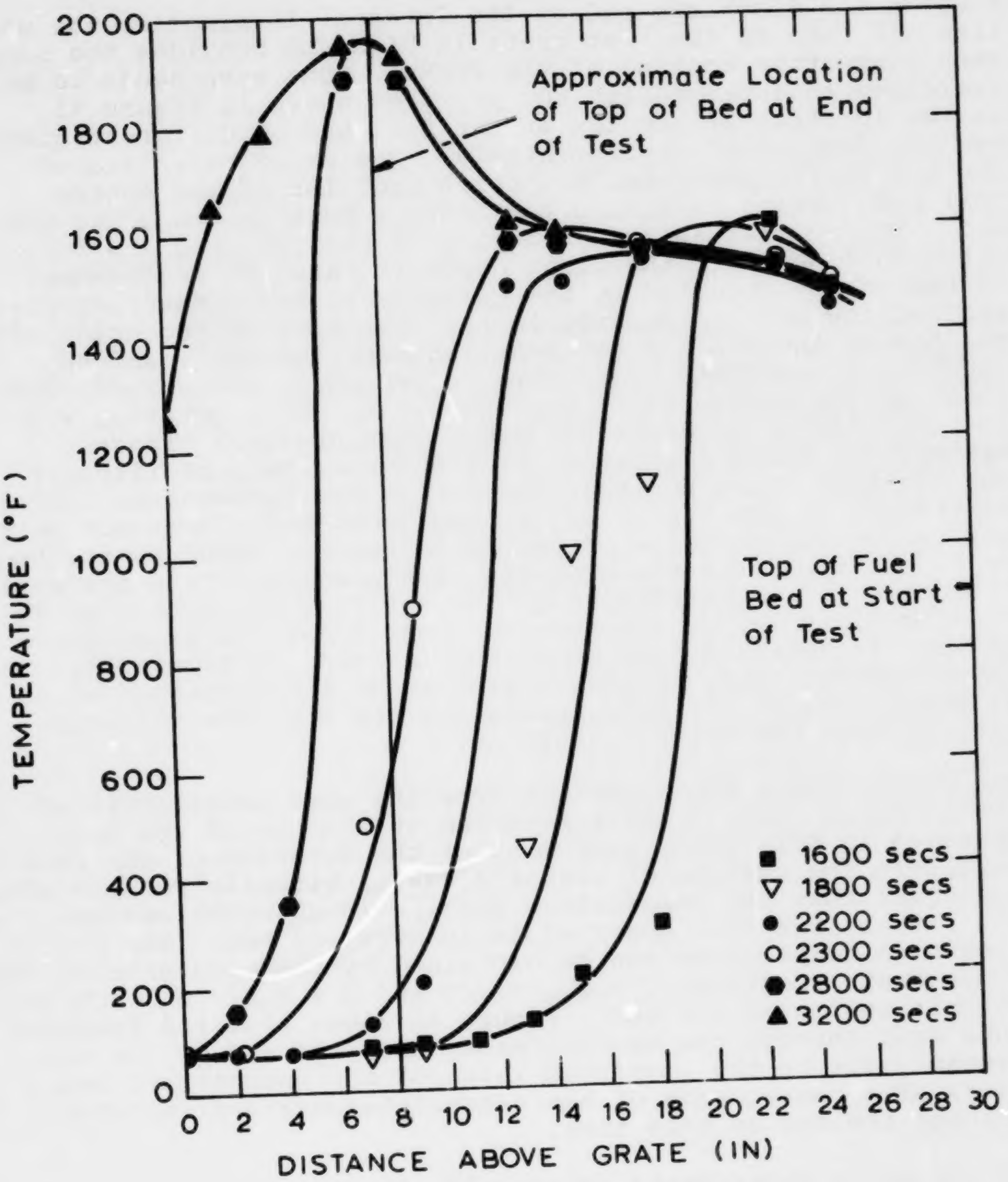

Fig. 51. Fuel Bed Temperature Profiles at Different Times throughout Run. Data from Run 18.

where the improved high pressure drop grate was used, the occurrence of channeling as manifested by high side wall temperatures was not noticed; this was confirmed by the two thermocouples used in these later experiments to measure the fuel bed temperatures at two different vertical and angular locations about one inch from the side wall (see Appendix H, Figures H.1 and H.2). These edge temperature measurements also showed that the ignition front appeared to propagate evenly across the width of the bed (see pages 210-211 , Figures 56 and 57).

Fuel Bed Temperature Distributions under Poor Ignition Conditions. In those runs where difficulty was experienced in igniting the bed at the start of the experiment, the bed temperature profiles were markedly different from those shown in Figure 50. Although this problem concerns mainly those runs in the second group of experiments (namely, Runs 5-9), similar experiences were found in Runs 12 and 13. The temperature profiles observed depended on the methods used in promoting active burning. A discussion will follow on the bed temperatures observed in Runs 5, 6, 7 and 9, as they represent the spectrum of behavior.

The fuel bed temperature data for Run 5, shown in Figure 52, indicated that the bed smoldered until enough of the moisture content of the bed had been removed for satisfactory burning to proceed. This was shown by the initial rise in the first 6-7 in. of the bed to 900°-1400°F by 900 sec, followed by a slow decrease in the temperature at this position in the bed and a slow rise of the temperatures through most of the remainder of the bed. The temperatures in the bed about 6 in. below the ignited portion of the bed plateaued around 200°F. During this period (0-2800 sec) the underfire air had been raised in an attempt to kindle the fire. After 2800 sec the temperatures started to rise slowly throughout the bed with the temperatures toward the top of the bed leading those lower down. By 4000 sec the whole bed had ignited and the temperatures throughout the bed steadily increased until they reached a peak of 2000°F at 4600 sec. At this time combustion was nearly completed and the temperatures started to fall. The underfire air was decreased at 4000 sec because visually the bed did not appear to be burning satisfactorily at this time. The data indicated that burning would have proceeded satisfactorily if the underfire air had been left at its previous level of 145 lb $hr^{-1}ft^{-2}$.

No satisfactory ignition of the bed could be obtained in Run 6 despite a number of underfire air changes and reignition of the gas burners so as to increase the heat flux to the top of the bed. Visual observation of the fire showed that it

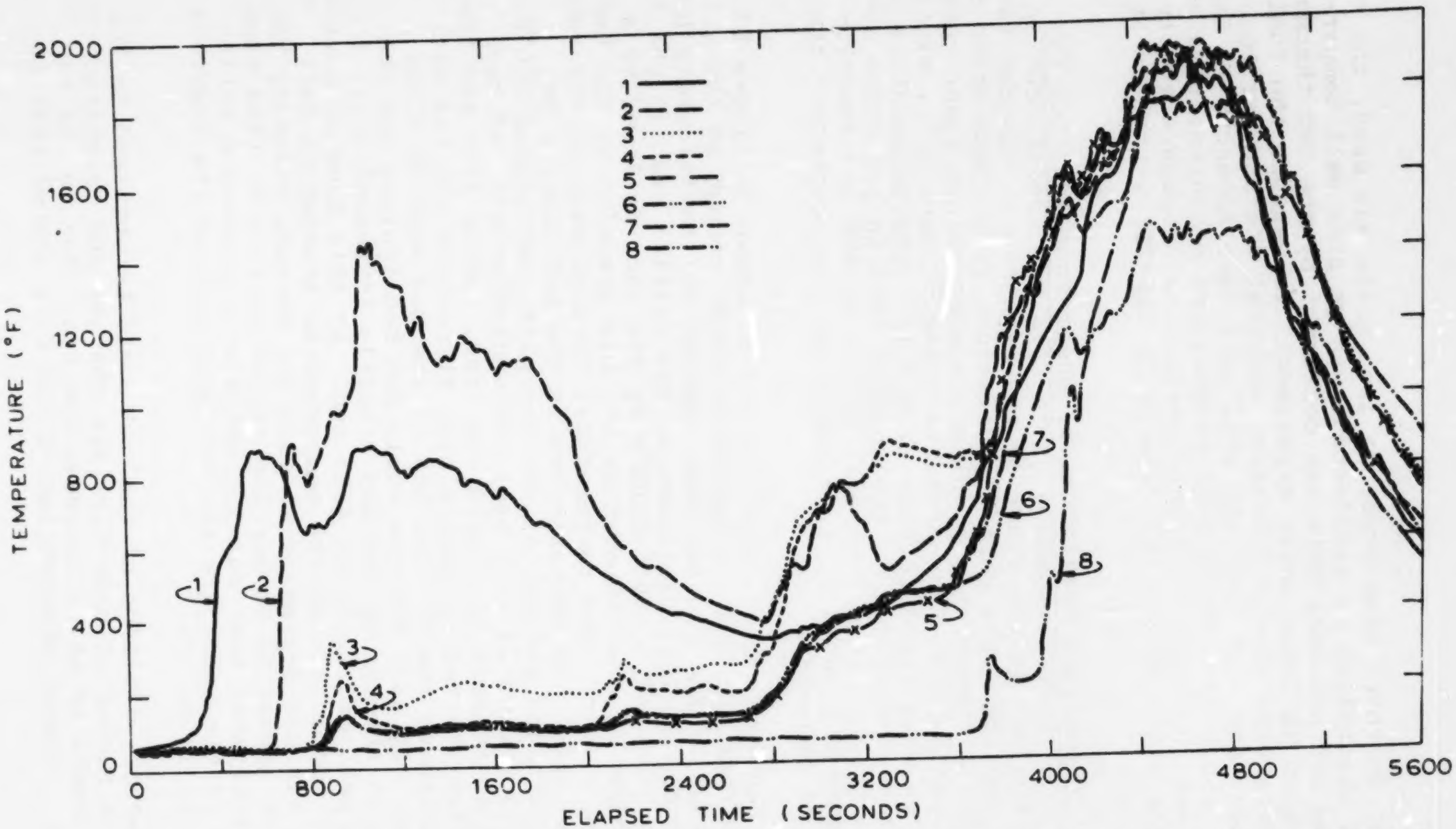

Fig. 52. Fuel Bed Temperatures (Run 5). Thermocouples 1, 2, 3, 4, 5, 6, 7, and 8 were located 25, 23, 19, 18, 11, 9, 7, and 2 in. from the grate. See Table VI.2 for experimental conditions.

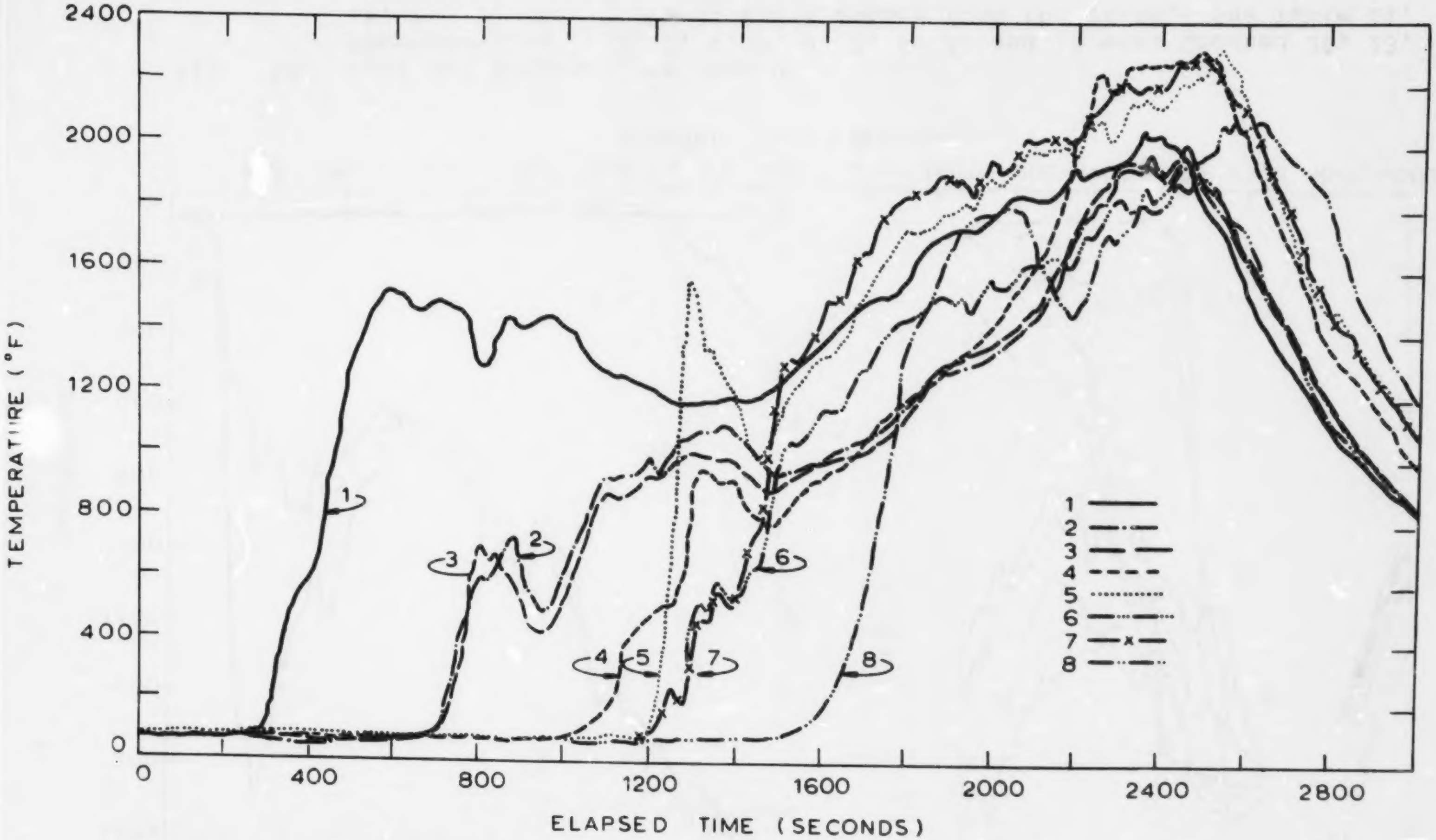

Fig. 53. Fuel Bed Temperatures (Run 7). Thermocouples 1, 2, 3, 4, 5, 6, 7, and 8 were located 23, 19, 18, 13, 11, 9, 7, and 0 in. from the grate. See Table VI.2 for experimental conditions.

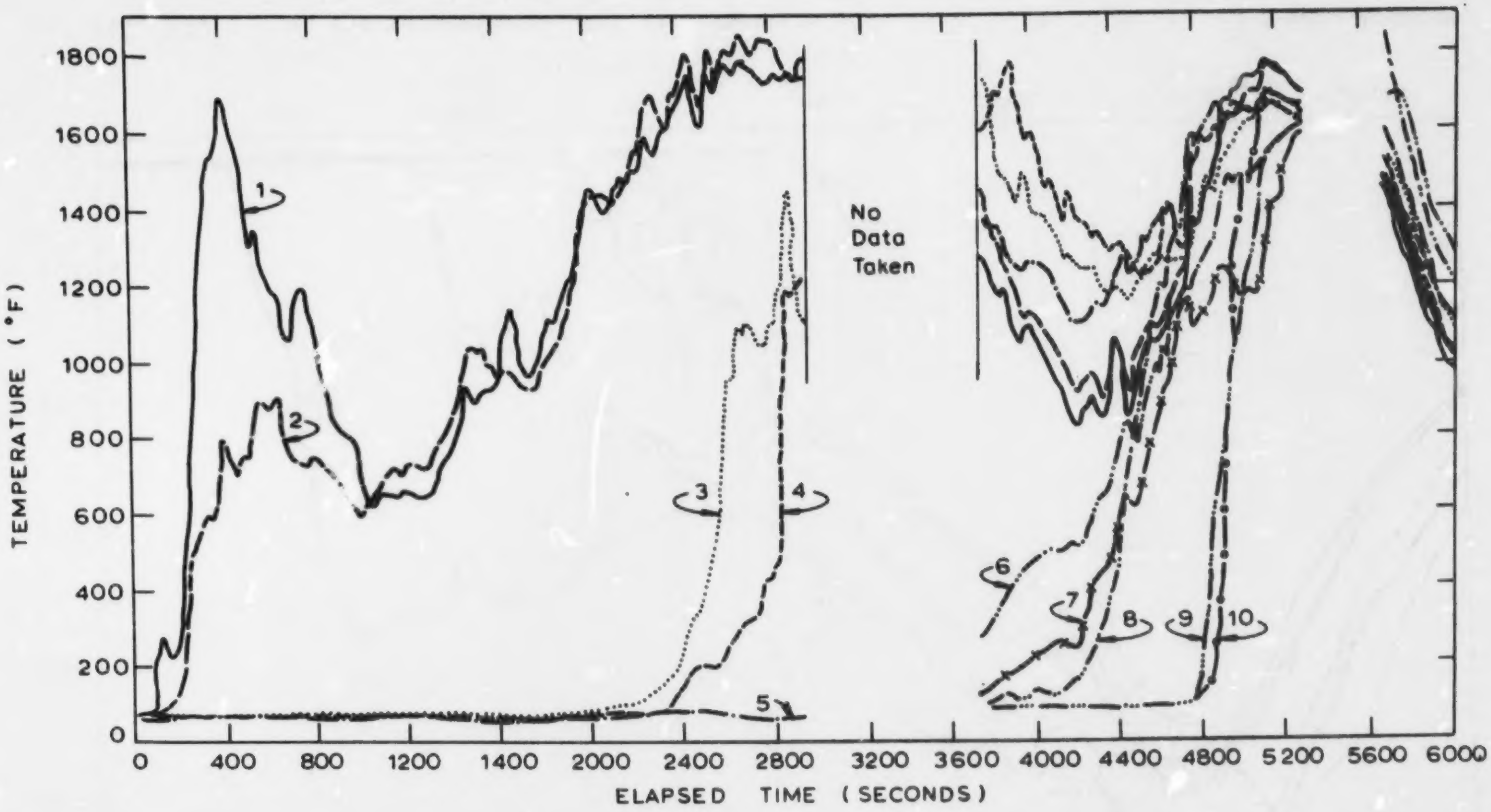

Fig. 54. Fuel Bed Temperatures (Run 9)
Thermocouples 1, 2, 3, 4, 5, 6, 7, 8, 9, and 10 were located 25, 23, 19, 18, 13, 11, 9, 7, 2, and 0 inches from the grate. See Table 11, for experimental conditions.

appeared to be almost totally quenched about 25 min after the run had started. Data taking was stopped at this time and a complete record does not exist for this run. It was observed that the bed continued to smolder for about 5 hr after the underfire air was cut off, and almost complete burn-out of the fuel was obtained. This result provided striking evidence of the tendency for air to be drawn down through the bed by natural draft. The bottom of the bed had been completely sealed by the grate and the combustion air could only have been supplied by air sinking down through the bed at the "cold" wall. The burning rate under these conditions was very low.

The data for Run 7 depicted a different picture of the bed temperatures, which are shown in Figure 53. In the first few inches of the bed, the temperatures rose quickly to well above ignition temperature, but at depths below 10 in. the temperatures rose slowly over a period of about 10 min to 1000°F. About halfway through the run (1500 sec) the whole bed had reached a temperature of around 1000°F; from this time until complete burn-out was achieved, the temperatures rose slowly throughout the bed over a period of 10 min to 2200°F (the maximum temperature observed, was achieved about 10 min before complete burn-out). The burning rate of the bed increased markely shortly after the bed temperatures reached their maximum and remained relatively constant until final burn-out. The underfire air was held constant for the major portion of this run at 146 lb hr^{-1}ft^{-2} since, visually, the bed appeared to be burning reasonably well.

For Run 9, yet another type of behavior was observed. The bed temperature profiles for this experiment are shown in Figure 54. The bed ignited rapidly down to 5 in. (about 400 sec into the run) despite the underfire air rate of 275 lb hr^{-1}ft^{-2}, and then the temperatures in this ignited section of the bed fell to around 600°F (at 1200 sec). The gas burners were reignited at 1500 sec to keep the top section refractories above 1400°F, and the underfire air was decreased since it was visually observed at this time that there had been poor ignition. From this time up to 2400 sec into the run, the temperature in the top few inches of the bed rose slowly to 1800°F, after which the ignition plane started to move through the bed until about two thirds of the bed was ignited. Visual observation showed that the bed appeared to be burning properly at this time and the underfire air was raised to 175 lb hr^{-1}ft^{-2}. The temperature data indicated that the underfire air rate must have been increased too quickly, for at 3000 sec the bed temperatures in the ignited portion of the bed began to decrease, dropping to a minimum of 800°-1400°F at 4400 sec. The temperature profile was still propagating into the virgin fuel at this time but temperatures did not reach the ignition level. The underfire air was again decreased and at 4400 sec the temperatures in the top two thirds of the bed began to increase. The remainder of the bed began to ignite, slowly at first and then more rapidly. The bed was fully ignited at 5000 sec, at which time the underfire air was again raised to 175 lb hr^{-1}ft^{-2} since the bed appeared to be burning satisfactorily. The burning rate was observed to increase in the later stages of the run but not to the extent noticed in Run 4.

Drying Front. As discussed on pages 192-208 , the drying rate of a fuel element is limited by the rate of transfer of energy from the burning front and by the rate of conduction of energy in the object being dried. When the latter resistance is low, for example in thin or porous objects, the temperature will plateau at 212°F and the drying wave will propagate ahead of the ignition wave. This was the case in the Bureau of Mines study (26,27), where the moisture was introduced with leafy vegetable material. In the present study the moisture was introduced in blocks of wood, in sizes such that the heating of the center of a block lagged behind the surface heating by times of the order of 1000 sec. For this case only a slight plateau was observed when the temperature measured within the bed reached 212°F and drying continued within the wood blocks even after the surface had ignited. The peak temperatures within the fuel bed observed toward the end of a run probably occurred subsequent to the drying of the entire bed.

Additional evidence for the protracted drying of elements of the fuel bed is provided by the data from runs in which difficulty was experienced igniting the bed (e.g., Run 5). In this case the temperature wave from the ignition front dissipated slowly enough that marked plateaus were observed when the temperature ahead of the ignited zone reached the vicinity of 212°F (see Figure 52). Under normal burning conditions this 212°F plateau would not be expected because of the much higher heating rates to which the fuel bed elements would be subjected (on pages 192-208). Under the normal burning conditions encountered in this study, the quenching effect of the wet wood blocks, where the internal diffusion of water was low relative to the heating rate, would not have been a hindrance to ignition and combustion.

Pyrolysis Front. In a number of runs a plateau at about 500°F was observed, corresponding roughly to the temperature of pyrolysis of cellulosic materials. It is difficult to determine if this was a real effect or was caused by temporary shielding of the thermocouples by inert material. The heat effects of pyrolysis will generally be rather lower than the drying heat effects and at the higher fuel bed heating rates it is unlikely that the pyrolysis "wave" would have been noticed. However, as in the case of drying, the pyrolysis of larger wood blocks was limited by the rate of propagation of energy into the center of the blocks. Pyrolysis would therefore have been initiated as the surface temperature of a block approached 500°F and continued internally within the block for extended periods.

Temperatures at the Ignition Front. The maximum temperatures observed at the ignition front for the different runs in which it was possible to obtain reasonable values are shown in Table 12;there was considerable scatter in the data, and selecting a range of values was often arbitrary. There was surprisingly little variation in the ignition front temperatures despite fairly considerable changes in the underfire air flow rate (86-175 $hr^{-1}ft^{-2}$) and the moisture content of the fuel (15-32%). The lowest temperatures observed occurred in Run 1, but these temperatures were quite possibly erroneous as they seem very low for the type of active burning usually observed. It appeared that the lower temperatures were associated with the lower air flow rates. A simple explanation for this is the greater effect of heat losses at these lower heat generation rates. There were no distinct trends with increasing moisture content although the theory developed earlier (a simple overall heat balance) suggested that the maximum temperature should decrease with moisture content, according to

$$T_{max} = \frac{Q^{net}}{\dot{G}C_{p_g} + \dot{U}C_{p_s}} \qquad (54)$$

This result may be attributed to the drying characteristics of the material used. The wood was known to dry over a protracted period of time, and the amount of moisture released up to the point when the temperature at the ignition front reached a maximum may have remained roughly constant, regardless of the moisture content. For material where the internal diffusion of water is high the effect of moisture on the maximum temperature will be much more pronounced. This will have a strong adverse effect on the ignition rate.

On the basis of equation (54), the maximum temperature for Run 15, would have been expected to be lower than in Runs 11 and 12 because of the higher ignition rate (based on the rate of

TABLE 12

Maximum Temperature Observed at Ignition Front with Varying Underfire Air Rates and Fuel Compositions

Run No.	Fuel Analysis			Underfire Air Rate (lb hr^{-1}ft^{-2})	Maximum Temperature Observed at Ignition Front (°F)
	% Inert	% Moisture	% Combustible		
1	-	8	92	Natural Draft	1100 - 1400
10	17.10	31.76	51.14	175	1600 - 1800[a] 1800 - 2000[b]
11	15.51	23.99	60.50	155	1800 - 2000
12	12.79	25.89	61.32	155	1800 - 2000[a] 1800 - 2200[b]
14	15.08	14.73	70.19	160	1800 - 2100
15	-	26.40	73.60	156	1600 - 2000
16	16.23	24.85	58.92	118	1600 - 1800[a] 1600 - 2200[b]
17	15.18	25.38	59.49	140	1700 - 1900[a] 1600 - 1900[b]
18	15.04	25.06	59.90	86	1500 - 1700[a] 1600 - 1900[b]

(a) Observed in top two thirds of bed

(b) Observed in bottom third of bed

ignition of both fuel and combustible). The range of maximum temperatures was observed to be slightly lower than in Runs 11 and 12 but the difference was hardly significant.

Temperature Profiles Below Ignition Front. From the temperature history of the different thermocouples in the bed and a knowledge of the ignition rate, the fuel bed temperature could be plotted as a function of distance below the ignition plane. The results for one test were not all the same because of the heterogeneous nature of the bed surrounding the thermocouples;however, it was possible to construct an average curve for the temperature-distance profile. These profiles are shown in Figure 55.

From equation 58 the temperature below the ignition plane is given by

$$T = T_{ign} \, e^{-(\alpha + \beta) z} \tag{58}$$

where

$$\alpha = \sqrt{\frac{h_v}{K_s^E} \left[1 + \frac{1}{4} \left(\frac{\dot{U} C_{p_s}}{\sqrt{h_v K_s^E}} + \frac{\sqrt{h_v K_s^E}}{\dot{G} C_{p_g}} \right)^2 \right]}$$

$$\beta = \frac{1}{2} \sqrt{\frac{h_v}{K_s^E}} \left(\frac{\dot{U} C_{p_s}}{\sqrt{h_v K_s^E}} - \frac{\sqrt{h_v K_s^E}}{\dot{G} C_{p_g}} \right)$$

Under most practical conditions $h_v \simeq 200$ Btu $hr^{-1} ft^{-3} {}^{\circ}F^{-1}$, $K_s^E \simeq 4$ Btu $hr^{-1} ft^{-1} {}^{\circ}F^{-1}$, $C_{p_g} \simeq C_{p_s} \simeq 0.5$ Btu $lb^{-1} {}^{\circ}F^{-1}$, $U \simeq$ 50 lb hr^{-1} ft^{-2} and $G \simeq$ 100 lb $hr^{-1} ft^{-2}$ giving

$$T \cong T_{ign} \, e^{-\sqrt{\frac{h_v}{K_s^E}} \, z} \tag{170}$$

Equation (170) predicts that as the volumetric heat transfer coefficient, h_v, increases or the effective thermal conductivity of the bed, K_s^E, decreases the profile below the ignition front will become steeper; conversely, as the heat transfer coefficient decreases or the effective thermal conductivity increases, the profile below the ignition front will become shallower. This prediction is confirmed by the results of Runs 18, 16 and 11 shown in Figure 55, in which progressively

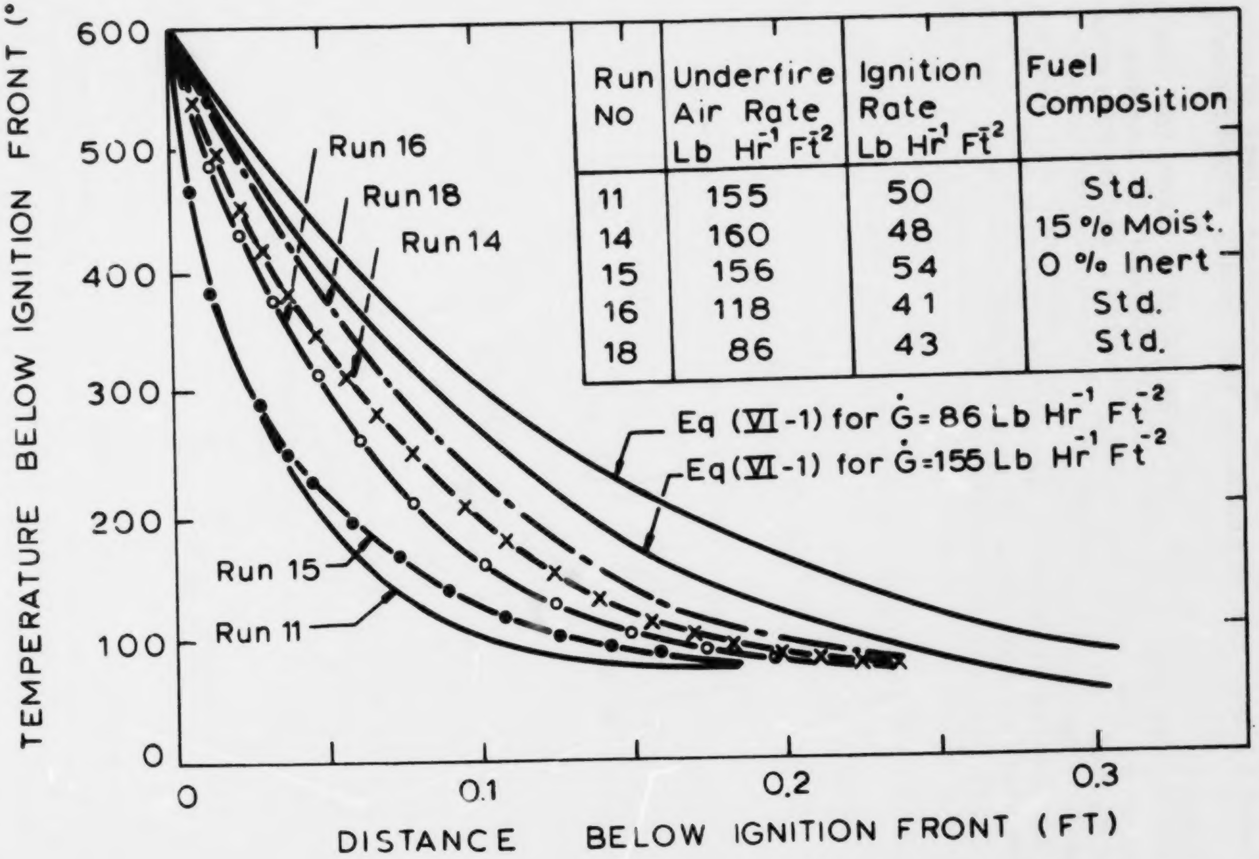

Run No	Underfire Air Rate Lb Hr^{-1} Ft^{-2}	Ignition Rate Lb Hr^{-1} Ft^{-2}	Fuel Composition
11	155	50	Std.
14	160	48	15 % Moist.
15	156	54	0 % Inert
16	118	41	Std.
18	86	43	Std.

Fig. 55. Fuel Bed Temperatures Below the Ignition Front for Different Fuel Types and Underfire Air Rates

greater underfire air flow rates were used (h_v scales approximately as $\dot{G}^{0.63}$). The temperature profiles of Run 15 also follow the trends indicated by equation (170). In this run the absence of the inert material (the components of which were slightly larger than those of the combustible portion of the fuel) very likely decreased the effective mean beam radiating length through the bed (see pages 198-203) and thus decreased the effective thermal conductivity.

Using the heat transfer correlation of Bradshaw *et al.* (64) and parameter values as follows: $C_{p_g} \simeq 0.4$ Btu $lb^{-1}\,^{o}F^{-1}$, $N_{pr}^{2/3} = 0.81$, $\mu = 0.1$ lb $hr^{-1} ft^{-1}$, $D_p = 0.125$ ft, $\delta = 0.4$, the heat transfer coefficient based on a unit volume of bed is found to be, $h_v = 10.4\dot{G}^{0.625}$ Btu $hr^{-1} ft^{-3}\,^{o}F^{-1}$. Figure 55 shows theoretical curves, calculated from equation (170) using the above relationship for h_v and $K_s^E = 4$ Btu $hr^{-1} ft^{-1}\,^{o}F^{-1}$ (see pages 198-203), for two different values of $\dot{G}$ corresponding to conditions for Runs 18 and 11. The theoretical profiles are of the correct order but the variation with changing underfire air rate is not as large as that observed experimentally. However, the theory is only approximate and the assumptions of constancy of effective thermal conductivity and particle isothermality, which are known not to be strictly true for many fuel bed conditions, will mitigate against precise prediction of the temperature profile below the ignition front.

From the results of the theory presented above, the temperature profiles of Run 14 should have been close to those of Run 11 as the only difference between the two runs lay in the moisture content of the fuel. The fact that the data fell between those obtained for Runs 16 and 18 is anomalous and no satisfactory explanation can be offered.

Ignition Rates

The ignition of the bed can be conveniently divided into two stages -- the initial ignition of the bed at the start of the run by the radiant heat from the hot refractory brickwork and the propagation of the ignition front through the bed. For all the runs performed, the fuel bed ignited at the start of the run, even when the top surface contained more than a proportionate amount of wet wood blocks, based on the total moisture content of the fuel. The initial radiant heat fluxes to the top of the bed were of the order 10^5 Btu $hr^{-1}ft^{-2}$, very much greater than required for ignition, even for blocks of wood containing 60% moisture (117), which was the maximum moisture content of any of the wet wood blocks used in this study.

The major difficulty with the ignition process lay in adjusting the underfire air rate so that the ignition front would propagate through the bed; this has been described on pages 198-203 for the cases of Runs 5-7 and 9. At the time these runs were conducted, it was felt that burning rates typically observed in a traveling-grate incinerator (60 lb $hr^{-1}ft^{-2}$) could be obtained with underfire air rates around 150 lb hr^{-1} ft^{-2} and it was thought that at these underfire air rates the burning rate would be close to its maximum. It was for this reason that underfire air rates varying from 120 to 275 lb $hr^{-1}ft^{-2}$ were employed. The range of underfire air rates was weighted to rates higher than 150 lb $hr^{-1}ft^{-2}$ because of the desire to map out the ignition-limited regime of burning.

Runs 5-9 clearly showed that raising the underfire air too quickly at the beginning of a run (on a traveling grate this would be equivalent of having too high an underfire air rate through the first few windboxes) seriously hampered the ignition rate; this behavior was not observed by Nicholls (24) in his studies on coke and coal as in his experiments the underfire air was raised to its final level very quickly after the fuel bed had been ignited. In addition, once the ignition front had propagated a few inches into the bed, the effect of changing the radiant heat flux to the top of the bed was found to be minimal because of the insulating effect of the inert and charred fuel. All the energy required to drive the ignition front forward had to come solely from the heat liberated by the reaction of oxygen with the char and pyrolysis products in the partially ignited bed. Once the temperatures in the ignited zone dropped low enough to provide a significant chemical resistance to combustion, it was very difficult to increase the heat generation rate to get the bed back into an active burning state because of heat losses to the cold fuel bed wall and the unignited fuel.

As discussed on pages 192-208, ignition temperatures differ between materials and with experimental conditions. For celluosic materials, piloted ignition occurs at temperatures of 550° to 600°F. In this study, a temperature of 600°F was selected for the derivation of curves, such as that shown in Figures 56 and 57 for the propagation of the ignition front. In active burning runs the temperature gradient near the ignition front was sufficiently steep that the values of the

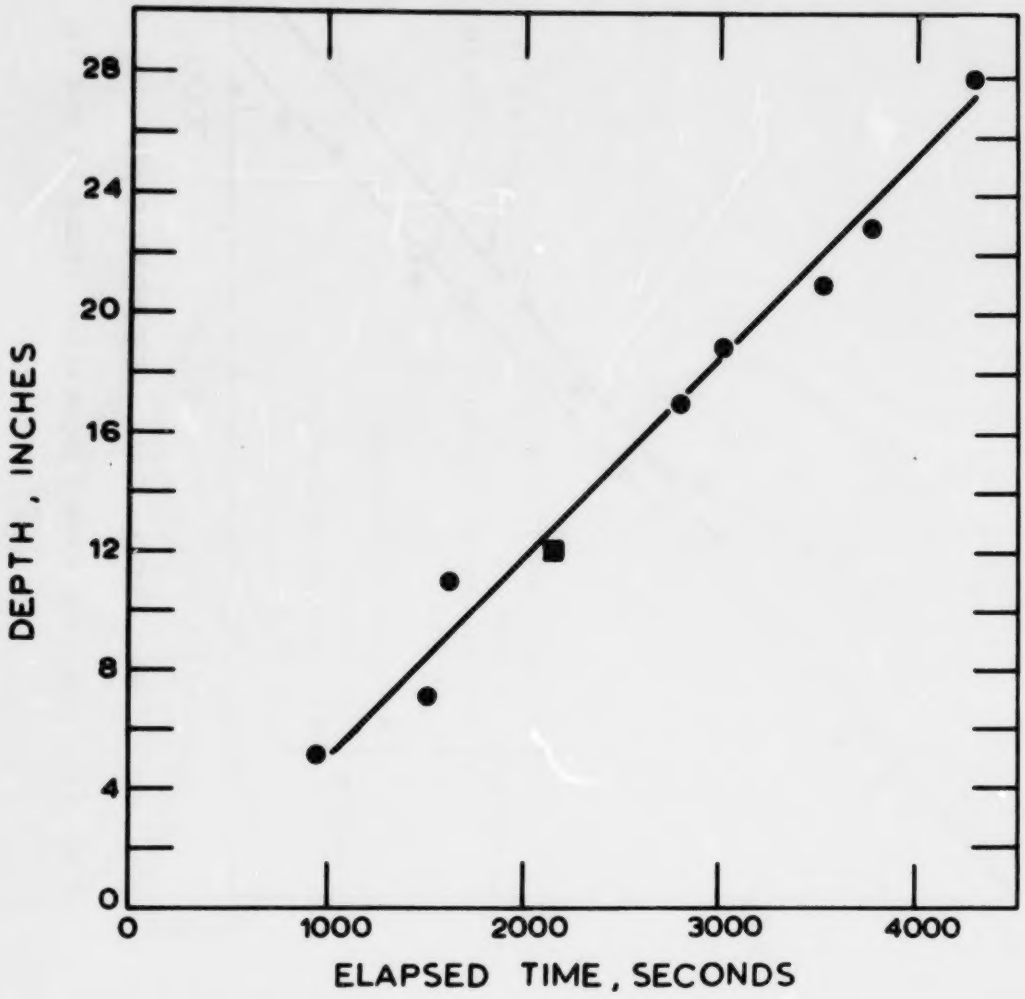

Fig. **56.** Ignition Wave Propagation (Run 10). Ignition temperature assumed equal to 600° F; underfire air flow 175 lb hr^{-1} ft^{-2}; bulk density of fuel 16.7 lb ft^{-3}; initial bed depth 30 in. ● measured at center of bed; ■ measured at edge of bed.

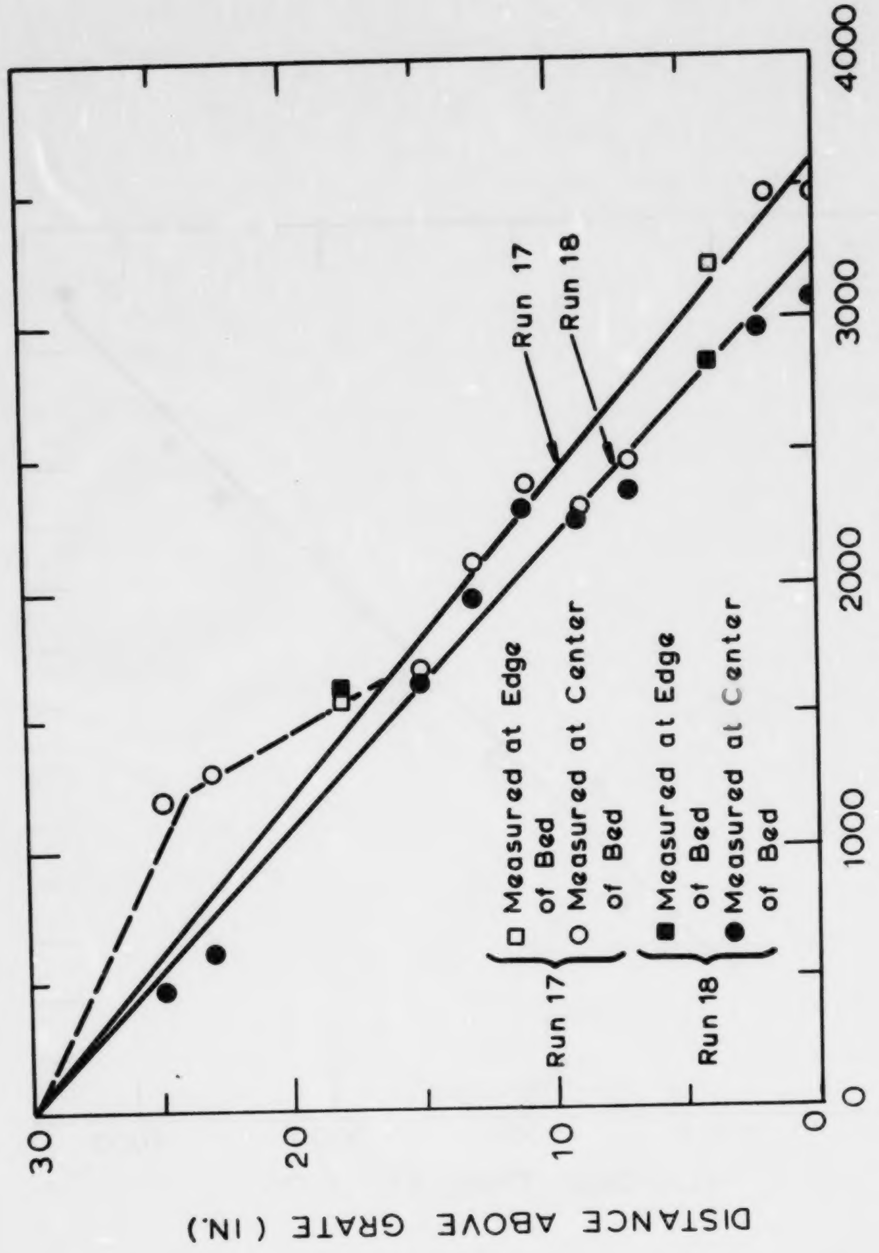

Fig. 57. Ignition Wave Propagation (Runs 17 and 18)

ignition rate were found to be insensitive to the value of ignition temperature selected. The ignition rates were computed as the product of the rate of travel of the ignition front and the initial bed density. For active burning runs the rate of travel of the ignition front was found to remain approximately constant over the duration of the experiment; the variation of the data shown in Figures 56 and 57 was typical of the deviation from linearity in the plot of depth of ignition front penetration versus elapsed time. Ignition rates were found to vary from 125 lb $hr^{-1}ft^{-2}$ for an underfire air rate of 127 lb $hr^{-1}ft^{-2}$ (Run 5) to 34 lb $hr^{-1}ft^{-2}$ for an underfire air rate of 175 lb $hr^{-1}ft^{-2}$ (Run 10). A summary of the ignition rates found in the experiments, the underfire air rates, and fuel compositions in given in Table 51.

The high ignition rates observed in the later stages of the runs where difficulty had been experienced in igniting the bed (e.g., Runs 5, 7 and 9) were undoubtedly much too high for the initial fuel composition employed. This descrepancy occurred because, at the times when these ignition rates were calculated, the bed had been partially dried (see page 203 and Figures 52, 53 and 54). The high ignition rate observed in Run 1 (110 lb $hr^{-1}ft^{-2}$) can be attributed to the low moisture content of the fuel. This ignition rate was probably close to the maximum achievable for the inert-free fuel used in this study. As clearly demonstrated in Nicholls' (24) experiments and by the embryonic ignition theory developed on pages 118-129, the ignition rate would be expected to pass through a maximum as the underfire air rate is increased. It is hypothesized that under natural draft conditions the underfire air rate increases to a level which gives an ignition rate close to its maximum. If this hypothesis is correct it lends credence to the belief that the ignition rate for Run 5 was measured for a fuel which had been almost completely dried. For Runs 11 through 18, where the calculated ignition rates were more truly representative of the initial fuel composition and of the conditions of the test, the observed ignition rates lay in the range 34-50 lb $hr^{-1}ft^{-2}$.

The ignition rates calculated for Runs 10, 11, 16, 17 and 18 which were all conducted with a fuel of approximately constant composition, show (with the exception of Run 11) a monotonic increase with decreasing underfire air rate (see Table 11). This result follows the general trend in ignition rates observed by Nicholls (24) in the equilibrium burning regime (equal ignition and burning rates). It may be postulated, therefore, that if underfire air rates below 86 lb $hr^{-1}ft^{-2}$ had been employed the ignition rate would have been observed to reach a maximum and then to decrease as the underfire air was further decreased. The ignition behavior observed in Run 11 is anomalous and no satisfactory explanation can be offered. More experiments are required to extend the range of underfire air rates and to duplicate the results presented here before a more quantitative picture of the ignition behavior can be drawn.

Camparison of the ignition rates obtained in Runs 11, 14 and 15 indicates that fuel composition changes had very little effect on the ignition rates. Within the limits of experimental error in determining the ignition rates, the rates were the same for the base case composition (15% inert, 25% moisture and 60% combustible) and for the cases where the inert and moisture content were both 15%, and where no inert was present and the moisture content was 25%. This is a somewhat surprising result, as decreasing both the inert and moisture fraction of the fuel would be expected to enhance ignition propagation. Further experiments are needed covering a wider range of inert (0-30%) and moisture 0-40%) contents before trends can be determined.

It is thought that the maximum underfire flow rate at which ignition will still be sustained for the type of fuel used in this study is in the vicinity of 275 lb $hr^{-1}ft^{-2}$. In Run 10 the underfire air rate was increased over a period of around 2 min to the 275 lb $hr^{-1}ft^{-2}$ level only after the bed had ignited and started to burn vigorously. About 10 min after the air rate had reached 275 lb $hr^{-1}ft^{-2}$ the bed appeared to have been almost totally quenched. The underfire air rate was then reduced to 175 lb $hr^{-1}ft^{-2}$ and visual observation of the fuel bed indicated that, within the space of a few minutes, the ignition and burning processes had started again. This behavior was borne out by the fuel bed temperature profiles, the first thermocouple (5 in. from the top of the bed) not reaching the ignition temperature until after 900 sec into the run; typically the time for the ignition plane to reach this level was around 300-400 sec. Similar experiences with early quenching were obtained from Run 9, where the underfire air rate was also increased to 275 lb $hr^{-1}ft^{-2}$ over the first few minutes of the run.

Burning Rates

Plots of weight loss of the fuel as a function of elapsed time for Runs 10, 17 and 18 are shown in Figures 58, 59 and 60. These plots were obtained using the load cell weighing

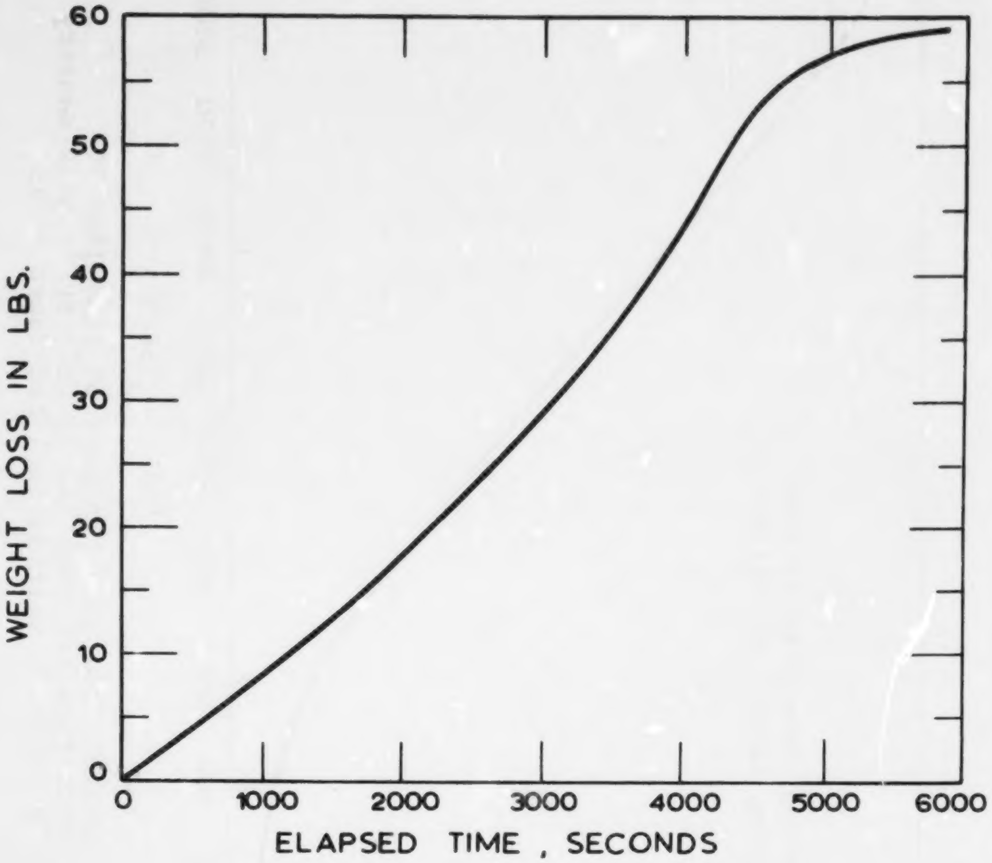

Fig. 58. Weight Loss as a Function of time (Run 10) Underfire air rate 175 lb hr^{-1} ft^{-2} and bulk density of the fuel 16.7 lb ft^{-3}; initial fuel bed depth 30 in.

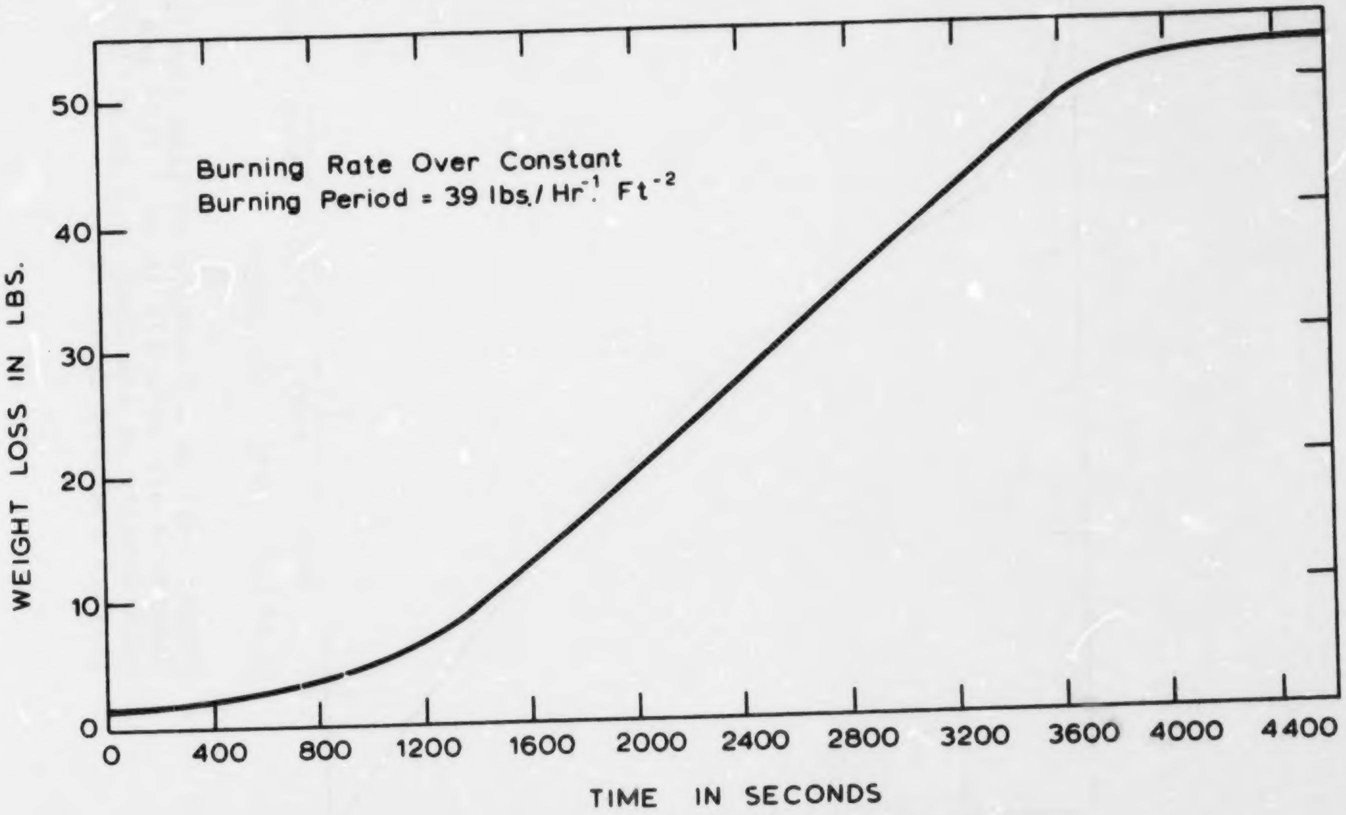

Fig. 59. Weight Loss as a Function of Time (Run 17)
Underfire air rate 140 lb hr^{-1} ft^{-1}; bulk density of fuel 15 lb ft^{-3}; initial fuel bed depth 30 in.

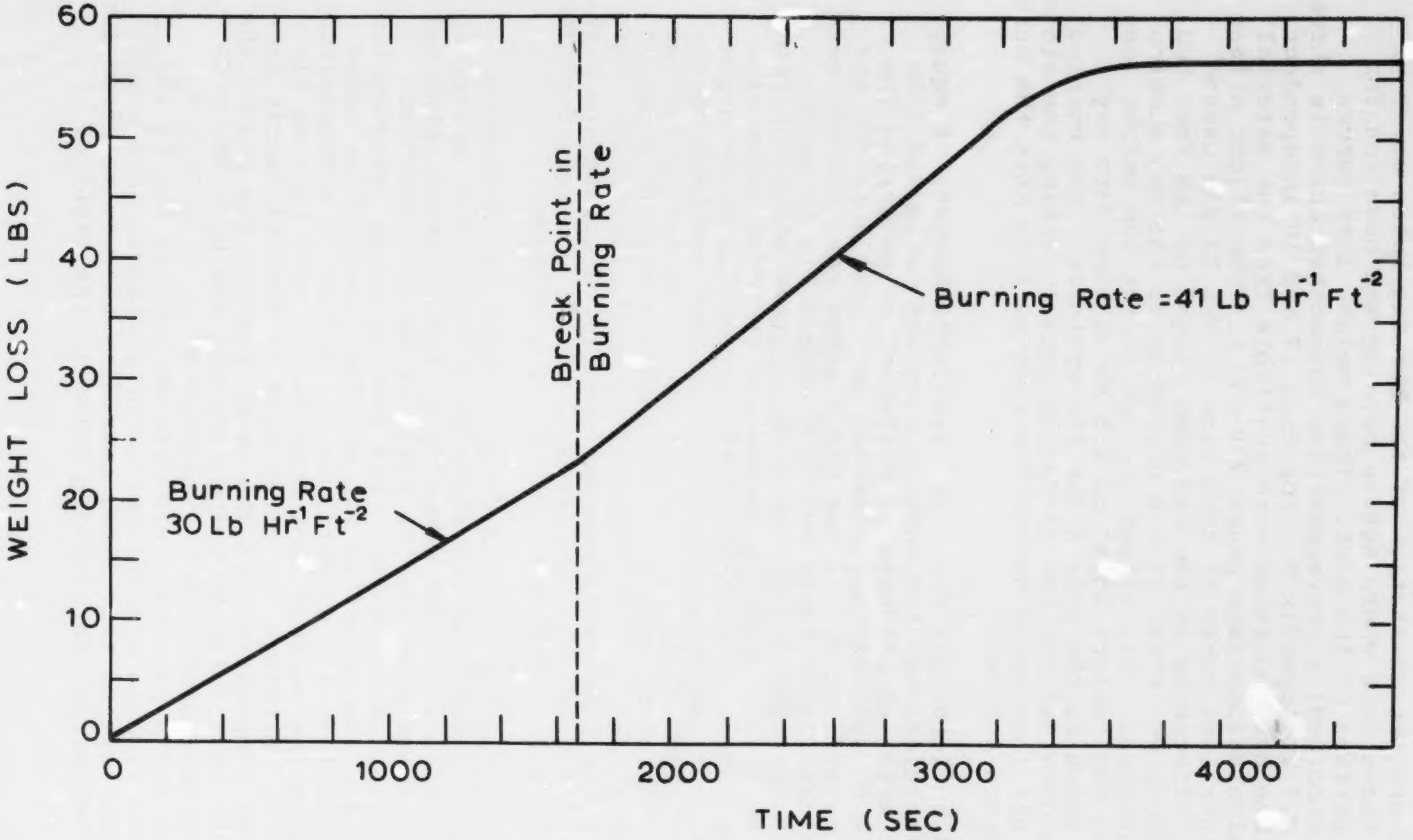

Fig. 60. Weight Loss as a Function of Time (Run 18)
Underfire Air Rate 86 lb hr^{-1} ft^{-2}, bulk density of fuel 16 lb ft^{-3}, initial bed depth 30 in.

system and are representative of the burning rate curves found for those runs where active burning was observed for the major portion of the test. These weight loss curves have been smoothed; a representative unsmoothed curve is shown in Figure H.7 in Appendix H. For Runs 17 and 18 independent checks on the burning rates were available from the material balance calculations (see pages 230-237). The slight offset in the weight loss curve at zero time in Run 17 was caused by slight differences in the recorded weight of the fuel bed section before and after it was butted up to the top section of the apparatus. This offset did not affect the weight loss results and the "weight loss" of 1.5 lb at time zero may simply be taken as the origin for the ordinate. The burning rates were obtained for the different runs by taking the slopes of the weight loss curve during the time periods that the burning rates were constant.

For Run 14 no load cell data were available because of equipment difficulties, but the burning rate was estimated from closure of material balances at different times during the run. Since no accurate measurements were available for the stack gas water content and the air leakage rate was not measured, the material balance was forced to close by selecting air leakage rates and stack gas moisture content correction factors that closed the carbon and hydrogen balances. The burning rates for Runs 15 and 16 were estimated by assuming that almost complete combustion had been achieved by the time the ignition front had reached the grate and by further assuming that the burning rate was constant over this period of time. This estimate is expected to be a little low. For comparison, the same technique was used to calculate the burning rate for Run 14; the result, 43 lb $hr^{-1} ft^{-2}$, agreed closely with that calculated from the material balances.

The burning rates for all the runs in which representative values could be obtained are shown as a function of underfire air rate in Figure 61; for comparison, the ignition rates calculated for these runs (on the basis of lb of combustible $hr^{-1} ft^{-2}$) are also indicated. For burning rates lying on the solid line AB, the underfire air and fuel consumption rates were in stoichiometric proportions for a fuel of a composition approximating the average fuel composition used in Runs 11-13 and 16-18. Although the rates were in stoichiometric proportions the compositions of the gases leaving the top of the bed were not restricted to being only CO_2 and H_2O; the offgases could have contained any mixture of O_2, CO, CO_2, H_2, H_2O, N_2 and trace pyrolysis products as long as the O_2 and combustibles were in stoichiometric proportions. For burning rates to the left of this line, secondary air was required for complete combustion; for burning rates to the right of

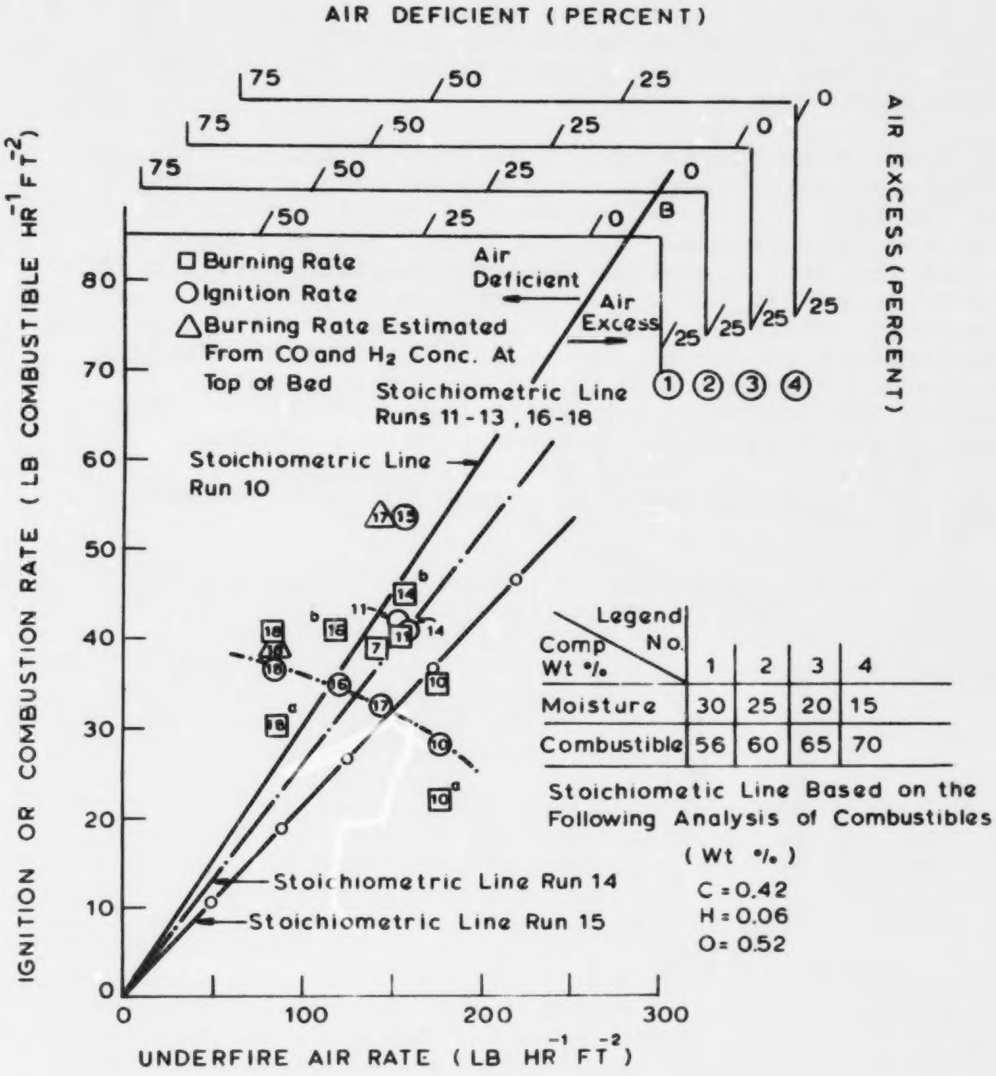

Fig. 61. Ignition and Burning Rates as a Function of Underfire Air Rate

the line, excess oxygen passed through the bed and secondary air was not strictly required if adequate mixing was achieved above the bed. The scales on the top and sides of Figure 61 permit the secondary air requirements at any burning rate to be obtained.

For all runs, with the exception of Runs 18 and 15, the observed burning rates suggest that oxygen passed completely through the bed. For example, at 2200 sec in Run 10 the burning rate was approximately 22 lb $hr^{-1}ft^{-2}$ while Figure 61 shows that the stoichiometric fuel consumption rate for this fuel is 57 lb $hr^{-1}ft^{-2}$ for the underfire air flow rate used in this test. There are three possible reasons for the apparent breakthrough of oxygen in the bed: (a) the underfire air channeled through the fuel bed at the side walls; (b) the burning bed depth was not sufficient for all the underfire air to react with the char and pyrolysis products; and (c) the underfire air channeled through the bed and in addition the bed depth was not deep enough for complete oxygen consumption.

The cause(s) could have been determined by comparing the carbon burning rate obtained from CO_2 and CO measurements at the center and top of the bed with the rate calculated from similar measurements in the stack gases; the carbon burning rate determined from the stack gas measurement would have been an average for the whole bed, while that determined from the top of the bed would have been indicative of the carbon burning rate in the core of the bed. These detailed comparisons were only possible in a few tests where extensive knowledge of the air leakage into the overfire region was available. For Run 10 a check on the carbon burning rate calculated from samples taken at the top of the bed and in the stack indicated that some channeling of the underfire air occurred, since the carbon burning rate derived from the fuel bed measurements was about 30% higher than that calculated from the stack gas concentration of CO_2. This result was previously reported by Rogers, Sarofim and Howard (140). However, in this calculation, the air leakage rate was not taken into account, and on the basis of later results it appears that the descrepancy was even higher ($\simeq$ 50-60%). This finding strongly indicates that serious channeling of the underfire air took place. The fuel bed gas samples for Run 10 (although taken at rather infrequent intervals) tend to support this conclusion, as the oxygen concentration observed near the center of the bed lay in the range 0.5 - 1.5% from 2400 to 3400 sec, at which time the burning rate was between 22 and 34 lb $hr^{-1}ft^{-2}$. Similar results were obtained for Run 17, the carbon burning rate estimated from the stack gas compositions being about 30% higher than that obtained from the fuel bed CO_2 and CO concentrations

This finding was confirmed by an estimation of the burning rate from the air deficiency calculated from the measured H_2 and CO concentrations within the fuel bed; this point is shown as a triangle in Figure 61.

For Run 18, the carbon burning rates calculated from fuel bed and stack gas measurements gave a different picture. From the material balance and the stack gas CO_2 content, an average carbon burning rate (from 2400 - 3200 sec) of 1.4 lb moles $hr^{-1}ft^{-2}$ was calculated, while the carbon burning rate estimated from the fuel bed gas composition was about 1.45 lb moles $hr^{-1}ft^{-2}$. In this run, therefore, channeling did not appear to be a problem. Further confirmation that no channeling occurred came from an estimation of the burning rate by calculating the air deficiency from the fuel bed gas compositions. The point shown as the triangle in Figure 61 was calculated from the gas compositions obtained from the topmost fuel bed probe at 2800 sec, at which time it was estimated that the probe was close to the top of the bed. The result agreed closely with the burning rate obtained from the load cell, which is an average rate for the whole bed. Nicholl's data (24) indicated that in his experiments channeling became more serious as the underfire air rate was increased. The results of this study indicated at similar trend.

For all runs the early burning rates increased as the run progressed. The shape of weight loss/time plots took on two basic forms as shown by Run 17, Figure 59 and Runs 10 and 18, Figures 58 and 60. For Run 17, the burning rate slowly increased with time until a constant rate was attained which was then maintained up to about the time the ignition front reached the grate. Similar behavior was seen in Runs 1 and 2. For Run 18 the burning rate started at a constant level and about halfway through the run suddenly increased to another constant level. This sudden break in the burning rate was confirmed by the material balance calculations. Similar trends were noticed in Run 10, but the burning rate appeared not to make such an abrupt change.

For Runs 10, 14, and 15-18, the data showed that, during the early stages of these runs, the burning rates were less than the ignition rate of the combustible content of the fuel, while during the later stages the burning rates were greater than the ignition rates. These findings were in marked contrast to Nicholls' (24) results, where equilibrium burning (equal ignition and burning rates) was observed at high underfire rates over the major portion of an underfeed burning test. Nicholls did not report any data on the developing thickness of the burning zone as burning rates were only measured (from stack gas compositions) after equilibrium burning was established. The results presented here, by contrast, were taken during the period when the depth of the active fuel bed was developing. It is obvious that a situation where the ignition rate is lower than the combustion rate is unstable since under these conditions, the active bed thickness will decrease until the burning and ignition rates equilibrate.

Before discussing these trends it will be worthwhile to indicate exactly what constituted the measured burning rate. The burning rate was made up of contributions from the drying and pyrolysis (or carbonization) of the combustible, char oxidation ($C + 1/2O_2 \rightarrow CO$ and $C + O_2 \rightarrow CO_2$) and char gasification ($C + H_2O \rightarrow H_2 + CO$ and $C + CO_2 \rightarrow 2\ CO$) throughout a depth slightly greater than the ignited zone (because some drying and to a lesser extent pyrolysis takes place ahead of the ignition front). Vaporization of metal coating and oxidation of steel are small enough to be neglected.

The observed increase in the burning rate as the runs progressed was in accord with the development of a burning depth. As the distance between the ignition front and the top of the bed increased, more time was available for the various gas phase and gas-solid reactions to occur. In addition, more depth was provided in which drying and pyrolysis could take place. (As indicated above, the observed burning rate was the sum of the weight losses associated with drying, pyrolysis and solid char consumption.)

As the burning zone developed, an increasing amount of the oxygen in the underfire air was consumed and in most experiments the burning zone eventually increased to the extent that all the oxygen was consumed. The depth required depended on the rate of mass transfer of the oxygen to the char surface and the rate of reaction of the oxygen with pyrolysis products. The oxygen consumption depth may be theoretically calculated from the correlation presented on pages 61 - 75, Figure 19, although the calculation must only be considered approximate. For this study the Reynolds numbers D_pG/u used lay in the range 80-200 and from Figure 19 the "effective" j_D factor was therefore about 0.15-0.20. On the assumption that the effective mass transfer area was 30 $hr^{-2}ft^{-3}$, the oxygen consumption distance (z_o), where the oxygen concentration fell to 0.1%, was of the order of 0.5 ft. This value of z_o is of the same order of magnitude as that observed experimentally - see pages 75 - 82 . As the depth of the burning zone increased, and more oxygen was consumed, the burning rate would be expected to increase partly as a result of increased char oxidation and partly as a consequence of the greater heat release within the bed. (From the analysis on pages   increasing the underfire air rate increases z_o ($z_o\ G^{0.41}$) and therefore low underfire air rates are preferable while the burning depth develops.)

Once enough depth had become available for all the oxygen to be consumed, further increases in depth provided a region in which the gasification reactions could proceed. The degree to which the gasification reactions occurred depended on there being adequate carbon left for reaction and high enough temperatures in the fuel bed (ca. 2000°F) for the reactions to have proceeded at reasonable rates. Burning rates in this regime would, on the basis of the theory of Niessen et al. (19), and on the assumption of no ignition rate limitations, be expected to increase proportionately with increases in the underfire air rate and would increase with decreasing heat losses from the bed (e.g., side wall losses or radiant heat losses from the top of the bed). The burning rate will obviously be dependant on the amount of channeling that takes place, but an effective burning rate could be calculated on the hypothesis that there are regions of the bed that act as gasifyers and regions where bypass of the underfire air occurs. For the fuel particles used in this study, where there was a major resistance to heat transfer within the elements, the weight loss that was associated with the drying and pyrolysis of each of the combustible fuel elements would have depended on the size and moisture content of the element and the length of time it had been in the ignited zone.

Towards the end of a run, after the ignition front had reached the grate the thickness of the burning zone started to decrease. Eventually the burning zone became thin enough for oxygen to break through the bed; the depth at which this occurred can be estimated using the methods outlined above for calculating z_o, but the effective mass transfer coefficient would be expected to be rather less in this case because of the lower probability of any reaction between oxygen and pyrolysis products. The rate of oxygen breakthrough and the burning rates at this stage in the combustion process may be estimated as follows. Assume that the oxygen concentration at the top fo the bed can be given by

$$P^T_{O_2}(t) = 0.21 \exp\left[\frac{-k_m}{\dot{G}} z^T(t)\right] \qquad (171)$$

where $P^T_{O_2}(t)$ is the mole fraction of oxygen at the top of the bed; k_m the effective mass transfer coefficient, lb hr^{-1}ft^{-3}; $\dot{G}$ the underfire air flow rate, lb hr^{-1}ft^{-2}; and $z^T(t)$ the height of the bed at any time t, ft. The burning rate, assuming a fuel comprising only carbon and inerts and that the reaction

$C + O_2 \rightarrow CO_2$ predominates, is then given by

$$\text{Burning Rate} = \frac{12}{29}\,\dot{G}\left[0.21 - P^T_{O_2}(t)\right] \tag{172}$$

The rate of recession of the top of the bed can be approximately expressed as,

$$-\Delta\rho\,\frac{dz^T}{dt} = \frac{12}{29}\,\dot{G}\left[0.21 - P^T_{O_2}(t)\right] \tag{173}$$

where $\Delta\rho$ is the density difference between the carbon and inert fuel and the inert alone. Substituting equation (172) into equation (173), integrating and substituting the resulting equation for z^T as a function of time back into equation (171) gives, with some approximation in the final answer, which becomes more correct as complete burn-out is achieved,

$$P^T_{O_2}(t) = 0.21\,\exp\left[\frac{-k_m}{2G}\left\{z^T_O + \frac{\dot{G}}{k_m}\left[1 + \log_e\left(1 - \exp\left\{\frac{-k_m z^T_O}{G}\right\}\right)\right] - \frac{0.0869Gt}{\Delta\rho}\right\}\right] \tag{174}$$

where z^T_O is the height of the bed when oxygen just starts to break through; since the oxygen concentration never reaches zero using the representation of equation (171), z^T_O is taken as when the oxygen concentration reaches an arbitrarily small number. From equation (174) the time required for the oxygen concentration to reach 21% after incipient breakthrough (t_F) is given by

$$t_F \simeq \frac{\Delta\rho}{0.0869G}\left[z^T_O + \frac{\dot{G}}{k_m}\right] \tag{175}$$

For typical values of $\Delta\rho \simeq 3$ lb ft^{-3} , $z^T_O \simeq 0.7$ ft , G $\simeq 100$ lb hr^{-1}ft^{-2} and $k_m \simeq 560$ lb hr^{-1}ft^{-3} , t_F is approximately of the order of the times experimentally observed for the burning rates to decrease to zero from their "steady state" values prior to oxygen breakthrough (Figures 58 - 60) and for the times it took the fuel bed oxygen concentrations to increase from 0% to 21% at the end of a test -- see pages 237-253 ; from the assumptions involved in this simplistic theory, the estimate of t_F would be expected to be too high.

(The above analysis indicates that underfire air rates should be decreased once the bed thickness has decreased to the point tht oxygen breakthrough occurs, for the following reasons: firstly decreasing the underfire air will decrease the excess air above the bed and secondly will help keep bed temperatures high and will, therefore, prevent premature quenching of the bed.)

The rate at which the active fuel bed depth (defined as the distance from the ignition front to the plane of zero combustible) increased was not strictly proportional to the difference between the ignition and burning rates as the measured weight loss (somewhat loosely called the burning rate here) included, as mentioned above, weight loss that did not affect the depth of the active bed (i.e., drying and pyrolysis). A distinction must be drawn here between the active fuel bed depth as defined above and the distance from the ignition front to the top of the bed. This latter distance will, under certain circumstances, be rather greater than the former because of the accumulation of inert material as the bed burns. Inert accumulation will depend on the relative rates of ignition and burning and has already been qualitatively discussed in regard to the work of Marskell and Miller (94) and on pages 192-198 . The inert content at the top of the bed insulated the burning zone from the radiant heat flux from the overfire flame and the hot refractory brickwork of the top section and helped occlude the oxygen present in the overfire section from the combustible in the bed. Presumably gas phase reactions took place in the void spaces in this "dead zone" of the bed; for instance, the oxygen in the underfire air could have reacted with CO, H_2, and pyrolysis products in this region of the bed.

No experimental determinations were made of the depth of either the active fuel bed or the accumulated inert. However, an approximate calculation was used to provide an estimate of the depth of the active burning zone and the rate of accumulation of inert above this zone; these calculations will be discussed below. The depth of the active fuel bed can only be calculated reasonable accurately if it is assumed that no volume change of the fuel particles takes place during the time required to completely dry and pyrolyze them; and if it is possible to estimate from the fuel bed gas composition what fraction of their carbon content can be attributed to char combustion. For a fuel, such as that used in this study with a large volatile content ($\simeq$ 75%) in comparison to fixed char content ($\simeq$ 25%), this latter estimation is particularly difficult. Faced with these difficulties more approximate methods were employed.

Figures 62 and 63 show the calculated depth of the active

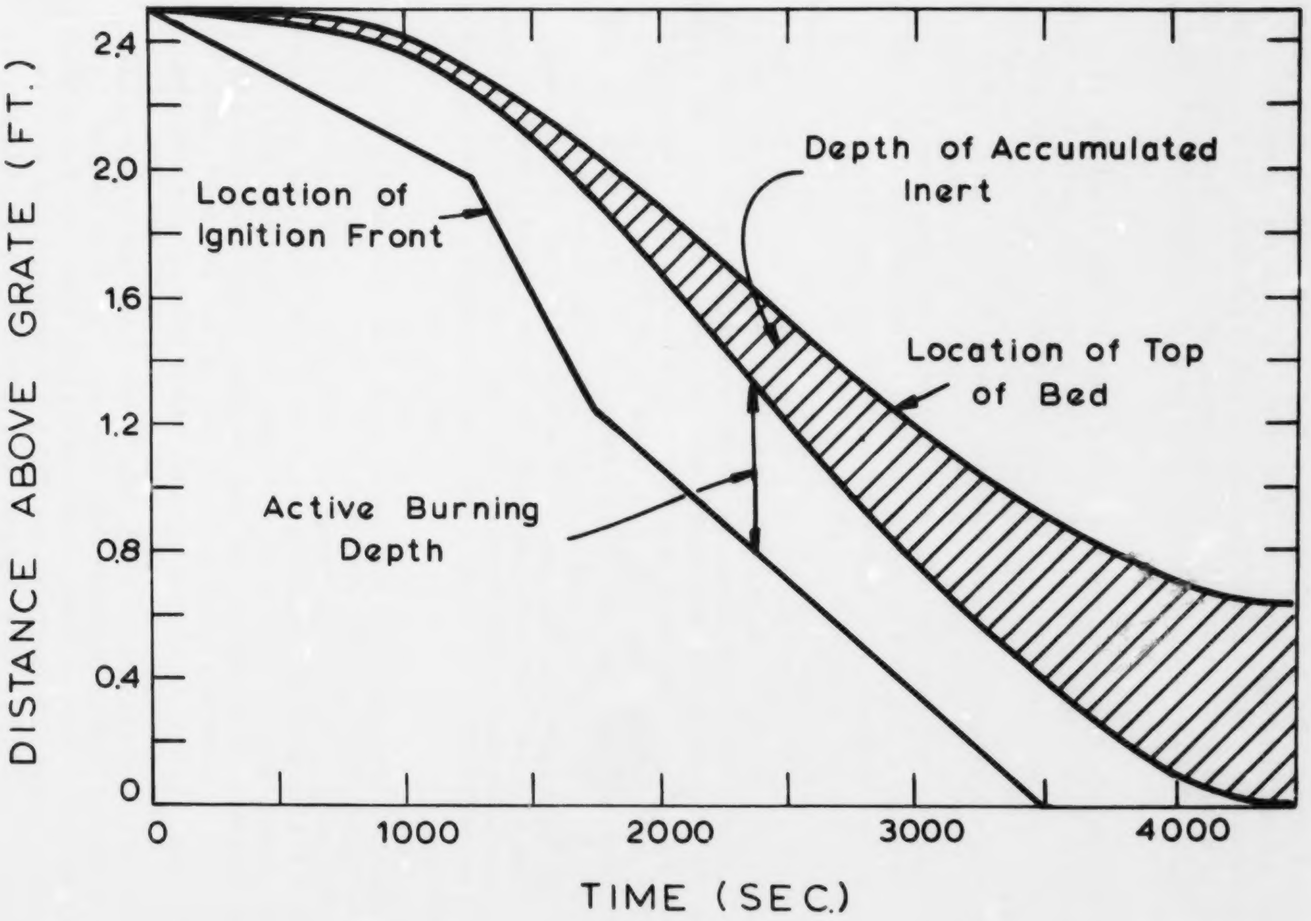

Fig. 62. Estimate of Fuel Bed Thickness and Accumulated Inert Layer (Run 17)

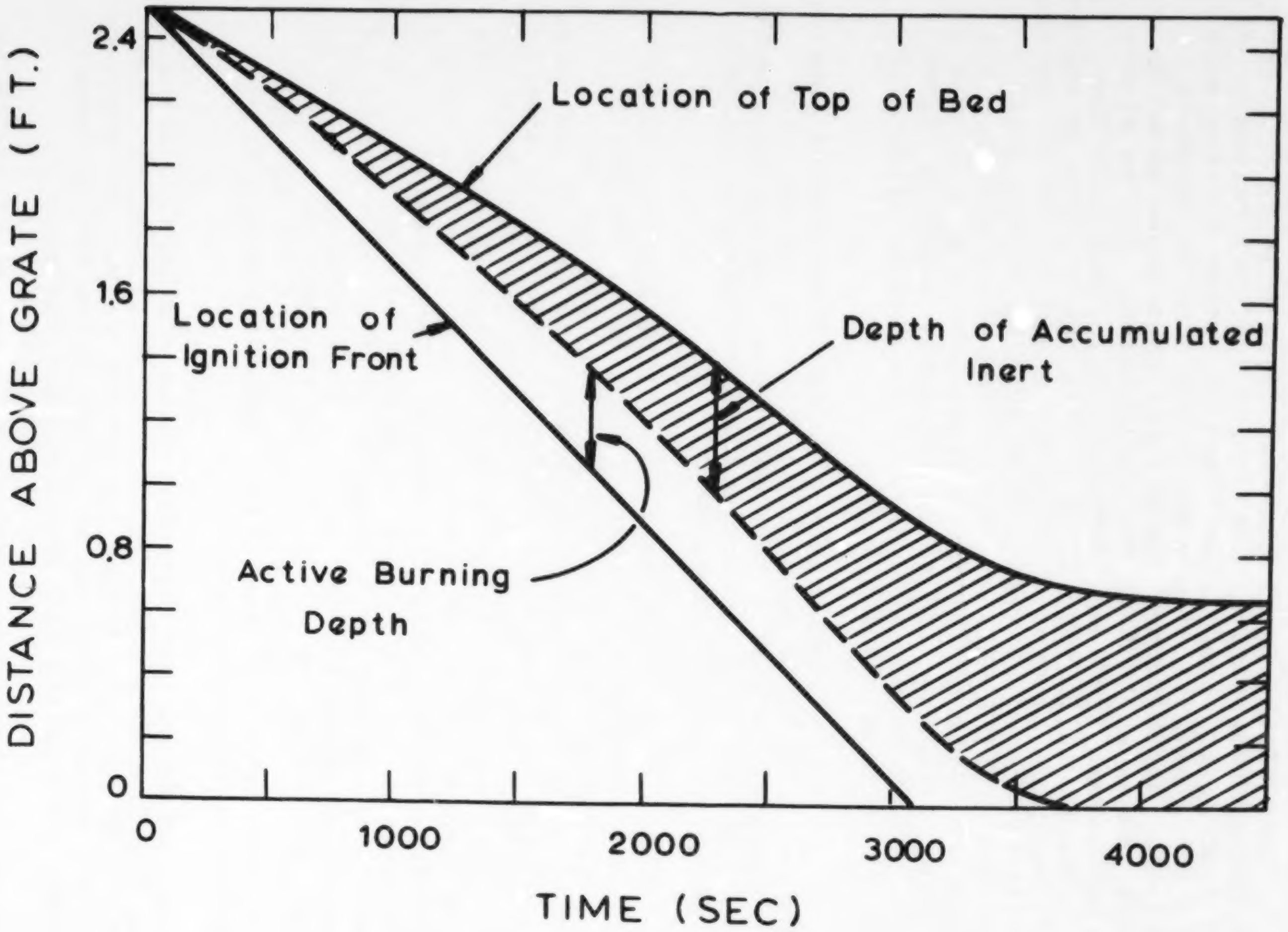

Fig. 63. Estimate of Fuel Bed Thickness and Accumulated Inert Layer (Run 18)

burning zone and the depth of accumulated inert over the course of Runs 17 and 18, respectively. For these calculations it was assumed that the fuel maintained its original density (ρ_o) until it was completely consumed, at which time its density dropped to that of the inert material ($\rho_I \approx 9$ lb ft^{-3}). For the case where the density of the active fuel bed varies linearly from ρ_o to ρ_I over the depth of active burning zone and where the inert fraction within this zone is constant, active burning depths about 30% greater than those shown in Figures 62 and 63 would have been calculated. For an alternative case, where the inert fraction (X_1) changes as the density changes, if it were assumed that the desnity of the non-inerts (i.e., wood blocks) remains unchanged during the course of combustion, the calculated active burning depths would have been about twice those shown in Figures 62 and 63. For this case the depth of the inert layer (where $x_I = 1$) would be much less than those indicated for early times in Figure 62 and 63. These models are expected to provide reasonable bounds on the active burning depth.

Figures 62 and 63 indicate how the depth of the active burning layer changed with variations in the burning and ignition rates. Figure 62 indicates that because of the varying ignition rate, the depth of the active fuel bed changed markedly during the course of the experiment.

For Run 18, Figure 63 shows that the active fuel bed depth changed gradually over the course of the test; the depth reached a maximum at the time the burning rate increased. In addition, a comparison between Figures 62 and 63 indicates that the active fuel bed depth in Run 17 was greater than that for Run 18. This result coupled with the fact that the underfire air rate used in Run 17 was greater than that used in Run 18 suggests that the burning rate for Run 17 should have been greater than that for Run 18. The observed average burning rate for Run 17 (39 lb combustible hr^{-1}ft^{-2}) was actually lower than that observed in the later stages of Run 18 (41 lb combustible hr^{-1}ft^{-2}). This apparent anomaly was caused by channeling in Run 17 and the burning rates based on the gas measurements at the centerof the bed for this test were rather higher (53 lb combustible hr^{-1}ft^{-2}) than the average burning rate.

Figures 64 and 65 present ignition rates and burning rates obtained from both the load cell and material balances (see pages 192-198) for Runs 17 and 18 respectively. The varying depth of the burning zone can be deduced from the different areas under the burning and ignition rate curves.

The increase in the burning rate in Runs 10 and 18 cannot be

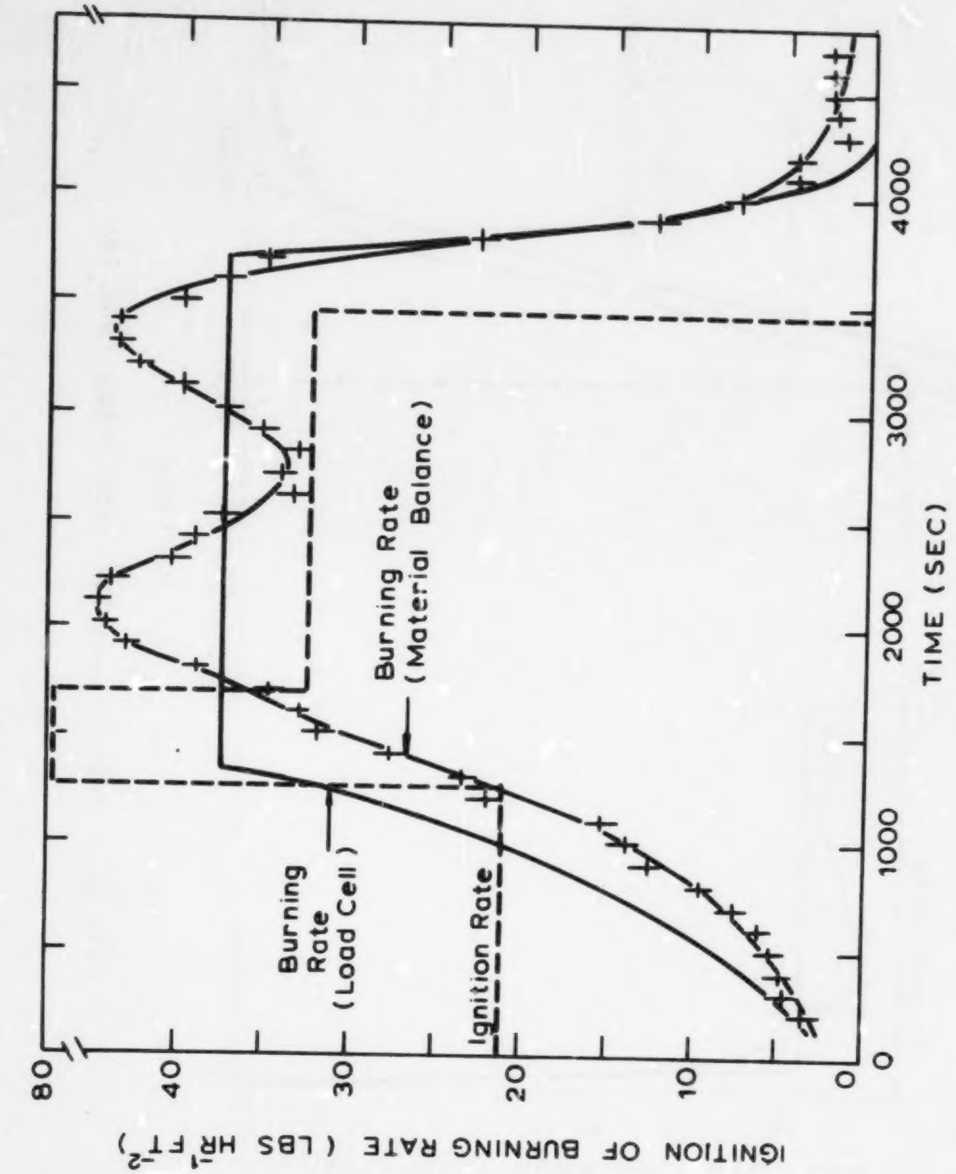

Fig. 64. Burning and Ignition Rates (Run 17)

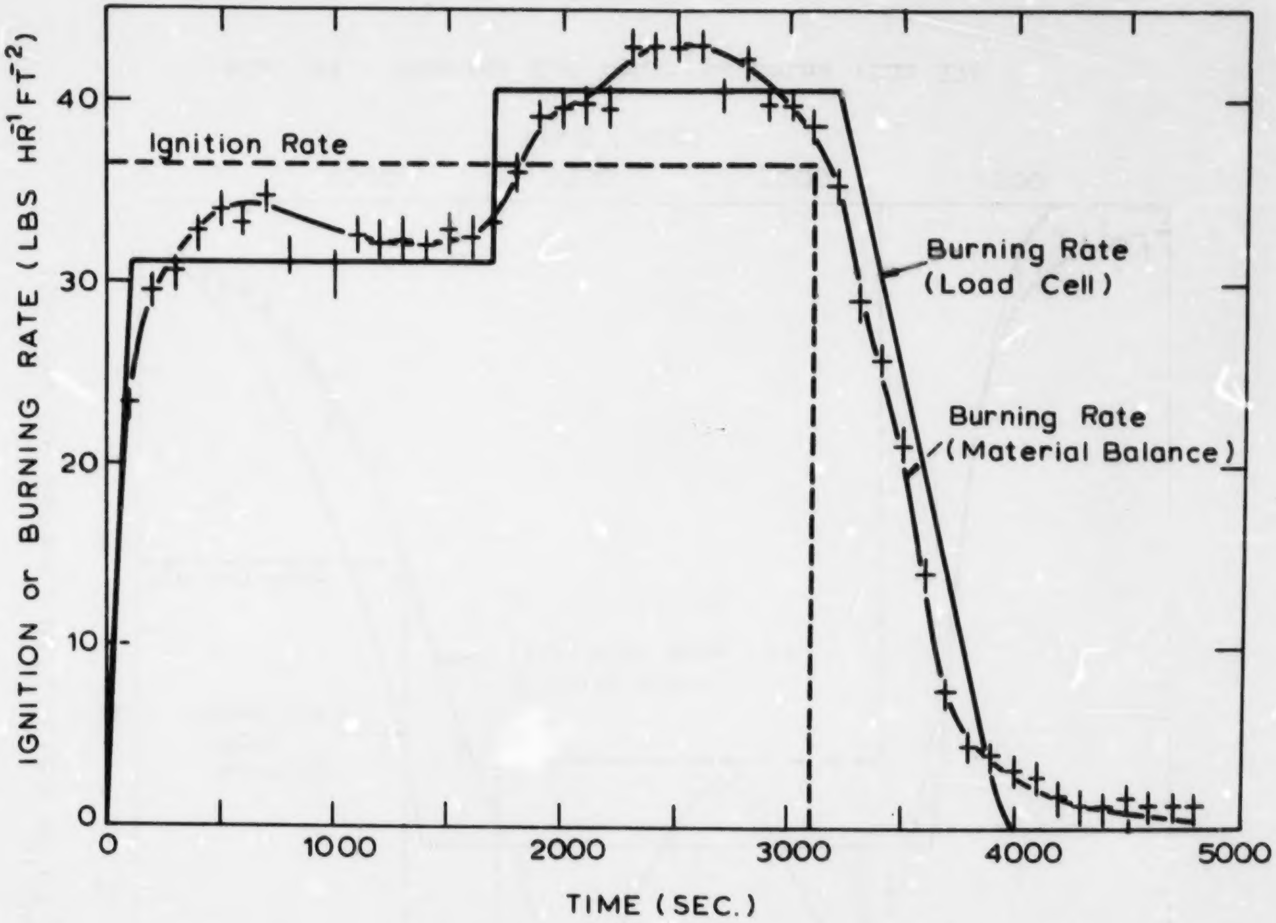

Fig. 65. Burning and Ignition Rates (Run 18)

explained strictly by the increase in fuel bed temperature observed towards the end of each run, as originally proposed by Rogers, Sarofim and Howard (140), since the increase in temperature always followed the increase in burning rate. No satisfactory explanation can be offered at this time to explain these results. It is likely that the degree of channeling changes as the bed burns and will give rise to different burning rates. Local changes in the way the fuel and inert were charged to the bed may also have affected the degree of channeling. This effect was probably aggravated by the larger size of the inert with respect to the fuel but could not be readily altered as the tin cans used were the closest to the fuel in size that were easily obtainable in bulk quantities. However, these effects would need to be very non-linear to explain the magnitude of the changes in burning rate observed. Although they probably did affect the burning rate to a certain extent it is very unlikely that they were the main cause of the observed increase. It is also possible that the burning rates changed because of changes in the rate of heat loss from the bed (e.g., by accumulation of inert on top of the bed) but this cannot be experimentally proven.

Material Balances

Complete material balances for Runs 17 and 18 are given in Tables 13 and 14. The symbols used in Tables 13 and 14 have the following meanings: F = total fuel burning rate, lb hr^{-1}; FC = carbon burning rate, lb hr^{-1}; FH = hydrogen burning rate, lb hr^{-1}; FO = oxygen burning rate, lb hr^{-1}; ALPHA = lb carbon/lb oxygen burnt; BETA = lb hydrogen/lb oxygen burnt; GAMMA = lb carbon/lb hydrogen burnt; G = stack gas flow rate, lb moles hr^{-1}; LEAK = air leakage rate, lb moles hr^{-1}; SUM = sum of CO_2 and H_2O concentrations within the stack gases, mole fraction; C = cumulative carbon loss, lb; O = cumulative oxygen loss, lb; H = cumulative hydrogen loss, lb; TLOSS = total cumulative loss, lb.

Tables 13 and 14 show good agreement on the overall material balance as indicated by the calculated carbon, hydrogen, and oxygen loss compared to the know weights of these materials in the fuel. The largest discrepancy is shown in the carbon balance for Run 17, and can be explained by either loss of carbon as particulates in the stack gases or by incomplete combustion. The former is very unlikely considering previous

Table 13. Material Balance Calculations (Run 17)

BURNING RATES AND INTEGRATED WEIGHT LOSS FOR RUN 17

TOTAL FUEL CHARGED = 62.630 WT.FRACTION MOISTURE = 0.2537 WT.FRACTION INERT = 0.1516
AMBIENT CONDITIONS YO2A = 0.2076 YN2A = 0.7808 YH2OA = 0.0115
INTEGRATION STARTED 200.0 SECONDS INTO RUN

TIME	F	FC	FH	FO	ALPHA	BETA	GAMMA	G	LEAK	SUM	C	O	H	TLOSS
200.0	6.204	0.777	0.934	4.492	0.1731	0.2080	0.8320	28.9763	7.7824	0.206	0.021	0.124	0.025	0.172
300.0	7.383	0.995	1.005	5.362	0.1856	0.1875	0.9901	28.4851	7.2463	0.206	0.046	0.261	0.052	0.360
400.0	8.125	1.308	1.049	5.767	0.2269	0.1819	1.2473	28.1099	6.8475	0.206	0.078	0.416	0.081	0.575
500.0	9.083	1.294	1.152	6.636	0.1949	0.1756	1.1229	27.8519	6.5366	0.206	0.114	0.588	0.112	0.814
600.0	10.952	1.914	1.165	7.872	0.2631	0.1480	1.6421	27.4776	6.1204	0.207	0.158	0.790	0.144	1.093
700.0	12.294	2.845	1.267	8.180	0.3478	0.1569	2.2447	27.2911	5.8986	0.206	0.225	1.013	0.178	1.416
800.0	16.894	4.087	1.403	11.404	0.3584	0.1230	2.9131	27.2076	5.6806	0.208	0.321	1.285	0.215	1.821
900.0	21.311	4.982	1.559	14.769	0.3373	0.1055	3.1945	27.0316	5.3601	0.210	0.447	1.648	0.256	2.352
1000.0	22.882	5.237	1.822	15.822	0.3310	0.1151	2.8739	26.8861	5.1162	0.210	0.589	2.073	0.303	2.965
1100.0	26.104	6.105	2.198	17.799	0.3430	0.1235	2.7772	26.8365	4.9107	0.208	0.746	2.540	0.359	3.646
1200.0	33.693	8.188	2.695	22.809	0.3590	0.1181	3.0374	26.9151	4.7085	0.210	0.965	3.104	0.427	4.476
1300.0	39.146	11.946	3.108	24.094	0.4957	0.1290	3.8426	26.7284	4.3785	0.208	1.224	3.755	0.507	5.488
1400.0	46.426	15.170	3.557	27.698	0.5476	0.1284	4.2637	26.8961	7.1311	0.208	1.601	4.475	0.600	6.677
1500.0	52.896	18.075	3.953	30.868	0.5855	0.1280	4.5722	26.9574	7.0345	0.208	2.063	5.288	0.704	8.056
1600.0	55.273	19.285	4.194	31.793	0.6065	0.1319	4.5979	27.1109	7.0988	0.207	2.582	6.158	0.817	9.558
1700.0	58.811	21.093	4.498	33.219	0.6369	0.1354	4.6890	27.2961	7.1635	0.206	3.143	7.061	0.938	11.143
1800.0	65.110	23.382	4.723	37.005	0.6318	0.1276	4.9503	27.6337	7.3265	0.208	3.760	8.037	1.066	12.864
1900.0	71.698	25.375	5.008	41.313	0.6142	0.1212	5.0661	27.9717	7.4586	0.210	4.437	9.124	1.201	14.764
2000.0	74.023	26.560	5.250	42.215	0.6291	0.1263	5.0589	28.3623	7.7607	0.209	5.159	10.285	1.344	16.788
2100.0	75.022	27.315	5.277	42.429	0.6437	0.1263	5.1752	28.5126	7.8973	0.208	5.907	11.460	1.490	18.858
2200.0	73.043	27.798	5.240	40.003	0.6949	0.1310	5.3043	28.9530	8.4229	0.206	6.673	12.605	1.636	20.915
2300.0	67.384	26.632	4.987	35.794	0.7432	0.1393	5.3339	29.1943	8.8590	0.205	7.428	13.658	1.778	22.865
2400.0	65.151	25.258	4.902	34.990	0.7218	0.1400	5.1526	29.7525	9.4637	0.204	8.148	14.641	1.915	24.706
2500.0	62.813	23.187	4.877	34.748	0.6672	0.1403	4.7537	29.9727	9.6975	0.204	8.821	15.610	2.051	26.483
2600.0	56.087	21.260	4.706	30.020	0.7115	0.1567	4.5379	30.0602	9.9755	0.202	9.440	16.509	2.184	28.135
2700.0	57.201	20.543	4.681	31.976	0.6426	0.1463	4.3885	30.2762	10.1368	0.203	10.022	17.370	2.315	29.708
2800.0	55.890	18.592	4.754	32.555	0.5708	0.1460	3.9083	30.3532	10.1775	0.203	10.565	18.266	2.446	31.279
2900.0	59.305	16.653	4.976	37.675	0.4420	0.1320	3.3466	30.5687	10.1775	0.206	11.055	19.242	2.581	32.879
3000.0	62.142	17.745	5.224	39.675	0.4346	0.1316	3.3010	30.5716	10.0559	0.206	11.526	20.316	2.723	34.565
3100.0	67.317	19.535	5.419	42.362	0.4611	0.1279	3.6044	30.6241	9.9755	0.208	12.036	21.456	2.870	36.363
3200.0	70.779	21.636	5.568	43.575	0.4965	0.1277	3.8853	30.4213	9.6975	0.208	12.608	22.649	3.023	38.281
3300.0	71.493	22.753	5.521	43.218	0.5264	0.1277	4.1707	30.1645	9.4637	0.208	13.225	23.855	3.177	40.257
3400.0	71.274	23.530	5.408	42.338	0.5558	0.1277	4.3502	29.8788	9.2337	0.208	13.868	25.043	3.329	42.240
3500.0	66.852	22.957	5.217	38.677	0.5935	0.1349	4.3998	29.4907	9.0077	0.206	14.513	26.168	3.477	44.159
3600.0	63.184	22.075	4.902	36.206	0.6097	0.1394	4.5025	29.0391	8.7120	0.206	15.139	27.208	3.617	45.965
3700.0	59.839	20.379	4.246	35.213	0.5787	0.1205	4.7991	28.5548	8.4229	0.210	15.728	28.200	3.744	47.674
3800.0	38.459	16.734	2.958	20.766	0.7095	0.1424	4.9801	27.3592	8.0007	0.206	16.216	28.977	3.844	49.039
3900.0	20.773	10.948	1.409	8.414	1.3012	0.1675	7.7660	26.3460	7.7607	0.206	16.573	29.383	3.905	49.861
4000.0	13.297	7.506	1.068	4.723	1.5886	0.2261	7.0236	25.8432	7.4586	0.204	16.829	29.565	3.939	50.335
4100.0	7.467	5.031	0.687	1.749	2.8764	0.3921	7.3166	25.2953	7.0988	0.205	17.003	29.655	3.964	50.623
4200.0	7.337	3.226	0.428	3.682	0.8761	0.1163	7.5272	24.9414	6.7492	0.208	17.118	29.731	3.979	50.829
4300.0	2.882	2.169	0.320	0.395	5.5129	0.8152	6.7626	24.5327	6.4704	0.206	17.193	29.787	3.990	50.971
4400.0	3.213	2.007	0.318	0.887	2.2615	0.3587	6.3040	24.3351	6.2578	0.207	17.251	29.805	3.999	51.055
4500.0	4.191	2.009	0.319	1.862	1.0794	0.1716	6.2902	24.3658	6.2578	0.208	17.307	29.843	4.007	51.158
4600.0	4.437	1.724	0.270	2.441	0.7064	0.1109	6.3651	24.3718	6.2578	0.208	17.358	29.903	4.016	51.278
4700.0	4.150	1.497	0.270	2.441	0.5886	0.1109	5.3042	24.3718	6.2578	0.209	17.402	29.971	4.023	51.397

INTEGRATED CARBON LOSS = 17.402 LBS
INTEGRATED HYDROGEN LOSS = 4.023 LBS
INTEGRATED OXYGEN LOSS = 29.971 LBS

INTEGRATED WEIGHT LOSS = 51.397 LBS

THEORETICAL CARBON CHARGED = 19.104 LBS
THEORETICAL HYDROGEN CHARGED = 3.985 LBS
THEORETICAL OXYGEN CHARGED = 30.040 LBS

TOTAL COMBUSTIBLE CHARGED = 53.129 LBS

CALCULATED FUEL C/H RATIO = 4.325
CALCULATED FUEL H/O RATIO = 0.134
CALCULATED FUEL C/O RATIO = 0.580

ACTUAL FUEL C/H RATIO = 4.793
ACTUAL FUEL H/O RATIO = 0.132
ACTUAL FUEL C/O RATIO = 0.635

BURNING RATE OVER CONSTANT BURNING PERIOD (FROM 1300.0 TO 3700.0 SECONDS) = 62.847 LBS/HR

Table 14. Material Balance Calculations (Run 18)

```
                 BURNING RATES AND INTEGRATED WEIGHT LOSS FOR RUN   18

TOTAL FUEL CHARGED = 66.500     WT.FRACTION MOISTURE = 0.2506  WT.FRACTION INERT = 0.1503
AMBIENT CONDITIONS    YO2A = 0.2059  YN2A = 0.7747  YH2OA = 0.0194
INTEGRATION STARTED 100.0 SECONDS INTO RUN


TIME      F      FC      FH     FO    ALPHA    BETA    GAMMA     G      LEAK     SUM     C       D       H    TLOSS
 100.0 39.116 11.370  2.466 25.280  0.4497  0.0975  4.6108 29.6485 10.5434  0.213   0.157   0.351  0.034   0.543
 200.0 49.441 14.273  3.155 32.013  0.4458  0.0985  4.5237 30.4517 10.9639  0.215   0.514   1.146  0.112   1.773
 300.0 50.923 16.495  3.452 30.975  0.5325  0.1114  4.7781 30.9269 11.3972  0.211   0.941   2.021  0.204   3.167
 400.0 54.721 16.989  3.687 34.045  0.4990  0.1083  4.6075 31.3032 11.6189  0.212   1.406   2.924  0.303   4.634
 500.0 56.906 18.612  4.007 34.284  0.5428  0.1168  4.6442 31.8443 12.0724  0.210   1.900   3.873  0.410   6.184
 600.0 56.367 17.707  4.180 34.479  0.5135  0.1212  4.2361 32.1843 12.3631  0.210   2.405   4.828  0.523   7.758
 700.0 57.866 17.569  4.093 36.204  0.4852  0.1130  4.2922 32.5129 12.6596  0.212   2.895   5.810  0.638   9.346
 800.0 52.400 17.606  3.885 30.908  0.5696  0.1257  4.5314 32.4762 12.8403  0.209   3.383   6.742  0.749  10.876
 900.0 33.814 17.350  1.849 14.614  1.1872  0.1265  9.3810 31.6409 13.0232  0.208   3.869   7.374  0.829  12.073
1000.0 50.485 15.988  3.717 30.779  0.5194  0.1207  4.3006 32.7363 13.1464  0.210   4.332   8.005  0.906  13.244
1100.0 54.134 16.414  3.665 34.055  0.4819  0.1076  4.4791 32.8255 13.1464  0.212   4.782   8.905  1.009  14.697
1200.0 53.288 16.348  3.580 33.359  0.4900  0.1073  4.5663 32.6594 13.0232  0.212   5.237   9.842  1.109  16.189
1300.0 53.247 15.890  3.629 33.728  0.4711  0.1075  4.3795 32.5002 12.8403  0.213   5.685  10.773  1.209  17.669
1400.0 52.906 15.776  3.741 33.389  0.4724  0.1120  4.2167 32.3370 12.6596  0.212   6.125  11.706  1.312  19.143
1500.0 54.086 15.988  3.984 34.113  0.4686  0.1168  4.0125 32.1828 13.8120  0.210   6.566  12.643  1.419  20.629
1600.0 53.332 16.825  4.234 32.303  0.5208  0.1301  4.0021 31.8892 14.4501  0.208   7.022  13.566  1.533  22.121
1700.0 54.658 19.388  4.435 31.834  0.5776  0.1393  4.1460 31.7030 14.2207  0.206   7.511  14.456  1.653  23.621
1800.0 60.170 19.269  4.816 36.085  0.5339  0.1334  4.0305 31.6493 13.9389  0.207   8.034  15.400  1.781  25.216
1900.0 64.964 20.554  5.076 39.333  0.5225  0.1290  4.0491 31.6492 13.7723  0.207   8.587  16.467  1.919  26.954
2000.0 65.271 21.677  5.363 38.230  0.5676  0.1403  4.0415 31.4676 13.7932  0.204   9.173  17.525  2.064  28.763
2100.0 66.286 22.876  5.465 37.946  0.6028  0.1440  4.1854 31.3218 14.6110  0.203   9.792  18.583  2.214  30.590
2200.0 65.368 23.779  5.508 36.059  0.6594  0.1527  4.3169 31.2200 14.5574  0.201  10.440  19.610  2.366  32.418
2300.0 72.124 24.906  5.472 41.747  0.5965  0.1310  4.5509 31.3352 14.5039  0.207  11.116  20.691  2.519  34.327
2400.0 72.729 24.970  5.398 41.951  0.5930  0.1286  4.6099 31.2698 14.4507  0.207  11.808  21.854  2.670  36.332
2500.0 72.521 24.543  5.467 42.510  0.5773  0.1286  4.4985 31.3067 14.4507  0.208  12.494  23.027  2.821  38.343
2600.0 71.825 25.137  5.449 41.238  0.6095  0.1321  4.6127 31.2073 14.3976  0.207  13.184  24.190  2.972  40.347
2700.0 68.432 24.708  5.494 38.229  0.6463  0.1437  4.4970 31.1265 14.3976  0.203  13.876  25.294  3.124  42.295
2800.0 70.326 25.408  5.902 39.415  0.6446  0.1396  4.6174 31.1636 14.3976  0.204  14.573  26.372  3.277  44.223
2900.0 66.364 25.646  5.408 35.310  0.7263  0.1531  4.7417 31.0118 14.3976  0.202  15.282  27.410  3.429  46.121
3000.0 66.872 25.074  5.156 36.642  0.6842  0.1407  4.8632 30.9903 14.3976  0.205  15.986  28.409  3.576  47.972
3100.0 63.842 24.481  4.761 34.598  0.7075  0.1376  5.1417 30.8808 14.4507  0.206  16.674  29.399  3.713  49.787
3200.0 55.954 23.810  4.287 30.806  0.7729  0.1391  5.5538 30.6438 14.4507  0.206  17.345  30.307  3.839  51.492
3300.0 48.020 22.010  3.650 22.360  0.9843  0.1632  6.0293 30.1676 14.3976  0.203  17.981  31.045  3.949  52.977
3400.0 43.251 21.305  2.822 19.123  1.1140  0.1476  7.5476 29.7015 14.2396  0.206  18.583  31.622  4.039  54.245
3500.0 34.738 18.539  2.181 14.017  1.3225  0.1556  8.4986 29.2254 14.0834  0.206  19.136  32.082  4.109  55.328
3600.0 23.392 15.052  1.547  6.792  2.2162  0.2279  9.7241 28.5846 13.8268  0.203  19.603  32.371  4.160  56.135
3700.0 12.897 11.609  0.995  0.298 38.9133  3.3397 11.6516 27.8922 13.4753  0.201  19.973  32.469  4.196  56.639
3800.0  9.216  8.908  0.643 -1.335 -6.6722 -0.4819 13.8444 27.3621 13.0843  0.203  20.258  32.455  4.218  56.933
3900.0  7.269  7.219  0.361 -0.309-73.2855 -1.1666 19.9600 26.8502 12.6110  0.206  20.482  32.432  4.232  57.148
4000.0  5.840  4.638  0.250  0.950  4.8793  0.2635 18.5119 26.4067 12.1538  0.208  20.647  32.441  4.241  57.330
4100.0  4.908  3.629  0.140  1.139  3.1860  0.1236 25.7695 25.7689 11.5396  0.209  20.762  32.470  4.246  57.479
4200.0  3.196  2.387  0.087  0.722  3.3057  0.1206 27.4093 25.4042 11.2013  0.208  20.845  32.496  4.250  57.592
4300.0  2.112  1.756  0.036  0.321  5.4541  0.1077 50.6122 24.8877 10.7104  0.208  20.903  32.510  4.251  57.665
4400.0  3.075  1.724  0.035  1.316  1.3117  0.0269 48.7447 24.4467 10.2382  0.210  20.951  32.533  4.252  57.737
4500.0  2.798  1.412  0.034  1.310  1.0781  0.0266 40.5027 24.0291  9.8209  0.210  20.995  32.570  4.253  57.818
4600.0  2.714  1.376  0.034  1.303  1.0557  0.0261 40.3220 23.4113  9.2033  0.210  21.033  32.606  4.254  57.896
4700.0  2.692  1.358  0.033  1.300  1.0442  0.0259 40.2269 23.0970  8.8894  0.210  21.071  32.642  4.255  57.970

   INTEGRATED CARBON LOSS   = 21.071 LBS      THEORETICAL CARBON CHARGED   = 20.433 LBS
   INTEGRATED HYDROGEN LOSS =  4.255 LBS      THEORETICAL HYDROGEN CHARGED =  4.226 LBS
   INTEGRATED OXYGEN LOSS   = 32.642 LBS      THEORETICAL OXYGEN CHARGED   = 31.840 LBS

   INTEGRATED WEIGHT LOSS   = 57.970 LBS      TOTAL COMBUSTIBLE CHARGED    = 56.499 LBS

   CALCULATED FUEL C/H RATIO =  4.951         ACTUAL FUEL C/H RATIO =  4.835
   CALCULATED FUEL H/O RATIO =  0.130         ACTUAL FUEL H/O RATIO =  0.132
   CALCULATED FUEL C/O RATIO =  0.645         ACTUAL FUEL C/O RATIO =  0.641

   BURNING RATE OVER CONSTANT BURNING PERIOD (FROM  100.0 TO 1700.0 SECONDS) = 51.439 LBS/HR

   BURNING RATE OVER CONSTANT BURNING PERIOD (FROM 1700.0 TO 3200.0 SECONDS) = 66.749 LBS/HR
```

experience with the smoke meter (not used in this test) which showed only trace particulates in the stack gases. The latter explanation is more likely and is confirmed by the weight loss plot of Figure 59, which shows a final weight loss of close to 51 lb. The incomplete combustion can be explained by the fact that small pieces of wood tended to fall inside the tin cans, where they burnt slowly and were incompletely burnt by the end of the run when fuel bed temperatures fell low enough for the carbon-oxygen reaction to be quenched.

The accumulative carbon, hydrogen and oxygen losses and their sum, TLOSS, for Runs 17 and 18 are plotted in Figures 66 and 67. Comparing the values of TLOSS versus the load cell data of Figures 59 and 60 gives an independent check on the accuracy of the weight loss determination; the agreement between the material balance calculations and the load cell data was very close for both these experiments. For Run 17 the average burning rate over the constant burning period (1300 to 3700 sec) calculated from the material balance is 38 lb $hr^{-1}ft^{-2}$, which is within 3 percent of the load cell result of 39 lb $hr^{-1}ft^{-2}$. For Run 18 two constant burning rate periods were observed, one lasting from about 100 sec to 1700 sec into the run and the other from 1700 sec to 3200 sec. For the former constant burning period, the load cell data gave a burning rate of 30 lb $hr^{-1}ft^{-2}$ and the material balance 31 lb $hr^{-1}ft^{-2}$ while for the latter the load cell data gave a burning rate of 41 lb $hr^{-1}ft^{-2}$ and the material balance 40 lb hr ft .

The material balance calculations were sensitive to the O_2 and CO_2 stack concentrations because they involved the computation of differences between large numbers; this sensitivity was most marked near the beginning and end of a test. The anomalous behavior indicated in both Tables 13 and 14 near the end of Runs 17 and 18 can be attributed to inaccurate data on these concentrations. Small changes in the measuring instrument calibration could have accounted for these errors. A check on the O_2 and CO_2 compositions measured in the stack was given by the SUM column; for the complete combustion of cellulose to CO_2 and H_2O the mole fraction of these two components in the stack should have equaled the mole fraction of O_2 in the combustion air (0.21). For all the points taken for the material balance this was found; the worst point at 2200 sec in Run 18 being less than 5 percent in error. (Actually, the fuel used contained net hydrogen so that the value of SUM should have been slightly less than 0.21.)

Figure 68 shows the values of the ratio of hydrogen to oxygen (BETA) and the ratio of carbon to hydrogen (GAMMA) in

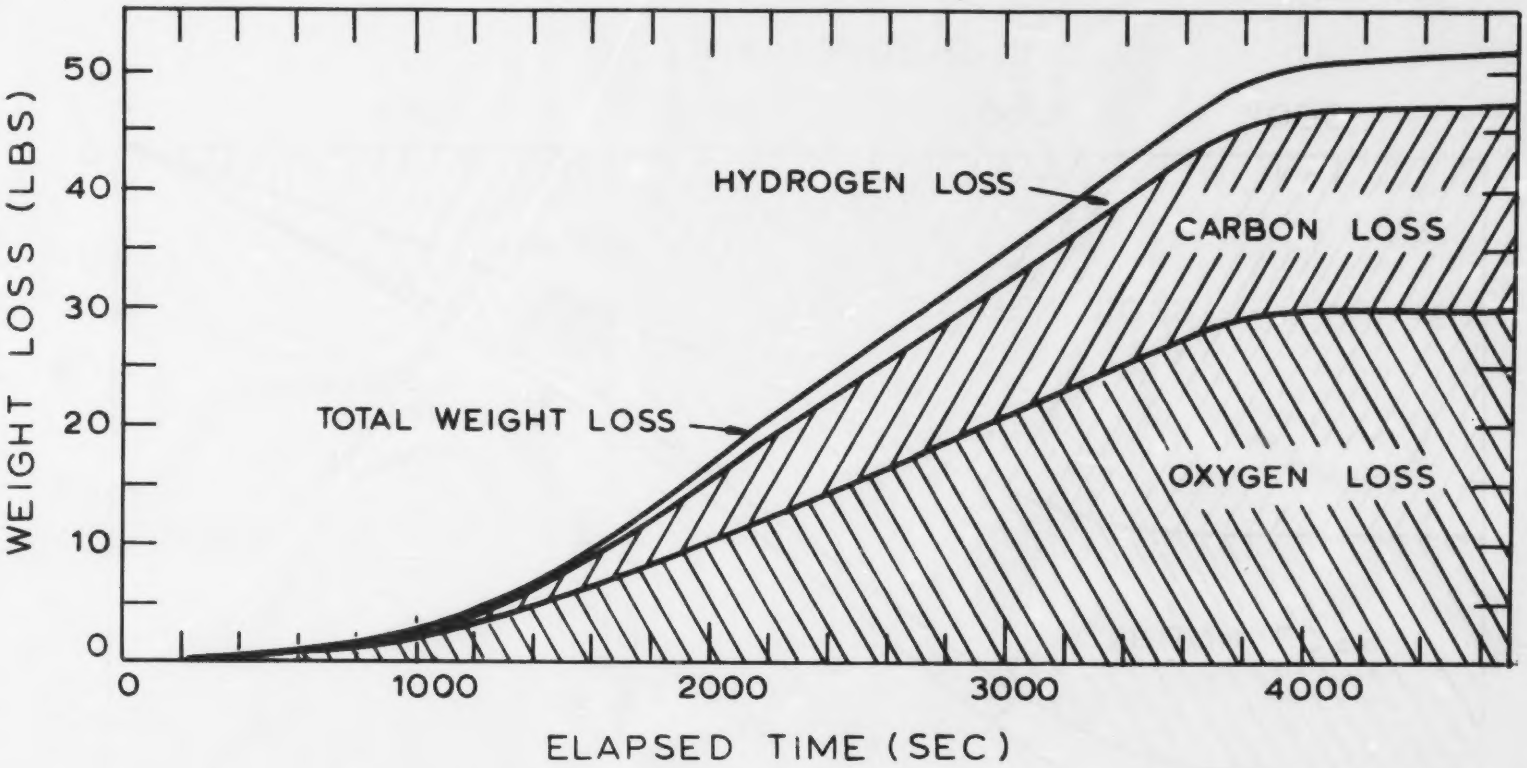

Fig. 66. Accumulated Carbon, Hydrogen and Oxygen Weight Loss of Fuel (Run 17)

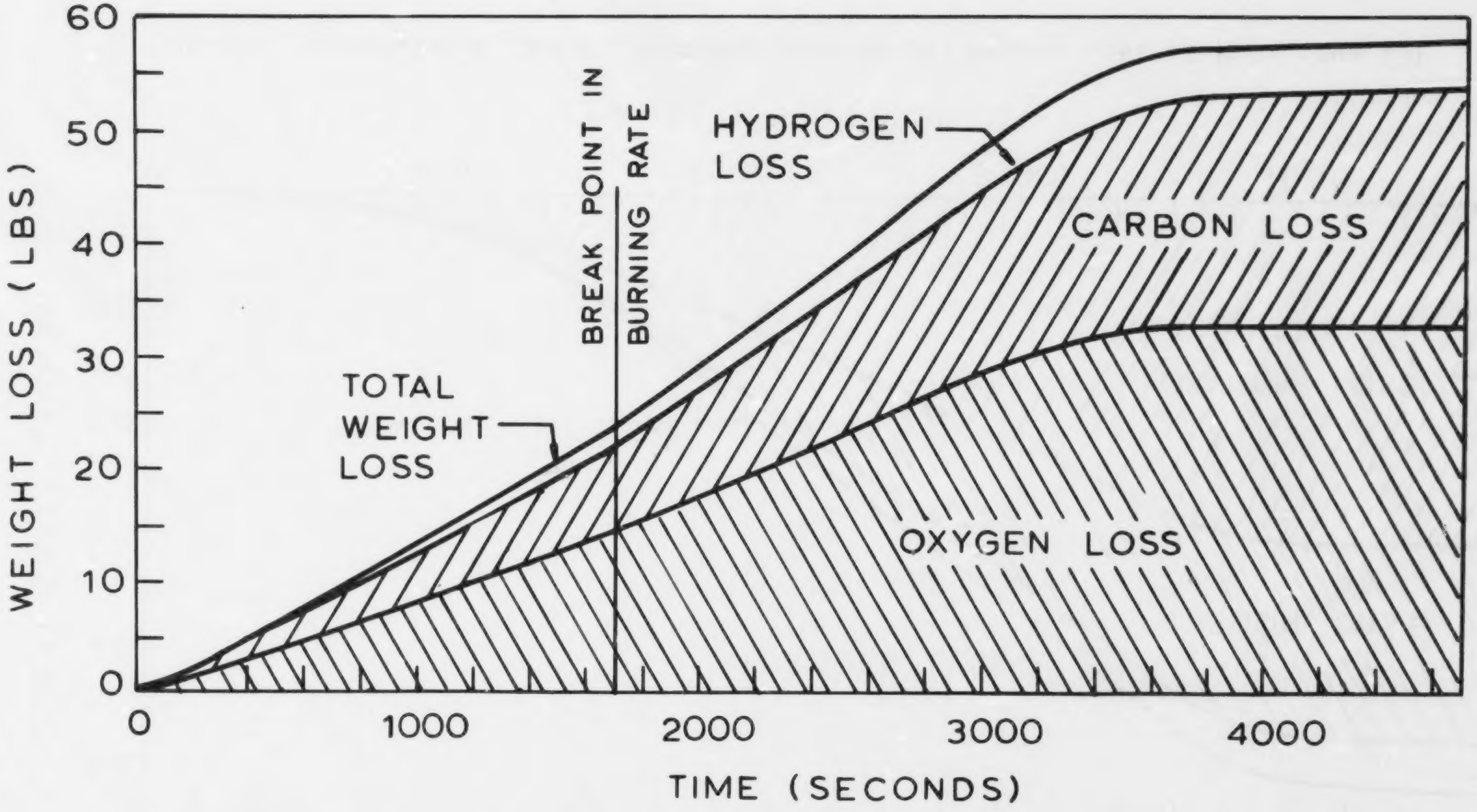

Fig. 67. Accumulated Carbon, Hydrogen and Oxygen Weight Loss of Fuel (Run 18)

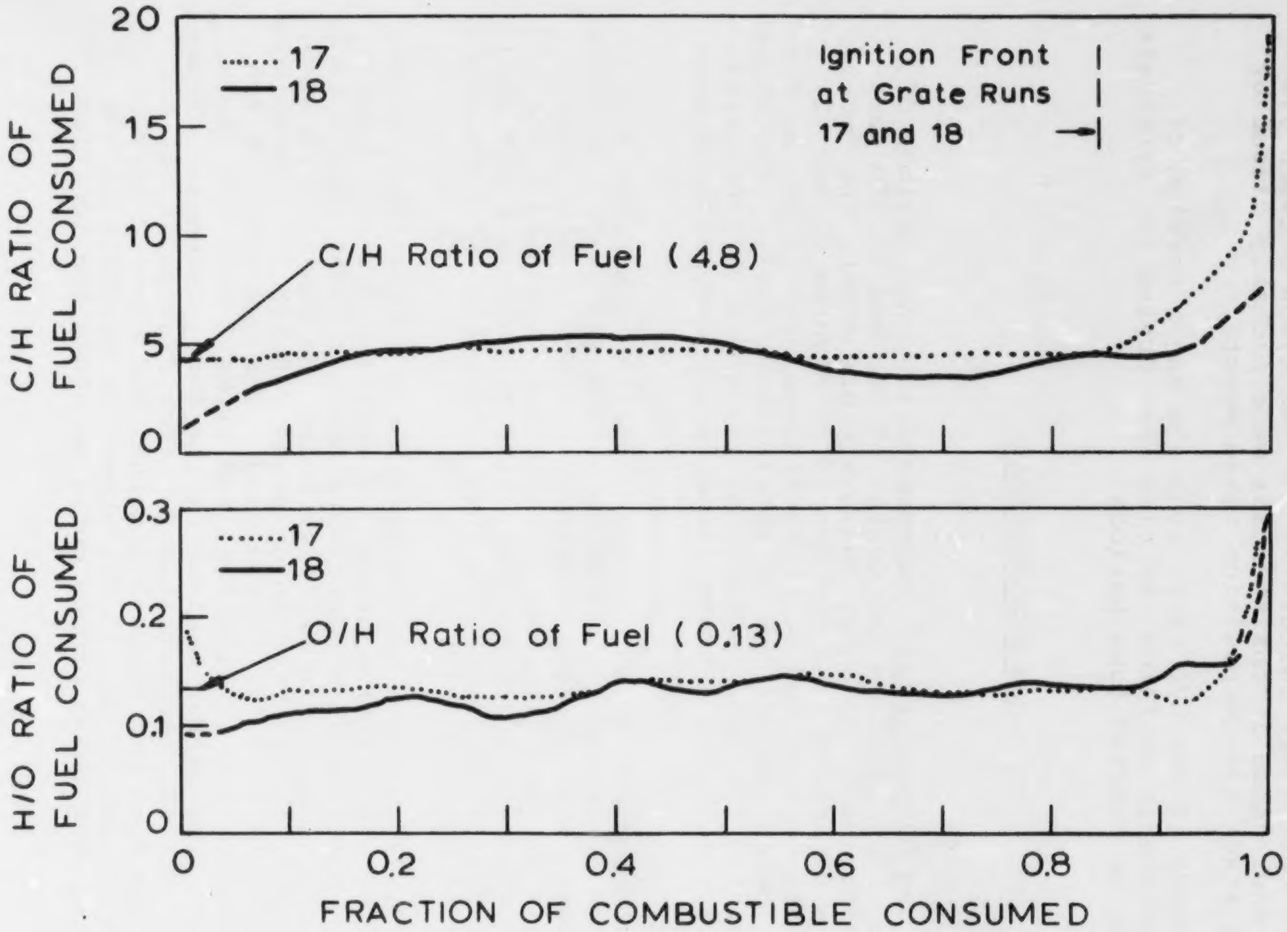

Fig. 68. Hydrogen/Oxygen and Carbon/Hydrogen Ratio of Fuel Burnt as a Function of Fraction of Combustible Consumed (Runs 17 and 18)

the fuel burnt for Runs 17 and 18; in this figure the regions where there was the most uncertainty in the calculated values are shown as dashed lines. For Run 18 some anomalous values of the H/O ratio were calculated for the times between 3700 and 3900 sec; these inconsistencies were probably caused by incorrect stack gas composition measurements.

The constancy of the H/O ratio over the major portion of these experiments confirms the view that drying and pyrolysis occur over protracted time periods.

Gas Compositions

Fuel Bed Gas Compositions. Representative compositions of the gases withdrawn from the center of the bed at two positions 20 in. and 12 in above the grate are shown, for Run 17, in Figures 69 and 70, and for Run 18 in Figures 71 and 72. Measurements of fuel bed gas compositions were taken, as described on pages 152-184, on an intermittent basis. The smooth curves joining the data points must therefore be considered only to represent the average trend in gas compositions with time.

The bias introduced by radial concentration gradients was checked for a number of runs by comparing the carbon contents of the gases at the sample points with those in the stack. For the gas samples from Run 18 there was little bias, but for other runs where larger quantities of underfire air were used, the degree of channeling increased; this has been fully discussed on pages 213-230.

Figures 73, 74 and 75 show the smooth gas composition curves replotted versus distance above the ignition front. These plots were obtained in a manner analogous to that used in calculating the temperature profiles below the ignition front and the reader is referred to on pages 206-208 for a more complete description of the method used. The gas compositions measured during Run 17 from Fuel Bed Probe 2 were not plotted in the above manner because of the incompleteness of the data on H_2 and CH_4 concentrations. (For Figures 70, 71 and 72, note the Fuel Bed Probe 1 and Fuel Bed Probe 2 were 20 in. (1.67 ft) and 12 in. (1 ft) above the grate; this was the maximum that these probes could be above the ignition front.)

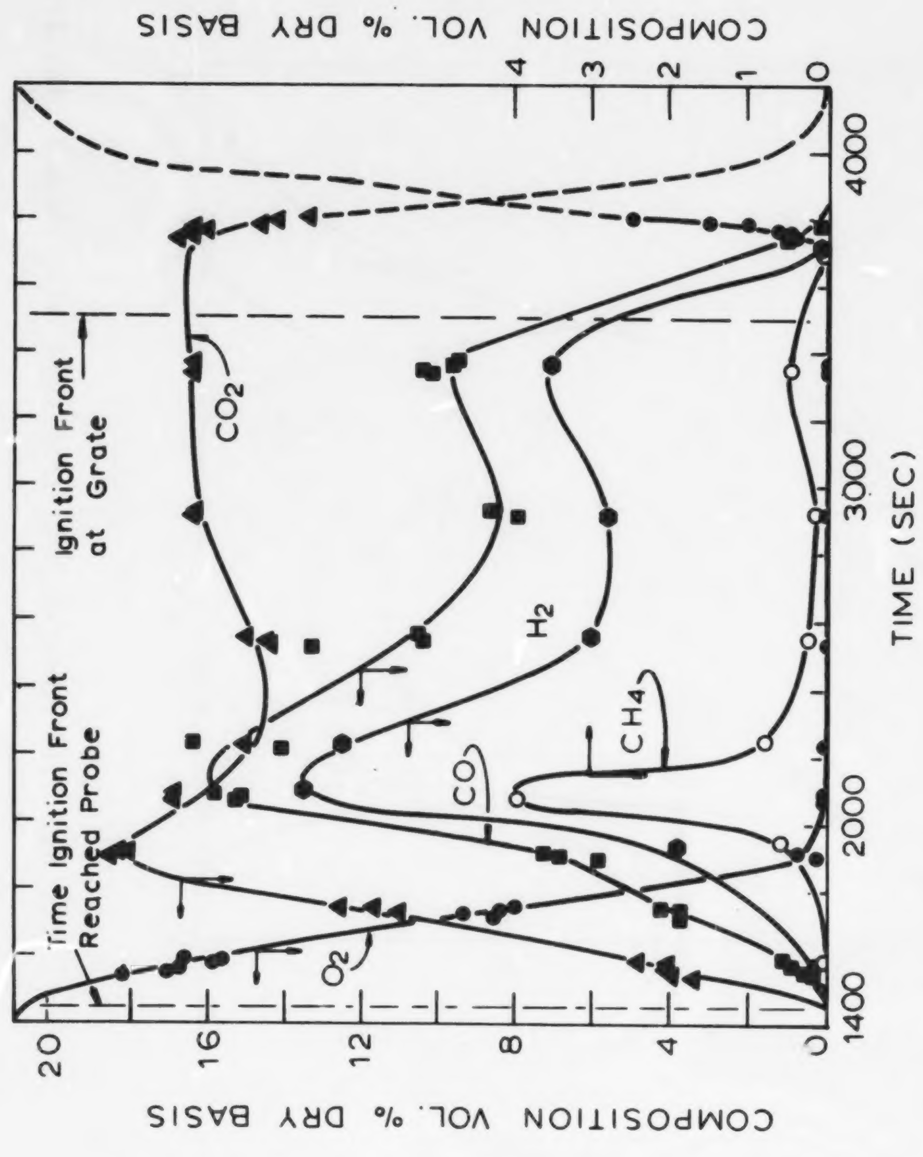

Fig. 69. Gas Compositions from Fuel Bed Probe 1 (Run 17)

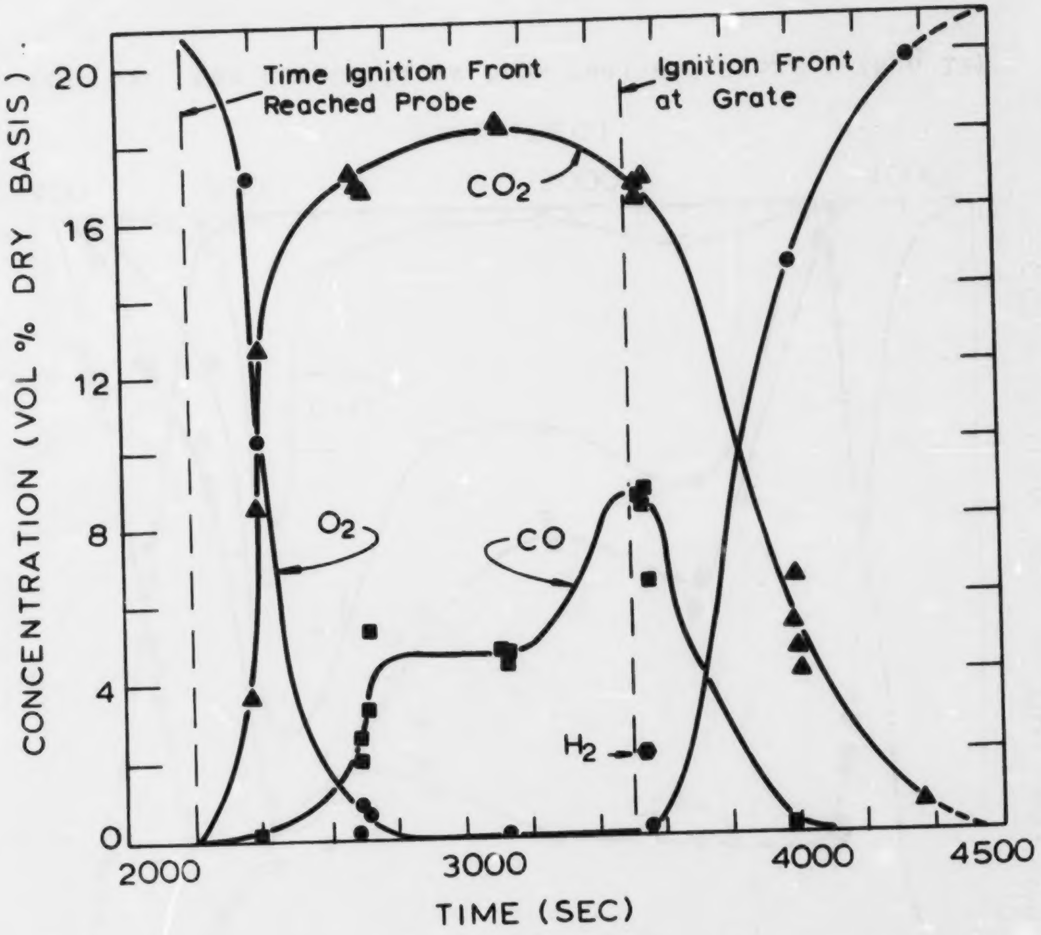

Fig. 70. Gas Compositions from Fuel Bed Probe 2 (Run 17)

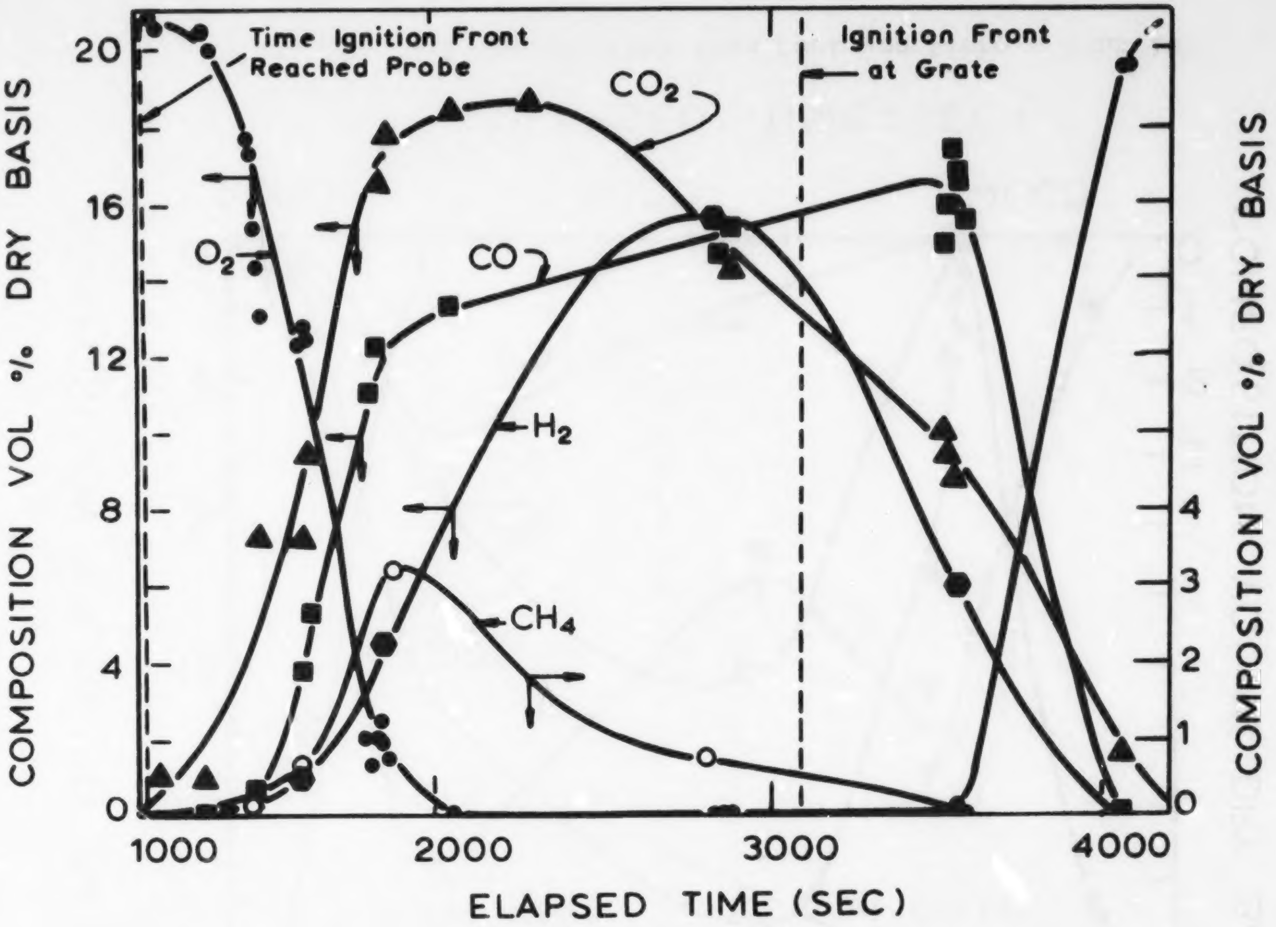

Fig. 71. Gas Compositions from Fuel Bed Probe 1 (Run 18)

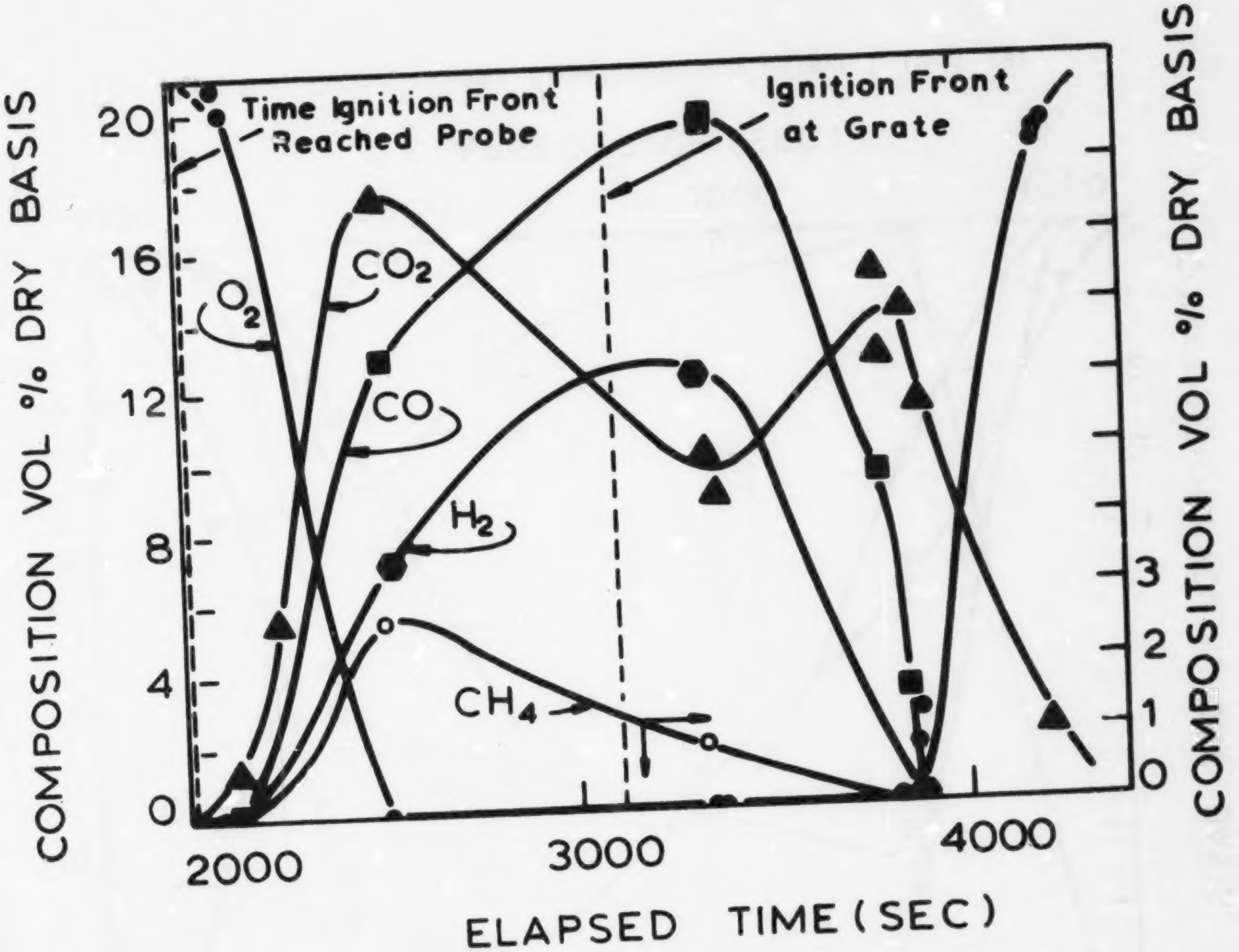

Fig. 72. Gas Compositions from Fuel Bed Probe 2 (Run 18)

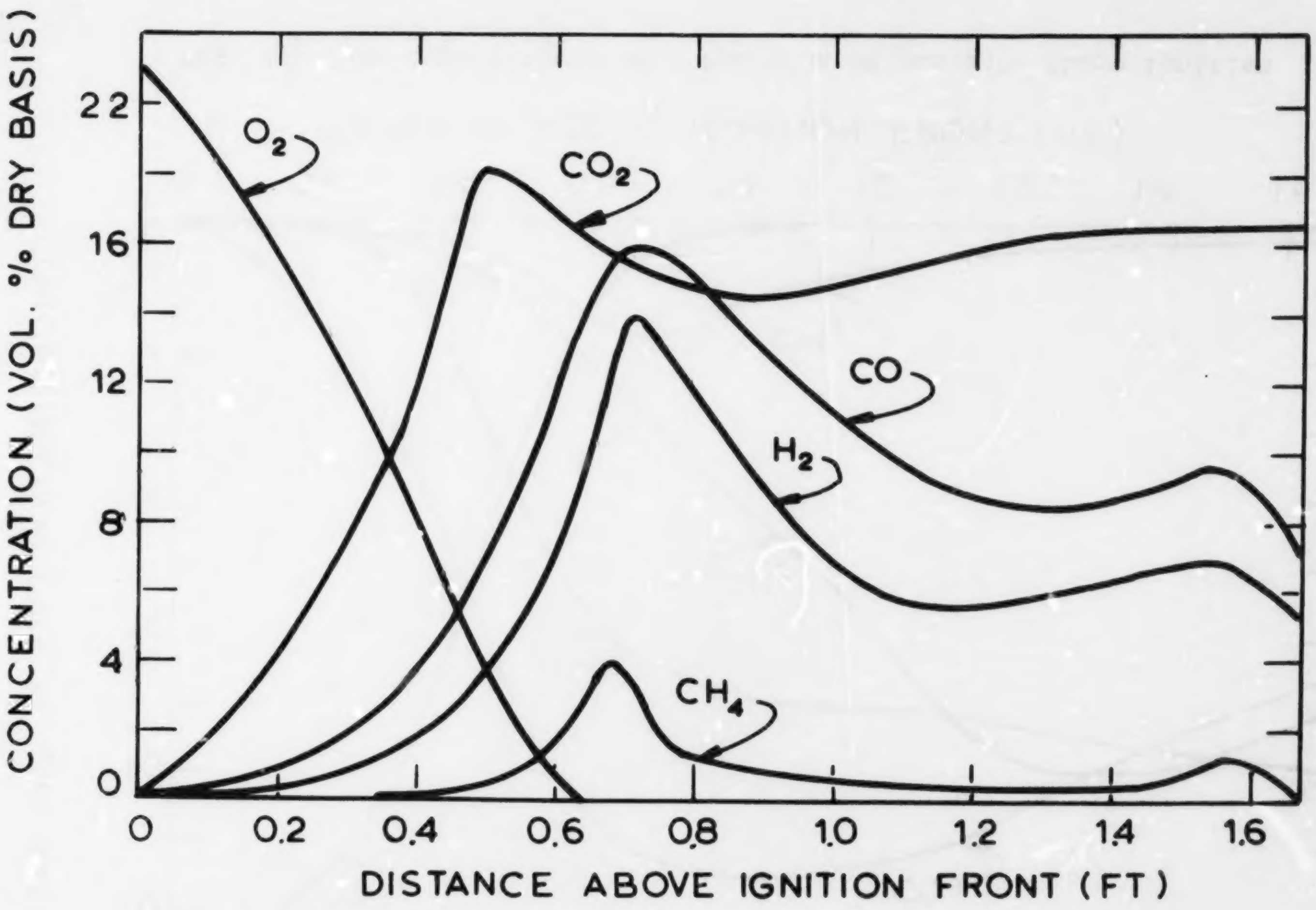

Fig. 73. Gas Compositions as a Function of Distance Above Ignition Front (Run 17)

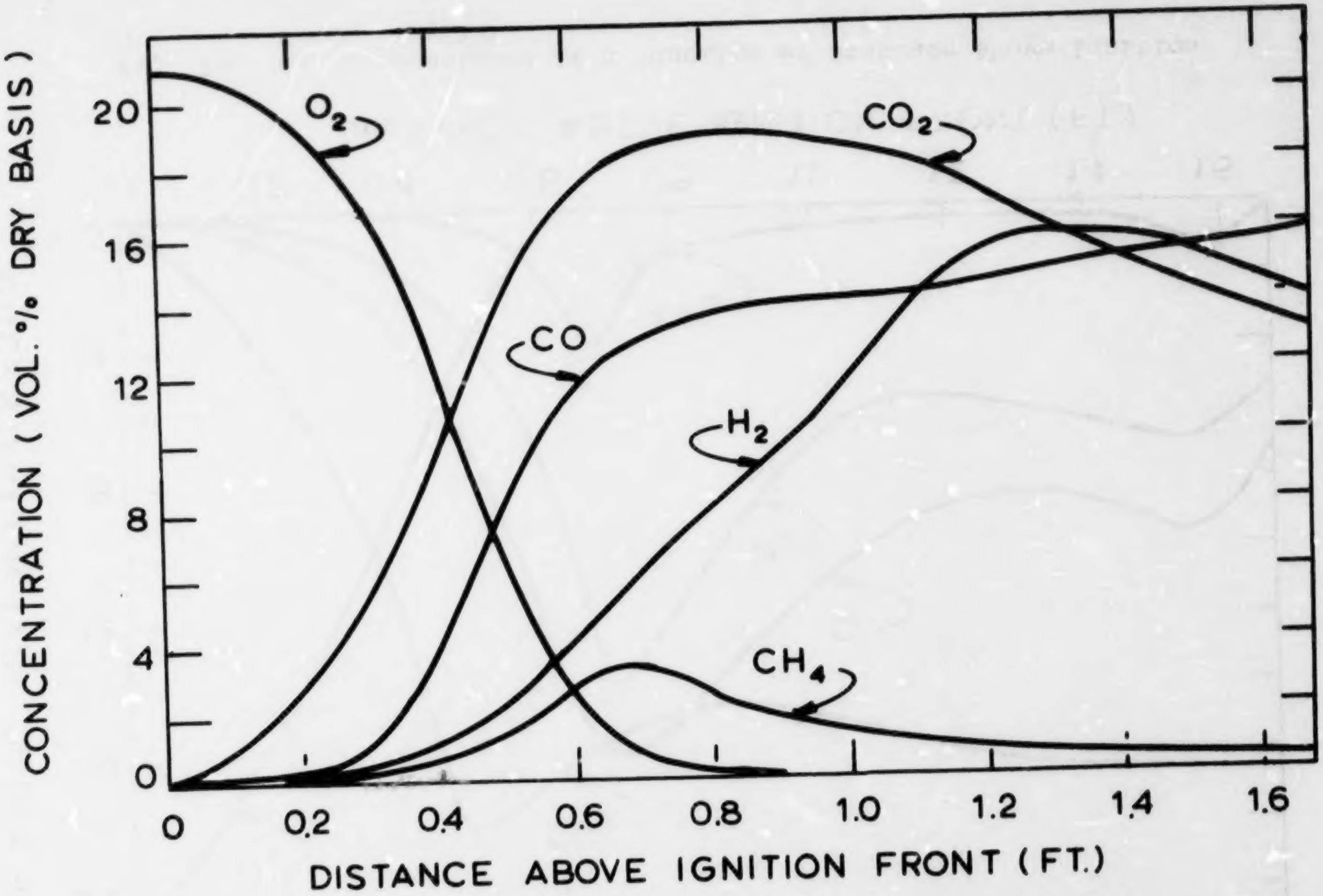

Fig. 74. Gas Compositions as a Function of Distance Above Ignition Front (Run 18)

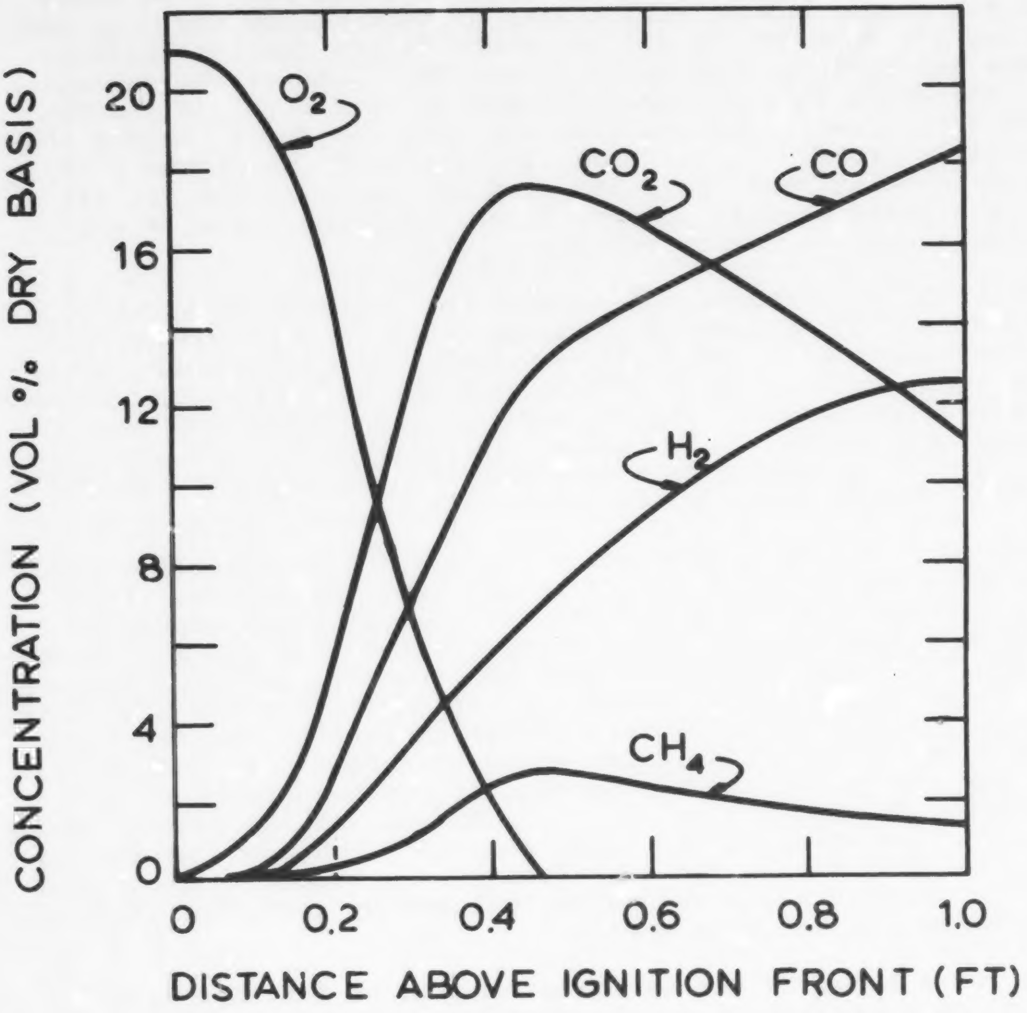

Fig. 75. Gas Compositions as a Function of Distance Above Ignition Front (Run 18) (Calculated using ignition velocity = 0.083 ft sec^{-1}); fuel bed probe located 12.n. above grate.

For these runs where low underfire air rates (150 lb hr^{-1} ft^{-2}) were employed, the oxygen concentration fell rapidly to zero as the ignition plane passed the probe and typically was consumed in a distance of 0.25 - 0.8 ft. The point at 2300 sec in Figure 68 appears to be spurious as there was no decrease in combustibles (CO and H_2) at this time. The decay of the oxygen concentration with distance below the ignition front for Runs 15, 17 and 18, where fairly complete records were available, is shown in Figure 76. Some of the variation of the shape of these profiles can be attributed to inaccurate determination of the time the ignition front reached the sampling probe. In addition, local variations of the ignition velocity could have affected the shape of the profile as the distance-time conversion was performed using a constant average ignition velocity.

As the O_2 concentration decreased, the concentrations of CO_2, CO, H_2 and CH_4 increased. The increase in CO_2 concentration always led the increases in concentration of the other gases; the same behavior was observed by Nicholls (24). Peak concentrations in both CO_2 and CH_4 were observed near the point of oxygen extinction, which again parallels Nicholls' (24) experimental results. Peak concentration of CO_2 were typically 16-20%; while those for CH_4 were 3-4%.

After all of the O_2 had been consumed, the conditions within the fuel bed appeared to differ between experiments. From the earlier discussions on the various processes occurring within a fuel bed, it would be postulated that due to the Boudouard reaction ($C + CO_2 \rightarrow 2CO$) the CO_2 concentration would decrease, while the CO concentration would increase with distance from the plane of zero oxygen concentration. Similarly the H_2 and CO concentrations would be expected to increase, at the expense of the H_2O because of the occurrence of the reaction $C + H_2O \rightarrow H_2 + CO$. In addition, if the assumption of the equilibration of the water-gas-shift reaction (except in the vicinity of the ignition front) is correct, increases in the CO concentration should be followed by increases in the H_2 concentration and vice versa.

The above behavior was exhibited in Run 18 (Figures 71 and 72) with the exception of the H_2 concentration measured with Fuel Bed Probe 1, at times greater than 2800 sec. (Figure 71 shows that, after this time, the H_2 concentration decreased while the CO concentration increased.) However, the exact location of the H_2 concentration profile was not known because of the paucity of the data for this species and it is possible that the H_2 concentration profile could have followed a similar shape to the CO profile. The gas compositions obtained from Run 17 exhibited behavior different from that observed in Run 18, as the CO and H_2 concentrations decreased with time (or,

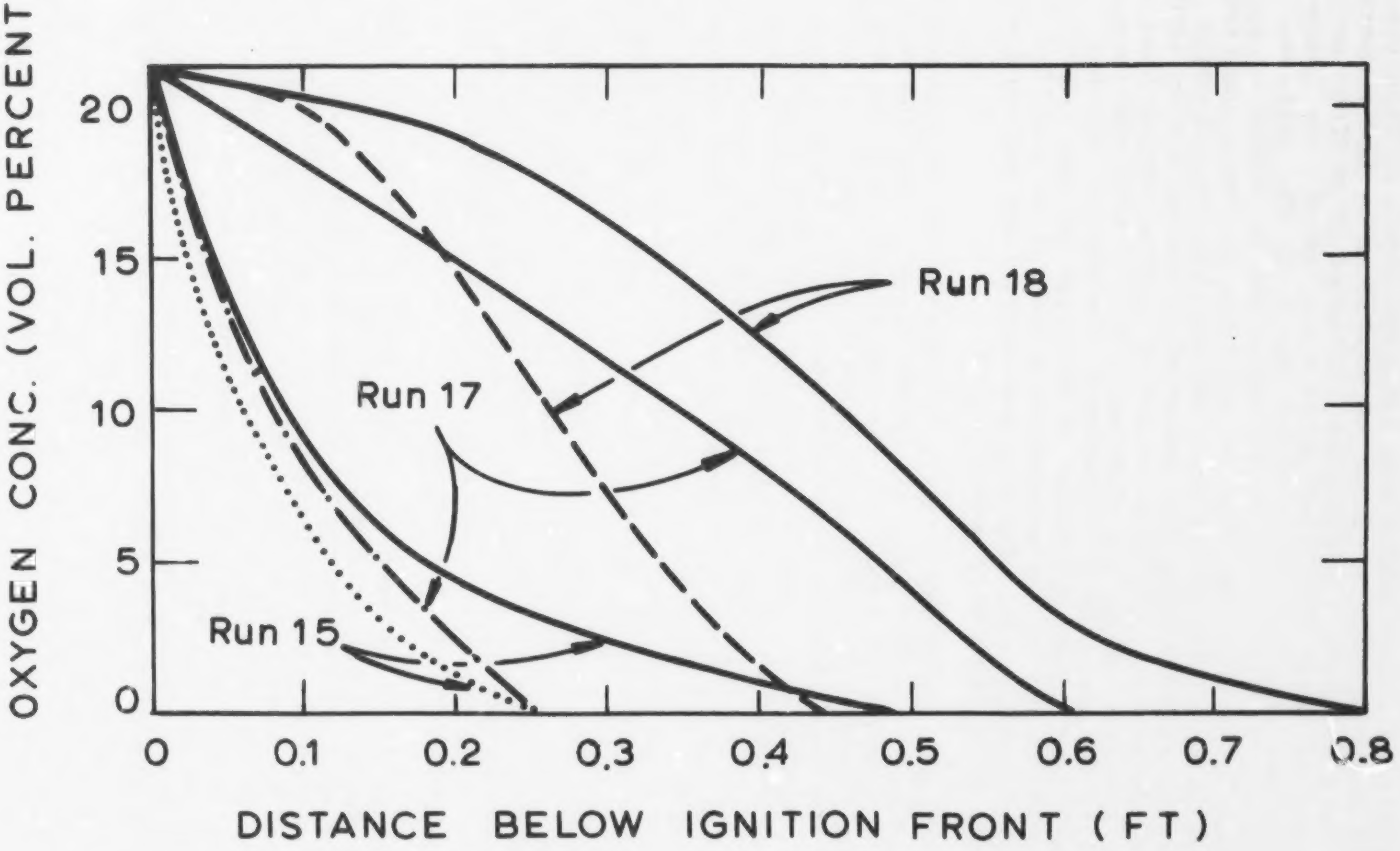

Fig. 76. Oxygen Concentration as a Function of Distance Below Ignition Front

equivalently, distance above the ignition front). This variation of gas composition cannot be explained by bed temperature changes as these temperatures increased from 2000 sec to 2800 sec by about 200°F and would have favored the formation of higher concentrations of CO and H_2O. The decrease in CO and H_2 in this run could be explained by mixing of bypass oxygen back into the core of the bed; at the higher temperatures which prevailed in this region, the oxygen would have reacted rapidly with the combustible and no oxygen would have been observed. The high amount of bypass oxygen that apparently channeled up the side wall during this run (see pages 213-230) makes this explanation plausible. Further confirmation of this hypothesis is supplied by the lower than normal CO and H_2 concentrations measured at position 12 in. above the grate. The CH_4 concentrations measured with this probe were also very small ($<0.1\%$).

For both Runs 17 and 18, as well as others, the CO_2 concentration within the bed fell off quite sharply near the end of active combustion (3800 sec for Run 17 and 3600 sec for Run 18 -- see Figures 59 and 60, which show that the major portion of the total weight loss was achieved by these times). Similar results were obtained from the stack gas measurements for these two experiments; this is discussed on pages 248-253 . The rapid decrease in CO_2 at the time when bed burnout is nearly complete may provide a relatively simple criterion for the burnout of the fuel bed on a travling grate incinerator as long as there is no gross back-mixing of the overfire combustion gas at the discharge end of the grate.

The gas compositions obtained from Fuel Bed Probe 2 in Run 18 (Figure 72) indicated that, near the end of the run, the CO_2 concentration started to increase as the CO concentration began to decrease. The CO_2 concentration continued to increase up to the time the CO concentration fell to zero at which point it started to fall.

From Figure 63 it is seen that even with a generous estimate for the depth of the active bed, the gas sampling probe was probably well above the top of the bed at the time the CO concentration started to decrease. This observation may be explained by the presence of a diffusion flame above the bed; the fuel to the flame was supplied by the combustible rising from the top of the bed and the oxidant was supplied by the oxygen from the overfire region. As the top of the bed receded from the probe, samples were first taken from the fuel regime of the diffusion flame, and then as the probe passed through the flame envelope from the oxidant side of the flame. The turbulence above the bed would make the location of the flame envelope ill-defined. Similar behavior would have been expected from the other gas compositions measured, but the intermittent sampling procedure may have obscured this trend.

Tables 15 and 16 (a) and (b) show the calculated ratio of the product of the CO and H_2O concentrations to the product of the CO_2 and H_2 concentrations within the fuel bed at various times during Runs 17 and 18. For both these runs, batch samples were taken from the fuel bed probes and analyzed for H_2. The H_2O content within the bed was back-calculated from the measured H_2O content in the stack gases. Table 15 shows that the water gas shift equilibrium was closely followed when oxygen began to penetrate through the bed (at 3760 sec). The two points, at 2080 sec and 2240 sec, where the calculated values are lower than would be predicted from equilibration of the water gas shift reactions could well be caused by interference from pyrolysis products (see Figure 66 or 70). Similar results were obtained from the two different sampling positions in Run 18, as shown in Table 16 (a) and (b) for two different locations within the fuel bed.

From the method of calculating the H_2O content in the bed the estimates of these concentrations were probably higher than those representative of conditions at the top of the bed for those cases where the sample was taken some distance from the top of the bed; this the estimate of $(CO)(H_2O)/(CO_2)(H_2)$ at these positions would have been higher than that observed at the top of the bed. These results although they must be considered of a preliminary nature tend to support the theoretical model of Niessen et al. (19) (see pages 106-112), and give a rough guideline for determining overfire air requirements.

Stack Gas Compositions. Figures 77 and 78 show the stack gas compositions for Runs 17 and 18. Although the burning rate was constant over the major portion of Run 17, there was some variation in the stack gas concentrations. This was caused by the varying air leakage into the top section. The air leakage would be expected to be proportional to the temperature differential between the ambient and the inside of the test incinerator. Figure 77 shows that the air leakage reached a maximum at around 3000 sec; at which time the inside refractory temperatures were at a maximum (see Appendix H, Figure H.4). The line marked "Start of Integration" at 200 sec in Figure 77 indicates the time when the first material balance was calculated -- see pages 230-237 .

TABLE 15

Check on Water Gas Equilibrium within Fuel Bed (Run 17)
(Fuel Bed Probe 1, 20 in. above grate)

Elapsed Time (sec)	Temperature (°F)	$\frac{[CO]}{[CO_2]}$	$\frac{[H_2O]}{[H_2]}$	$\frac{[CO]\,[H_2O]}{[CO_2]\,[H_2]}$ (Experimental)	$\frac{[CO][H_2O]}{[CO_2]\,[H_2]}$ (Calculated assuming water gas shift equilibrium)
1570	just at ignition	0.2	77.0	15.0	> 0.10
1930	1700	0.4	6.6	2.6	1.42
2080	1700	1.0	0.3	0.3	1.42
2240	1750	1.0	0.66	0.66	1.54
2540	1800	0.75	2.9	2.2	1.65
2930	1900	0.52	4.3	2.2	1.86
3350	1750	0.59	1.7	1.0	1.65
3760	1800	0.09	∞	∞	1.65

[A] denotes concentration of A

TABLE 16 (a)

Check on Water Gas Shift Equilibrium within Fuel Bed (Run 18)

(Fuel Bed Probe 1, 20 in. above grate)

Elapsed Time (sec)	Temperature (^oF)	$\frac{[CO]}{[CO_2]}$	$\frac{[H_2O]}{[H_2]}$	$\frac{[CO][H_2O]}{[CO_2][H_2]}$ (Experimental)	$\frac{[CO][H_2O]}{[CO_2][H_2]}$ (Calculated assuming water gas shift equilibrium)
1450	?	0.1	90	9.0	--
1600	?	0.4	59	24.0	--
1850	∿ 1400	0.7	4.7	3.3	0.8
2830	1500	1.0	1.2	1.2	1.0
3550	1650	0.57	2.1	1.2	1.3

TABLE 16 (b)

Check on Water Gas Shift Equilibrium within Fuel Bed (Run 18)

(Fuel Bed Probe 2, 12 in. above grate)

Elapsed Time (sec)	Temperature (^oF)	$\frac{[CO]}{[CO_2]}$	$\frac{[H_2O]}{[H_2]}$	$\frac{[CO][H_2O]}{[CO_2][H_2]}$ (Experimental)	$\frac{[CO][H_2O]}{[CO_2] H_2]}$ (Calculated assuming water gas shift equilibrium)
2550	1100-1500	0.74	4.1	3.1	≈ 0.5
3320	1700	2.0	1.8	3.6	1.6

[A] denotes concentration of A

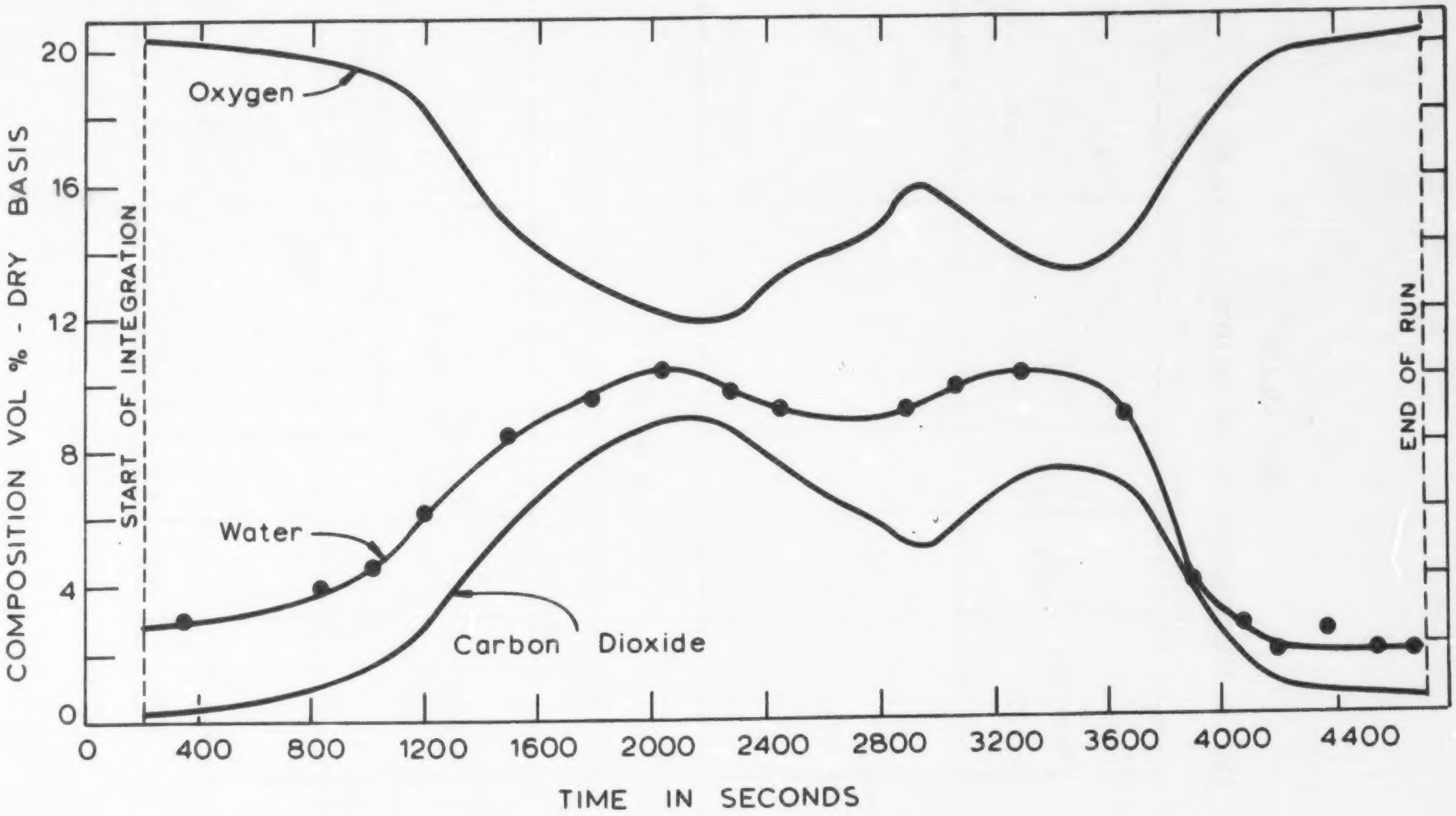

Fig. 77. Stack Gas Compositions (Run 17)

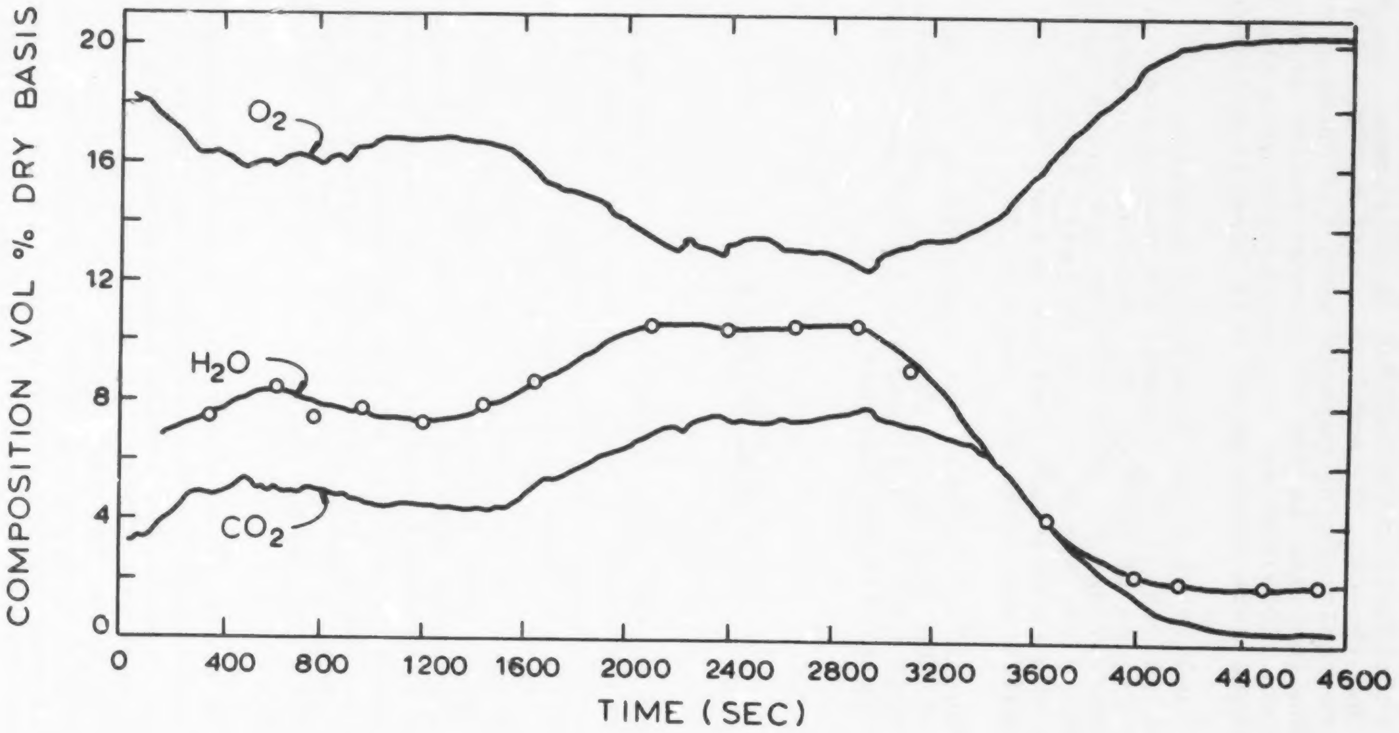

Fig. 78. Stack Gas Compositions (Run 18)

For Run 18 the temperatures inside the overfire section did not change as markedly as those for Run 17; the leak rate was therefore relatively constant during this test (see pages 230-237) and the CO_2, O_2 and H_2O concentrations did not change appreciably during periods when the burning rate was steady. The increase in the CO_2 concentration that was observed around 1600-1800 sec was consistent with the increase in the burning rate observed at this time (see Figure 60).

Figures 77 and 78 show the same rapid decrease of the concentrations of CO_2 towards the end of the run as indicated by Figure 66 through 72. For Run 17 a comparison between Figures 77 and 59 shows that at the point where the concentrations of CO_2 and H_2O began to fall (3600 sec) about 95 percent of the combustible fuel content had been consumed. Similar results were obtained for Run 18.

For both Runs 17 and 18 the H_2O concentration in the stack decreased at the same point that the CO_2 concentration decreased. This result confirmed the hypothesis of protracted drying and pyrolysis of the fuel.

Energy Balances

Differential energy balances taken at different times during an experiment can provide information on the total heat release rate (the sum of the heat release rates within and above the bed) at those times, while an integral heat balance taken over the duration of active burning can give an estimate of the total heat released which can be checked against that calculated from the known fuel composition and amount consumed. Attempts were made to calculate both types of balance but only integral heat balances could be calculated with any certainty because of the unsteady-state nature of the combustion processes and the "thermal flywheel" provided by the top section refractory lining. The difficulties encountered with the energy balance calculations will be discussed below.

Prior to the start of an experiment a steady temperature profile was established in the refractory brickwork of the overfire section; typically, inside temperatures were 2100°F and outside temperatures 275°F. At the start of an experiment, a few seconds after the refractory shield was opened the temperature dropped sharply (generally from 2100°F to 1700°F in about 200 sec) as the energy stored in the refractory section was transferred to heat the fuel bed surface and the underfire and overfire air. Stack gas temperatures typically fell a few hundred degrees Fahrenheit during this "ignition" period. Once active burning was established the temperatures of the refractories changed slowly to an "equilibrium" level. For those runs where adjustments were made in the amount of overfire air employed or where the burning rate varied, the temperatures changed continually during the course of the experiment.

For the purposes of calculating differential energy balances it was important to be able to estimate the effective heat sources and sinks associated with the changes in temperature level of the refractories. This was particularly important at the beginning and end of a run if heat release rates were to be determined for these times but no reasonable method for calculating this effect was available. Assuming a linear temperature profile within the top section refractories, the change in total energy content of this section per ^{o}F change in the temperature of the inside surface $\Delta O/\Delta T_s$ was calculated to be

$$\frac{\Delta O}{\Delta T_s} = 90 \text{ Btu } {}^{o}\text{F}^{-1} \qquad (176)$$

This equation can be used to calculate the integral heat source or sink effects but clearly would give an erroneous result under conditions of rapid heat transfer. (When the temperature of the top section dropped rapidly at the start of a test, the temperature profile within the refractories reached a maximum some distance from the inside surface.) With the temperature measurements taken, there was no simple method available which could be used to improve the calculation of the source sink effect of the refractories and therefore limited the use of differential energy balances.

The other difficulty encountered concerned the estimation of the heat loss through the feul bed wall. Heat losses through the fuel bed wall were determined from the temperatures measured with the heat loss probes and from the theoretical calculations of heat loss through the fuel bed wall (see Appendix B). From Figure B.1 the maximum heat loss (at a short time after the wall was exposed to the burning fuel) was estimated to be of the order of 10×10^3 Btu hr^{-1} per foot of bed height, while at times greater than about 0.6 hr the heat loss dropped to approximately 6×10^3 Btu hr^{-1} per foot of bed height. From the heat loss probe data for Run 18 the heat losses were estimated as 8×10^3 Btu hr^{-1} per foot of bed height. For calculational purposes a value of 8×10^3 Btu hr^{-1} ft^{-1} was chosen as representing a mean heat loss rate. The heat loss depended on the amount of wall exposed to the ignited solid. From the ignition rate and the estimates given above, a mean heat loss for Run 18 was calculated to be 10 x 10^3 Btu hr^{-1}. This value was considered to be typical for the majority of experiments conducted in this study.

For simplicity, heat losses were considered constant throughout the duration of a run; estimates of the fuel bed heat losses would be most markedly affected by this assumption but the effects proved to be fairly small in relation to the other heat losses, so this assumption was reasonable. Heat losses were considered to take place in three places: overfire region, top section cooling coils, and fuel bed. Heat losses to the grate were neglected because, for the run in which heat release rates were calculated, the ignition front reached the grate at a time close to the end of the experiment. Heat losses from the top section (assumed to include the refractory tray) were estimated using

$$Q_1 = \frac{2Lk_s(T_s^i - T_s^o)}{\ln(r_1/r_o)} \quad \text{Btu hr}^{-1} \qquad (177)$$

where L was the length of the top section area (416 ft); k_s the mean thermal conductivity of the refractory brickwork (0.18 Btu hr^{-1}ft^{-1} °F); T_s^i and T_s^o the inside and outside refractory temperature respectively; and r_o and r_1 the inside and outside radius of the overfire section respectively (r_o = 0.75 ft; r_1 = 1.3 ft).

The heat loss to the top section cooling plate was calculated from the mass flow rate of the cooling water used (450 lb hr^{-1}) and the temperature rise (∿ 30°F max.). These heat losses were therefore about 14 x 10^3 Btu hr^{-1} and were roughly constant over the duration of a run and between different experiments.

For the specific case of Run 18, the heat loss from the top section, using equation (177) with $T_s^i \simeq 1600$°F and $T_s^o \simeq 275$°F, was about 12 x 10^3 Btu hr^{-1}. Total heat losses for this test were therefore about 36 x 10^3 Btu hr^{-1}. For this run the temperature of the top section refractories remained practically constant from 1800 to 3000 sec. During this time the average rate of enthalpy loss via the stack gas was 256 x 10^3 Btu hr^{-1}. (This value was calculated using the molar flow rates determined from the material balance program, a mean flue gas specific heat of 8.1 Btu lb mole^{-1} °F^{-1}, the recorded stack gas temperatures and a datum temperature of 80°F.) From the burning rate of 68.5 lb combustible hr^{-1} (41 lb combustible hr^{-1}ft^{-2}) the average heating value of the combustible was 4300 Btu lb^{-1}.

The above calculation was repeated for times from 200-1600 sec. In this case, however, the temperatures of the top section fell an average of 200°F over this time period. The total heat generated from 200-1600 sec (82×10^3 Btu) was computed by summing the integrated enthalpy losses to the stack, fuel bed wall and cooling coils and subtracting the net enthalpy change in the refractory brickwork given by equation (176). The total weight loss over this period was approximately 20 lb, giving an average heating value of the combustible of 4100 Btu lb^{-1}. The calculated heating values for the two different periods of the experiment agree closely.

Using a heating value for the dry wood of 8090 Btu lb^{-1} (calculated from the Du Long formula, $\Delta H = 14600C + 62000 (H - O/8)$, Btu lb^{-1}) and subtracting from this the amount of energy required to vaporize any water present (the heat of absorption term is small: $\sim$ 30 Btu lb^{-1}), the heating value of the fuel used in this experiment was calculated to be 5450 Btu lb^{-1}. The agreement with the experimental values is reasonable considering the approximate nature of the calculations.

Energy balances were not caluclated for Run 17 because of the difficulties encountered in correcting for the changes in temperature level of the refractories which occurred during this experiment.

Overfire Air Regime

From the fuel bed gas concentrations shown in Figures 69 through 72, it is apparent that the oxygen required to complete the combustion of the gases leaving the fuel bed varied with operating conditions and with time. For a traveling grate incinerator this means that overfire air requirements will vary with position along the grate as well as with operating conditions.

For the experiments conducted in this study the average overfire (or secondary) air requirements for the burning rates observed could be readily evaluated from Figure 61. However, this calculation could not be performed on an a priori basis because there were no theories available that could be used to determine the achievable burning rate for a given underfire air rate. For cases where the burning rate was known as a function of underfire air rate (i.e., from experimental observation) a plot similar to Figure 61 could be of use in determining the appropriate secondary air requirements. For example, this technique could be used to evaluate the secondary air requirements for a traveling grate incinerator if the average burning rate and the underfire air rate were known. For this particular example, however, some care would have to be exercised, as the total oxygen feed rate through the fuel bed would need to be known. Oxygen can be supplied to the bed both in the underfire air and in any overfire air induced through the bed by temperature gradients; for the latter case, the overfire air (which has a lower mass fraction of oxygen and a lower density than the underfire air) will tend to sink down at the "cold" walls of the furnace and to rise up through the "hot" core of the bed. The oxygen in this air would be expected to be rapidly consumed near the edges of the bed. The estimation of the quantity of air being induced into the bed in this manner is difficult but a rough estimate of the expected magnitude of this effect can be found as follows.

If only the significant forces are those of momentum $(U^2 \rho L^2)$ and buoyancy $(L^3 \Delta\rho g)$, the entrainment velocity U is found to be

$$U = \sqrt{\frac{L\Delta\rho g}{\rho_c}} \qquad (178)$$

where L is a characteristic length given by the distance from the top of the bed to the roof of the incinerator; $\Delta\rho$ the density difference of the gas at the hot and cold temperatures; ρ_c the density of the cold gas; and g the gravitational constant. The mass flux of oxygen through a unit area of the bed by this natural draft $(\dot{G}_{ND})$ will be

$$\dot{G}_{ND} = U\rho_c \, (M_{O_2})_c = \rho_c \, (M_{O_2})_c \sqrt{\frac{L\Delta\rho g}{\rho_c}} \qquad (179)$$

where $(M_{O_2})_c$ is the mass fraction of oxygen in the overfire air. The mass flux of oxygen through a unit of bed in the underfire air $(\dot{G}_{FD})$ is given by

$$\dot{G}_{FD} = V\rho_a \, (M_{O_2})_a \qquad (180)$$

where V is the superficial velocity of the underfire air and ρ_a and $(M_{O_2})_a$ the density and mass fraction of oxygen in the underfire air, respectively.

If the effect of the natural draft is to be negligible

$$V\rho_a(M_{O_2})_a >> \rho_c(M_{O_2})_c \sqrt{\frac{L\Delta\rho g}{\rho_c}} \qquad (181)$$

and using $\rho_c = \frac{\rho_a T_a}{T_c}$ and $\rho_H = \frac{\rho_a T_a}{T_H}$, where T_a, T_c and T_H are the ambient cold and hot air and gas temperatures, gives

$$V\ (M_{O_2})_a >> \frac{T_a(M_{O_2})_c}{T_c} \sqrt{L\left[1 - \frac{T_c}{T_H}\right] g} \qquad (182)$$

Putting typical values into equation (177) as follows: $V = 0.5$ ft/sec (≈ 120 lb $hr^{-1}ft^{-2}$); $(M_{O_2})_a = 0.23$; $(M_{O_2})_c = 0.08$; $T_a = 520^oR$; $T_c = 2000^oR$; $T_H = 2500^oR$, gives

$$0.12 >> 0.053\sqrt{L} \qquad (183)$$

For many furnaces, L, one of the driving forces for the buoyancy term, is of the order of 10-20 ft. Substituting this value into equation (183) indicates that the oxygen mass flux induced by natural draft may well be greater than that supplied in the underfire air. The uncertainty associated with estimating the unknown amount of air which is entrained through the bed imposes a serious constraint upon the above method of calculating the secondary air requirements.

The theoretical model of Niessen et al. (19) may also be used to determine secondary air requirements if the average burning rate and fuel composition have been determined. This model assumes that relatively small amounts of higher hydrocarbon pyrolysis products are present in the gases at the top of the bed and that these gases are equilibrated with respect to the water gas shift reaction at the temperature of the bed. The results of this study indicated that this assumption was relatively good for the simulated refuse used; results from full scale operating units have also suggested that this assumption holds for a real refuse (149). Details of the Niessen et al. (19) model are given on pages 106-112 .

For this study the mixing above the bed supplied by the overfire jets was sufficient to provide nearly complete combustion of all combustibles. Carbon monoxide was never detected in the stack for any of the runs; for the later runs the limit of detection was only about 0.1 - 0.2% but earlier runs where the detection limit was about 0.05% also failed to show the presence of CO. Trace quantities of soot and smoke were recorded, but only during periods of smoldering was any smoke visually noticeable. Although this synthetic refuse was not inherently a "smoky" fuel, these results are encouraging and suggest that if, in operating units, adequate mixing is achieved and high enough temperatures are maintained in the overfire region, clean combustion of the volatiles and combustible can be achieved.

As will be discussed below, for the very low degree of turbulence encountered in all incinerators, and in the test incinerator of this study, the rate of mixing of the combustible and oxygen is generally expected to provide the limiting step in the combustion process. The ensuing discussion follows that of Sarofim (150). From the studies (e.g., 151, 152, 153) in well-stirred reactors the following general conclusions can be drawn:

(a) The kinetics of oxidation for a large number of fuels are so fast that volumetric heat release rates of 10^6 to 10^8 Btu $hr^{-1}ft^{-3}$ are achievable over the temperature range 2000° to 3000°F.

(b) The reactions of the hydrocarbons and ketones studied are very fast relative to that of the carbon monoxide intermediate formed in the reactions.

(c) The rate of burnout of the carbon monoxide, which provides the rate limiting step, in the overall combustion process, is given by

$$-\frac{df_{CO}}{dt} = 1.8 \times 10^{10} \exp\left[\frac{-25000}{RT}\right] f_{CO}\sqrt{f_{O_2}}\sqrt{f_{H_2O}}\left(\frac{P}{RT}\right)^2 \text{ liters}$$

$$\text{g/mole}^{-1}\text{sec}^{-1} \qquad (184)$$

where f_{CO}, f_{O_2}, f_{H_2O} are the mole fractions of CO, O_2 and H_2O; T is the absolute temperature in °K, and (P/RT) is in g moles/liter. Using equation (184) and representative values of temperature, oxygen and water vapor concentrations found under most incinerator conditions, the time required to reduce the carbon monoxide concentration to less than .01 percent is of the order of a millisecond. Thus it can be concluded that if the turbulence above the fuel bed is high enough to provide perfect mixing and if there is no equilibrium constraint imposed by the reaction $CO_2 + H_2 \rightarrow CO + H_2O$ no CO would be expected in the flue gases and complete reaction of the pyrolysis products could be achieved. Moreover, the very rapid rate of chemical reaction suggests that if the mixing were greatly improved above the fuel bed, furnace volumes could be considerably reduced.

The rate of soot burn-out can be estimated from the expression for mass transfer and chemical reaction. The rate of soot oxidation can be determined from the semi-empirical formula proposed by Nagle and Strickland-Constable (154) to correlate the measurements of the oxidation rate of polycrystalline pyrographite. Appleton (155) has summarized various experimental evidence on surface structure to support the assumption that the kinetics of soot oxidation are similar to those for pyrographite. Park and Appleton (156) have provided experimental evidence that at high temperatures (> 1500°K) the rate of soot oxidation is closely predicted by the theory for the rate of oxidation of pyrolyzable graphite. Assuming that the Nagle and Strickland-Constable relationship holds for soot oxidation at the low temperatures typical of incinerator operation, the rate of soot oxidation can be given approximately by:

$$K_{chem} = 12 \left[\frac{20 \exp\left\{-15{,}000/T\right\} P_{O2}}{1 + 21.3 \exp\left\{2060/T\right\} P_{O_2}} \right] \text{g cm}^{-2} \text{ sec}^{-1} \qquad (185)$$

where T is in °K and P_{O2} in atmospheres. From equation (185) it can be concluded that for all conceivable conditions within an incinerator the chemical rate will provide the rate limiting step for the oxidation of soot. Therefore the time to burn a soot particle (t_b) of original diameter (d_o cm) is given by

$$t_b = \frac{\rho_s d_o}{2k_{chem}} \approx \frac{d_o}{k_{chem}} \qquad (186)$$

On the assumption that the density of the soot particle is about 2 g. cm^{-3}, equation (186) shows that the time for burnout of the particles will be weakly dependent on the oxygen partial pressure (P_{O_2}), will increase with particle size d, and will decrease with increasing temperature. Using equation (186) and typical incinerator conditions, $P_{O_2} \approx 0.1$ atm and T ≈ 1500°F (≈ 1090°K), the time to burn out a 1-micron particle is 61 sec and a 200Å particle is 1.2 sec.

It is evident from the kinetic control of soot oxidation that the temperatures in the overfire region should be kept as high as possible. This result suggests that the addition of air too high above the fuel bed may cool the gases and quench the reaction, since the rate of reaction falls markedly with decreasing temperature (at incinerator temperatures the rate changes an order of magnitude with $200^{\circ}K$ change in temperature). The importance of the proper design and placement of the overfire air jets has been emphasized in the early studies at Battelle under Engdahl (157).

Finally, in this study, the combustion intensities for active burning runs were of the order of 40,000 Btu ft , assuming that all the overfire volume and 50% of the fuel bed section volume were needed for complete combustion. The complete oxidation of the combustibles was probably achieved in a volume rather less than that used in this calculation. This combustion intensity is twice that typically used in most incinerators. No difficulties were encountered in using a combustion intensity of this magnitude, even for those runs where paper was used as a constituent of the fuel; there have been suggestions that for light material, such as paper, high combustion intensities aggravate the problem of entrainment. Extrapolating the combustion intensity results from this study to full-scale units would be unjustified, but the results suggest that the possibility of using higher combustion intensities (which would allow furnace volumes to be decreased) should be investigated further.

Fuel Bed Conductivity and Rate of Heat Release within Bed

An attempt was made to calculate the effective thermal conductivity of the fuel bed and the net rate of heat release within the bed following the methods proposed by Stewart and Saville (87). These methods have been outlined on pages 34 - 39 and can be seen to rely upon accurate measurement of the temperature profiles within the bed, as they require the evaluation of the second derivative of temperature with distance $\frac{\partial^2 T_s}{\partial z^2}$. The temperature measurements obtained in this study were not of a high enough quality to permit meaningful estimates of either the effective thermal conductivity or the net heat release rate using the Stewart and Saville technique.

ACKNOWLEDGEMENTS

Financial support from the Solid Waste Research Division of the Environmental Protection Agency is gratefully acknowledged. The principal investigators are particularly grateful to Mr. Louis W. Lefke and Mr. Daniel J. Keller for their guidance and patience during the early stages of design and construction. The authors are indebted to Mr. Robert C. Thurnau for his encouragement and advice in the later phases of the program.

The report is based largely on the Sc.D. thesis of Joseph L. Rogers.

The building of the experimental equipment could have been achieved only with a great deal more trial and tribulation if it were not for the outstanding contributions of Steven R. LeMott and Charles T. Johnson. Grateful acknowledgement goes also to Reed C. Fulton, for his many helpful suggestions and practical assistance in constructing much of the heavy equipment; and to Paul W. Bletzer, Allan H. Merrill and Arthur Clifford, for the generous donation of their time in completing many smaller but no less important tasks. Special thanks are due Stanley R. Mitchell, who not only participated in numerous aspects of building the equipment, but who also lent enthusiastic assistance with its operation. The guidance of Dr. Anwar E.Z. Wissa of the Department of Civil Engineering with the selection of the load cell weighing system is much appreciated.

Credits for typing and assembling the final manuscript are due to Mrs. Alice Biladeau and Mr. Wayne Wendler. We are grateful to Mr. Donald C. Aldrich for his careful proofreading.

REFERENCES

1. Wallabark, J.W., and Taylor, A.M. "Civilization Past and Present," Rev. Ed., vol. 1, p. 148, Chicago, Scott Foresman and Co. (1949).

2. American Public Works Association, Public Administration Service, "Municipal Refuse Disposal," 2nd Edition, p. 7 (1966).

3. Hering, R., and Greely, S.A. "Collection and Disposal of Municipal Refuse," McGraw-Hill, New York (1921).

4. Black, R.J., Muhich, A.T., Klee, A.J., Hickman, H.L., Jr., and Vaughan, R.D. "The National Solid Wastes Survey, an Interim Report," presented at the 1968 Annual Meeting of the Institute of Solid Wastes of the American Public Works Association, Miami Beach, Florida (October 24, 1968).

5. Solid Wastes Management/Refuse Removal Journal, Vol. 14 (4), No. 16, p. 24 (1971).

6. Anderson, D.R., and Colliman, J.P. "Gas Generation and Movement in Landfills," Proceedings National Industrial Solid Wastes Management Conference, Houston, Texas, March 24-26, pp. 311-316 (1970).

7. Vaughan, R.D. "National Goals for Solid Waste Management," Proceedings National Industrial Solid Wastes Management Conference, Houston, Texas, March 24-26, pp. 14-16 (1970).

8. Prindle, R.A. "Health Aspects of Solid Waste Disposal," Proceedings The Surgeon General's Conference on Solid Waste Management, Washington, D.C., Public Health Service, PHS-Pub-1729, pp. 15-20 (1967).

9. Kenahan, C.B., Sullivan, P.M., Ruppert, J.A., and Spano, E.F. "Composition and Characterization of Municipal Incinerator Residues," Report No. 7204, Bureau of Mines, U.S. Department of Interior (1968).

10. Ostrowski, E.J. "Recycling of Ferrous Scrap from Incinerator Residue in Iron and Steel Making," Proceedings National Incinerator Conference, ASME, New York, pp. 87-96 (1972).

11. "Municipal Refuse Disposal," loc. cit., p. 159, (1966).

12. Johnson, A.J., and Auth, G.H., Eds. "Fuel and Combustion Handbook," p. 355, McGraw-Hill, New York, (1951).

13. Orning, A.A. "Principles of Combustion" in "Principles and Practices of Incineration," Corey, R.C., ed., p. 20, Wiley Interscience, New Yok (1969).

14. Meissner, H.G. "Central Incineration of Community Wastes," in "Principles and Practices of Incineration," loc. cit., p. 195.

15. "Municipal Refuse Disposal," loc. cit., p. 164, (1966).

16. Hollander, H.I. "Developing Thermal Energy Release Intensity Parameters for Solid Waste," Proceedings National Industrial Solid Wastes Management Conference, Houston, Texas, March 24-26, pp. 129-132, (1970).

17. Niessen, W.R., and Alsobrook, A.F. "Municipal and Industrial Refuse: Composition and Rates," Proceedings National Incinerator Conference, ASME, New York, pp. 319-337, (1972).

18. Niessen, W.R., and Chansky, S.H. "The Nature of Municipal Solid Waste," American Society of Mechanical Engineers Incinerator Division, May 15, 1969, New York, New York.

19. Neissen, W.R., Sarofim, A.F., Mohr, C.M., and Moore, R.W. "An Approach to Incinerator Combustible Pollutant Control," Proceedings National Incinerator Conference, ASME, New York, pp. 248-259, (1972).

20. Stephenson, J.W. "Burning Wet Refuse," Proceedings National Incinerator Conference, ASME, New York, pp. 260-264, (1972).

21. Thurnau, R.C., Project Manager, Thermal Degradation Project, Solid Waste Research Laboratory, U.S. Environmental Protection Agency, National Environmental Research Center, Cincinnati, Ohio, personal communication, March, 1972.

22. Koenig, L. "The Cost of Municipal Research," Proceedings National Industrial Solid Wastes Management Conference, Houston, Texas, March 24-26, pp. 436-442, (1970).

23. Kreisinger, H., Ovitz, F.K., Augustine, C.E. "Combustion in the Fuel Bed of Hand-Fired Furnaces," U. S. Bureau of Mines, Technical Paper No. 137, (1916).

24. Nicholls, P. "Underfeed Combustion, Effect of Preheat and Distribution of Ash in Fuel Beds," U.S. Bureau of Mines, Bulletin No. 387, (1934).

25. Rose, A.H., and Crabaugh, H.R. "Incinerator Design Standards: Research Findings," Publications of the Los Angeles County Air Pollution Control District, No. 60.

26. Weintraub, M., Orning, A.A., and Schwartz, C.H. "Experimental Studies of Incineration in a Cylindrical Combustion Chamber," U. S. Dept. of the Interior, Bureau of Mines Investigation 6908, (1967).

27. Orning, A.A., Pfeiffer, J.J., Harold, W.C., and Schultz, J.F. "Experimental Study of Incineration," 51st Annual Meeting of APCA, Philadelphia, Pa., May 25-29, paper 58-12, (1958).

28. Schwartz, C.H., Orning, A.A., Snedden, R.B., Demeter, J.J. and Bienstock, D. "Development of a Vortex Incinerator with Continuous Feed," Proceedings National Incinerator Conference, ASME, New York, pp. 145-154, (1972).

29. Stenburg, R.L., Hangerbrauck, R.P., VonLehunden, D.J., and Rose, A.H. "Effects of High Volatile Fuel on Incinerator Effluents," 53rd Annual Meeting of APCA, Cincinnati, Ohio, May 22-26, (1960).

30. Essenhigh, R.H. "Incineration-A Practical and Scientific Approach," Environmental Sci. and Tech., Vol. 2, p. 524, (1968).

31. Stumbar, J.P., and Essenhigh, R.H. "Flame Spread Down Cardboard Sticks and Paper Cylinders," Fire Research Abstracts and Reviews, Vol. 10, p. 112, (1968).

32. Essenhigh, R.H. "Burning Rates in Incinerators, Parts I and II," Proceedings National Incinerator Conference, ASME, New York, p. 87, (1968).

33. Rao, S.T.R., Gelernter, G., and Essenhigh, R.H. "Scale-up Factors for Combustion Pot Behavior in Predicting Incinerator Performance," Proceedings Third National Incinerator Conference, New York, p. 232, (1968).

34. Biswas, B.K., and Essenhigh, R.H. "Heat Value of Refuse," Mech. Eng., Vol. 91, p. 68, (1969).

35. Kuwata, M., Stumbar, J.P., and Essenhigh, R.H. "Combustion Behavior of Suspended Paper Spheres," Proc. Twelfth Symposium (International) on Combustion, Poitiers, France, July, 1968, The Combustion Institute Pittsburgh, pp. 663-675, (1969).

36. Essenhigh, R.H., and Kuo, T.J. "Combustion and Emission Phenomena in Incinerators: Development of Physical and Mathematical Models of Incinerators, Part I: Statement of the Problem," Proceedings National Incinerator Conference, ASME, New York, pp. 261-271, (1970).

37. Kuwata, J., Kuo, T.J., and Essenhigh, R.H. "Combustion and Emission Phenomena in Incinerators: Burning Rates and Operational Limits in a Solid Fuel Bed," Proceedings National Incinerator Conference, ASME, New York, pp. 272-287, (1970).

38. Stumbar, J.P., Kuwata, M., Kuo, T.J., and Essenhigh, R.H. "Combustion and Emission Phenomena in Incinerators: Propagation Velocity and Flame Spread Through Simulated Fuel Beds, Part I: Flame Spread Down a Simulated Fuel Bed, Part II, The Mechanism of Flame Spread Over a Cellulosic Surface," Proceedings National Incinerator Conference, ASME, New York, pp. 288-293, 293-303, (1970).

39. Biswas, B.K., Kuo, T.J., and Essenhigh, R.H. "Combustion and Emission Phenomena in Incinerators: Studies on Combustion Behavior and Extinction Limits of Smoke Flames," Proceedings National Incinerator Conference, ASME, New York, pp. 304-313, (1970).

40. Rao, S.T.R., Kuo, T.J., and Essenhigh, R.H. "Combustion and Emission Phenomena in Incinerators: Characterization of Stirring Factors by Cold Model Simulation," Proceedings National Incinerator Conference, ASME, New York, pp. 314-326, (1970).

41. Kuo, T.J., Kuwata, M., Shieh, W.S., and Essenhigh, R.H. "Combustion and Emission Phenomena in Incinerators: Physical and Mathematical Model of a Simple Incinerator: Part II, The Mechanistic Analysis," Proceedings National Incinerator Conference, ASME, New York, pp. 327-330, (1970).

42. Biswas, B.K., and Essenhigh, R.H. "Some Characteristics of Stabilized Smoke Flames," *Combustion and Flame*, Vol. 15, pp. 93-96, (1970).

43. Essenhigh, R.H., and Kuo, T.J. "Development of Fundamental Basis for Incinerator Design Equations and Standards," *Proceedings Third Mid-Atlantic Industrial Waste Conference*, University of Maryland, Nov. 1969, pp. 105-146, (1970).

44. Rao, S.T.R, and Essenhigh, R.H. "Experimental Determination of Stirring Factors Generated by Straight and Swirling Jets in Isothermal Combustion Chamber Models," *Proceedings Thirteenth Symposium (International) on Combustion*, University of Utah, August 1970, The Combustion Institute, pp. 603-614, (1971).

45. Biswas, B.K., and Essenhigh, R.H. "The Problem of Smoke Formation and Control," Paper No. 39f presented at A.I.Ch.E. 70th National Meeting, Atlantic City, Aug/Sept. 1971.

46. Shieh, W.S., and Essenhigh, R.H. "Experimental Behavior of Waste Combustion in a Test Incinerator," *Fourth Mid-Atlantic Industrial Waste Conference*, University of Delaware, November, (1970).

47. Shieh, W.S., and Essenhigh, R.H. "Combustion of Computer Cards in a Continuous Test Incinerator: A Comparison of Theory and Experiment," *Proceedings National Incinerator Conference*, ASME, New York, pp. 120-134, (1972).

48. "Municipal Refuse Disposal," *loc. cit.*, pp. 45-54, (1966).

49. Kaiser, E.R. "Chemical Analyses of Refuse Components," publication 65-WA/PID-9, ASME, New York, 1965.

50. "Municipal Refuse Disposal," *loc. cit.*, p. 12, (1966).

51. Kaiser, E.R. "Refuse Composition and Flue Gas Analyses from Municipal Incinerators," *Proceedings National Incinerator Conference*, ASME, New York, p. 180, (1964).

52. "Municipal Refuse Disposal," *loc. cit.*, p. 47, (1966).

53. "Control Techniques for Particulate Air Pollutants," U.S. Dept. of HEW, PHS, Consumer Protection and Environmental Health Service, National Air Pollution Control

administration Publication No. AP-51.

54. "Proposals for a Refuse Disposal System in Oakland County, Michigan," Report SW-7d prepared by Jones and Henry Engineers Limited under Grant D01-U1-00068 from the Bureau of Solid Waste Management, Public Health Service Publication No. 1960 (1970).

55. Bortz, S.A., and Pincus, A.G. "High Temperature Incineration," Proceedings National Industrial Solid Wastes Management Conference, University of Houston, March 24-26, (1970).

56. Bernard, R.A., and Wilhelm, R.H. "Turbulent Diffusion in Fixed Beds of Packed Solids," Chem. Eng. Prog., Vol. 46, No. 5, pp. 233-244, (1950).

57. Schotte, W. "Thermal Conductivity of Packed Beds," A.I.Ch.E. Journal, Vol. 6, No. 1, p. 63 (1960).

58. Yagi, S., Kunii, D., and Wakao, N. "Internal Developments in Heat Transfer," Part IV, p. 742, ASME, New York, (1961).

59. Luikov, A.V., Shashkov, A.G., Vasiliev, L.L., and Fraiman, Yu.E. "Thermal Conductivity of Porous Systems," Int. Journal of Heat and Mass Transfer, Vol. 11, pp. 117-140, (1968).

60. Barker, J.J. "Heat Transfer in Packed Beds," Ind. and Eng. Chem., Vol. 57, No. 4, p. 43 (1965).

61. Heggs, P.J., and Handley, D. "Momentum and Heat Transfer Mechanisms in Regular Shaped Packings," Trans. Instn. Chem. Engrs, Vol. 46, T251 (1968).

62. Furnas, C.C. "Heat Transfer from a Gas Stream to a Bed of Broken Solids," U.S. Bureau of Mines Bulletin 261 (1932).

63. Gillespie, B.M., Crandall, E.D., and Carberry, J.J. "Local and Average Interface Heat Transfer Coefficients in a Randomly Packed Bed of Spheres," A.I.Ch.E. Journal, Vol. 14, pp. 483-490, (1968).

64. Bradshaw, A.V., Johnson, A., McLachlan, N.H. and Chin, Y-T. "Heat Transfer Between Air and Nitrogen and Packed Beds of Non-reacting Solids," Trans. Instr. Chem. Engrs., Vol. 48, pp. T77-T84, (1970).

65. Kitaev, B.I. "Heat Exchange in Shaft Furnaces, Metallurgizdat, (1945).

66. Yoshida, F., Ramaswami, D., and Hougen, D.A. "Temperatures and Partial Pressures of the Surfaces of Catalyst Particles," A.I.Ch.E. Journal, Vol. 8, pp. 5-11, (1962).

67. Kitaev, B.I., Yaroshenko, Yu. G., and Suchkov, V.I. "Heat Exchange in Shaft Furnaces," p. 90, Pergammon Press, Oxford, (1967).

68. Baumeister, E.B., and Bennett, C.O. "Fluid-Particle Heat Transfer in Packed Beds," A.I.Ch.E. Journal, Vol. 4, No. 1, pp. 69-74, (1958).

69. Denton, W.H. "Proceedings of the General Discussion on Heat Transfer," Inst. of Mech. Eng. (London), p. 370 (1951).

70. Yagi, S., and Kunii, D. "Studies on Effective Thermal Conductivities in Packed Beds," A.I.Ch.E. Journal, Vol. 3, No. 3, pp. 373-381 (1957).

71. Deissler, L.G., and Eian, G.S. Natl. Advisory Comm., Aeronaut., RME.52005 (1952).

72. Yagi, S., Kunii, D., and Wakao, N. "Studies on Axial Effective Thermal Conductivities in Packed Beds," A.I.Ch.E. Journal, Vol. 6, No. 4, pp. 543-546 (1960).

73. Spalding, D.B. "Some Fundamentals of Combustion," pp. 53-81, Gas Turbine Series, Vol. 2, Butterworths Scientific Publications, London (1955).

74. Kays, W.M. "Convective Heat and Mass Transfer," McGraw-Hill, New York, pp. 327-329 (1966).

75. Amundson, N.R. "Solid-Fluid Interactions in Fixed and Moving Beds: Part 2, Fixed Beds with Large Particles," Ind. and Eng. Chem., Vol. 48, p. 35 (1956).

76. Sauders, O.H., and Ford, H. "Heat Transfer in the Flow of Gas Through a Bed of Solid Particles," J. Iron and Steel Inst., Vol. 1, pp. 292-328 (1940).

77. Chukhanov, Z.F. "Thermal Regime of Semi Coking, Burning and Gasification of Particles in a Solid Fuel," Dokl. Akad. Nauk. SSSR, Vol. 47, No. 3, 1945. Clearing House for Scientific and Technical Information, Washington, D.C. 20230 Translation No. 62-10785.

78. Handley, D., and Heggs, P.J. "The Effect of Thermal Conductivity of the Packing Material on Transient Heat

Transfer in a Fixed Bed," Int. J. Heat Mass Transfer, Vol. 12, pp. 549-570, Pergammon Press (1969).

79. Schumann, T.E.W., "Heat Transfer: A Liquid Flowing Through a Porous Prism," J. Franklin Inst., Vol. 208, No. 3, p. 405 (1929).

80. Klinkenberg, A. "Numerical Evaluation of Equations Describing Transient Heat and Mass Transfer in Packed Solids," Ind. and Eng. Chem., Vol. 40, Pt. 2, No. 10, p. 1992 (1948).

81. Singer, E., and Wilhelm, R.H. "Heat Transfer in Packed Beds: Analytical Solution and Design Method; Fluid Flow, Solids Flow and Chemical Reaction," Chem. Eng. Prog., Vol. 46, No. 7, p. 343, (1950).

82. Brinkley, S.R. "Heat Transfer Between Fluid and Porous Solid Generating Heat," J. App. Physics, Vol. 18, No. 6, p. 582 (1947).

83. Wilhelm, R.H., Johnson, W.C., and Acton, F.S. "Conduction, Convection and Heat Release in Catalytic Converters," Ind. and Eng. Chem., Vol. 35, No. 5, p. 562 (1963).

84. Kasten, P.R., Lapidus, L., and Amundson, N.R. "Mathematics of Absorption in Beds: Part V, Effect of Intraparticle Diffusion in Flow Systems in Fixed Beds," J. Phys. Chem., Vol. 56, No. 6, P. 683, (1952).

85. Munro, W.D., and Amundson, N.R. "Solid-Fluid Exchange in Moving Beds," Ind. and Eng. Chem., Vol. 42, No. 8, p. 1481 (1950).

86. Amundson, N.R. "Solid-Fluid Interactions in Fixed and Moving Beds: Part I, Fixed Beds with Small Particles," Ind. and Eng. Chem., Vol. 48, No. 1, P. 26 (1956).

87. Stewart, M.C., and Saville, J. "A Simplified Heat Transfer Equation for Sinter Beds," Trans. Australian Mech. and Chem. Eng., p. 135 (1968).

88. Woods, S.E., and Harris, C.F. "Heat Transfer in Sinter Roasting," Proceedings Symposium on Chemical Engineering in the Metallurgical Industries, Edinburgh 25-26, Sept. 1963, London I. Chem. E., p. 77 (1963).

89. Walker, P.L., Rusinko, R., and Austin, L.G. "Gas Reactions of Carbon," in "Advances in Catalysis," Vol. XI,

p. 135, Academic Press (1959).

90. Mayers, M.A. "Temperatures and Combustion Rates in a Fuel Bed," Trans. ASME, Vol. 59, Paper No. FSP-59-8 (1937).

91. Kolodtsev, K.I. "Dynamics of Gas Formation in Carbon Beds," J. Phy. Chem. U.S.S.R., Vol. 19, p. 417 (1945).

92. Yagi, S., and Kunii, D. "Studies on Combustion of Carbon Particles in Flames and Fluidized Beds," 5th Symposium (International) on Combustion, Reinhold, New York, p. 231 (1955).

93. Parker, A.S., and Hottel, H.C. "Combustion Rate of Carbon: Study of Gas-Film Structure by Microsampling," Ind. and Eng. Chem., Vol. 28, No. 11, pp. 1334-1341 (1936).

94. Marskell, W.C.,and Miller, J.M. "Mode of Combustion of Coal on a Chain Grate Stoker," Fuel, Vol. 25, No. 1, pp. 4-12 (1946).

95. Kreisinger, H., Augustine, C.E., and Harpster, W.C. "Combustion Experiments with North Dakota Lignite," U.S. Bureau of Mines, Technical Paper 207 (1919).

96. Mayers, M.A. "Combustion Characteristics of Coke," Fuel in Science and Practice, Vol. 21, No. 1, p. 4 (1941).

97. Mayers, M.A. "Some Factors Affecting Combustion in Fuel Beds," ASME Tech. Publication, No. 77 (1937).

98. Thring, M.W. "Physics of Fuel Bed Combustion," Fuel, London, Vol. 31, p. 355 (1952).

99. Thring, M.W. "Physical Processes in a Bed of Fuel," Inst. of Fuel Journal, Vol. 24, No. 75, pp. 47-65 (1940).

100. Silver, R.S. "Theoretical Treatment of Combustion in Fuel Beds I, Gas Compositions and Heat Release," Fuel, Vol. 32, p. 121, (1953).

101. Silver, R.S. "Theoretical Treatment of Combustion in Fuel Beds II - Temperature Attained in Combustion," Fuel, Vol. 32, p. 138 (1953).

102. De Acetis, J., and Thodos, G. "Flow of Gases Through Spherical Packings," Ind. and Eng. Chem., Vol. 52, p. 1003 (1960).

103. Terres, E., Tjia, Hie A., Herrmann, W., Johswich, F., Patscheke, G., Pfeiffer, J., and Schwarzmann, H. Beitrage zur Kenntris der thermischen grundlagen der Verschwelung und Verkokung von Braunkohlen (Ausang)," *Angew. Chm.*, Vol. 48, pp. 17-21 (1935).

104. Bangham, D.H., and Thring, M.W. *Coal Research*, p. 48 (Sept., 1944).

105. Gamson, B.W. "Heat and Mass Transfer: Fluid Solid Systems," *Chem. Eng. Prog.*, Vol. 47, No. 1, pp. 19-28 (1951).

106. Nichols, L.H.F. "Gas Sampling and Temperature Measurement in Fuel Beds," *Inst. of Fuel Journal*, Vol. 14, No. 75, pp. 71-73, (1940).

107. Mott, R.A., and Wheeler, R.V. "Coke for Blast Furnaces," *Iron and Steel Industry Research Council Report No. 1*, *Midland Coke Research Committee* (1930).

108. Löf, G.O.G., and Hawley, R.W. "Unsteady State Heat Transfer Between Air and Loose Solids," *Ind. and Eng. Chem.*, Vol. 40, p. 1061 (1948).

109. Thring, M.W. *Coal Research*, p. 70 (Sept. 1944).

110. Essenhigh, R.H. "The Speed of Combustion of Solid Fuel on Beds," in "The Science of Flames and Furnaces," Thring, M.W., p. 184, 2nd Edition, John Wiley & Sons, Inc., New York (1962).

111. Wu, P.C. "The Kinetics of the Reaction of Carbon with Carbon Dioxide," Sc.D. Thesis, Dept. of Chem. Eng., M.I.T. (1949).

112. Arthur, J.R. "Reactions Between Carbon and Oxygen," *Trans. Faraday Soc.*, Vol. 47, pp. 164-178 (1951).

113. Rice, C.W., "Forced Convection of Heat in Gases and Liquids - II," Ind. and Eng. Chem., Vol. 16, No. 5, pp. 460-467 (1924).

114. Kaiser, E.L., personal communication to Niessen, W.R., Mohr, C.M., and Sarofim, A.F. (1970).

115. von Fredersdorff, C.G., and Elliott, M.A. "Coal Gasification," Chapter 20 in "Chemistry of Coal Utilization," Lowry, H.H., ed., Supplemental volume, John Wiley and Sons, New York (1945).

116. Lewis, W.K., Gilliland, E.R., McBride, G.T., Sr. "Gasification of Carbon by Carbon Dioxide in Fluidized Powder Bed," Ind. and Eng. Chem., Vol. 41, No. 6, pp. 1213-1226 (1949).

117. Simms, D.L., and Law, M. "The Ignition of Wet and Dry Wood Ignited by Radiation," Combustion and Flame, Vol. 11, p. 377-388 (1967).

118. Spalding, D.B. "Conditions for the Stable Burning of Carbon in an Air Stream," Inst. of Fuel Journal, Vol. 26, No. 155, pp. 289-294 (1953).

119. Vortmeyer, D. "Das Verhalten von Zündzonen in exotherm reagierenden gasdurchströmten Körnerschuttungen," Zeitschrift fur Elektrochemie, Vol. 65, pp. 282-289 (1961).

120. Eigenberger, G. "On the dynamic behavior of the catalytic fixed-bed reactor in the region of multiple steady states - I. The influence of heat conduction in two phase models," Chem. Eng. Sci., Vol. 27, pp. 1909-1915 (1972).

121. Vortmeyer, D., and Jahnel, W. "Moving reaction zones in fixed bed reactors under the influence of various parameters," Chem. Eng. Sci., Vol. 27, pp. 1485-1496 (1972).

122. Wicke, E. "Einfluss des Stofftransportes auf den Verlauf heterogener Gasreaktionen," Chem. Eng. Sci., Vol. 8, p. 61 (1958).

123. Wekmeister, H. "Verbrennungsverlauf bei Steinkolen mittlerer Korngrossen," Arch. fur Warmewirtschaft, Vol. 12, pp. 225-232 (1931).

124. Maughan, J.D., Spalding, H.B., and Thornton, B.M. "A Method of Controlling the Temperatures of Travelling Grate Stokers," Engineering, Vol. 137, pp. 587-589, 656-658, 669-671 (1934).

125. Williams, C.C. "Damage Initiation in Organic Materials Exposed to High Intensity Thermal Radiation," Technical Report No. 2, Fuels Research Laboratory, Massachusetts Institute of Technology, Cambridge, Mass. (1953).

126. Gardon, R. "Temperature Obtained in Wood Exposed to High Intensity Thermal Radiation," Technical Report No. 3, Fuels Research Laboratory, Massachusetts Institute of Technology, Cambridge, Mass. (1953).

127. Kreith, F., and Romie, F.E. "A Study of the Thermal

Diffusion Equation with Boundary Conditions Corresponding to Solidification or Melting of Materials Initially at the Fusion Temperature," Proc. Phys. Soc. B., Vol. 68, pp. 277-291 (1955).

128. Goodman, T.R. "The Heat-Balance Integral and Its Application to Problems Involving a Change of Phase," Trans. ASME, Vol. 8, No. 2, pp. 335-342 (1958).

129. Rosseland, S. "Astrophysik und Atom-Theoretisches Grundlage," Springer Verlag, Berlin, 1931, pp. 41-44.

130. Bamford, C.H., Crank, J., and Malan, D.H. "The Combustion of Wood. Part I," Proc. Camb. Phil. Soc., Vol. 42, pp. 146-181, (1946).

131. Tao, C.H., "Generalized Numerical Solutions of Freezing a Saturated Liquid in Cylinders and Spheres," A.I.Ch.E. Journal, Vol. 13, No. 1, pp. 165-169 (1967).

132. Shih, Yen-Ping, and Chou, Tse-Chuan, "Analytical Solutions for Freezing a Saturated Liquid Inside or Outside Spheres," Chem. Eng. Sci., Vol. 26, pp. 1787-1793 (1971).

133. Siegel, R., and Savino, J.M. "An Analytical Solution for Solidification of a Moving Warm Liquid onto an Isothermal Cold Wall," Int. J. Heat Mass Transfer, Vol. 12, p. 803 (1969).

134. Goodman, T.R. "Integral Methods for Non-Linear Heat Transfer," Advan. Heat Transfer, Vol. 1, pp. 51-122 (1964).

135. Rossini, F.D., Pitzer, K.S., Arnett, R.L., Braun, R.M., and Pimental, G.C. "Selected Values of Physical and Thermodynamic Properties of Hydrocarbons and Related Compounds," Carnegie Press, Pittsburgh (1953).

136. Hougen, B.A., and Watson, K.M. "Chemical Process Principles," Part I. p. 254, Wiley and Sons, New York, 1950.

137. Dunningham, A.C., Grummell, E.S. "Contribution to the Study of the Ignition of Fuel Beds," Inst. of Fuel Journal, Vol. 11, pp. 117-122, 129-133 (1937).

138. Johnstone, R.E., and Thring, M.W. "Pilot Plants, Models and Scale-up Methods in Chemical Engineering," McGraw-Hill, New YOrk, 1957, p. 214.

139. Spink, L.K. "Principles and Practices of Flow Meter

Engineering," The Foxboro Company, March 1967, Chapter 6.

140. Rogers, J.E.L., Sarofim, A.F., and Howard, J.B. "The Effect of Underfire Air Rate on a Burning Simulated Refuse Bed," Proceedings National Incinerator Conference, ASME, New York, pp. 135-144 (1972).

141. Wheeler, A. "Reaction Rates and Selectivity of Catalyst Pores," Chapter in "Advances in Catalysis," Vol. 3, pp. 249-327, Academic Press, Inc., New York, 1951.

142. Weisz, P.B., and Prater, C.D. "Interpretation of Measurements in Experimental Catalysis," Chapter in "Advances in Catalysis," Vol. 6, pp. 143-196, Academic Press, Inc., New York, 1954.

143. Van Heerden, C. "The Character of the Stationary State of Exothermic Processes," Chem. Eng. Sci., Vol. 8, p. 133 (1958).

144. Liu, S., and Amundson, N.R. "Stability of Adiabatic Packed Bed Reactors: An Elementary Treatment," Ind. Eng. Chem. Fundamentals, Vol. 1, p. 200 (1962).

145. Aris, R. "Some Problems in the Analysis of Transient Behavior and Stability of Chemical Reactors," Advances in Chemistry, No. 109, p. 578, American Chemical Society (1972).

146. Aris, R. and Schruben, D.L. "Transients in Distributed Chemical Reactors, Part I: A Simplified Model," Chem. Eng. J., Vol. 2, p. 179 (1971).

147. Aris, R., and Fatina, I.H. "Transients in Distributed Chemical Reactors, Part 2: Influence of Diffusion in the Simplified Model," Chem. Eng. J., Vol. 4, p. 149 (1972).

148. Rhee, Hyun-Ka, Foley, D., and Amundson, N.R. "Creeping Reaction zone in a Catalytic, Fixed-Bed Reactor: A Cell Model Approach," Chem. Eng. Sci., Vol. 28, pp. 607-615 (1973).

149. Sarofim, A.F., personal communication, March 5, 1973.

150. Sarofim, A.S. "Combustion Reactions in Overfire Volumes," Presented to the Grates and Combustion Committee ASME Incinerator Division, Thursday, Jan. 15, 1970.

151. Longwell, J.P. and Weiss, M.A., "High Temperature Reaction Rates in Hydrocarbon Combustion," Ind. Eng. Chem.,

Vol. 47, p. 1534 (1955).

152. Hottel, H.C., Williams, G.C., Nerheim, M.N., and Schneider, G.R., "Kinetic Studies in Stirred Reactors: Combustion of Carbon Monoxide and Propane," Tenth Symposium (International) on Combustion, pp. 111-121, The Combustion Institute (1965).

153. Williams, G.C., Hottel, H.C., and Morgan, A.C. "The Combustion of Methane in a Jet Mixed Reactor," Twelfth Symposium (International) on Combustion, pp. 913-925, The Combustion Institute (1969).

154. Nagle, J. and Strickland-Constable, R.F. "Oxidation of Carbon Between 1000-2000°C," Proceedings of Fifth Carbon Conference, Vol. 1, p. 154 (1962).

155. Appleton, J.P. "Soot Oxidation Kinetics at Combustion Temperatures," Presented at AGARD Propulsion and Energetics Panel, 41st Meeting on "Atmospheric Pollution by Aircraft Engines," London, England, 9-13 April (1973).

156. Park, C., and Appleton, J.P. "Shock-Tube Measurements of Soot Oxidation Rates," Combustion and Flame, (in Press), (1973).

157. Engdahl, R.B., and Major, W.S. Bituminous Coal Research, Inc., Tech. Paper No. VII, 1957.

158. American Gas Association Report No. 3 (1954).

APPENDIX K

Biographical Note

Joseph Edward Lloyd Rogers was born on January 30, 1945, in Salisbury, Rhodesia, and is the son of Dr. and Mrs. Edward Rogers of Salisbury, Rhodesia. He attended Ruzawi Preparatory School in Marandellas, Rhodesia, and Prince Edward High School, Salisbury, Rhodesia. After completing high school in December 1962, he was awarded a four year Student Engineer Scholarship from the Anglo American Corporation of South Africa and worked with Anglo American at the Rhokana mine in Zambia until entering the University of Edinburgh, Scotland, in the fall of 1963. He graduated with honors from the University of Edinburgh in June 1967. In the summer of 1967 he was awarded a Fulbright Travel Grant and he entered M.I.T. in the fall of that year as a teaching assistant. He attended the School of Chemical Engineering Practice in the fall of 1968 and received the degree of Master of Science in Chemical Engineering Practice in February 1969. He then accepted a one-semester appointment as the Assistant Director of the Bound Brook Practice School in the spring of 1969. In the summer of 1969 he returned to M.I.T. as a Research Assistant and commenced work on his doctorate.

Joseph Rogers is a member of the honorary society of the Sigma Xi, the American Society of Chemical Engineers, the Institution of Chemical Engineers (London), the Combustion Institute, and is an honorary citizen of the State of Tennesse. He is co-author of

> "The Effect of Underfire Air Rate on a Burning Simulated Refuse Bed," Proceedings National Incinerator Conference, ASME, New York, pp. 135-144, (1972).
>
> "Combustion Characteristics of a Simulated Refuse Bed," presented at the 1973 Technical Session of the Central States Section of the Combustion Institute, March 27, 28, Champaign, Illinois.

He was married to the former Sally Ann Doonan in August 1972 and has accepted a position with Halcon International, Inc., in New York City.

NOMENCLATURE

Dimensional units are expressed in terms of length (L), mass (M), quantity of heat (H), time (t) and temperature (T). Dimensional quantities are given in terms of Btu, hr, ft, °F unless otherwise specified.

Symbol	Meaning	Dimensions
English		
A	Frequency factor in kinetic expression	Dimensions of reaction rate constant
A	Ash fraction of fuel, equation (95)	-
a	Specific heat ratio, C_{p_s}/C_{p_g}	-
A_s	Interfacial area per unit volume of bed	L^2L^{-3}
B	Mass transfer driving force	-
C_j	Concentration of specie j	ML^{-3}
C_{p_g}	Heat capacity of gas	$HM^{-1}T^{-1}$
C_{p_s}	Heat capacity of solid	$HM^{-1}T^{-1}$
D	Coefficient of molecular diffusion	L^2t^{-1}
D^E	Effective coefficient of diffusion	L^2t^{-1}
D_p	Particle diameter	L
d	Mean radiating beam length, equation (65)	L
E	Turbulent eddy diffusion	L^2t^{-1}
E	Activation energy	H lb mole

F_A	Area firing rate, equation (95)	$Mt^{-1}L^{-2}$
F_{RCS}	Relative Carbon Saturation factor, defined by equation (82)	-
$\dot{G}$	Mass velocity of fluid	$ML^{-2}t^{-1}$
g	Mass transfer conductance	$Mt^{-1}L^{-2}$
g^*	Mass transfer conductance for very small mass transfer rates	$Mt^{-1}L^{-2}$
$\bar{H}_v$	Effective latent heat of vaporization, $\Delta H_v \left[\frac{\rho_s^w}{\rho_s^d} - 1 \right]$	HM^{-1}
H_v	Latent heat of vaporization	HM^{-1}
H^c	Overall heat of combustion	HM^{-1}
H_j	Heat of reaction per mole of j - endothermic negative, exothermic positive	H mole $^{-1}$
h_r	Radiation contribution to effective thermal conductivity of porous solid - defined by equation (14)	$Ht^{-1}L^{-2}T^{-1}$
h_s	Heat transfer coefficient based on unit area	$Ht^{-1}L^{-2}T^{-1}$
h_s^E	Effective heat transfer coefficient based on unit area, defined by equation (6)	$Ht^{-1}L^{-2}T^{-1}$
h_v	Heat transfer coefficient based on unit volume	$Ht^{-1}L^{-3}T^{-1}$
j_D	$\frac{k_c \rho_g}{\dot{G}} (N_{Sc})^{2/3}$	-

j_H	$\frac{h_s}{\dot{G}C_{p_g}} \; (N_{Pr})^{2/3}$	-
$J_0(x)$	Bessel's function of the first kind and zeroth order	-
K	Constant for reaction rate	Lt^{-1}
K_s	Packed bed thermal conductivity	$Ht^{-1}L^{-1}T^{-1}$
K_s^E	Effective packed bed thermal conductivity	$Ht^{-1}L^{-1}T^{-1}$
K_g	Effective gas conductivity	$Ht^{-1}L^{-1}T^{-1}$
$\bar{k}$	Effective reaction rate constant, equation (149)	$M_t{}^{-1}L^{-3}$
$\bar{k}$	$K_s^E + \left(\frac{\dot{G}C_{p_g}}{\sqrt{h_v}}\right)\beta$	$Ht^{-1}L^{-1}T^{-1}$
k_c	Mass transfer coefficient	Lt^{-1}
k_g	Molecular gas conductivity	$Ht^{-1}L^{-1}T^{-1}$
k_m	Mass transfer coefficient $(k_c\rho_g)$	$Mt^{-1}L^{-2}$
k_s	Molecular solid conductivity	$Ht^{-1}L^{-1}T^{-1}$
L	Characteristic dimension	L
L_0	Characteristic reaction depth, equation (96)	-
L_c	Combustion bed depth, equation (96)	-
m_j	Mass fraction of specie j	-
M	Moisture fraction of fuel, equation (95)	-
M_j	Molecular weight of specie j	-

N_{Bi}	Biot Number $\left(\frac{h_s D_p}{2k_s}\right)$	-
N_{Le}	Lewis Number $\left(\frac{N_{Pr}}{N_{Sc}}\right)$	-
N_{Pr}	Prandtl Number $\left(\frac{C_p \mu_g}{k_g}\right)$	-
N_{Re}	Modified Reynolds Number $\left(\frac{D_p \dot{G}}{\mu}\right)$	-
N_{Sc}	Schmidt Number $\left(\frac{\mu}{\rho_g D}\right)$	-
N_{Sh}	Sherwood Number $\left(\frac{k_c D_p}{D}\right)$	-
Q^{net}	New total heat release from $z=0$ to $z=\infty$	$Ht^{-1}L^{-2}$
$Q(z)$	Net heat release	$Ht^{-1}L^{-3}$
$\overline{Q}(z)$	Conductivity normalized net heat release	TL^{-2}
R	Gas constant	$ML^2t^{-2}T^{-1}mole^{-1}$
R_p	Radius of particle	L
r_i	Rate of reaction i	$ML^{-3}t^{-1}$
r_i^{eff}	Effective rate of reaction i	$ML^{-3}t^{-1}$
R^*	Rate of reaction	$ML^{-3}t^{-1}$
T_o	Ambient temperature	T
T_{ad}	Adiabatic temperature	T
T_g	Gas temperature	T

T_s	Solid temperature	T
t	Time	t
U	Mass velocity of solid	$Mt^{-1}L^{-2}$
V	Volatile fraction of fuel, equation (95)	-
V	$\dot{U}C_{p_s} + \dot{G}C_{p_g}$	$Ht^{-1}L^{-2}T^{-1}$
w_p	Weight fraction of pyrolyzable material	-
x	Defined by equation (35)	-
y	Defined by equation (34)	-
z	Vertical position	L
z_O	Oxygen consumption distance	L

Symbol	Meaning	Dimensions
Greek		
β	Defined by equation (45)	-
γ	$V/\bar{k}$, equation (51)	L^{-1}
γ	$\frac{GC_{p_g}}{h_v}$, equation (41)	L
δ	Void fraction	-
ε	Emissivity	-
ν_{ij}	Stoichiometric coefficient of component i in reaction j	-
ρ_g	Gas density	ML^{-3}
ρ_s	Solid density	ML^{-3}

ψ	Shape factor (unity for spheres), equation (10)	-
μ	Gas viscosity	$ML^{-1}t^{-1}$
σ	Stefan-Boltzman constant	$Ht^{-1}L^{-2}T^{-4}$
$\phi(T_s)$	Net heat absorbed in endothermic reactions, equation (4)	$Ht^{-1}L^{-3}$
$\psi_j(T_s)$	Mass rate of appearance of specie j, equations (3) and (5)	$Mt^{-1}L^{-3}$

Symbol	Meaning
Superscript	
b	Bulk
d	Dry
i	Interface
o	Initial
v	Vaporization
w	Wet
Subscript	
j	Specie j